

Instytut Podstawowych Problemów Techniki

Polska Akademia Nauk

Marek Bukowicki

**Dynamics of settling pairs of elastic
particles at low Reynolds number regime**

rozprawa doktorska

Promotor rozprawy

prof. dr hab. Maria Ekiel-Jeżewska

Instytut Podstawowych Problemów Techniki

Polskiej Akademii Nauk

Warszawa 2019

Oświadczenie autora rozprawy

Oświadczam, że niniejsza rozprawa została napisana przeze mnie samodzielnie.

data

podpis autora rozprawy

Oświadczenie promotora rozprawy

Niniejsza rozprawa jest gotowa do oceny przez recenzentów.

data

podpis promotora rozprawy

Dziękuję w szczególności:

Pani prof. Marii Ekiel-Jezewskiej,

koleżankom i kolegom z IPPT,

Rodzinie i Przyjaciołom.

Marek Bukowicki was supported in part by the National Science Centre under grant No. 2014/15/B/ST8/04359.

Parts of the results presented in this thesis have been published in articles:

M. Bukowicki, M. Gruca, M. L. Ekiel-Jeżewska, “Dynamics of elastic dumbbells sedimenting in a viscous fluid: oscillations and hydrodynamic repulsion”, *Journal of Fluid Mechanics*, **767**, pp. 95-108 (2015).

M. Bukowicki, M. L. Ekiel-Jeżewska, “Different bending models predict different dynamics of sedimenting elastic trumbbells”, *Soft Matter*, **14**, pp. 5786-5799 (2018).

Streszczenie

Jednym z ważnych zagadnień dotyczącym dynamiki cząstek w lepkim płynie jest opadanie sprężystych włókien w polu grawitacyjnym. W literaturze zajmowano się opadaniem pojedynczego włókna lub niedużych grup takich cząstek. Celem niniejszej rozprawy jest teoretyczne i numeryczne zbadanie dynamiki par mikrowłókien opadających w cieczy przy wartości liczby Reynoldsa znacznie mniejszej od jedności. W większości rozprawy rozważane są cząstki ustawione symetrycznie względem płaszczyzny pionowej. Zbadano również wpływ niewielkich niesymetrycznych zaburzeń konfiguracji początkowej. Oprócz sprężystych włókien, przedmiotem analizy są cząstki sztywne oraz dwa uproszczone modele cząstek: hantle (ang. dumbbells) i tryplety (ang. trumbbells).

Rozprawa wnosi wkład w dotychczas słabo poznany problem oddziaływania hydrodynamicznego pomiędzy parami opadającymi włóknami. Dotychczas taki układ był badany jedynie dla kilku wybranych wąskich klas położenia początkowych, często jedynie dla krótkiego czasu obserwacji. Rozszerzenie zakresu badanych konfiguracji pozwoliło na znalezienie nowych typów dynamiki, które są kluczowe dla zachowania układu.

W celu świadomego wyboru jednego z kilku stosowanych w literaturze potencjałów zginania przeanalizowano jego różne formy za pomocą metod teoretycznych i numerycznych. Okazało się, że powszechnie stosowany potencjał Kratkyego-Poroda systematycznie nie doszacowuje energii zginania. Potencjał harmoniczny jest pozbawiony tej wady. Wykazano też, że wartości i kierunki sił zginania uzyskane przy użyciu różnych potencjałów mogą się znacznie różnić. Ponadto pokazano na przykładach że w niektórych układach potencjały harmoniczny i Kratky'ego-Poroda mogą prowadzić do skrajnie odmiennych wyników.

Znaleziono nowe rozwiązania periodyczne w symetrycznym układzie podłużnych cząstek sztywnych. Podczas opadania cząstki koziółkują, jednocześnie przesuując się okresowo w kierunku poziomym równoległym do płaszczyzny symetrii. Rozwiązania periodyczne dla cząstek sztywnych stanowią ważną część pracy, będąc granicznym rozwiązaniem dla sprężystych włókien, których sztywność dąży do nieskończoności.

Opadanie pary giętkich włókien charakteryzuje się bogatą dynamiką. W zależności od współczynnika giętkości cząstek oraz parametrów konfiguracji początkowej występują różne typy ruchu. Przykładowo, w początkowej fazie bardzo giętke włókna mogą przybliżać się lub oddalać. W tej pracy szczególnie skupiono się na cząstkach o umiarkowanej giętkości.

W takich układach włókna zbiegają do pozycji w której oba ich końce znajdują się na takim samym poziomie i w takiej samej odległości od płaszczyzny symetrii („konfiguracja równoległa”), zaś środkowe odcinki włókien są wygięte ku dołowi. Zbieganie do takiej konfiguracji często charakteryzuje się gasnącymi oscylacjami, których amplituda i tempo zaniku zależą od sprężystości cząstek. Tu warto nadmienić że w granicy cząstek sztywnych tłumienie oscylacji nie występuje i obserwowane są ruchy periodyczne. Po tym jak sprężyste włókna zbiegną do opisanej konfiguracji równoległej, w zależności od swojej giętkości mogą się odpychać, przyciągać, lub zbiegać do określonej odległości. W szczególnym przypadku pary sprężystych cząstek leżących początkowo w płaszczyźnie pionowej, z powodu braku zaburzeń zewnętrznych, cząstki nie mogą jej opuścić podczas ruchu. Dla takich konfiguracji zaobserwowano przewidziany w literaturze „koziołkujący” typ ruchu włókien podczas gdy dla dwóch trypletów odkryto nową rodzinę ruchów periodycznych.

Analiza układów niesymetrycznych pokazała, że dla badanych zaburzeń również w tym przypadku włókna, o ile nie są zbyt sztywne, zbiegają do konfiguracji równoległej. W przypadku bardziej sztywnych cząstek początkowe niesymetryczne zaburzenie jest wzmacniane. Dynamika układu staje się znacznie bardziej skomplikowana, cząstki często w sposób sztuczny zderzają się ze sobą. Odkryto, że dość sztywne włókna mogą zbiegać do nowych, niesymetrycznych konfiguracji o długim czasie trwania.

Oprócz dynamiki włókien, przebadano również zachowanie uproszczonych modeli cząstek: hantli i trypletów. Zastosowanie uproszczonych modeli cząstek w szczególności pokazało kluczową rolę zginania w procesie zbiegania do konfiguracji równoległej. Tryplety, nie ograniczone do płaszczyzny pionowej, zachowują się analogicznie do włókien – jedno i drugie cząstki zbiegają do konfiguracji równoległej, co poprzedzone jest gasnącymi oscylacjami. Również zachowanie trypletów po osiągnięciu konfiguracji równoległej - przyciąganie lub odpychanie - ma swój odpowiednik w dynamice włókien. Dynamika hantli jest inna. Cząstki wykonując koziołkujący ruch stopniowo oddalają się od siebie. Co więcej, hantle powoli dążą do płaszczyzny pionowej, zamiast do konfiguracji prostopadłej do tej płaszczyzny, jak to czynią tryplety i włókna.

Niniejsza rozprawa wzbogaca wiedzę na temat dynamiki jednego z podstawowych układów mikrohydrodynamicznych: dwóch włókien opadających w płynie pod wpływem grawitacji. Wnosi ona zarazem wkład w zagadnienie modelowania podobnych układów. Nowo odkryte zjawiska pozwalają lepiej zrozumieć nie tylko zachowanie pary włókien, lecz także większych układów, w których dwucząstkowe oddziaływania hydrodynamiczne mają duże znaczenie.

Abstract

The system of a few elastic fibres settling under gravity in low Reynolds number regime is one of important problems studied in the field of microhydrodynamics. In the literature it was concerned for a single or a couple of filaments. The topic of this dissertation is to elucidate the dynamics of pairs of microfibrils settling in the system where Reynolds number is much smaller than unity. Majority of results are obtained for initial configurations of particles which are symmetric with respect to a vertical plane. The dynamics of the system were evaluated also for small perturbations from the symmetric state. Apart from elastic fibres, this dissertation includes results for rigid particles and two types of simplified models: dumbbells and trumbbells.

This work contributes to the knowledge about the problem of two hydrodynamically interacting fibres settling under gravity in a viscous fluid. Until now such system was investigated only for a few narrow classes of initial configurations, often only for short time scales. Broad range of initial configurations analysed in this dissertation allowed to discover new types of dynamics, which are essential for the system behaviour.

In order to thoughtfully choose the form of bending potential, a few options present in the literature were theoretically and numerically analysed. It turned out that the popular cosine (Kratky-Porod) bending potential systematically underestimate the bending energy. Harmonic model does not have this flaw. It was also demonstrated that the discrepancy between bending forces calculated with different bending potentials can be large in terms of both magnitude and direction. Furthermore, it was shown that in some systems harmonic and Kratky-Porod bending potentials may lead to completely different results.

New periodic solutions have been found in the symmetric system of rigid, elongated particles. During the settlement the particles tumble and at the same time periodically swing along the horizontal direction which is parallel to the symmetry plane. Periodic solutions found for the rigid particles are an important part of this work and for the elastic filaments they serve as a limiting case of the infinite bending stiffness.

The dynamics of settling pair of elastic filaments is reach. Depending on their flexibility and the initial configuration parameters the particles may perform different types of motion. For example, in the initial phase of dynamics very flexible fibres may effectively repel or attract each other. In this work I mainly focused on moderately flexible particles. In such kind of

systems the fibres converge to the configuration in which both ends of each particle are located at the same level and within equal distance from the symmetry plane (“aligned configuration”), while the middle parts of fibres are bent downward. During the convergence toward aligned configuration particles usually oscillate: the amplitude and decay rate of the oscillations depend on the filaments flexibility. In the limit of rigid particles the damping is absent and periodic motions are observed. After the elastic fibres have converged to the aligned configuration, depending on the flexibility they can repel each other, attract or converge to a specific distance. In the special case when the initial configuration of particles is restricted to the vertical plane, in absence of external noise the particles have to stay within the plane throughout the motion. In such configurations some fibres performed the predicted in the literature tumbling motion, while for trumbbells a new family of periodic motions was found.

The analysis of non-symmetric systems showed that for the range of perturbations considered in this work the filaments keep to converge to the aligned configuration, unless the particles are too stiff. In case of more stiff particles, the initial perturbations are amplified. The dynamics of the system become much more complex, particles often spuriously collide. It was discovered that quite rigid filaments can converge to alternative long-lasting configurations, which are not symmetric.

Apart from fibres, also simplified models of particles were considered: dumbbells and trumbbells. The application of simplified models of particles showed the key role of particles bending capability in the process of the convergence to the aligned configuration. Trumbbells, if not restricted to the vertical plane, behave similarly as filaments: they converge to the aligned configuration, what is preceded with damped oscillations. Also after the alignment the dynamics of trumbbells is analogous to those of fibres: particles attract or repel each other. The dynamics of dumbbells is different. Particles perform tumbling motion and gradually move away from each other. Moreover, dumbbells slowly tend toward the vertical plane, unlike trumbbells and fibres which tend to orient themselves perpendicularly to it.

This dissertation expands the knowledge concerning one of the basic systems in the microhydrodynamics: two fibres settling under gravity in a viscous fluid. It also contributes to the methodology of modelling similar systems. The new phenomena discovered in this work allow to better understand not only the behaviour filament pairs, but also the dynamics of larger assemblies of fibres in which two-particle hydrodynamic interactions play important role.

Contents

1	Introduction	1
1.1	Basic concepts of low Reynolds number regime	2
1.2	Characteristic features of the system considered in this work	7
1.3	Dynamics of particles settling in low Reynolds number regime	9
1.4	Simplified models: dumbbells and trumbbells	12
1.5	Dynamics near interfaces	14
1.6	Scope and outline of the thesis	14
2	Methodology	17
2.1	Particle representation - bead model	17
2.2	Elastic response	20
2.3	Hydrodynamic interactions and equations of motion	23
2.4	Normalization	25
2.5	Outline of similar models used in the literature	25
2.6	Symmetry of the system	27
3	Two sedimenting dumbbells	30
3.1	Problem statement - initial configurations in the vertical plane	30
3.2	Limits of very stiff bond and lack of bonds	31
3.3	Dynamics of elastic dumbbells in vertical plane	36
3.4	Analytic considerations	41
3.5	Dynamics of dumbbells out of vertical plane	45

4	Dynamics of rigid particles	50
4.1	Dynamics of rigid filaments (rods) in plane	50
4.2	Notation of the particles orientation in the 3D motion	54
4.3	Dynamics of rigid filaments out of plane	55
4.4	Dynamics of rigid dumbbells and trumbbells	58
4.5	Periodicity of the motion	60
5	Analysis of different forms of bending potential in bead model of elastic particles	62
5.1	Correspondence between continuous and bead models	63
5.2	Comparison of energy in different bending models	65
5.3	Comparison of forces in discrete models for different bending potentials	67
5.4	Impact of the form of bending potential on the dynamics of elastic particles settling in a viscous fluid	72
6	Flexible particles in the vertical plane	80
6.1	Dynamics of filaments	80
6.2	Dynamics of trumbbells	83
6.3	Example of spurious dynamics caused by inappropriate bending potential	86
7	Dynamics of elastic particles out of the vertical plane	90
7.1	Dynamics of filaments -general picture	90
7.2	Oscillations	92
7.3	Dynamics of aligned filaments	96
7.4	Trumbbells	99
7.5	Conclusions	102
8	Dynamics of particles in non-symmetric configurations	104
8.1	Initial configurations and notation	105
8.2	More flexible filaments, $B \geq 10$	107
8.3	More stiff filaments, $B \leq 5$	111
8.4	Drift and rotation of the system	114
8.5	Discussion	115

9	Conclusions	119
9.1	Summary	119
9.2	Original elements of the thesis	120
9.3	Perspectives for future studies	122
	Appendices	125
A	Comparison of point-particle and Rotne-Prager approximations of hydrodynamic interactions in application to dumbbells' dynamics	126
B	Stability of single sedimenting trumbbell	130
	Bibliography	132

1 Introduction

Dynamics of microparticles in water solution is very different from the everyday experience and from physical intuition brought from classical mechanics classes. In such environment effects of viscosity dominate the motion, inertia is typically negligible and velocities of both fluid and immersed particles are proportional to the instantaneous forces acting in the system.

At the same time, the area of microhydrodynamics is becoming increasingly important for medical, industrial and environmental applications due to rapid progress in observation and manipulation techniques [1–4]. One of the approaches taken in order to better understand behaviour of microparticles in fluids is focusing on basic, fundamental systems which can be comprehensively analysed and understood. Concerning a broad problem of microparticles sedimentation, in recent years a lot of attention was devoted to a basic system of a single microfibre settling in a quiescent fluid [5–12]. Other publications discussed dynamics of a group consisting of a couple of sedimenting elastic particles, for particular classes of initial configurations [10, 13].

This dissertation adopts a similar approach: it is a comprehensive study of the system of two fibres settling in a viscous fluid. Initial configuration of particles is symmetric with respect to a vertical plane. Both flexible and stiff particles are considered. In comparison to previous studies, this work greatly extends the range of analysed configurations, what allows to obtain a more global view on the landscape of different behaviours of the filaments. The benefit of analysing both stiff and flexible particles is a better understanding of the mechanism underlying the observed dynamics. The more so, I investigate whether the form of bending potential applied in the simulations can be qualitatively alter the dynamics and argue which form of bending potential may be the preferred choice.

The results obtained in this work give a valuable insight into fundamental properties of a basic class of systems consisting of hydrodynamically interacting pairs of elastic particles, what can be considered as a next step after the problem of a single settling filament has been extensively studied. Furthermore, the two-particle interactions are essential to analyse dynamics of large assemblies of settling particles in semi-dilute regime [14, 15].

1.1 Basic concepts of low Reynolds number regime

1.1.1 Stokes equations

Dynamics of fluid is described by Navier-Stokes equations [16]. In low Reynolds number regime, where the viscosity dominates the dynamics and the influence of inertia is small, Navier-Stokes equations reduce to Stokes equations [16, 17]:

$$\eta \nabla^2 \mathbf{u} - \nabla p = 0 \quad (1.1)$$

$$\nabla \cdot \mathbf{u} = 0 \quad (1.2)$$

where \mathbf{u} is the fluid velocity, p – pressure and η – dynamic viscosity. The first equation (1.1) is the balance of forces, while equation (1.2) indicates that the considered fluid is incompressible. At the same time non-hydrodynamic forces acting on each particle¹ (in context of this work: on each particle segment – bead) are balanced by hydrodynamic forces acting on its surface:

$$\mathbf{F}_i = \oint_{S_i} \boldsymbol{\sigma} \cdot \mathbf{n} dS \quad (1.3)$$

where \mathbf{F}_i is the total non-hydrodynamic force acting on the i -th particle segment, S_i is the surface of the segment, \mathbf{n} is the surface normal vector and $\boldsymbol{\sigma} = -p\boldsymbol{\delta} + \eta [\nabla \mathbf{u} + (\nabla \mathbf{u})^T]$ is the stress tensor. Non-hydrodynamic torques are coupled with the stress tensor on the surface in a similar way. As in the system considered in this dissertation external torques are absent, their influence is not described in more details.

The Reynolds number, which is crucial to determine whether the Stokes equations can be a proper description, is a ratio of the characteristic viscous relaxation time scale τ_B to the advection time scale τ_S . The former can be written as:

$$\tau_B = \frac{m}{\zeta} \quad (1.4)$$

where m is the mass of a fluid element and ζ is hydrodynamic friction (inverse mobility). If L is the characteristic length scale, the mass of fluid element with is proportional to ρL^3 , where ρ is the fluid density, while $\zeta \sim L\eta$. Taken together, the viscous relaxation time scale is equal to

¹Sometimes in the literature ‘non-hydrodynamic forces’ are called ‘external forces’. In the system considered in this work there are three types of forces acting on particle segments: gravity, elastic constraint forces and hydrodynamic forces. Because in many contexts elastic forces in the body by no means are described as ‘external’, throughout the thesis I will reserve this name for gravity, or an analogous force. Elastic forces and gravity together will be called ‘non-hydrodynamic forces’.

$\tau_B = \rho L^2 / \eta$. The advection time scale is given by:

$$\tau_S = \frac{L}{U} \quad (1.5)$$

where U is the characteristic velocity in the system.

In terms of characteristic velocity U , length L , density ρ and viscosity η the Reynolds number can be written as:

$$Re = \frac{\rho U L}{\eta} \quad (1.6)$$

Stokes equations are valid for vanishing Reynolds number, $Re \ll 1$. Reynolds number close to zero can be found in various systems. Undoubtedly, the most common context is a water solution in microscale. In case of sedimentation, the Reynolds number is very small for objects which sizes vary from macromolecules ($\sim 100nm$) up to at least large algae cells ($\sim 10\mu m$) for virtually the whole available spectrum of densities (more precisely, it is the difference between density of particles and the fluid what matters). In glycerine, honey or silicon oil, which are much more viscous than water, Reynolds number is small even for macroscopic objects of the order of millimetres or more. Owing to this property, macroscopic experiments can be used to study the dynamics of microsystems. Such approach was adopted in case of sedimentation of suspensions [18–21], groups of particles [22–28] and recently also single filaments [12]. Sometimes Stokes equations are used to describe even larger objects, like bubbles in magma [29].

In low Reynolds number regime the dynamics is Aristotelian: unlike in the familiar Newtonian systems, it is the velocity, not the acceleration, what is a linear response to forces. This happens because accelerations in the system are practically instantaneously relaxed due to large friction. Velocities are proportional to the forces, and in absence of the latter the system is motionless. The Aristotelian dynamics takes its name after the Greek philosopher, who claimed that otherwise static objects can move only as long as forces are applied. Clearly, such observation is true as long as a strong damping is present in the systems.

An important feature of Stokes equations is time-reversal-symmetry of the motion. This property means that if velocity \mathbf{u} and pressure p constitute the solution of Stokes equations for given boundary conditions on the fluid velocity and pressure, by switching $\mathbf{u} \rightarrow -\mathbf{u}$, $p \rightarrow -p$, and reversing the signs of \mathbf{u} and p in boundary conditions, another solution is obtained. Equation (1.3) couples non-hydrodynamic forces exerted on particle segments with the stress tensor integrated on the particle surface, which is defined by velocity and pressure of the fluid. For the system considered in this dissertation, which in absence of non-hydrodynamic forces is motionless, reversing the direction of non-hydrodynamic forces is equivalent to reversing signs

of \mathbf{u} and p in boundary conditions. In other words, when all non-hydrodynamic forces change direction to the opposite, the systems follows the dynamics backward in time. This property is the origin of many non-intuitive phenomena observed in viscous fluid. One striking example is the ‘unmixing’ of a smeared drop of dyed glycerine shown by Taylor [30]: after having reversed the direction of mixing, the smeared drop reforms itself back to its initial shape². Time-reversal-symmetry is also readily used in theoretical analysis, because it often allows to discover important features of the dynamics without laborious calculations. For example it can be reasoned that the two identical spherical particles settle down without changing their relative position [17] or that an microorganism (or microrobot) cannot propel itself repeating back and forth the same motion, the latter called ‘scallop theorem’ [31]. In this dissertation time-reversal-symmetry will be useful in showing periodicity of the motion in some systems.

1.1.2 Hydrodynamic interactions

It is trivial to say that every force acting in the fluid has an impact on the fluid velocity and pressure fields. Non-trivially however, in Stokes regime this influence is instantaneous, what follows from the limit of vanishing viscous relaxation time. Fluid motion caused by forces acting on a single particle influences the dynamics of all other particles in the system and such influence is called hydrodynamic interactions (HI).

The instantaneous relaxation of velocities gives potentially large computational advantage. This property guarantees that there exists a relation between non-hydrodynamic forces and the motion of each element of the system. In other words, knowing the boundary conditions, positions of particles and non-hydrodynamic forces we are able to determine the particle velocities in the system without explicit calculations of the fluid motion. The motion of bulk of fluid does not need to be resolved, unlike in other popular methods such as Lattice-Boltzman method [32, 33] or multiparticle collision dynamics [34, 35]. Of course the expressions describing hydrodynamic interactions – relation between non-hydrodynamic forces and velocities – can be very complicated, but it is at least granted that they actually exist.

In Stokesian dynamics velocities of particles (or segments of particles) are calculated by multiplying vector of all non-hydrodynamic forces³ by the (grand) mobility matrix, which depends on the configuration of particles. The process of calculating mobility matrix is described in more details in chapter 2. Dynamics of the system (time-dependent positions of particle segments) is resolved by numeric integration of expressions for particle

²This experiment was presented to the general audience by our research group at the Science Picnic of Polish Radio. Educational resources from our group, including experiments presented at the Science Picnic, can be found at <http://hydro.ippt.pan.pl>

³And in general torques and ambient flow multipoles, both absent in this work.

segment velocities, calculated as described above. Unlike in the Newtonian dynamics the accelerations of the particles do not enter into equations of motion. As mentioned before, in low-Reynolds-number dynamics the full information about motion of the fluid is not necessary to determine the dynamics of particles. However, if the motion of fluid is the matter of interest, it can be straightforwardly calculated at any point of the space, basing on particles positions and forces acting in the system.

Hydrodynamic interactions can be calculated with different approximations. In general there is no superposition principle (interactions are not pairwise additive), however approximations where such principle holds are very popular. For spherical particles hydrodynamic interactions have a relatively simple form, which additionally can be expanded into series of terms of the order of $1/r^n$, where r is the distance from the centre of the sphere. Basing on such expansion, reliable and convenient approximations can be derived for long distance interactions. In particular, point particle approximation [17] (containing terms up to $1/r$) and Rotne-Prager-Yamakawa [36, 37] approximation (up to $1/r^3$) are often used. In both of them the equations of motion can be expressed exclusively in terms of pairwise interactions, what makes them very convenient for numerical calculations. If even higher accuracy is required, higher order terms may be also included [38–42]. Relatively simple expressions for hydrodynamic interactions between spheres gave rise to the modelling approach in which more complex shapes of particles are represented as made of spherical beads [6, 43–46]. Such bead models are also used in this dissertation, as described in section 1.4 and chapter 2.

An important property of hydrodynamic interactions in viscous fluids is that they have very long range. Their influence on velocity decays with distance r as $\sim 1/r$. In consequence, large systems of particles are challenging to be modelled numerically and, maybe even more, theoretically, because the influence of even very distant particles cannot be omitted.

1.1.3 Important examples

Hydrodynamic interactions between microparticles can lead to complex, often nonintuitive and interesting behaviours. In this section some illustrative examples are presented in order to give broader context for the results described in this dissertation.

The most basic system, already mentioned before, is a pair of identical spheres settling under gravity. Regardless of their relative positions, the particles move with the same velocity and there is no relative motion between them. Such behaviour is different from the same system for higher Reynolds number, where for example if the spheres initially are located one above the other, the upper particle would catch up the lower one (so called drafting-kissing-tumbling behaviour [47]).

Two non identical settling beads in the Stokes regime can perform periodic motions [48]. It was recently shown, that if the particles are additionally charged, a new, stable and attracting equilibrium may appear, in which beads are located one above the other with a certain equilibrium distance between them [49].

Larger groups of neutral point particles, settling under gravity, have been shown to exhibit interesting properties. For particles located at the vertices of a single horizontal polygon it was shown that the system is stable up to 6 particles, whereas it becomes unstable for larger groups [50]. For certain regular configurations of beads, periodic motions have been discovered [39, 51–55], coupled with settling down. In some cases, probably there is no upper limit for the number of involved particles [54, 55]. Recently it was shown, that periodic motions of particles can exist also in Brinkmann medium [56, 57].

Random groups of particles perform non-periodic, yet long-lasting dynamics, before finally the cloud decays [58, 59]. Their multi-step life cycle, consisting of quasi-periodic oscillations, shape evolution and decay, is a topic of studies in various aspects. Long-lasting, yet non-periodic dynamics is present also in regular arrangements of particles [54, 55] and in systems consisting of only three [60] or four [53] spheres.

Sedimentation of elongated particles, rigid or elastic, is another broad topic in the field of microhydrodynamics. In such systems hydrodynamic interactions are essential for the relative motion of particles. Since sedimentation of filaments is also the topic of this dissertation, the state of art in this matter will be reviewed more broadly later in the text. In case of closed (looped) filaments, numerical simulations show a wide range of different behaviours observed for different elasticity of particles [61]. For closed filaments which are knotted, numerical results have been also successfully confronted with experiments [62].

Although in this dissertation particles fall in a quiescent fluid, it is worth to briefly mention also the dynamics of neutrally buoyant microfilaments in external flow. Vast literature of the topic covers problems like influence of filament elasticity [63–65] or vicinity of walls [66–68] in various types of the flow. Often the migration of fibres is the primary matter of interest [63, 66, 69, 70], however other issues like the filament shape during the motion [64], its knotting due to external flow [69, 71] or pair formation [46] are also considered. It was also shown that hydrodynamic interactions between filaments (and not only between segments of a single filament) may be relevant for the dynamics [72]

Examples described in this section present basic systems of microparticles in fluid, which fundamental features have been discovered in recent decades. Their behaviours are often complex, interesting and significant for applications or further studies. This dissertation aims to extend the list given above.

1.2 Characteristic features of the system considered in this work

In this section I will describe the scale of real world systems to which the results of this work apply.

Stokes equations for the problem of sedimentation in water solution are valid up to the length scale of the order of tens of microns. In more viscous media, like glycerine or silicon oil, the upper boundary for the particle size is moved up, what allows to perform macroscopic experiments. The bottom boundary for Stokes equations is given by the scale at which due to coarse nature of solvent molecules the fluid cannot be approximated as homogeneous, what is usually assumed to be at tens of nanometers.

The Brownian motions are known to play an important role in nanoscale. The characteristic time scale of thermal (Brownian) noise is:

$$\tau_R = \frac{a^2}{D} = \frac{a^2 \zeta}{k_B T} \quad (1.7)$$

where a – particle size, D – diffusion coefficient, k_B – Boltzmann constant, T – temperature and ζ is the hydrodynamic friction coefficient, which is proportional to the particle size a and to the fluid viscosity η , e.g. for a sphere of a radius a is equal to $\zeta = 6\pi\eta a$. The relative influence of Brownian motions is often described by the dimensionless Péclet number, which is the ratio of the diffusion time scale τ_R to advection time scale τ_S .

In this work, large value of Péclet number, $Pe \gg 1$, (negligible diffusion effects) is assumed and the thermal noise is not applied in the simulations. Large Péclet number establish the lower limit for the size of particles considered in this dissertation. In water solution it is around fractions of micron, below which the thermal noise becomes relevant [17]. However, the experiments conducted with micro- and nanofilaments have shown that in many cases even at smaller scales the Brownian effects do not affect significantly the motion, and main features of the dynamics are the same both in Brownian and non-Brownian systems [62, 73–78].

Apart from that, any non-hydrodynamic surface interactions (van der Waals forces, charges, wetting effects etc.) are neither taken into account. Such approach is common in similar studies and allows to obtain more basic results. Additional surface interactions could be added to the model as the next step in more detailed simulations, which aim to capture behaviour of a specific real word system, instead of general, universal features of the dynamics like in this work. Moreover, in this dissertation I focus on the dynamics of particles which are not very close to each other.

Sedimentation is a very important process in biological context [79–83]. Among the microobjects important from the environmental point of view it is worth to mention bacteria [84], pollens and plankton [85–87], in particular diatoms which can form long, elastic fibres [74, 76]. In broad field of medical sciences, the particles of interest are for example microfilaments [73, 88], dust in lungs [] or red blood cells [89]. In the industry, the most prominent applications are probably processes involving cellulose fibres [90, 91]. Nanofibres (‘nano’ refers to the diameter– typically tens to hundreds of nanometres– much smaller than the fibres length), which have amazing range of applications [92, 93], are also within the range of scales that can be modelled with Stokesian dynamics.

The filaments examined in the dissertation have certain elasticity. It is usually assumed, that for settling fibres the dynamics are primarily controlled by dimensionless parameter B , which couples gravity force G exerted on the fibre, its length L and bending stiffness A :

$$B = \frac{L^2 G}{A} = \frac{4L^2 G}{\pi E_Y a^4} = \frac{4gL^3 \Delta\rho}{E_Y a^2} \quad (1.8)$$

where E_Y is Young modulus, a is the fibre radius, g is gravitational acceleration and $\Delta\rho$ is the difference in density between the particle and the solvent. The latter equation is valid if the settling of particles is caused by gravity, what is not the only possible application. Saggiorato et al. argued that dynamics in centrifugation is another option, which would allow to control the parameter B for a particle with given physical properties (length and stiffness) by tuning G . Yet another realisation is the motion of charged particles in electric field, which would play the role of driving force instead of the gravity. Schlagberger and Netz [6, 94] used results obtained in simulations of a sedimentating filament to explain anomalous birefringence in suspension of charged filaments. The difference between sedimentation under gravity and electrophoresis is that in the latter case segments of charged particle interact with each other electrostatically, however this additional effect was neglected by authors cited above.

In this work I mainly focus on the values of flexibility parameter $B \in [1, 300]$ or rigid particles $B \ll 1$. When necessary, values out of these limits are also considered. The selected range of B is consistent with other publications in the topic, except that it does not include very flexible filaments $B > 300$. One reason for omitting regime of very flexible particles was that the larger values of B were difficult (and sometimes impossible) to be reached with short filaments considered in this work. Even more importantly, virtually all real-world examples of filaments are either within the range of B selected in this work, or even below it (more stiff). Additionally, the investigated range of B was adopted in the course of development of the study in order to follow important patterns of the dynamics.

For the important biopolymers the parameter B calculated for settling under gravity was estimated as $B \approx 0.01$ for actin filaments and $B \approx 0.1$ for microtubules [10]. Larger value

of this parameter can be reached for artificially made microfibrils: filaments used by Perazzo et al. [95] had $B < 80$ and in studies by Pawłowska et al. [77, 96] B was also of the order of $B \sim 10$. In macroscopic experiments [12] performed in the silicon oil the examined range of B was approximately $B \in [60, 1000]$.

Value of B depends strongly on the aspect ratio of the particle $L/2a$. Values of B given above have been calculated for filaments with large aspect ratio. Results presented in this dissertation are obtained for rather short particles. It was shown however, that it is the value of B parameter, rather than the aspect ratio, what is the most important factor for the dynamics of elongated, elastic particles [7, 12, 13].

1.3 Dynamics of particles settling in low Reynolds number regime

The problem of sedimentation in viscous fluids has been studied for both rigid and elastic particles. In this section I briefly review main results, with particular interest in publications closely related to the topic of this dissertation.

1.3.1 Sedimentation of rigid particles

A single ellipsoid or rod in viscous fluid settles down without change of configuration [17], what can be derived from time-reversal-symmetry of Stokes equations. Objects with more complex shapes can orient themselves during sedimentation, as it was shown for bent, stiff filaments [97, 98]. Dynamics of chiral particles, which constantly rotate at the settlement, is also a subject of interest [99].

Dynamics of two rigid particles is even more interesting. Kim [100, 101] has shown that some symmetric configurations lead to periodic tumbling of particles, combined with the settlement. This kind of motion was later explored in different contexts [43, 102] but even more importantly was observed in macroscopic experiments [23, 28]. Jung et al. [23] examined dynamics of pairs of objects with various shapes: rods, discs and hemispheres. In all cases they found periodic, tumbling motion, predicted by Kim. Recently more detailed experiments with pair of discs are conducted by Chajwa et al. [28]. Tumbling motion of two rigid particles is wider discussed in chapters 3.2 and 4 of this dissertation.

Larger groups of rigid particles have also been studied. Dynamics of a ‘cloud’ of rods was investigated numerically and experimentally by Park et al. [26]. Suspension of rigid particles was a subject of theoretical [14], numerical [103] and experimental [19, 21] studies. Recently Goldfriend et al. [104] have shown that the irregular shape of rigid particles may be important for global properties of the suspension.

1.3.2 Single flexible filament

The problem of a single, elastic filament settling under gravity has been extensively studied in recent years. Xu and Nadim [5] by means of theoretical analysis discovered that the weakly flexible fibre under gravity would bent and orient itself horizontally. In April 2005 two articles by Schlagberger and Netz [6] and Lagomarsino and coauthors [7] were published, which addressed the problem of a filament sedimentation by numeric simulation, for wide range of filament flexibility. In both studies the filament was initially straight, and therefore restricted to the vertical plane – the dynamics was quasi-2D.

The results indicate that independently on the initial tilt of the particle, its configuration converges to a steady ‘U’-shape. Only very flexible fibres are shown be able to adopt unstable ‘W’-shape configuration, but this behaviour was observed for filaments much more flexible than those considered in this dissertation. Form the technical point of view, it is worth to point out that in both works the dynamics was performed with bead model, described later in the text and used also in this dissertation⁴. Results for the single filaments are almost insensitive to the aspect ratio as such (number of beads it consists of). It was shown that the stationary shape of the particle depends mainly on the dimensionless number B , introduced before in section 1.2. More information about definition of fibres elasticity is given in chapter 2.

Dynamics of a single filament was later a subject of further studies [8–12]. Li et al. [8] investigated particles with both uniform and non-uniform cross-sectional thickness using slender body approximation. The authors confirmed previous results and in addition they explicitly showed that the horizontal distance travelled by a single filament during relaxation is always finite. In work by Saggiorrato et al. [10] dynamics of a single, two and three filaments was studied. Unlike in other articles cited above, stochastic simulations were performed with the presence of low-amplitude white noise, which however did not intend to directly simulate the Brownian forces. Regarding the problem of a single particle, the authors discovered that for large $B > 1200$ the particles start to deviate from the vertical plane and for $B > 1800$ the filaments become asymmetric and settle down along helical trajectories. Both of these new types of behaviour were observed for B above the range considered in this work and therefore also much larger than in majority of interesting systems with the gravity as the driving force.

In a recent article by Marchetti et al. [12] the authors provided a broad review of previous studies, performed numerical simulations with two different models and conducted experiments for a macroscopic elastic fibre in the silicon oil. In general, the experimental results confirmed earlier numerical predictions, however their limited accuracy does not allow for detailed comparison so far.

⁴The details of the models used by Schlagberger&Netz and by Lagomarsino et al. are different. The model used in this dissertation is more similar to the former one, as described in chapter 2, in particular in section 2.5.

1.3.3 Two flexible filaments

The most comprehensive work considering sedimentation of two microfilaments is the article by Llopis et al. [13] in which short term dynamics was analysed for three different classes of initial configurations, referred by the authors as three ‘geometries’. In all geometries the filaments were initially straight and horizontal. Gravity pointed downward along ‘ z ’ axis and both filaments are parallel to ‘ x ’ axis.

In geometry (I) the second filament is shifted along y axis with respect to the first one by distance d . The authors showed that for sufficiently large d the influence of the second filament on the bending amplitude scales as d^{-3} and the influence on the settling velocity of the particles scales as d^{-1} . Unfortunately the authors do not comment on the velocity of the filaments along y direction (attraction or repulsion) which in this dissertation is shown to be an important feature of the dynamics in such configuration (chapter 7.3).

In the second geometry studied by Llopis et al. the two filaments were initially placed one above the other (shift along z axis). The authors found that the upper filament always sediments faster and catches up the lower one. The relative velocity of the filaments scales as d^{-2} and also strongly depends on the filaments flexibility.

The last studied geometry was the ‘collinear’ configuration in which the second filament is shifted along x axis. Such configurations of particles are also studied in this dissertation (chapters 6 and partially 3). In this family of initial configurations the behaviour of particles was shown to be qualitatively dependent on the elasticity parameter: more rigid particles approach each other and collide, while more flexible repel each other [13]. Apart from that, the authors investigated settling velocity and asymmetry of the filaments shapes.

The dynamics of two filaments was also a topic of study by Saggiorato et al. [10]. The authors investigated initial configuration in which one filament is above the other. They considered not only the case in which filaments are in the same vertical plane (‘geometry II’ in ref. [13]) but also the more general situation where the upper filament is additionally rotated around the vertical axis. The authors found that in the latter case the pair of filaments rotates while settling down, what was also observed in this dissertation for some non-symmetric configurations investigated in chapter 8. Moreover, Saggiorato et al. [10] showed that in the long time scale the filaments gradually converge to the parallel configuration.

The class of initial configurations studied in this dissertation is broader than those investigated in the literature. In the major part of the thesis I consider particles which are initially horizontal, parallel to ‘ x ’ axis and symmetrical with respect to a vertical plane. If we denote $\varphi(0)$ as the initial angle between the ‘right’ particle and ‘ x ’ axis, then 1st and 3rd

geometries in study of Llopis et al. [13] correspond to $\varphi(0) = \pi/2$ and $\varphi(0) = 0$, respectively. In this dissertation I investigate the range of $\varphi(0)$ in between these values. Additionally new analysis of already studied configurations is performed, revealing new important features of the dynamics. Apart from flexible fibres, in this work I consider also rigid rods and simplified models of dumbbells and trumbbells, described in section 1.4.

1.3.4 Larger groups of flexible filaments

The system of three filaments was considered by Saggiorato et al. [10]. The initial configurations of particles were ‘randomly chosen’, however the authors do not reveal details of this procedure. Results presented for three filaments were obtained for absence of noise and flexibility $B = 60$ (which is within the range considered in this dissertation). In majority of simulations, two of the filaments form a ‘bundle’ which settles faster than the third, isolated particle. Additionally they observed that in some cases all three fibres perform periodic motions. The described dynamics is therefore somewhat similar to the system of three point particles in the vertical plane, studied by Janosi et al. [60]. In point particles dynamics, likewise the dublet of particles eventually leave the third one behind, and the separation may be preceded by long and complex three-particle interaction. The filaments however, in opposite to point particles, are able to establish periodic motions of three particles⁵. Moreover, the periodic solution for the filaments seems to be stable and have basin of attraction large enough to be discovered when starting from random configurations.

Larger groups of flexible fibres have been considered as a suspension of particles. The problem was investigated with theoretical and numerical methods [15, 106–108]. For example it was recently demonstrated that the self-reorientation effect of flexible filaments has large influence on the microstructure (size of the instabilities) of the suspension [108]. In this dissertation the reorientation of elastic particles is shown to play an important role also in the two-particle dynamics.

1.4 Simplified models: dumbbells and trumbbells

In modelling of particles settling in low Reynolds number regime, bead model is arguably one of the most popular [6, 9, 10, 12, 13]. In this approach the fibre is modelled as a chain of

⁵Interestingly, in an analogous system, with hard spheres instead of point particles, periodic solutions have been found [105]. Such solutions obtained for three spheres are however different from those observed for filaments, because all three spheres perform the same type of motion, while in case of filaments two particles oscillate differently than the third one.

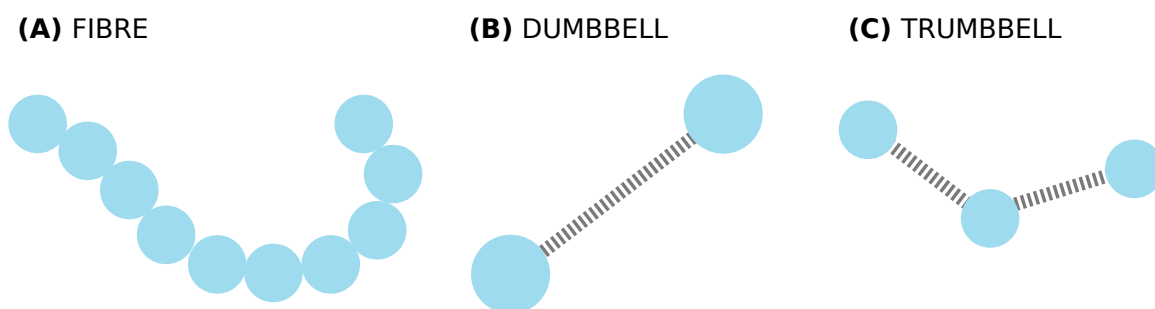


Figure 1.1: Types of particles modelled as chains of beads: (A) fibre, (B) dumbbell, (C) trumbell.

connected beads, what is described in more details in chapter 2. Apart from such filaments, in this dissertation I consider the dynamics of more basic models: dumbbells and trumbells. All three types of particles are shown in figure 1.1. Dumbbell consists of only two beads, connected with a spring. Trumbell consists of three sequentially connected beads with an additional elastic bending potential. The simplified models are important, because they can enable broader theoretical analysis and help to elucidate the mechanisms of certain behaviours. For example dumbbell may serve as an example of a particle which can deform and elastically respond to the deformations, while trumbell is the simplest of beads models, which can bend.

Dumbbells have been used in a range of problems. In context of migration of particles in vicinity of walls such model was used e.g. in works by Jendrejack et al. [66], Ma & Graham [109] or Singh [110]. Dumbbells are also used to model active particles [111–115]. In particular it was shown that although according to the scallop theorem a single dumbbell cannot swim, two dumbbells are enough to overcome this limitation [111, 112]. Larger groups of dumbbells also have been studied [116–119], for example in context of separation of passive and active particles [119].

Trumbell model (sometimes called trimer) is typically used to determine the primary influence of bending on the dynamics [13, 120–125]. The simplicity of the model allows to filter out features which originate from more complex, and therefore more case-specific, properties of the system, like higher modes of deformations. Trumbell models are also relatively simple to theoretical analysis. Their applications in microhydrodynamics are quite common. Often the area of interest is the dynamics of particles in flow [120–125]. Llopis et al. [13] used trumbell model to analytically estimate the rate at which the upper elastic particle from the pair catches up the bottom one, in the second geometry described above in section 1.3.3. Uspal and Doyle [126] considered groups of trumbells to investigate phenomena of self-organization of many particles in flow.

1.5 Dynamics near interfaces

In recent years a lot of studies have been devoted to dynamics near flat interfaces. Generally three basic types of interfaces are considered [17]: fluid-wall (no-slip), fluid-gas (free slip) and fluid-fluid (with different viscosity) which is a superposition of no-slip and full-slip cases. Dynamics in presence of boundaries is an interesting problem, because they can significantly affect the motion and they are common both in natural environment [] and microfluidic applications [127–129]. Influence of the interfaces was studied in various contexts, like dynamics of microswimmers [130, 131], relaxation of elastic filament near free surface [132] or sedimentation in vicinity of wall [27, 133, 134].

In simulations and theoretical analysis of objects near interfaces the method of images is often used. Recent review of some aspects of this method for fluid-wall and fluid-gas interfaces is given in the article by Ekiel et al. [135] with contribution of the author of this dissertation. Many results for two particles presented in later chapters are also relevant for a single particle near a fluid-gas interface, what is described in section 2.6 together with a brief note about the application of method of images in microhydrodynamics.

1.6 Scope and outline of the thesis

This work intends to give a comprehensive description of the symmetric system of two elongated particles settling under gravity in low Reynolds number regime. It covers wide range of initial configurations. Both stiff and elastic particles are considered. Different forms of bending potential are critically analysed in comparison to the continuous reference model. Particular attention is paid to the relatively stiff particles, with $B \leq 100$, due to their importance in context of experiments. Extensive analysis of the problem, including rigid rods, elastic fibres and simplified models, allows in-depth understanding of behaviour of the system and drawing general conclusions. Additionally, dynamics of slightly non-symmetric systems are studied in order to investigate robustness of obtained results.

The system of particles which is being studied in this work has not been investigated before. The main part of results is obtained for two elongated particles which are initially located symmetrically with respect to a vertical plane. For such symmetric system, the main questions which this work aims to answer are:

I What is the dynamics of elastic fibres?

II What is the dynamics of rigid rods?

III What is the dynamics of simplified models: dumbbells and trumbbells? Do they capture main features of behaviour observed for fibres?

In order to elucidate robustness of results I also analyse the following problem:

IV What is the dynamics of slightly non-symmetric system of elastic particles? Are the perturbations attenuated or amplified?

Additionally this dissertation analyses the following issue, which may be important for numerical studies which use popular bead models:

V Does the choice of bending potential form influence the dynamics? Which one is the most adequate?

The text is organized as follows. In this chapter I describe the goal of the thesis and present the analysed system. I also introduce Stokes regime and give a short review of relevant literature. The range of application of obtained results is outlined.

In the second chapter I present methodology used in this work. I characterize the representation of particles – bead model, define elastic forces acting on the beads and the approximation of hydrodynamic interactions between them. Equations of motion are given. Similarities and differences in comparison with other similar studies are discussed. Also correspondence of the two-particle system with system of a single particle near interface is presented, what is an alternative interpretation of the obtained results.

In the third chapter the dynamics of two dumbbells is described. Dumbbells are the simplest models of particles considered in this work. First, the limits of rigid particles and lack of bonds are discussed. Arguments for periodicity of motion are presented. Next, the dynamics of elastic dumbbells in a vertical plane is described, with particular focus on attracting, universal trajectory and hydrodynamic repulsion phenomena. Scaling arguments, regarding interplay between beads size and elasticity are developed. Finally, the dynamics of dumbbells out of vertical plane are investigated.

The fourth chapter describes the dynamics of rigid particles, for which flexibility coefficient B is close to zero. Dynamics of fibres (rods) in vertical plane and out of vertical plane is discussed. Additionally the dynamics of rigid dumbbells and trumbbells is investigated and compared to results obtained for fibres. Dynamics of rigid particles serves as a reference for elastic fibres, described in later chapters.

In the next chapter the influence of different forms of bending potential is investigated. First, the correspondence between bead model and a continuous fibre is established. Next, the bending energies in different bending potentials are compared to the reference value of a continuous filament. Moreover, the resulting bending forces for different bending potentials are compared. Finally, the influence of the form of bending potential is examined in a few model systems of settling particles.

In chapter 6 the dynamics of elastic fibres in a vertical plane is investigated. The system is studied for different lengths of filaments and different elasticities. For very short particles a new type of behaviour is observed (tumbling), which was predicted, but not observed, by Llopis et al. [13]. Long term properties of tumbling dynamics is examined for the first time. In the same chapter the dynamics of elastic trumbbells is studied, which are simplified models of particles which can bend. Interesting, new type of periodic motion is observed. Additionally, spurious effects of commonly used cosine (Kratky-Porod) bending potential are shown.

In chapter 7 the dynamics of flexible particles out of the vertical plane is described. This is the most prominent part of this dissertation. First, different types of dynamics are investigated for a wide range of flexibility and initial configurations. Next, I focus on the regime of relatively small B , in which particles converge to a horizontal, parallel configuration. The mechanism of such alignment is discussed and oscillations, which occur prior to the alignment, are characterized. Moreover, the dynamics of particles after the alignment is investigated. Finally, I show that the simplest model of bending particles, trumbbells, is sufficient to capture the dynamics characteristic for elastic filaments.

In chapter 8 the influence of non-symmetric perturbations of the initial configuration is analysed. I show that the behaviour of the system is robust to perturbations in the major part of flexibility parameter range investigated in this work: it converges to the horizontal, parallel configuration of particles. For more stiff fibres the perturbations initially amplify, what can be followed by later attenuation, spurious collision or, interestingly, other types of long-lasting configurations.

Chapter 9 summarizes the results, outlines most important findings of this work and indicates promising areas for the future studies.

2 Methodology

In this chapter I introduce methodology used to simulate dynamics of particles in viscous fluid. First, representation of particles is described, along with necessary notation (sec. 2.1). In next sections, models of particle elastic response (sec. 2.2) and hydrodynamic interactions (2.3) are presented. In the latter section, equations of motion are included. Normalization is given in section 2.4. Subsequently, short comparison with other, similar models used in literature is provided (sec. 2.5). Finally, the system symmetry is discussed and a correspondence between dynamics of symmetric pair of particles settling in bulk and single particle near liquid-gas interface is established (sec. 2.6).

2.1 Particle representation - bead model

In this dissertation the dynamics of elongated particles with constant circular cross section is described. One of most common approaches to simulate motion of such particles in viscous fluid is to represent each particle as a chain of identical beads [6, 7, 10, 12, 44–46, 62, 124, 136–141], what is called ‘bead model’. The reason for such simplification is the existence of convenient approximations for hydrodynamic interactions between spherical beads (sec. 2.3). For a cylindrical shape of particle, hydrodynamic interactions are much more difficult to calculate. An advantage over another popular simplification, slender body limit, is that the bead model takes the thickness of the particle into account.

Information about particle positions and configurations in the bead model is carried by a vector containing positions of centres of all beads that the particle consists of. Usually rotational dynamics of beads is not subject of interest [6, 7, 10, 12, 44–46, 62, 124, 136–141] and it is also omitted in this dissertation. Centres of subsequent beads are connected with virtual bonds, which do not interfere with the fluid. In the presented model, vector \mathbf{r} which carries full information about state of the system comprises of positions of all centres of beads in the system: $\mathbf{r} = (\mathbf{r}_1, \dots, \mathbf{r}_M)$, where M is the total number of beads in the system and \mathbf{r}_i is the position of i -th bead centre: $\mathbf{r}_i = (x_i, y_i, z_i)$. We often consider systems consisting of more than one particle, in which case vector \mathbf{r} comprises positions of beads belonging to distinct particles. By convention consecutive beads in a particle are labelled with consecutive numbers.

Let us introduce and summarize notation used in this dissertation:

- \mathbf{r}_i – position of centre of i -th bead,
- $\mathbf{t}_i = \mathbf{r}_{i+1} - \mathbf{r}_i \equiv \mathbf{r}_{i,i+1}$ – vector connecting centres of subsequent beads (referred also as i -th bond),
- $l_i = \|\mathbf{t}_i\|$, (for $i > 0$) – length of i -th bond,
- l_0 – bond’s equilibrium length (further explained in section 2.2),
- β_i – angle between \mathbf{t}_{i-1} and \mathbf{t}_i . Vertex of this angle is in the center of i -th bead,
- \mathbf{f}_i – non-hydrodynamic force acting on i -th bead,
- a – bead radius,
- $a_{max} = l_0/2$ – radius of bead such that consecutive beads touch each other in the equilibrium configuration,
- N – number of beads in particle,
- L – ‘length’ of the particle, equal to sum of bonds’ lengths $L = \sum_{i=1}^{N-1} l_i$,
- L_0 – equilibrium length of the particle, $L_0 = (N - 1)l_0$ (further explained in section 2.2),
- \mathbf{G} – gravity force acting on all beads: $\mathbf{G} = (\mathbf{f}_1^g, \dots, \mathbf{f}_M^g)$, where M is the total number of beads in the system and \mathbf{f}_i^g is gravitational force, with buoyancy taken into account, acting on i -th bead. In systems considered in this dissertation gravitational forces acting on all beads are equal to each other and given by $\mathbf{f}_i^g = (0, 0, -G/N)$, where G is the magnitude of the total gravitational force acting on a single particle consisting of N beads.

Apart from listed above, some common notation conventions are used: hat for unit vector: $\hat{\mathbf{x}} = \mathbf{x}/\|\mathbf{x}\|$, and non-bold font for vector length: $x = \|\mathbf{x}\|$ (except for G which is not the length of \mathbf{G} , as described above). The values of all variables which appear in later chapters are given in dimensionless units, defined in sec. 2.4, apart of a few initial sections of chapter 5 where dimensional quantities are considered.

Below I introduce and briefly discuss three types of bead-modelled particles used in this work, consisting of different number of beads N : dumbbell ($N = 2$), trumbell ($N = 3$) and fibre ($N \geq 4$).

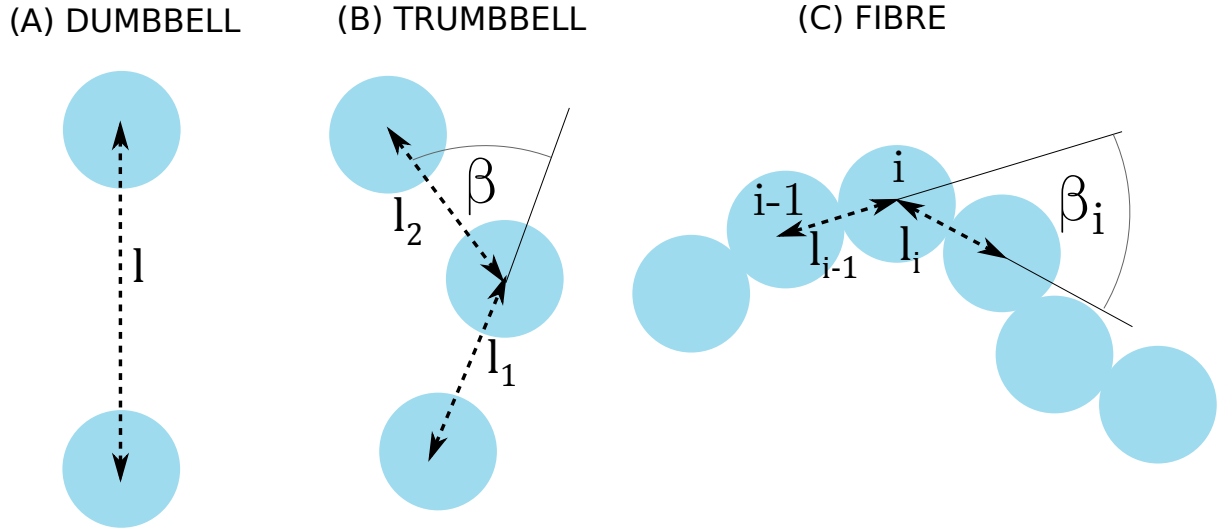


Figure 2.1: Types of particles studied in this work: dumbbell, trumbbell and fibre (filament).

2.1.1 Dumbbell

Dumbbell is the simplest non-trivial case of bead model. It consists of two beads, centres of which are connected with a spring. Importantly, the dumbbell cannot bend and the only allowed alteration of its shape is change of the spring length. Typically, the dumbbell's beads are widely separated [109, 111], in this work usually $a = a_{max}/5$.

2.1.2 Trumbbell

Trumbbell is the simplest of bead models which can bend. It consists of three beads, so that the shape of a trumbbell is described by lengths of the two springs and the bending angle. Analysis of trumbbells dynamics allows to identify what is the influence of bending on dynamics of flexible objects.

In literature trumbbells are often studied with the assumption that bonds lengths are constant in time, therefore with only one variable (angle β) describing the shape [120–122, 125, 126]. In this dissertation lengths of trumbbell's bonds are not fixed (as in e. g. ref. [123]), in order to be consistent with the case of filaments, where in agreement with the elasticity theory, extensible bonds are considered. It was checked that small variation of bond lengths, caused by its elasticity, does not have a significant effect on the dynamics of particles.

Trumbbell model usually does not intend to represent a real shape of a particle. It is rather a model system aimed to capture basic properties of dynamics of particles, which can bend [120, 122, 124, 125, 142]. In order to study behaviour of elongated particles, trumbbells with small bead radius are used, such that beads do not touch each other: in this work typically $a = a_{max}/4$ or $a = a_{max}/2$. The limit of large, touching beads with $a = a_{max}$ is also studied.

2.1.3 Fibre

Fibres (filaments) are modelled with so called ‘shish-kebab model’ [10, 13, 143], or simply ‘bead model’, where a cylindrical continuous fibre is represented by a chain of touching ($a = a_{max}$) or almost touching beads. In equilibrium configuration, the filament is straight.

Unlike dumbbell or trumbbell, which mainly serve as simplified models, the filament is a common shape of particles occurring in nature and in technical applications, whose dynamics is aimed to be revealed. Therefore it is worth to discuss the relation between the bead model of a filament, used in simulations, and continuous, cylindrical shape of real-world, yet idealized, fibre. Unlike the cylinder, the chain of beads does not have constant width, since it varies from $2a$ in the widest point to 0 at beads joints. Also the length is somewhat ambiguous: it may be defined as the ‘total length’ (equal to $L + 2a$ in our notation) or may be measured from centre of first bead to the centre of the last one (equal to L), excluding the marginal hemispheres of the fibre. Tentatively we will refer to L as the fibre length and $2a$ as the width. Correspondence between continuous fibre and bead model of the fibre will be further discussed in chapter 5.

2.2 Elastic response

At rest and in the absence of external flow and forces, the particle (made of beads) in the equilibrium configuration: particle is straight, what means that $\forall_{i,j \in 1, \dots, N-1} \hat{\mathbf{t}}_i \cdot \hat{\mathbf{t}}_j = 1$, and all bonds have equilibrium length $\forall_{i \in 1, \dots, N-1} l_i = l_0$. In this section there it is defined what elastic forces appear when the particle is out of its equilibrium.

2.2.1 Extensional forces

For modeling particle response to stretching and compression, harmonic elastic potential is applied, given by:

$$U^e = \frac{k}{2} \sum_{i=1}^N (l_i - l_0)^2, \quad (2.1)$$

where $l_0 = L_0/(N - 1)$ and k is Hookean spring constant. The resulting force \mathbf{f}_i^e acting on i -th bead is equal to:

$$\mathbf{f}_i^e = -\frac{\partial U^e}{\partial \mathbf{r}_i} = k [(l_i - l_0)\hat{\mathbf{t}}_i - (l_{i-1} - l_0)\hat{\mathbf{t}}_{i-1}], \quad (2.2)$$

for non marginal beads ($1 < i < N$). For marginal beads there is only one term in this sum, as either \mathbf{t}_i or \mathbf{t}_{i-1} does not exist.

2.2.2 Bending forces

In this work two main types of bending potentials are used: cosine Kratky-Porod¹ and harmonic. Additionally in some contexts also logarithmic bending potential is considered. Different forms of bending potential are described briefly in this section, while further discussion can be found in chapter 5 and 6.3.

In order to represent bending, positions of at least three beads are necessary. Therefore, the input for bending potential functions is pair of unit vectors, representing directions of two consecutive bonds.

Kratky-Porod bending potential for each particle is given by [146]:

$$U_{KP}^b = \frac{A}{l_0} \sum_{i=2}^{N-1} (1 - \hat{\mathbf{t}}_{i-1} \cdot \hat{\mathbf{t}}_i) = \frac{A}{l_0} \sum_{i=2}^{N-1} (1 - \cos \beta_i) \quad (2.3)$$

Kratky-Porod potential is often used in simulations [6,7,10,12,44,45,137,138,140,141,144] of particles because it is easy and effective to implement, at the same time being an accurate approximation for small bending angles.

Another popular form of bending model is the harmonic potential [62, 125, 136, 139, 147–156]. It is given by:

$$U_H^b = \frac{A}{2l_0} \sum_{i=2}^{N-1} \beta_i^2 \quad (2.4)$$

It may be noticed, that the calculations of harmonic bending potential from unit vectors $\hat{\mathbf{t}}_{i-1}$ and $\hat{\mathbf{t}}_i$ are numerically more costly than in case of Kratky-Porod potential, as the relevant formulas involve inverse trigonometric functions, e. g. by $\beta_i = \arccos(\hat{\mathbf{t}}_{i-1} \cdot \hat{\mathbf{t}}_i)$.

Logarithmic form of bending potential, used by Förtsch et al. [157], is much less common than the previous two. It is given by:

$$U_{Log}^b = -\frac{2A}{l_0} \sum_{i=2}^{N-1} \ln(1 + \cos \beta_i) \quad (2.5)$$

Unlike harmonic and Kratky-Porod models, the logarithmic potential grows to infinity as the bending angle approaches π , what means that the resistance to bending for large angles is significantly larger than in other models.

¹Following other studies(e.g. ref. [144]), in this work the expression ‘Kratky-Porod’ bending potential refers only to the formula which relates bending energy and angles between segments of the particle. In general context Kratky-Porod model [145] has wider meaning, not explored in this dissertation.

All forms of bending potential presented in this chapter are identical in the limit of small bending angles, where the term proportional to β_i^2 dominates. Further discussion and comparison of bending potentials may be found in chapter 5. The choice of an adequate bending model was a part of research conducted in this dissertation.

Elastic forces, resulting from bending, acting on each bead, are calculated by differentiation of chosen bending potential function with respect to the position of a given bead:

$$\mathbf{f}_i^b = -\frac{\partial U^b(\mathbf{r})}{\partial \mathbf{r}_i}. \quad (2.6)$$

2.2.3 Elasticity coefficients

Elasticity coefficients responsible for bending (A) and stretching (k) can be coupled, based on continuous elasticity theory [158]. Assuming that the fibre made of beads of radius a aims to model continuous, cylindrical shape with the same radius a , coefficient k is related to A by:

$$k = \frac{4A}{a^2 l_0}. \quad (2.7)$$

In this work, following other articles in this topic [6, 12, 94], such relation is applied. However, because change of bonds length usually does not play important role in the dynamics, in the literature value of parameter k sometimes is chosen independently from A , typically as a large number to assure that the filament is practically inextensible [44, 64, 138].

Taking into account the elasticity theory, values of bending coefficients are also related to the material property of the filament, Young modulus E_Y :

$$A = \frac{E_Y \pi a^4}{4}, \quad (2.8)$$

$$k = \frac{E_Y \pi a^2}{l_0}. \quad (2.9)$$

In the literature [7, 10, 12, 13], the ratio of gravity to bending stiffness of the filament is often characterized by dimensionless value B :

$$B = \frac{L_0^2 G}{A}. \quad (2.10)$$

Later in this work, B is referred as ‘gravity-to-bending’ ratio or simply ‘elasticity’ or ‘flexibility’ parameter of the particle: the larger B , the more flexible the filament (or trumbbell)

is. Gravity-to-bending ratio ‘ B ’ is an inverse of elasto-gravitational number, used e. g. by Li et al. [8].

For trumbbells a modified elasticity coefficient will be used, denoted as B' :

$$B' = B \cdot \frac{a}{a_{max}} \quad (2.11)$$

The reason for this modification is to obtain an elasticity coefficient for which in the first approximation the dynamics would be independent from the size of beads. We may observe from the expressions for bending potentials (2.3)-(2.5) and from eq. (2.13) that the bending force is inversely proportional to B and that the primary effect of any force on beads velocity is proportional to magnitude of the force divided by the bead radius a . In consequence the contribution of bending force to the beads velocity is roughly inversely proportional to $B' \sim B \cdot a$. At the same time it can be noticed that the second important factor contributing to the relative velocities of beads, influence of gravity does not depend on the elasticity of the particle and is almost insensitive to beads’ size² (eq. (2.15)). Therefore in many cases the overall dynamics of the systems with conserved value of $B' \sim B \cdot a$ may be very similar, even if values of bead size a and elasticity B vary. Indeed, such rescaling was shown to be convenient for trumbbells [159] as it allows to consider similar range of elasticity parameter B' for particles with different sizes of beads.

2.3 Hydrodynamic interactions and equations of motion

In general hydrodynamic interactions are not additive, however there exist approximations where superposition principle holds. Here the ‘additivity’ means that hydrodynamic interactions in a system of many particles can be calculated as the sum of independent pairwise contributions from all particles. Lack of additivity means that hydrodynamic interactions between two particles (in context of this dissertation: two beads) are affected by presence of a third one.

Among additive models arguably the most common are point-particle (PP) approximation [17] (which model interactions between particles of any shape which are separated widely enough) and Rotne-Prager-Yamakawa (RPY) approximation [36, 37], which is the simplest version of model for hydrodynamic interactions between spherical particles. Additive models of hydrodynamic interactions are particularly useful, because they allow to simulate systems consisting of points (PP approximation) or spheres (RPY) with relatively low computational cost. Indeed, in vast majority of studies where the bead model is involved, one of these additive

²For gravity, the self terms in eq. (2.12) are identical, what means that the gravity contributes to relative velocities of beads only by pairwise hydrodynamic interactions.

approximations of hydrodynamic interaction is used, although more precise approaches, such as multipole method, are also present in the literature [38–42, 45, 64, 97, 160–167]. In this dissertation Rotne-Prager-Yamakawa and point-particle models are used.

For an additive model of hydrodynamic interactions, in the bead model, the velocity of i -th bead $\dot{\mathbf{r}}_i$ is given by:

$$\dot{\mathbf{r}}_i = \boldsymbol{\mu}^{ii} \cdot \mathbf{f}_i + \sum_{j \neq i} \boldsymbol{\mu}^{ij}(\mathbf{r}_i, \mathbf{r}_j) \cdot \mathbf{f}_j, \quad (2.12)$$

where $\boldsymbol{\mu}^{ii}$, is the self-mobility matrix of size 3×3 and $\boldsymbol{\mu}^{ij}$ is the part of mobility matrix which defines hydrodynamic interactions between i -th and j -th bead. For identical beads in bulk, the self-mobility matrix is given by:

$$\boldsymbol{\mu}^{ii} = \mathbb{1}\mu_0 = \mathbb{1}\frac{1}{6\pi\eta a}, \quad (2.13)$$

where a is the radius of the bead, $\mathbb{1}$ is 3×3 unit matrix. It is worth to stress that interaction terms $\boldsymbol{\mu}^{ij}$ in additive models depend only on position of i -th and j -th beads, and not on any other factors. The more so, if the system is translationally invariant – as is the bulk considered in this study – the matrix $\boldsymbol{\mu}^{ij}$ depends only on *relative* position of the beads: $\boldsymbol{\mu}^{ij}(\mathbf{r}_i, \mathbf{r}_j) = \boldsymbol{\mu}^{ij}(\mathbf{r}_j - \mathbf{r}_i) \equiv \boldsymbol{\mu}^{ij}(\mathbf{r}_{ij})$. The form of $\boldsymbol{\mu}^{ij}$ depends on chosen approximation: in this work point particle model or RPY.

In point-particle approximation $\boldsymbol{\mu}^{ij}$ is given by Oseen tensor (fundamental solution of Stokes equations for velocity) [17]:

$$\boldsymbol{\mu}^{ij}(\mathbf{r}_{ij}) = \mathbf{T}(\mathbf{r}_{ij}) = \frac{1}{8\pi\eta r_{ij}} (\mathbb{1} + \hat{\mathbf{r}}_{ij} \otimes \hat{\mathbf{r}}_{ij}). \quad (2.14)$$

Rotne-Prager-Yamakawa approximation is more accurate than point-particle model due to comprising terms up to the order of $(r_{ij})^{-3}$. An additional advantage of RPY approximation is that it ensures that the mobility matrix is positively defined (all eigenvalues are greater than 0) and therefore that the dissipation of energy is positive. Although RPY model describes dynamics of spherical particles, one should keep in mind that it allows for overlaps of beads. In RPY approximation $\boldsymbol{\mu}^{ij}$ is given by formula, which distinguish whether beads do not overlap ($r_{ij} \geq 2a$) or they do ($r_{ij} < 2a$):

$$\boldsymbol{\mu}^{ij}(\mathbf{r}_{ij}) = \begin{cases} \frac{1}{8\pi\eta r_{ij}} \left[\left(1 + \frac{2a^2}{3r_{ij}^2}\right)\mathbb{1} + \left(1 - \frac{2a^2}{r_{ij}^2}\right)(\hat{\mathbf{r}}_{ij} \otimes \hat{\mathbf{r}}_{ij}) \right] & \text{if } r_{ij} \geq 2a, \\ \frac{1}{6\pi\eta a} \left[\left(1 - \frac{9r_{ij}}{32a}\right)\mathbb{1} + \frac{3r_{ij}}{32a}(\hat{\mathbf{r}}_{ij} \otimes \hat{\mathbf{r}}_{ij}) \right] & \text{if } r_{ij} < 2a. \end{cases} \quad (2.15)$$

In order to simulate the dynamics of beads, equations of motion (eq. (2.12)) are solved for $\mathbf{r}_i(t)$ with appropriate form of hydrodynamic interaction matrix $\boldsymbol{\mu}^{ij}(\mathbf{r}_{ij})$ and forces \mathbf{f}_i calculated as the sum of elastic forces (eq. (2.2) and (2.6)) and external body force (gravity). Point particle approximation is used in chapter 3, describing dynamics of dumbbells, while RPY model is used in all other chapters of the dissertation. In appendix A both models of hydrodynamic interactions are applied and shown to give very similar results.

2.4 Normalization

As mentioned in section 2.1, all calculations in this dissertation are made on dimensionless quantities. If not stated otherwise, normalization units are as follows:

- **Length** L_0 - equilibrium length of the particle: $L_0 = (N - 1)l_0$,
- **Force** G - value of external force due to gravity exerted on the whole particle (after correction for bounciness). Since all beads are identical force exerted on a single bead is equal to G/N ,
- **Velocity** $v = G/(8\pi\eta L_0)$, where η is the dynamic viscosity of the fluid,
- **Time** $\tau = L_0/v$.

From these units all the others may be constructed, such as units of spring constant k (equal to G/L_0) or bending stiffness A (equal to GL_0^2). In the following chapters all variables are dimensionless and given in the units described above, except for sections 5.1-5.3 in chapter 5. In order to avoid excessive notation, the normalized values are denoted by the same symbols as the dimensional ones and the additional clarification is given whenever there might be a risk of confusion.

2.5 Outline of similar models used in the literature

In this section I will try to outline the model used in this dissertation in the background of other works which use bead model. The rationale for devoting particular attention to this issue is the fact, that up to date there is no ‘golden standard’ for a bead model in studies of particle dynamics. Therefore, models used by different authors usually differ to some extent, usually by applying various forms of bending potential, extensional potential or different

hydrodynamic interaction model. I believe it is useful to recapitulate what are the common parts, and what are the differences between model used in this work and models used in related studies. The comparison includes three main features: bending potential, extensional potential and hydrodynamic interactions. When necessary, other features of models are also mentioned such as Brownian motions or short-range repulsive potential (both absent in this work).

As stated before, in this dissertation two main bending potentials are used: Kratky-Porod and harmonic. First, let us review models which apply KP potential. The model used in this work (with KP bending potential) is identical as in studies e. g. by Schlagberger & Netz [6], Gauger & Stark [44] and Marchetti et al. [12]. Almost the same model, but with more accurate hydrodynamic interactions (multipole method instead of RPY) is used e. g. by Słowicka et al. [45, 64, 70], typically with no coupling between elasticity parameters A and k . With less accurate hydrodynamics (point-particle model) it was also applied in study by Saggiorato et al. [10], where additionally random noise was introduced. From the other side, Matthews et al. [138] used a model with RPY approximation of hydrodynamic interactions (the same as in this work) and KP bending potential, but with FENE (finitely extensible nonlinear elastic) extensional potential, instead of harmonic extensional potential used here and in all other works mentioned in this paragraph.

The second type of bending potentials used in this dissertation is harmonic one. A good example of this approach is model used by Gruziel et al. [62] for looped filaments, which is identical as the one applied in this work, except for additional, short-range repulsive potential added by the authors to prevent overlaps of beads, and lack of coupling between k and A elasticity parameters. The same model of bending potential, hydrodynamic interactions and elastic response as in this dissertation was also used in the work by S. Allison [147], where additional Brownian forces were also introduced due to of small size of simulated filaments.

Harmonic bending potential is the most common choice in simulations of trumbbells [123, 125, 155]. In a study by Díaz and García de la Torre [123] it is accompanied by harmonic extensional potential, whereas in works by Ali et al. [155] and Plan & Vincenzi [125] the bonds are inextensible. In publications regarding trumbbell's dynamics cited above, hydrodynamic interactions were not taken into account, however in other works considering dynamics of trumbbells the influence of hydrodynamic interactions is included [121, 142].

Among other, less closely related, models of filaments it is worth to mention studies published by Llopis et al. [13] and Delmotte et al. [9] where filaments with inextensible bonds are considered. A bead model with logarithmic bending potential, harmonic extensional potential and point-particle approximation of hydrodynamic interactions may be found in work by Förtsch et al. [157]. In articles by group of C. Likos [46, 144] yet another type bending potential is used, proportional to $\sum_i (1 - \cos \beta_i)^2$.

2.6 Symmetry of the system

2.6.1 Symmetrized dynamics

The vast majority of systems considered in this work consists of two particles, with a vertical symmetry plane between them. Since we are mainly interested in the dynamics of the systems where the reflection symmetry is conserved, this property is used to simplify equations of motions solved during the simulations. Except for results presented in chapter 8, velocities of beads of the ‘first’ particle are calculated with the explicit assumption that the ‘second’ particle is placed in an exactly symmetric configuration. In consequence the system of equations of motion (eq. (2.12)) may be simplified and the number of differential equations to solve is reduced by half: for a system consisting of two particles, each made of N beads, the number of differential equations is equal to $3N$ instead of $6N$ as it would be for the case without the assumption of the symmetry. For non-symmetric configurations considered in chapter 8 such simplification obviously cannot be applied and configurations of the two particles are independent from each other. Results presented in chapter 8 allow to study the consequences of even a slight symmetry breaking, what is an important question for a real-world pair of particles. It turns out that the main results obtained in this work for the symmetrized dynamics are relevant also for slightly non-symmetric systems.

In the next section it is shown that the strictly symmetric system of two particles is equivalent to a single particle near free surface parallel to the external force. This advocates for embedding of the system symmetry into equations of motion.

2.6.2 Correspondence to a problem of single particle near free surface by method of images

Symmetric systems studied in this dissertation allow to explore correspondence with a system where a fluid-gas interface is present in place of the symmetry plane and one of the particles (the one on the ‘gas’ side of the interface) is replaced with an ‘image’ particle, what is described in this section.

Method of images is used to calculate value of a given scalar or vector field under requested boundary conditions. Best known examples of its application come from electrostatics, e. g. in the problem of calculating electric field around a charge near infinite conducting plane. In this example the bounded system is replaced by unbounded one with additional image charges located in the non-physical region. In the fluid dynamics, often the relevant question is the

velocity field of the fluid (at Stokes regime) near liquid-gas interface, for given forces acting in the system.

In the method of images additional ‘image’ agents (called ‘images’) are introduced at the other side of interface, such that imposed boundary conditions are met without need of considering the boundary explicitly. For the problem forces-velocities relation in viscous fluid, the aim is to find a relevant system of images: forces and force multipoles, that fulfils boundary conditions.

First let us discuss boundary conditions for fluid-fluid interface, next a more specific case of liquid-gas interface is to be presented. Let us denote σ_1 , σ_2 and \mathbf{u}_1 , \mathbf{u}_2 as stress tensors³ and fluid velocities on two sides of the interface, respectively. Normal vector of the interface is denoted as $\hat{\mathbf{n}}$. Boundary conditions required at fluid-fluid interface are as follows [17]:

- fluid velocities on both sides of interface are equal to each other and at the interface parallel to the surface (interface is impermeable): $\mathbf{u}_1 = \mathbf{u}_2$, $\mathbf{u}_1 \cdot \hat{\mathbf{n}} = 0$,
- tangential components of the traction⁴ on both sides of the interface are equal: possible jump of normal component of the traction is balanced by surface tension γ multiplied by curvature of the surface: $\sigma_1 \cdot \hat{\mathbf{n}} + \gamma(1/R_1 + 1/R_2)\hat{\mathbf{n}} = \sigma_2 \cdot \hat{\mathbf{n}}$, where R_1, R_2 are radii of curvature. In case of planar interface: $\sigma_1 \cdot \hat{\mathbf{n}} = \sigma_2 \cdot \hat{\mathbf{n}}$.

In case of fluid-gas interface (i.e. free surface) the viscosity of fluid ‘2’ is equal to 0, and therefore $\hat{\mathbf{t}} \cdot \sigma_2 \cdot \hat{\mathbf{n}} = 0$, where $\hat{\mathbf{t}}$ is an arbitrarily chosen unit vector parallel to the surface. In summary, for flat fluid-gas boundary the conditions are as follows: $\hat{\mathbf{n}} \cdot \mathbf{u}_1 = 0$ and $\hat{\mathbf{t}} \cdot \sigma_1 \cdot \hat{\mathbf{n}} = 0$.

For a planar free surface, image of non-hydrodynamic forces are located symmetrically to the forces themselves, on the opposite side of the boundary. Image of a non-hydrodynamic force is the reflection of the original force with respect to the boundary plane [17, 135]. In this dissertation a planar interface which satisfies equation $x = 0$ is considered. In this case, image of a force $\mathbf{f} = (f_x, f_y, f_z)$ at position $\mathbf{r} = (r_x, r_y, r_z)$ is located at $\mathbf{r}^{im} = (-r_x, r_y, r_z)$ and the image force is given by: $\mathbf{f}^{im} = (-f_x, f_y, f_z)$.

It can be noticed that any system in the bulk which maintains planar symmetry regarding particle positions and acting forces is equivalent to a half of such a system near fluid-gas interface located in the place of the symmetry plane. In this situation, particles on the other

³Stress tensor σ is defined as $\sigma = -p\delta + \eta [\nabla\mathbf{u} + (\nabla\mathbf{u})^T]$, where p is the pressure, \mathbf{u} is the fluid velocity, η is the fluid viscosity and T denotes matrix transposition.

⁴Traction is the force exerted by the fluid on unit surface. Traction vector \mathbf{T} for a unit surface perpendicular to vector $\hat{\mathbf{n}}$ is given by $\mathbf{T} = \sigma \cdot \hat{\mathbf{n}}$ where σ is the stress tensor.

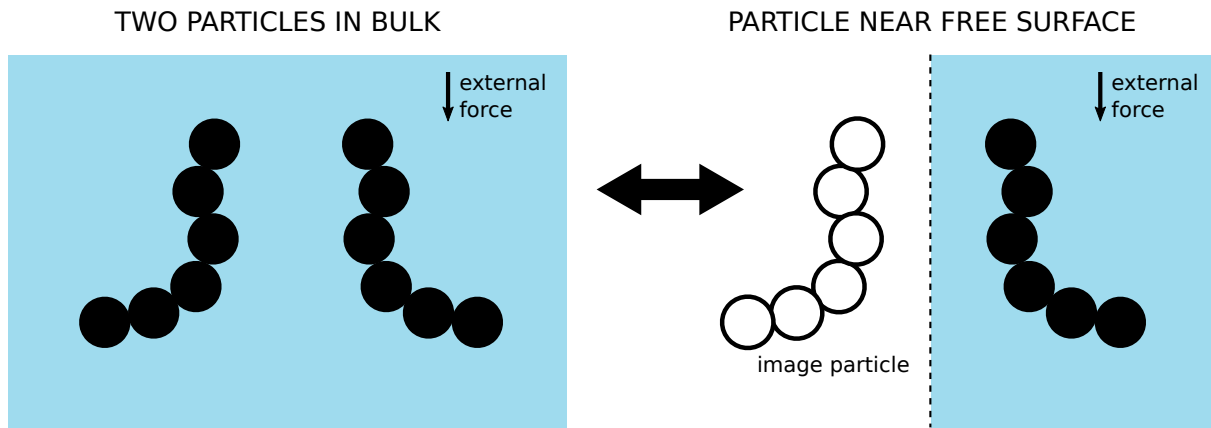


Figure 2.2: In Stokes flow, symmetric pair of particles (on the left) is equivalent to single particle near free surface (on the right), given that external forces are parallel to the symmetry plane.

side of symmetry plane in bulk are equivalent to images of particles in the system with fluid-gas interface, and dynamics of corresponding systems are identical. In the symmetric system of two settling particles this condition is met if the external force (e. g. gravity) is parallel to the symmetry plane: from symmetry of the system it is known that elastic forces acting on the particles maintain mirror symmetry. Therefore dynamics of two particles in symmetric system in bulk, given that external forces are parallel to the symmetry plane, are identical to dynamics of single particle near fluid-gas interface (see Fig. 2.2).

3 Two sedimenting dumbbells

Dumbbell is a particle consisting of two spheres connected with an ideal spring. Ideal spring has no mass, does not interfere neither with the fluid nor with beads' surfaces, and its ends are attached directly to the centres of two beads. Dumbbell shape has only one degree of freedom - spring length - and is arguably the simplest model of an elastic particle. By definition, axial symmetry of a dumbbell particle is conserved during its motion.

Dynamics of elastic dumbbells is a good starting point for studying systems of elastic particles [66, 109] and contributes, as a reference, to understanding the behaviour of elastic particles which can bend. Apart from that, dumbbells can represent a particular class of real particles, which are deformable along longer axis, but conserve axial symmetry.

Results for the dynamics of dumbbells presented in this chapter were calculated with point-particle approximation of hydrodynamic interactions (eq. (2.14)). It was checked that application of Rotne-Prager approximation, used in other chapters of this work, does not have a significant impact on the results obtained for dumbbells, what is described in Appendix A.

Large part of results described in this chapter was published in the article 'Dynamics of elastic dumbbells sedimenting in a viscous fluid: oscillations and hydrodynamic repulsion' written by me, Marta Gruca and Maria Ekiel-Jeżewska [168]. Due to different normalizations, the dimensionless values given in the article, e.g. of time or spring constant k , are not the same as presented in this chapter.

3.1 Problem statement - initial configurations in the vertical plane

Configurations of two dumbbells, considered in this chapter are mainly restricted to a vertical plane, with exception of section 3.5. In absence of forces perpendicular to this plane, the dumbbells' centres move only in two dimensions, although the whole system is three dimensional.

Let us summarize the notation: l is a distance between centres of beads which form the same dumbbell (equivalent to the particle length L), a is the bead's radius and k is the spring

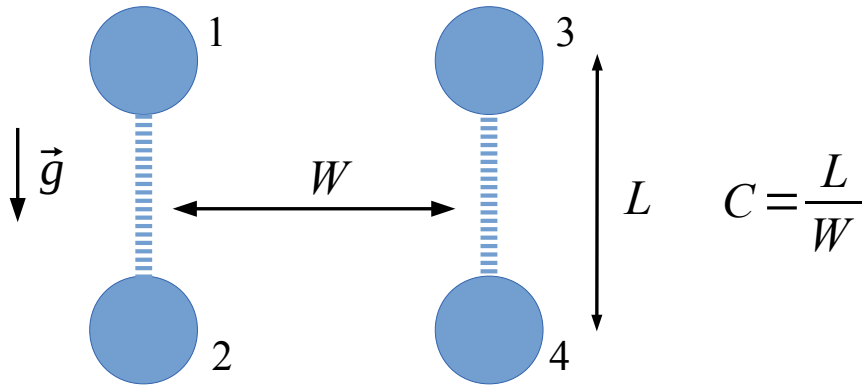


Figure 3.1: Initial configuration of dumbbells, referred as ‘vertical configuration’. Parameters L , W and $C = L/W$ are defined. Figure reprinted from [168].

constant. As stated in section 2.4, lengths are normalized by L_0 (for dumbbells equal to l_0) and k is normalized by G/L_0 .

The main family of dumbbells’ initial configurations considered here can be described as follows: two dumbbells in vertical position, located at the same height (see fig. 3.1). Usually at time $t = 0$ dumbbells have equilibrium length, $L(0) = L_0 = l_0$. The parameter which characterizes a given initial configuration from this family is defined as $C = L/W$, where W denotes distance between dumbbells’ centres. Dynamics of dumbbells which initially are not vertical will be described in section 3.3.4.

The family of ‘vertical’ initial configurations is chosen differently than in closely related works by Hocking [51] and by Jung et al. [23] (in case of rods), where ‘horizontal’ configuration of particles was used, in which all 4 beads were positioned along horizontal line. The reason for this is greater generality of obtained results, what will become clear in the next section 3.2. In short, when starting from horizontal configuration of dumbbell with $k > 0$, particles will always reach the vertical configuration; in contrast there exist vertical configurations, which would not lead to horizontal ones. Therefore the chosen family of vertical configuration allows to explore broader range of dynamics. In the cited publications, this point was not relevant. In work by Hocking four separated beads were considered ($k = 0$) and in such system there exist also horizontal configurations which cannot be reached when starting from vertical ones. In the article devoted to rigid particles, by Jung et al., horizontal initial configuration of rods was chosen for practical reasons: in their experiments symmetric horizontal configurations were much easier to initiate, than a vertical one.

3.2 Limits of very stiff bond and lack of bonds

In this section I will recover and discuss results for limits of rigid particles, $k \rightarrow \infty$, and complete lack of bonds, $k = 0$. The first case - rigid dumbbells - is a model of stiff, elongated

particles, which were shown to perform periodic motions [23, 100, 101]. It is calculated by applying very large values of k . The other limit, $k = 0$, corresponds to the system of four independent point particles, studied by Hocking [51], and is a simple repetition of his results in our setup, yet for broader range of parameters. Also in this limit periodic orbits are observed.

It may be noticed that in both discussed limits the relative dynamics of dumbbells may be described by only two variables: orientation of particles and the distance between dumbbells divided by their length¹. It is not the case for elastic dumbbells, where a third variable enters, e. g. the dumbbells' length scaled by the spring equilibrium length.

3.2.1 Description of periodic motion

Periodic motions, performed by 'dumbbells', for both $k = 0$ and $k \rightarrow \infty$ are schematically shown in fig. 3.2 (top and bottom panels, respectively) and trajectories of beads are shown in fig.3.3. Dynamics can be described as follows: in the initial configurations dumbbells form two side edges of a vertical rectangle, with beads located at its vertexes. At the initial moment hydrodynamic interactions lead to contraction of the upper edge of the rectangle, and elongation of the bottom edge: in consequence, an isosceles trapezoid is formed. Once this has happened, dumbbells centres drift apart from each other. At the same time dumbbells continue to rotate in the inward direction. After a quarter of the period, particles reach horizontal configuration: all beads lay at one horizontal line. In this position, distance between centres of dumbbells is maximal. It is important to notice, that the horizontal configuration, similarly as the initial vertical one, is symmetric with respect to bottom-up reflection. In the horizontal configuration dumbbells do not stop to rotate: the inner two beads tend to settle faster, and again an isosceles trapezoid is formed, this time with the upper edge longer the bottom one. Due to time-reversal symmetry of Stokes equations (described in the introduction, sec. 1.1.1) the further trajectories of beads, after reaching the horizontal configuration at time $T/4$, are reflections of trajectories from the first quarter of the period: if we denote vertical coordinates 'z' of beads in the horizontal configuration (which are all equal) as $z_i(T/4) = z_{T/4}$, than the future z_i and x_i coordinates of beads are given by: $z_i(T/4 + t) = 2z_{T/4} - z_i(T/4 - t)$ and $x_i(T/4 + t) = x_i(T/4 - t)$ (and $y_i(t) = 0$ for all time).

Since the implication between reaching horizontal configuration and periodicity of dumbbells motion may not look straightforward, I will devote this paragraph to discuss this matter in some details. Let us denote M_z as an operator of reflection in a horizontal plane, and

¹For $k \rightarrow \infty$ this statement is obvious. For $k = 0$ in point-particle approximation it is true because relative motion of beads does not depend on the size of the system (e. g. on $L(t)/a$): if the system is scaled by the factor λ , relative velocities conserve directions and their values are scaled by $1/\lambda$.

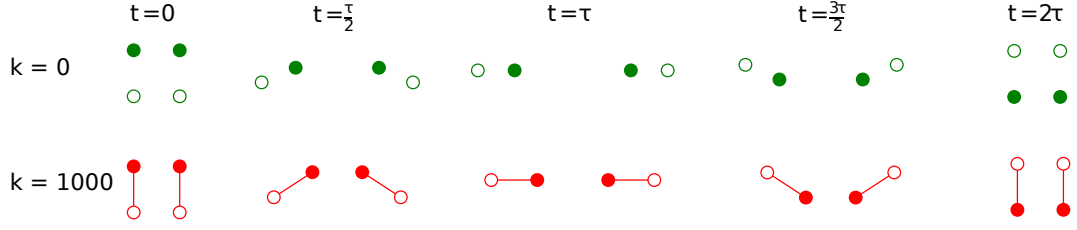


Figure 3.2: Tumbling dynamics of dumbbells. For each value of k the configurations are shown for 5 moments separated by τ time interval. Time interval τ is equal to $1/4$ of the period and is different for $k = 0$ and $k = 1000$.

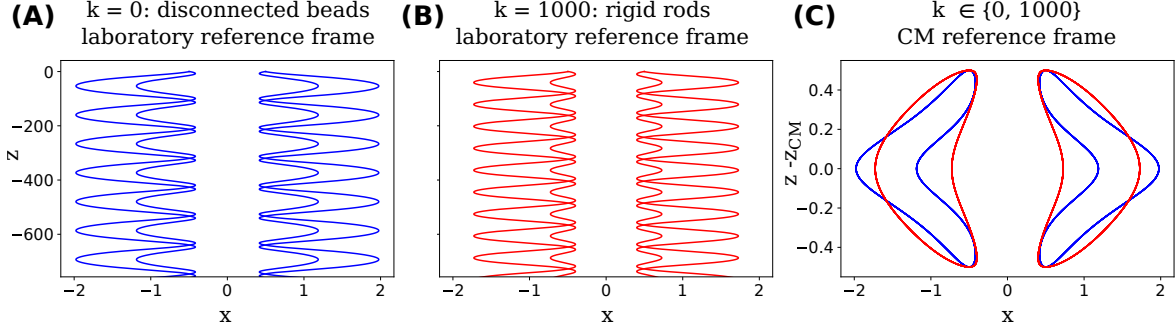


Figure 3.3: (A) Trajectories of beads for $k = 0$, when all four beads are disconnected. Shape parameter $C = L/W = 1$. (B) Trajectories of beads for $k = 1000$, when dumbbells are practically stiff. $C = 1$. (C) Trajectories of beads from panels (A) and (B) shown in centre of mass reference frame: $k = 0$ (blue) and $k = 1000$ (red).

τ as a time when the configuration is symmetric with respect to this reflection: $\mathbf{r}(\tau) = M_z \mathbf{r}(\tau)$ (e. g. ‘horizontal’ configuration of dumbbells). In the described problem both vertical and horizontal configurations are symmetric with respect to reflection in a given horizontal plane. It is worth to recall here that \mathbf{r} is the vector containing positions of centres of all beads and \mathbf{G} denotes vector of gravitational forces acting on all beads. Expression $\mathbf{v}(\mathbf{r})$ will be used to denote velocities of all beads centres. In order to proof the symmetry of beads’ trajectories, defined as $\forall_t \mathbf{r}(\tau + t) = M_z \mathbf{r}(\tau - t)$, it is enough to meet the following conditions:

$$\exists_{\tau} \mathbf{r}(\tau) = M_z \mathbf{r}(\tau), \quad (3.1)$$

$$\forall_{\mathbf{r}} \mathbf{v}(\mathbf{r}) = -M_z \mathbf{v}(M_z \mathbf{r}), \quad (3.2)$$

where (3.1) assumes existence of a symmetric configuration at time τ , while (3.2) states that the given function of velocity $\mathbf{v}(\mathbf{r})$, which depends only on beads positions \mathbf{r} , fulfils the required condition of the reflection symmetry. Importantly, the fact that velocity depends only on position of beads is true due to lack of inertia in the system, specific for the Stokes regime.

I will now show that the second condition is met for rigid particles or group of disconnected beads for a vertical external force, where vector of velocities $\mathbf{v}(\mathbf{r})$ can be expressed in terms of

\mathbf{G} and the mobility matrix $\boldsymbol{\mu}(\mathbf{r})$ as ² $\mathbf{v}(\mathbf{r}) = \boldsymbol{\mu}(\mathbf{r}) \cdot \mathbf{G}$. We can write:

$$-M_z \mathbf{v}(M_z \mathbf{r}) = M_z \boldsymbol{\mu}(M_z \mathbf{r}) \cdot (-\mathbf{G}) \quad (3.3)$$

$$= M_z \boldsymbol{\mu}(M_z \mathbf{r}) \cdot M_z \mathbf{G} \quad (3.4)$$

$$= M_z M_z \boldsymbol{\mu}(\mathbf{r}) \cdot \mathbf{G} \quad (3.5)$$

$$= \boldsymbol{\mu}(\mathbf{r}) \cdot \mathbf{G} = \mathbf{v}(\mathbf{r}) \square \quad (3.6)$$

In the first step (eq. (3.3) \rightarrow (3.4)) relation $-\mathbf{G} = M_z \mathbf{G}$ is applied. In the second transition (3.4) \rightarrow (3.5) we use the fact that $\boldsymbol{\mu}(M_z \mathbf{r}) \cdot M_z \mathbf{G} = M_z \boldsymbol{\mu}(\mathbf{r}) \cdot \mathbf{G}$ for all \mathbf{r} and \mathbf{G} , what is a fundamental property of the dynamics. Transition (3.5) \rightarrow (3.6) is a simplification and final return to the explicit notation velocity $\mathbf{v}(\mathbf{r})$ in eq. (3.6).

If the particles start from vertical configuration and reach the horizontal one, it means that trajectory has at least two horizontal symmetry planes. It is easy to show, that in such situation motion of the beads consists of sedimentation in vertical direction coupled with periodic motion in centre-of-mass reference frame. Given that τ_1 and τ_2 are two consecutive times when the configuration is symmetric, than the period of the relative motion is equal to $4(\tau_2 - \tau_1)$. Twice as frequent, with period $2(\tau_2 - \tau_1)$, configuration of beads in centre-of-mass reference frame is repeated but with permutation of beads: e. g. if at time t bead with label 1 is higher than 2, at $t + 2(\tau_2 - \tau_1)$ time the situation is opposite.

3.2.2 Dependence on the initial configuration

The presented family of initial vertical configurations, with $L(0) = 1$, has only one parameter which can be varied, namely the ‘length to distance’ ratio C . Dynamics of disconnected beads ($k = 0$), which has been already studied [51, 54, 55], is shown here as a useful reference and in some aspects a complementary study (in previous studies other class of initial configurations was considered), while the limit of rigid dumbbells $k \rightarrow \infty$ includes new results.

Periodic dynamics is observed only if the dumbbells are not too distant in the vertical configuration, what means that C is not smaller than a certain threshold, denoted as C_0 . Above

²For $k = 0$ this statement is obvious, since external force \mathbf{G} is the only force acting in the system. In rigid particles, apart from \mathbf{G} , also elastic forces of constraints $\mathbf{F}_{constraint}$ act on the beads. In Stokes flow such constraint forces are linear to external forces, so there exists matrix $\mathbf{A}(\mathbf{r})$ such that $\mathbf{F}_{constraint} = \mathbf{A} \cdot \mathbf{G}$ and therefore total force \mathbf{F} is equal to $\mathbf{F} = \mathbf{G} + \mathbf{F}_{constraint} = (\mathbb{1} + \mathbf{A}) \cdot \mathbf{G}$. In consequence also for rigid particles there exist mobility matrix $\boldsymbol{\mu}$ which links dynamics of beads $\dot{\mathbf{r}}$ with external forces: $\dot{\mathbf{r}} = \boldsymbol{\mu}(\mathbf{r}) \cdot \mathbf{G}$, although this matrix it is not given by expressions written in sec. 2.3, valid for vector of explicit non-hydrodynamic forces acting on each bead. If $\boldsymbol{\mu}'(\mathbf{r})$ denotes mobility matrix for explicit non-hydrodynamic forces acting on each bead, mobility matrix for rigid particles $\boldsymbol{\mu}(\mathbf{r})$ can be expressed as $\boldsymbol{\mu}(\mathbf{r}) = \boldsymbol{\mu}'(\mathbf{r}) \cdot (\mathbb{1} + \mathbf{A}(\mathbf{r}))$.

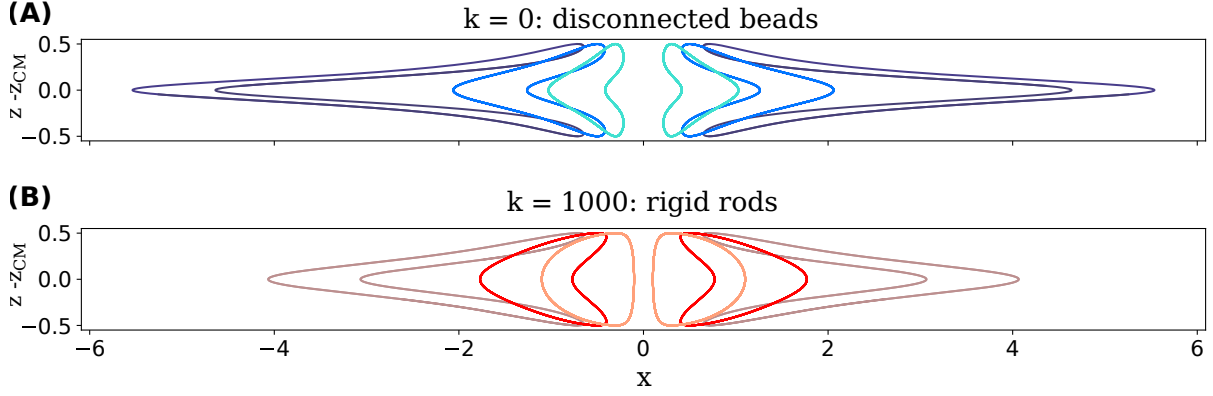


Figure 3.4: Trajectories of beads in the centre-of-mass reference frame for different values of $C \in \{0.7, 1.0, 1.65\}$ for disconnected beads (A) and stiff dumbbells (B). Wider trajectories correspond to lower value of C .

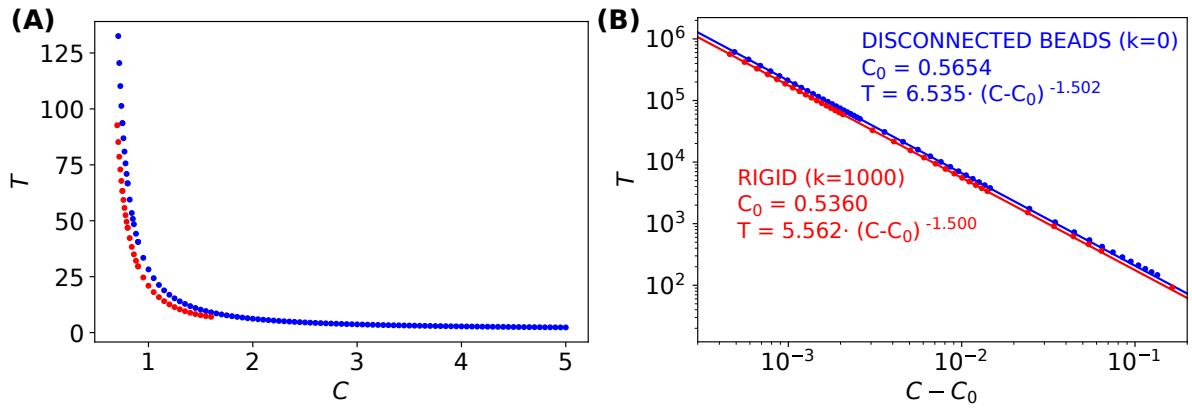


Figure 3.5: Period T for the range of shape parameter C for stiff dumbbells (red) and independent beads (blue). (A) Results for wide range of C . Values of the period are not shown for large C and stiff dumbbells because particles overlap under applied point-particle approximation of hydrodynamic interactions. (B) Period T in logarithmic scale with fitted dependence on C and fitted C_0 . For values of C close to C_0 in both cases period scales as approximately $\sim (C - C_0)^{3/2}$, as proven in [54] for $k = 0$ in a wide class of similar systems.

C_0 , parameter C affects shape (fig. 3.4) and period (fig. 3.5) of the trajectory. For both disconnected beads and rigid dumbbells the period is shorter for smaller initial distance between dumbbells, what is equivalent to larger C .

When initial parameter C approaches limiting value for periodic motions, C_0 , length of the period grows to infinity. Ekiel-Jezewska [54] showed, that for $k = 0$ there is a power law relation between period length T and $C - C_0$, with exponent equal to $3/2$. Results shown in figure 3.5B suggest that the same kind of relation applies to rigid dumbbells. In comparison to disconnected beads, for rigid dumbbells the value of C_0 is slightly smaller and for a given value of $C - C_0$ the period is shorter. Values of parameters fitted for power law expression are shown in fig. 3.5B.

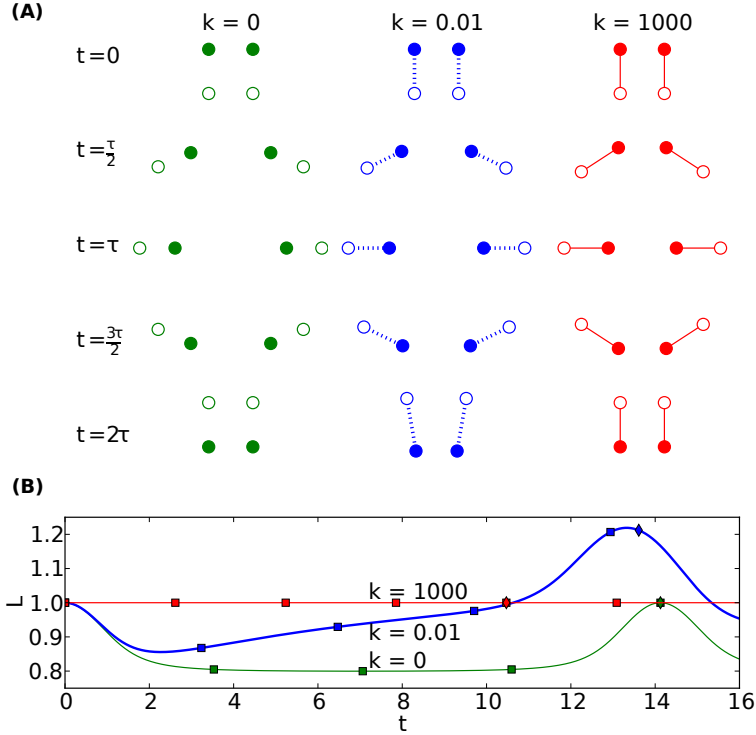


Figure 3.6: Dynamics of 4 disconnected beads (limit $k = 0$, green), elastic dumbbells ($k = 0.01$, blue) and almost rigid dumbbells ($k = 1000$, red). (A) Snapshots of the system taken at equal time intervals $\tau/4$ for each k : at time τ the particles reach horizontal configuration. (B) Dumbbells' length in time. Squares represent moments when snapshots were taken. Diamonds denote moments when particles reach vertical configuration. For independent beads and rigid particles it happens at half of the period and squares overlap the diamonds. The dumbbells with $k = 1000$ may be considered as practically rigid: the deviations of their lengths are as small as 3×10^{-5} only. Figure reprinted from [168] with minor changes.

3.3 Dynamics of elastic dumbbells in vertical plane

3.3.1 General picture

Dynamics of elastic particles may be significantly different from dynamics of rigid ones. The argumentation on periodicity of the motion, elaborated in the previous section, does not hold if particles are deformable and elastic because condition (3.2) is not met for all configurations: $\exists_r \mathbf{v}(\mathbf{r}) \neq -M_z \mathbf{v}(M_z \mathbf{r})$.

The dynamics of two elastic dumbbells is shown in figure 3.6A, upper central panel. Tumbling motion is maintained, however it is not periodic any more. As it was discussed in the previous paragraph, there is no mirror symmetry of the beads dynamics. Let τ denote transition time from vertical to horizontal configuration: it appears that in case of elastic dumbbells the subsequent transition time, from horizontal configuration to the next vertical one, is longer than

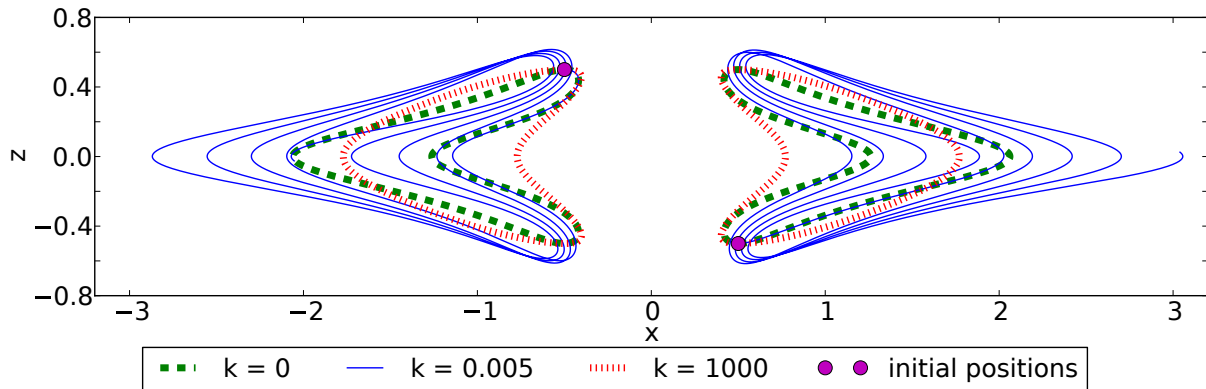


Figure 3.7: Trajectories of beads for dumbbells with rigid bonds ($k = 1000$, red), elastic bonds ($k = 0.005$, blue) and independent beads ($k = 0$, green). Since the motion of left and right dumbbells is symmetric, the trajectory of the bead which is initially in the top is drawn on the left, and trajectory of the bead which is initially on the bottom is drawn on the right side of the figure, in order to be more illustrative. Trajectories of beads from elastic dumbbells are not closed and become wider with the time. Figure reprinted from [168] with minor changes.

τ . Lack of time symmetry of relative motion is also visible in the bottom panel of fig. 3.6, where lengths of the dumbbells is shown.

It is convenient to analyse dynamics of particles in the centre of mass reference frame, in which trajectories are closed if the motion is periodic. Trajectories of dumbbells' beads are shown in fig. 3.7 for rigid bonds ($k = 1000$), elastic bonds ($k = 0.005$) and lack of bonds ($k = 0$). In case of elastic particles, the non-periodicity of the dynamics manifests in open trajectory. We can also observe, that the width of trajectory (along x direction) systematically increases with every tumbling. Before describing these phenomena, I will focus on the influence of initial configuration on the system's dynamics.

3.3.2 Convergence to the universal trajectory

A single dumbbell in a viscous fluid, when stretched or compressed, returns exponentially to its equilibrium length. In the investigated system of two dumbbells the situation is slightly more complicated: the system is attracted to a universal non-periodic trajectory. A good way to illustrate this, is to look at subsequent vertical configuration of dumbbells, occurring two times for a period. When dumbbells are vertical, configuration may be described by two variables: dumbbells length L and distance between dumbbells W . Since we are now tracking dumbbells in centre of mass reference frame, we are not interested in absolute position of the system in z (vertical) axis. For convenience, sometimes the shape parameter $C = L/W$ will be also used.

The dynamics of elastic dumbbells has two main phases. Initially the system converges to a certain universal (the same for different initial conditions) phase space trajectory, what is called

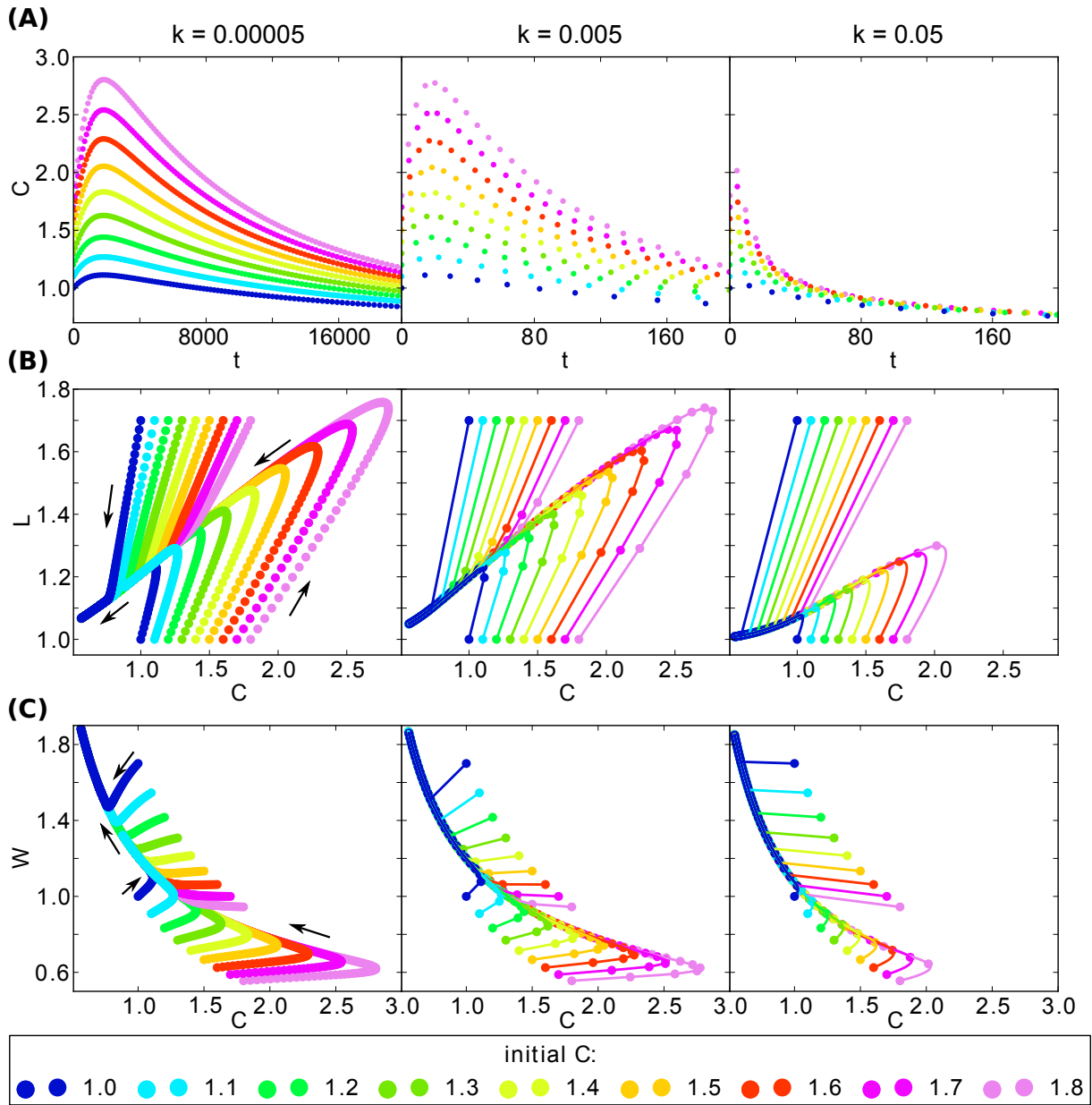


Figure 3.8: Relaxation of the system and the universal dynamics. Dots represent parameters in subsequent vertical configurations of the dumbbells. (A) Shape parameter C in time. Relaxation phase is visible as a ‘hill’ in the initial phase of the motion. Note the different scale of time for $k = 5 \cdot 10^{-5}$. (B) Dumbbell length L versus shape parameter C . Convergence of the dynamics for different initial configurations (given by C and L) is visible. At the universal trajectory, the values of C and L decrease with time. Lines are drawn to guide the eye. (C) Distance between dumbbells W versus shape parameter C . Figures show the same features of the dynamics as (B) from a different perspective. At the universal trajectory, the distance between dumbbells W increases with time. Figure reprinted from [168] with minor changes.

relaxation. In the second phase the system follows the universal trajectory. Relaxation phase can be easily distinguished in figure 3.8. In the first row (fig. 3.8A) shape parameter C in consecutive vertical configurations is plotted against time. At the universal trajectory value of C decreases with time (dimensionless, normalization is given in sec. 2.4). Initial ‘hill’ visible in the figure corresponds to relaxation phase. Relaxation time scale may be estimated from the shape of the plot and it can be noticed that it scales as $1/k$, as it is visible that with such scaling the shapes of the curves are very similar for different k between $5 \cdot 10^{-5}$ and 0.005; results for these two values are presented in fig. 3.8A. Relaxation phase is not visible for $k = 0.05$ because it is shorter than a single tumble, and therefore there are no vertical configurations before convergence to the universal trajectory.

The convergence to the universal trajectory during relaxation is clearly visible in figure 3.8B,C. Results show that starting from different values of shape parameter C and different dumbbells length L the dynamics converges to the same trajectory in phase space. The convergence may take dozens of tumblings in case of very elastic dumbbells ($k = 5 \cdot 10^{-5}$), only a few for more stiff ones ($k = 0.005$) and none for even more stiff ($k = 0.05$).

Existence of an universal solution is very important for the dynamics. One of advantages is that it allows to investigate general properties of the system without extensive probing different initial configurations.

3.3.3 Hydrodynamic repulsion

After relaxation, dumbbells repel each other. In figure 3.9 successive (but not consecutive) vertical configurations are shown: distance between dumbbells systematically increases. The strongest effect is observed for $0.005 \leq k \leq 0.05$. It can be noticed that as the time passes not only the distance becomes larger, but also the ‘length to distance’ ratio C decreases. As stated before, for limit cases $k = 0$ and $k \rightarrow \infty$ the width of trajectory (maximal horizontal distance between dumbbells) increases for decreasing C , and tends to infinity for $C \rightarrow C_0$. Similar dependence may be observed for elastic particles: the distance between dumbbells in horizontal configuration (local maximum of the distance) rises much faster than the distance in vertical configuration (local minimum). For example, in the system illustrated in fig. 3.9 the distance in vertical configuration roughly triples, while that in horizontal configuration raises more than 100 times, from 1.27 at the beginning to almost 170 at $t \approx 5800$. Since in the system of elastic dumbbells the value of C systematically decreases, it is not excluded that after certain time system reaches $C < C_0$ and does not return to vertical configuration (or even horizontal one), but rather particles drift away to infinity. However, the studies necessary to confirm this hypothesis have not been conducted for this dissertation.

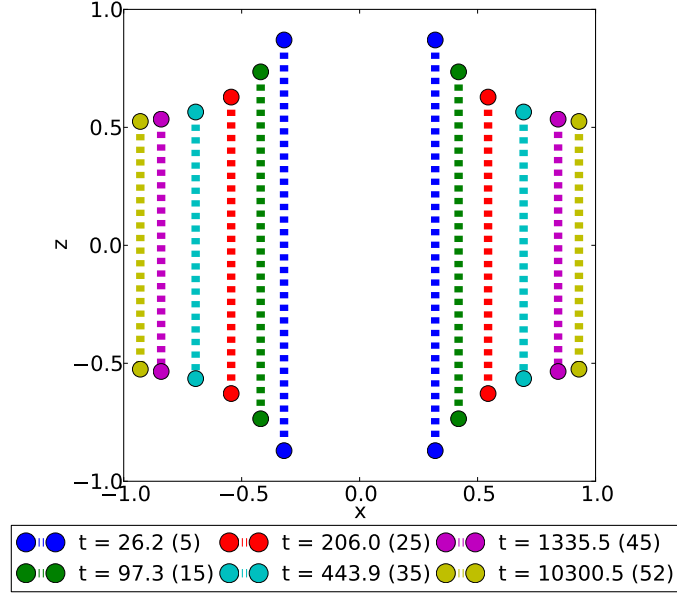


Figure 3.9: Snapshots of elastic dumbbells in successive (but not consecutive) vertical configurations. For each snapshot time and number of the performed flips is indicated in the legend. Hydrodynamic repulsion is clearly visible, as the distance between dumbbells systematically increases. Parameters of the simulation are: $k = 0.005$, $C = 1.8$, $L(0) = 1$. For the sake of clarity, the bead size is reduced three times. Figure reprinted from [168] with minor changes.

3.3.4 Non-vertical initial configurations in a vertical plane

Until now we have considered the vertical initial configuration. In this section the dynamics of a symmetric pair of dumbbells is studied for non-vertical configurations which are still restricted to the vertical plane. It was already discussed that during the motion the dumbbells rotate and either tumble reaching consecutive horizontal and vertical configurations or drift away to infinity without tumbling. It was also shown that the particles starting from the vertical initial configurations, after the relaxation phase, follow a universal trajectory in the phase space, in which particles repel each other. In consequence, also the dumbbells which start from non-vertical initial configuration will either drift away, staying non-vertical, or after some time they reach vertical configuration and converge to the universal trajectory, in agreement with results presented in previous sections.

The dynamics of dumbbells for selected initial configurations is shown in figure 3.10, which illustrates that the non-vertical configurations lead to the same type of dynamics as vertical ones, described before. In fig. 3.10A the chosen initial configurations are presented: in each case dumbbells have the same length $L(0) = 1$, spring constant $k = 0.005$ and the horizontal distance between centres of particles, $W(0) = 1.4$. For the vertical configuration (blue), the value of parameter C is approximately equal to 0.71. Trajectories of centres of dumbbells are plotted in fig. 3.10B. In all cases the width of trajectory increases with time. It can be observed,

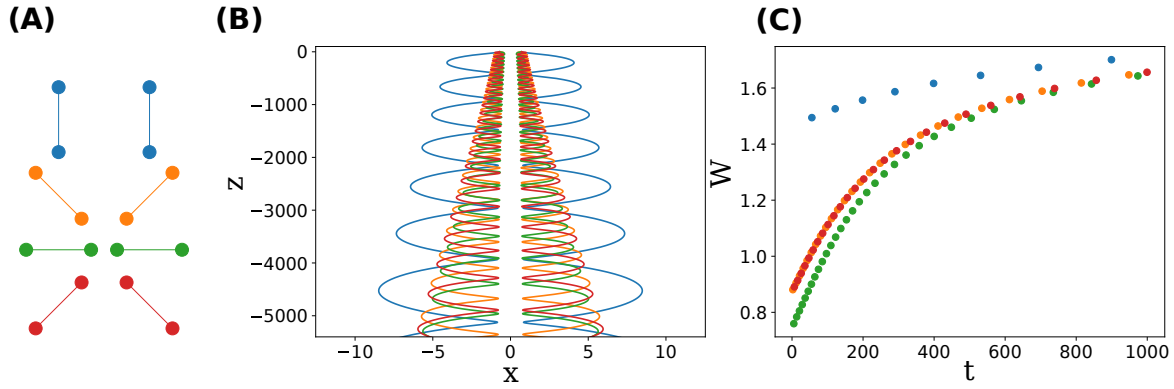


Figure 3.10: Dynamics of elastic dumbbells for initial configurations shown in panel (A). (B) trajectories of centres of the dumbbells; (C) hydrodynamic repulsion illustrated by the distance between particles in consecutive vertical configurations.

that for the second and the fourth initial configurations the trajectories are almost identical. As expected, the first trajectory (blue, for vertical initial configuration) is the widest, because it corresponds to the smallest C . In figure 3.10C the distance between particles in consecutive vertical configurations is shown. The effect of hydrodynamic repulsion is clearly visible for all studied initial configurations. In conclusion, this example illustrates that for different symmetric configurations, restricted to the vertical plane, the effect of hydrodynamic repulsion between dumbbells is observed. Such behaviour is a natural consequence of the convergence to the universal trajectory, described in section 3.3.2.

3.4 Analytic considerations

3.4.1 Elastic forces in comparison to gravity

The hydrodynamic repulsion phenomena, described in previous sections, are caused by elastic forces acting between dumbbells' beads. For this reason it is interesting to investigate how large the elastic forces are in comparison to gravity. Let us begin with an analytical estimation for the limit $a \ll l_0$.

Velocity of the first bead is given by:

$$\dot{\mathbf{r}}_1 = \frac{4}{3a}(\mathbf{S}_1 + \mathbf{f}^g) + \mathbf{T}(\mathbf{r}_{12}) \cdot (\mathbf{S}_2 + \mathbf{f}^g) + \mathbf{T}(\mathbf{r}_{13}) \cdot (\mathbf{S}_3 + \mathbf{f}^g) + \mathbf{T}(\mathbf{r}_{14}) \cdot (\mathbf{S}_4 + \mathbf{f}^g) \quad (3.7)$$

where \mathbf{S}_i denotes elastic force acting on i -th bead and $\mathbf{f}^g = (0, 0, -1/2)$ denotes the gravity force acting on a single bead. The equation is expressed in dimensionless units, as described in section 2.4. Velocity of the second bead may be easily derived from eq. (3.7) by replacements

1 \rightarrow 2 and 2 \rightarrow 1. Elastic force acting on i -th bead is given by $\mathbf{S}_i = S\hat{\mathbf{r}}_{ij}$, where j is the index of another bead from the same dumbbell, and $S = k(l - l_0)$ is the signed value of elastic force. Absolute value of elastic force $|S|$ is the largest when deviation of dumbbell length is maximal, and therefore at that moment $dl/dt = 0$. In terms of the whole system it means that at this instance the length of dumbbells is not changing, but dumbbells may have rotational and translational components of motion. From equation (3.7) we obtain:

$$\begin{aligned} \frac{d|\mathbf{r}_{12}|}{dt} &= \hat{\mathbf{r}}_{12} \cdot (\dot{\mathbf{r}}_2 - \dot{\mathbf{r}}_1) = \\ &= \hat{\mathbf{r}}_{12} \cdot \left\{ \frac{-8S}{3} \frac{S}{a} \hat{\mathbf{r}}_{12} - f^g [\mathbf{T}(\mathbf{r}_{23}) + \mathbf{T}(\mathbf{r}_{24}) - \mathbf{T}(\mathbf{r}_{13}) - \mathbf{T}(\mathbf{r}_{14})] \cdot \hat{\mathbf{z}} \right. \\ &\quad \left. + S [2\mathbf{T}(\mathbf{r}_{12}) \cdot \hat{\mathbf{r}}_{12} + \mathbf{T}(\mathbf{r}_{23}) \cdot \hat{\mathbf{r}}_{34} - \mathbf{T}(\mathbf{r}_{24}) \cdot \hat{\mathbf{r}}_{34} - \mathbf{T}(\mathbf{r}_{13}) \cdot \hat{\mathbf{r}}_{34} + \mathbf{T}(\mathbf{r}_{14}) \cdot \hat{\mathbf{r}}_{34}] \right\} \end{aligned} \quad (3.8)$$

On the right-hand site of eq. (3.8) the first term in the curly brackets is of the order of S/a , the second f^g/r_{ij} and the third S/r_{ij} (because $\|\mathbf{T}(\mathbf{r}_{ij})\|$ is of the order of $r_{ij}^{-1} = |\mathbf{r}_{ij}|^{-1}$), where r_{ij} is distance between i -th and j -th beads. Since the assumption states that $a \ll r_{ij}$, the third term is much smaller than the first one and can be neglected. In consequence, for the maximal deformation, when $dl/dt = 0$, we obtain $S/a \sim f^g/r_{ij}$, and finally $S/f^g \sim a/r_{ij} \ll 1$. This result shows that in the limit of small beads the elastic forces are always much smaller than gravity; nevertheless, they have huge impact on the dynamics, causing hydrodynamic repulsion between particles.

Figure 3.11 shows actual elastic forces acting on the beads in case of $a = l_0/10$, scaled by the gravitational force. It shows that the magnitude of elastic force stays below 1.5% of gravitational force. We may also notice that the values of the elastic forces are the largest for practically rigid particles. In case of elastic dumbbells with $k = 0.05$ and $k = 0.005$, although in both cases we observe strong repulsion, the values of elastic forces are very different from each other: close to the rigid case for $k = 0.05$ and an order of magnitude smaller for $k = 0.005$.

In the derivation of analytic approximation for limit $a \ll r_{ij}$ we dropped the third term in eq. (3.8), which describes hydrodynamic interactions originated from elastic forces. After such simplification only the first term, of the order of $S/a = k(l - l_0)/a$, and the second term, of the order of f^g/r_{ij} , remain. As a result, the dynamics in limit $a \ll r_{ij}$ depends exclusively on the ratio k/a , rather than on k and a parameters independently. This prediction is in a good agreement with numerical results. In figure 3.12 relevant trajectories of beads are shown: we can observe that dynamics is almost indistinguishable if k/a ratio is kept constant. The bead radius presented in this comparison is equal to $l_0/10$, what shows that the relevance of approximation described above is not restricted to very small beads.

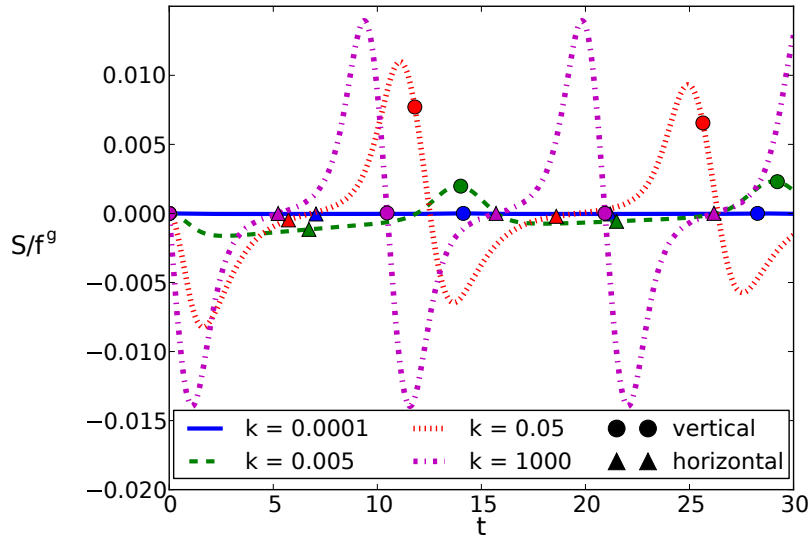


Figure 3.11: Elastic forces in the dynamics of two dumbbells. Colours indicate results for different values of spring constant k . Circles and triangles indicate time of vertical and horizontal configurations, respectively. The figure shows that elastic forces are the largest for the most stiff dumbbells. It may be also observed that for different k the maximal magnitude of force occurs in different moments of the period: for $k = 0.005$ very close to vertical configuration, for $k = 0.05$ slightly before it, and for almost rigid dumbbells somewhere in the middle between horizontal and vertical configuration. In the latter case when the system is in the vertical configuration force is very close to 0. Figure reprinted from [168] with minor changes.

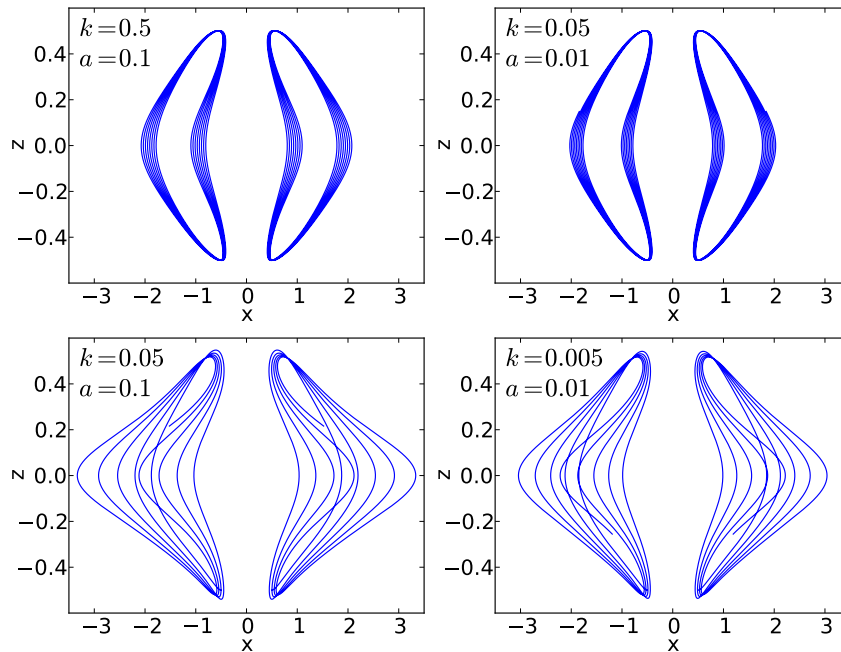


Figure 3.12: Trajectories of beads for different values of radius a and spring constant k . In the top row $k/a = 5$, in the bottom $k/a = 0.5$. Results for different bead radii, but with the same ratio k/a are practically undistinguishable. Figure reprinted from [168].

3.4.2 Compression and stretching phases in tumbling motion

During the tumbling motion of particles, hydrodynamic interactions cause compression or stretching of particles, with neutral instances in between. Dumbbells are perfect model to study impact of such stresses, since resulting change of dumbbell lengths is the only allowed deformation.

Here, only contribution of gravity is discussed. The reason behind this is that the direct contribution of elastic forces depends on the dumbbell length, what introduce another degree of freedom, and more importantly its effect is easy to predict: elastic forces cause compression when dumbbell is stretched and stretching when dumbbell is compressed. The secondary contribution from elastic forces, by hydrodynamic interactions, is much smaller than both direct effect of these forces and than analogous contribution from gravity, because elastic forces are much weaker than gravity (sec. 3.4.1).

It is worth to stress that elastic forces are very important for the dynamics of dumbbells and their significance should not be underestimated. Indeed, they are the source of non-periodicity of the motion and of the hydrodynamic repulsion phenomena. As discussed in the previous section, contributions to the relative velocities of beads by the elastic forces (by direct action on the beads) are of the same order as by the gravity (by hydrodynamic interactions between beads). The discussion presented here, considering compressive/stretching contribution to dumbbells' dynamics originating from the gravity, aims to supplement the description of the system and help in better understanding of its dynamics, but does not intend to suggest that the influence of elastic forces is negligible.

Let us consider symmetric pair of dumbbells, each consisting of two point particles. By convention presented in fig. 3.1 the left dumbbell consists of beads number 1 and 2 while the right one of beads 3 and 4. Configuration of dumbbells in an arbitrary, yet symmetric configuration is given by the vector $\mathbf{r} = (x_1, y_1, z_1, x_2, \dots, z_4) = (-x_3, 0, z_3, -x_4, 0, z_4, x_3, 0, z_3, x_4, 0, z_4)$. For convenience, let us denote $\Delta x = x_4 - x_3$, $\Delta z = z_4 - z_3$, $x_{cm} = (x_3 + x_4)/2$.

In the new variables, the squared dumbbell length is equal to: $l^2 = (\Delta x)^2 + (\Delta z)^2$. We can write:

$$\mathbf{v}_i^g = \sum_{j \neq i} \mathbf{T}(\mathbf{r}_j - \mathbf{r}_i) \cdot \mathbf{f}_j^g, \quad (3.9)$$

$$\frac{dl}{dt} = \frac{1}{l} \left[\Delta x \frac{d\Delta x}{dt} + \Delta z \frac{d\Delta z}{dt} \right] = \frac{1}{l} [\Delta x (\mathbf{v}_4^g - \mathbf{v}_3^g) \cdot \hat{\mathbf{x}} + \Delta z (\mathbf{v}_4^g - \mathbf{v}_3^g) \cdot \hat{\mathbf{z}}] \quad (3.10)$$

where \mathbf{v}_i^g is the contribution to i -th particle velocity from gravity (without self-term $\boldsymbol{\mu}^{ii} \cdot \mathbf{f}_i^g$, identical for all beads and therefore omitted here) and \mathbf{T} is the Oseen tensor (2.14). After some transformations we end up with the equation:

$$\frac{dl}{dt} = \frac{f^g}{2l} \frac{\Delta x \Delta z}{x_{cm}^2} \left\{ \left[1 - \left(\frac{\Delta x}{2x_{cm}} \right)^2 \right]^{-1} - \left[1 + \left(\frac{\Delta z}{2x_{cm}} \right)^2 \right]^{-\frac{3}{2}} \right\} \quad (3.11)$$

Let us analyse the sign of dl/dt . By definition the dumbbell's length l and magnitude of gravitational force acting on each bead f^g are both positive. We may also observe that the first term in the braces is always greater than unity and the second term is always smaller than unity. In consequence the overall sign of expression in braces is always positive what means that dumbbells are compressed when Δx and Δz have different signs, that is when dumbbells move away from each other, and stretched in the opposite case. In vertical and horizontal configurations hydrodynamic interactions originated from gravity do not cause compression nor stretching, but dumbbells' rotation only. If elastic dumbbells are considered, the influence of gravity described in this section acts alongside with influence of elastic forces, which depend on the instantaneous length of the spring l .

3.5 Dynamics of dumbbells out of vertical plane

In this chapter the dynamics of two dumbbells in symmetric configurations, non restricted to the vertical plane, will be described. As before, the system is symmetric with respect to reflection in the $x = 0$ plane. Initially the dumbbells are in a parallel configuration, tilted by angle $\theta(0)$ with respect to $y = 0$ plane and both have the equilibrium length. The initial coordinates of beads $\mathbf{r}_1(0), \dots, \mathbf{r}_4(0)$ are given by:

$$\mathbf{r}_1(0) = \left[-x_{CM}(0), \frac{l_0}{2} \sin(\theta(0)), \frac{l_0}{2} \cos(\theta(0)) \right], \quad (3.12)$$

$$\mathbf{r}_2(0) = \left[-x_{CM}(0), -\frac{l_0}{2} \sin(\theta(0)), -\frac{l_0}{2} \cos(\theta(0)) \right], \quad (3.13)$$

$$\mathbf{r}_3(0) = \left[x_{CM}(0), \frac{l_0}{2} \sin(\theta(0)), \frac{l_0}{2} \cos(\theta(0)) \right], \quad (3.14)$$

$$\mathbf{r}_4(0) = \left[x_{CM}(0), -\frac{l_0}{2} \sin(\theta(0)), -\frac{l_0}{2} \cos(\theta(0)) \right]. \quad (3.15)$$

For the sake of brevity, systems restricted to the vertical plane will be called 'in-plane', and otherwise 'out-of-plane' systems. First, let us consider limits of stiff bonds and lack of bonds.

3.5.1 Limits $k = 0$ and $k \rightarrow \infty$

For a pair of dumbbells not restricted to the vertical plane the periodic motions also exist. In figure 3.13 the dynamics is shown for an exemplary initial configuration. The projection of

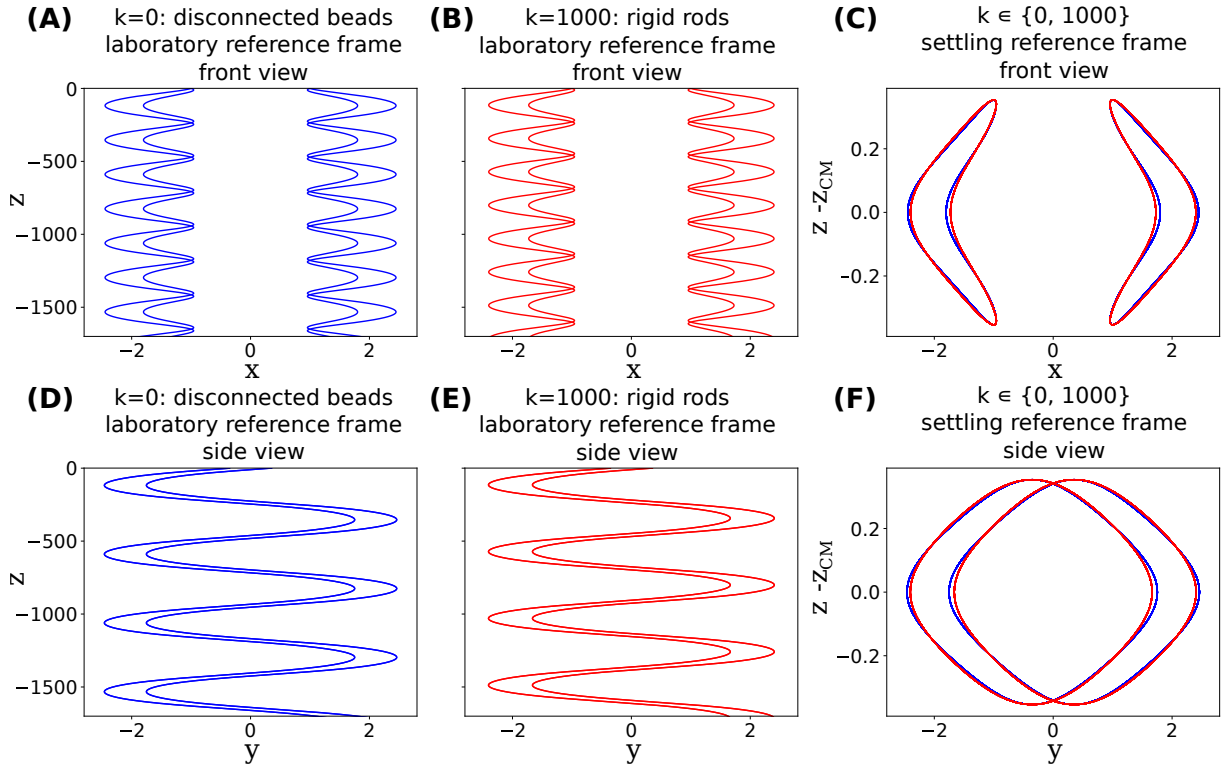


Figure 3.13: Trajectories of beads in the limit of lack of bonds ($k = 0$, blue lines) and stiff dumbbells ($k = 1000$, red lines). Front (A-C) and side (D-F) views are presented. Figures (C) and (F) are shown in the reference frame settling with the centre of mass of the particles. In all cases $x_{CM}(0) = 1$ and $\theta(0) = \pi/4$.

trajectory on the vertical xz plane (fig. 3.13A-C) is very similar to the quasi two dimensional in-plane dynamics described before. Additionally, the dumbbells move along y axis, what is visible in the figure 3.13D-F. In the horizontal configurations, beads are located at vertexes of an isosceles trapezoid. Periodic dynamics described in this section has not been reported before in the literature. The case of $k = 0$ generalizes Hocking's results for four point particles in a vertical plane [51], while the limit $k \rightarrow \infty$ corresponds to rigid elongated particles and generalizes findings by Kim [100]. Dynamics of rigid particles with shapes other than dumbbells will be described broadly in chapter 4.

Similarly as in the quasi-2D dynamics, the shape of trajectory depends on the initial configuration of dumbbells. For the dynamics out of plane, with initial positions of beads given by equations (3.13)-(3.15), each configuration is characterized by two parameters: the distance x_{CM} of the particles from the symmetry plane $x = 0$ and the tilt angle $\theta(0)$. In figure 3.14 the shape of trajectory is shown for different values of x_{CM} and fixed value of $\theta(0) = \pi/4$. Results for different tilt angles are similar. It can be observed that both for disconnected point particles ($k = 0$, fig. 3.14A,B) and stiff particles ($k = 1000$, fig. 3.14C,D) larger initial distances between particles lead to wider trajectories. Similarly as for the dynamics of dumbbells in plane, if the initial distance is too large, the particles drift away from each other and do not

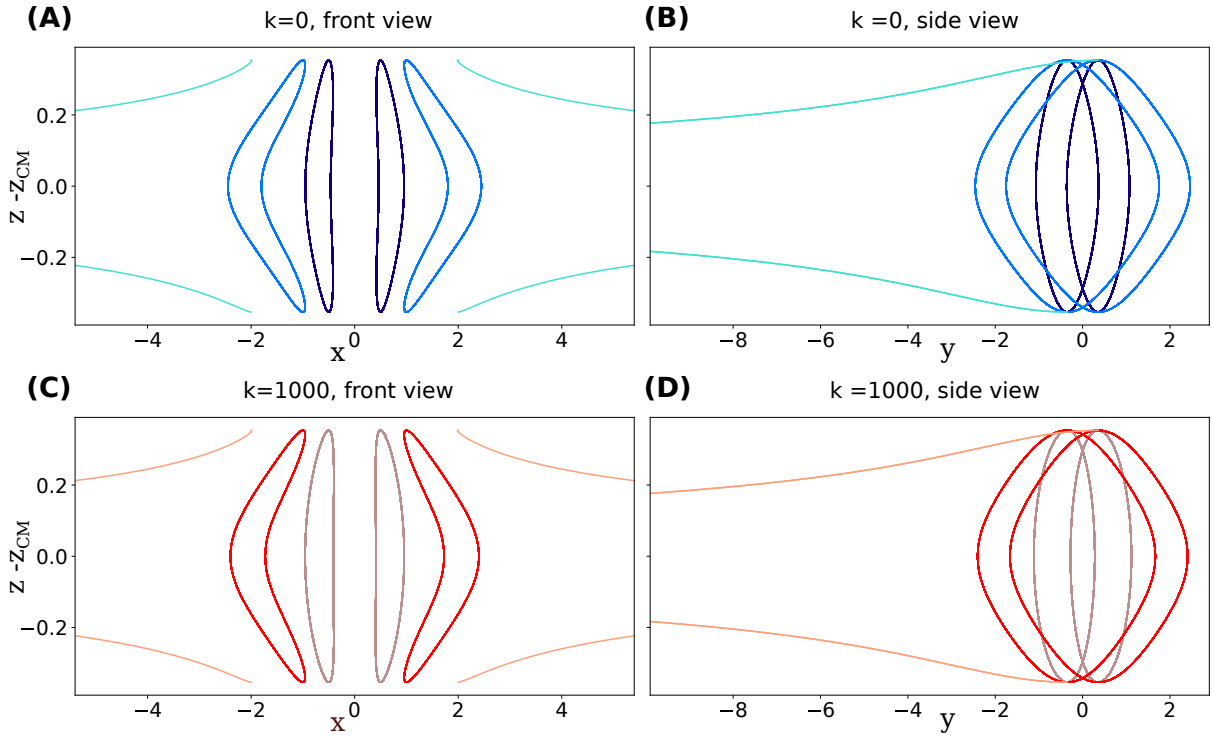


Figure 3.14: Dependence of the trajectory shape on the initial distance between particles for $k = 0$ (A,B) and $k = 1000$ (C,D). Results are shown for $\theta(0) = \pi/4$ and three different values of $x_{CM}(0)$: 0.5, 1 and 2. Different values of $x_{CM}(0)$ are represented by different colours. Results for $\theta(0) = \pi/4$.

come back again [54, 100]. Examples of trajectories, which most likely are non-periodic, are shown in the figure 3.14 for $x_{CM}(0) = 2$.

3.5.2 Elastic dumbbells

Dynamics of elastic dumbbells in three dimensions is very similar to the dynamics restricted to the vertical plane. It is illustrated in figure 3.15, where trajectories of beads are shown for two elastic dumbbells with spring constant $k = 0.01$, initial $x_{CM}(0) = 0.5$ and tilt angle $\theta(0) = \pi/4$. Similarly as in the quasi-2D dynamics, a significant change of trajectory shape is observed: the trajectory becomes wider and wider. Interestingly, the width of the trajectory grows not only in x direction (fig. 3.15A,C), but also in y direction (fig. 3.15B,D).

The influence of elasticity on the dynamics depends on the value of spring constant k . For very small or very large k the dynamics is close to periodic. In order to illustrate the dependence on k , trajectories of centres of the dumbbells (not trajectories of beads as in previous figures) are plotted in the figure 3.16 for different values of elasticity. In both front and side projections of trajectories it is visible that the dynamics of dumbbells with $k = 0.001$ and $k = 1$ is almost periodic in the presented time scale. Larger deviations from periodicity are present for $k = 0.01$

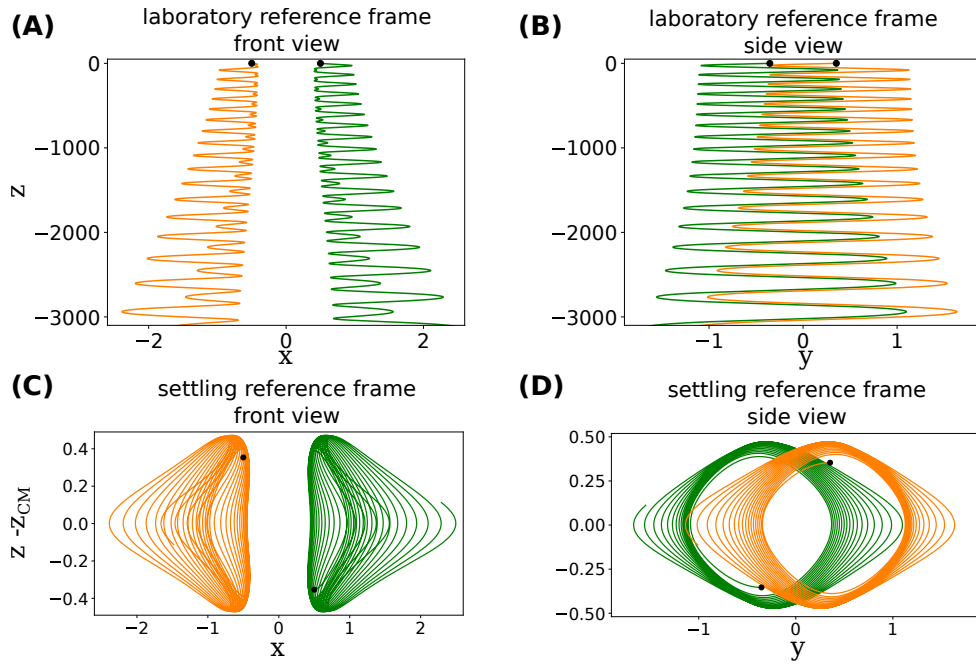


Figure 3.15: Trajectories of the 1st (orange) and 4th (green) beads. Dots indicate initial positions of beads. Results for $k = 0.01$, $x_{CM}(0) = 0.5$ and $\theta(0) = \pi/4$.

and $k = 0.1$. It is worth to remind that for similar values of k the strongest hydrodynamic repulsion was observed also for the in-plane dynamics [168].

An important property of hydrodynamic repulsion phenomena for dumbbells, is that not only the maximal width of trajectory increases, but also the values of local minima of the distance between dumbbells grow. For the dynamics in the vertical plane local minimum of the distance corresponds to the vertical configuration, for the motion out of plane it corresponds to the configuration parallel to the $x = 0$ plane. It turns out that also for the out-of-plane dynamics the same effect of hydrodynamic repulsion is observed. Values of local minima of x_{CM} for different k are shown in figure 3.17A. Here it is clearly visible that for moderate

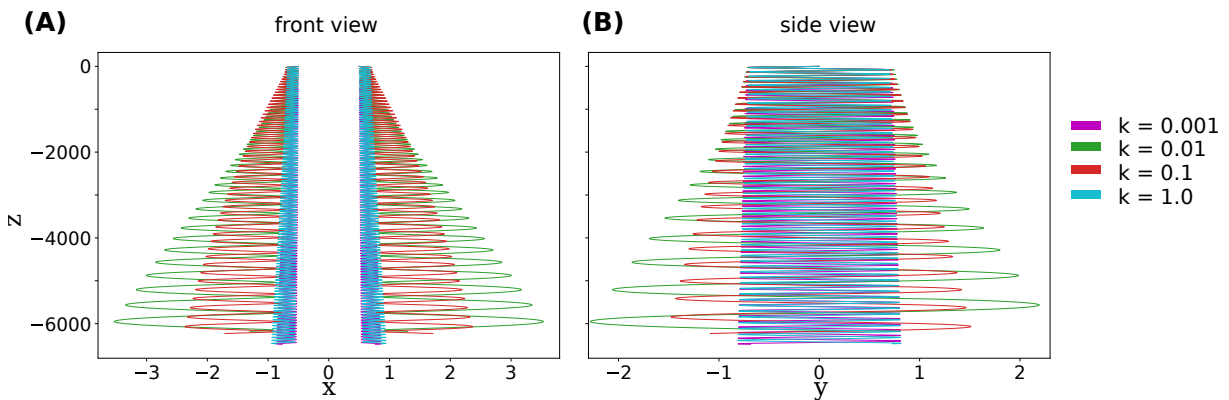


Figure 3.16: Trajectories of dumbbells' centres for $x_{CM}(0) = 0.5$ and $\theta(0) = \pi/4$. Different colours of lines indicate different values of elasticity k . Dynamics was calculated for 1000 time units.

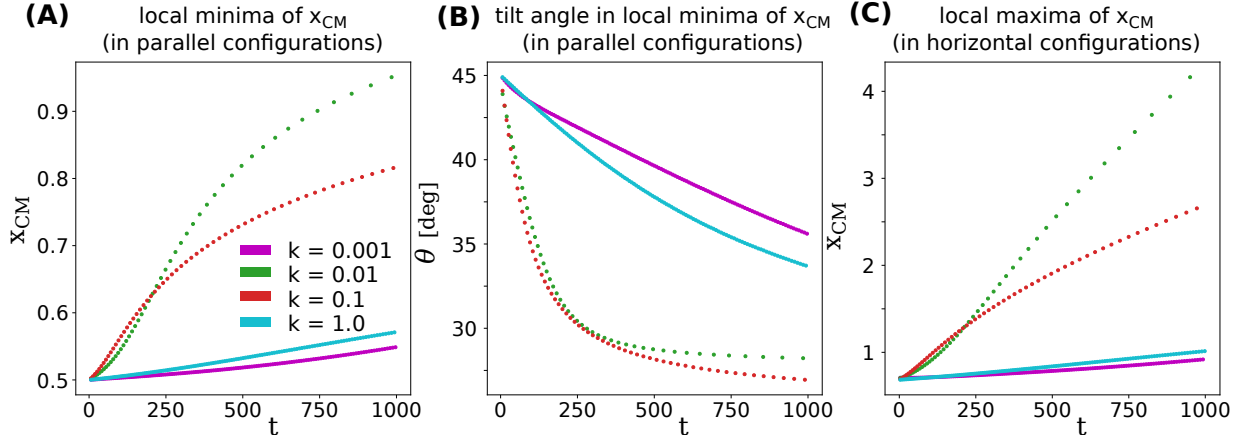


Figure 3.17: Hydrodynamic repulsion between dumbbells. (A) Values of local minima x_{CM} ; (B) values of tilt angle θ for the moments when x_{CM} reaches local minima; (C) values of local maxima of x_{CM} . Results for $x_{CM}(0) = 0.5$, $\theta(0) = \pi/2$ and values of k indicated in the legend.

values of k , including $k = 0.001$ and $k = 1$, the distance between particles gradually increases, although for some values of k much faster than for others. In the figure 3.17B it can be observed that the tilt angle in the parallel configuration slightly decreases during the motion, what is an interesting feature of the dynamics, not possible to be observed when the particles are restricted to the vertical plane. The width of the trajectory (more precisely half of the width, namely the local maxima of x_{CM}), shown in figure 3.17C, grows much faster than local minima of x_{CM} , similarly as for the dynamics in the vertical plane.

In conclusion, the dynamics of dumbbells out of the vertical plane is similar to that restricted to the plane. Periodic motions are observed for the lack of bonds (four independent point particles) and for the rigid dumbbells. In case of elastic bonds the periodicity is lost and an effective repulsion between particles appears. Distance between particles grows both in terms of its local minima and local maxima. The increase of the trajectory width is observed in both horizontal directions: x and y . Hydrodynamic repulsion is weak when spring constant is too small or too big: the strongest effect is observed for $k \approx 0.01$, similarly as for the dynamics of elastic dumbbells in the vertical plane. Apart from hydrodynamic repulsion, in the out-of-plane dynamics the dumbbells become more and more vertical in the consecutive parallel configurations - value of the azimuthal angle θ systematically decreases.

4 Dynamics of rigid particles

In this chapter I present the dynamics of rigid particles, modelled as very stiff chains of beads. The rigidity is obtained by applying very small value of elasticity B , usually $B \in [0.001, 0.01]$. In this study relatively short particles are considered, consisting of $N = 6$ beads and $N = 10$ beads.

First, the dynamics of two filaments settling in the vertical plane is investigated (sec. 4.1). Next, I introduce the notation which is used for tracking of three dimensional motion of particles (sec. 4.2) and subsequently, in section 4.3, the dynamics of the system of two particles not restricted to the vertical plane is described.

Dynamics of rigid particles is similar for a range of shapes with axial and fore-aft symmetries. Results obtained for rigid filaments are compared with dynamics of stiff dumbbells and trumbbells in section 4.4. Finally, some theoretical considerations on the periodicity of the motion are presented in section 4.5.

4.1 Dynamics of rigid filaments (rods) in plane

In this section quasi-2D dynamics of two settling rigid filaments, represented by chains of beads, are investigated. Although studied for ellipsoids [23, 100] and some other shapes [23, 43] up to my knowledge this system was not evaluated for particles modelled as chains of beads. Even though in the closely related article by Llopis et al. [13] the authors consider case of two weakly flexible filaments made of beads, they do not explore range of B close to the limit $B \rightarrow 0$, probably due to collision of the studied particles, consisting of $N = 30$ beads, for such value of B . In this section I will show that in simulations with the bead model applied in this dissertation (Rotne-Prager approximation, lack of additional short-range repulsion), only very short particles may avoid collision. The dynamics of two rigid filaments in a vertical plane, described here, is also very closely related to dynamics of rigid dumbbells [168] (see sec. 3.2), however with some important differences.

Unlike for the dumbbells, the main family of initial configurations considered for the filaments consists of systems where the particles are initially horizontal. For the case of two filaments restricted to the vertical plane, the only parameter of initial configuration is the

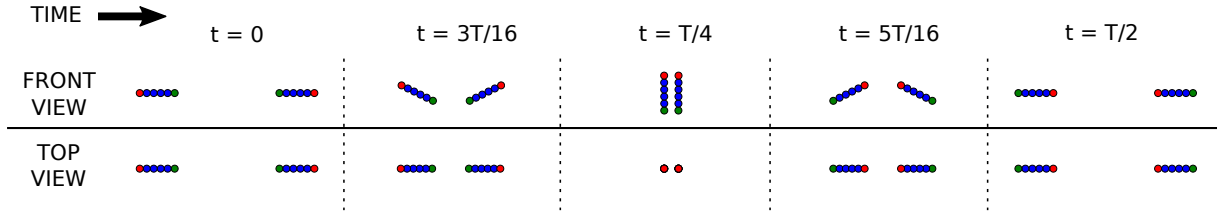


Figure 4.1: Snapshots of rigid filaments configurations at chosen moments, where the period of the motion is denoted by T . Front and top projections are presented. Results for $x_{CM}(0) = 2$. Figure reprinted from ref. [169].

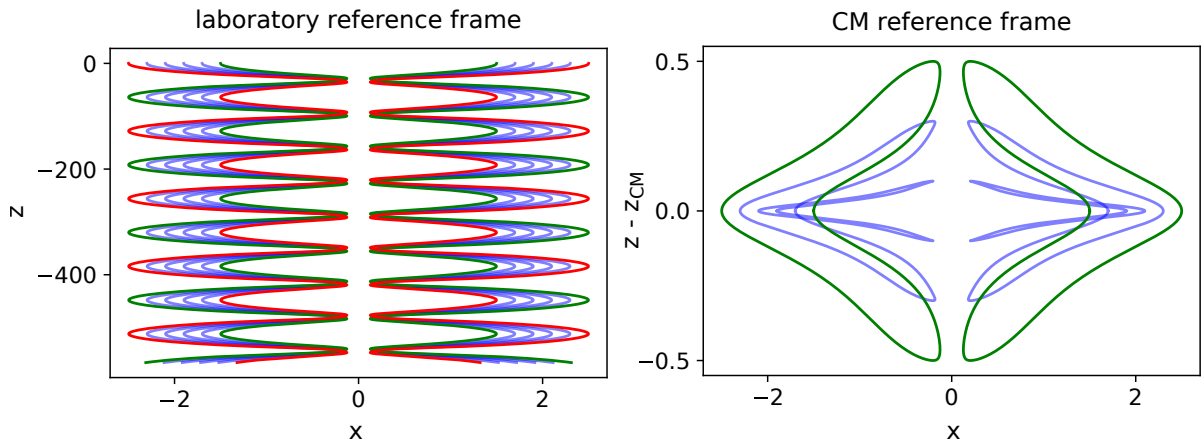


Figure 4.2: Trajectories of beads: (A) in the laboratory reference frame; (B) in the centre of mass reference frame. Trajectories of the 1st and N -th beads are marked with green and red, respectively. Trajectories of other beads are shown in blue. In the centre of mass reference frame only trajectories of 1st, 2nd and 3rd beads shown, because they are identical to trajectories of 6th, 5th and 4th beads, respectively. Results shown for $x_{CM}(0) = 2$ and $N = 6$.

distance between particles. In this work I use the initial x component of centre of the right particle, denoted as $x_{CM}(0)$, as a characteristic parameter of the initial configuration.

The dynamics of the rigid filaments consisting of $N = 6$ beads is presented in fig. 4.1 by a series of snapshots of the particles. Trajectories of beads, in the laboratory reference frame and in the settling reference frame are shown in fig. 4.2A and B, respectively. The dynamics is very similar to the dynamics of the dumbbells: periodic oscillations are coupled with vertical translation. Starting from horizontal configuration the particles begin to rotate and approach each other. After a certain time τ particles reach vertical configuration, when they are again parallel to each other. Next, the particles continue to rotate and start to drift away. Exactly after time 2τ they reach horizontal configuration, which is identical to the initial one, except for switching positions of particles $i \leftrightarrow N + 1 - i$. The time of full period is equal to $T = 4\tau$.

Similarly as in the case of dumbbells, initial configuration affects non only the width, but also the shape of trajectory. A few exemplary results are shown in fig. 4.3A. We can observe that trajectories of beads are most sensitive to $x_{CM}(0)$ when the particles which are close to each other: trajectories for $x_{CM}(0) = 1.1$ and $x_{CM}(0) = 1.5$ are significantly different. If particles are too close, $x_{CM}(0) \leq 1$, the particles collide. Interestingly, even initially quite remote particles approach each other up to a very close distance. In fig. 4.3B the minimal distance between particles is plotted as a function of $x_{CM}(0)$. The results indicate that even if in the horizontal configuration the distance between particles is as large as almost 7 times the filament length ($x_{CM}(0) = 4$ corresponds to 6.8 distance between surfaces of particles), the minimal distance between particles during the motion is still smaller than the bead radius, which for the particle consisting of $N = 6$ beads is equal to 0.1. The conclusion from this study is that even if the width of the trajectory is large, the particles are close to collision during the tumbling process.

Particles which consist of $N = 10$ beads initially behave in the same way as shorter rigid filaments. During rotation they approach each other, but unlike in the $N = 6$ case, the rotation is not fast enough to avoid collision. Trajectories of beads and configuration of particles at the collision are shown in fig. 4.4. The phenomena of collision of rigid filaments are consistent with work by Llopis et al. [13] where such behaviour was observed for longer filaments $N = 30$ for B below certain positive threshold, what suggests that also for $B \approx 0$.

It is worth to notice that ‘collision’ of filaments can not actually happen under Stokes regime. In such system particles which are separated cannot establish contact, and particles in contact cannot separate. If we aimed to determine accurate dynamics of particles in near-contact phase, a more sophisticated method than Rotne-Prager approximation would be required, for example multipole approximation with lubrication correction [41]. We can speculate that with use of an accurate hydrodynamic model, at least in some cases, after the near-contact encounter the particles would ‘tumble’, as observed in experiments for rigid particles [23].

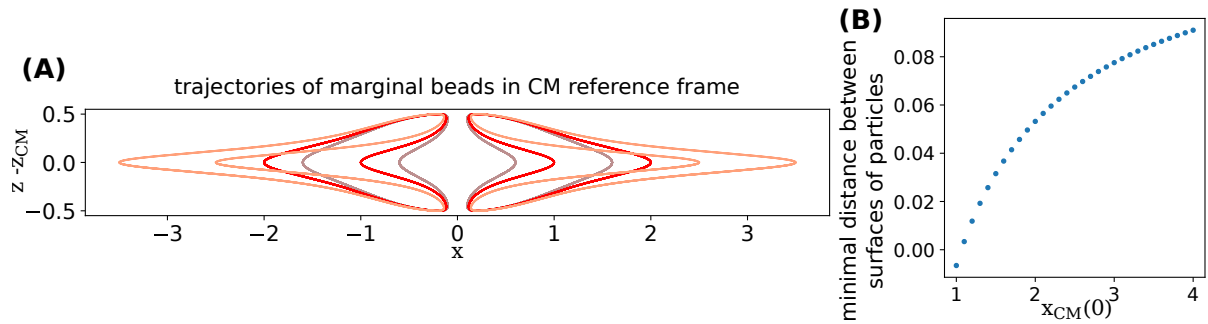


Figure 4.3: The influence of initial separation on the dynamics. (A) Shapes of trajectories of marginal beads (identical for the 1st and the N th bead) shown in the centre of mass reference frame for $x_{CM}(0) \in \{1.1, 1.5, 3.0\}$. Wider trajectories correspond to larger values of $x_{CM}(0)$. (B) Minimal distance between surfaces of particles as a function of $x_{CM}(0)$. Result for $x_{CM}(0) = 1.0$ is included for comparison regardless its non physical value, which is slightly negative (beads overlap).

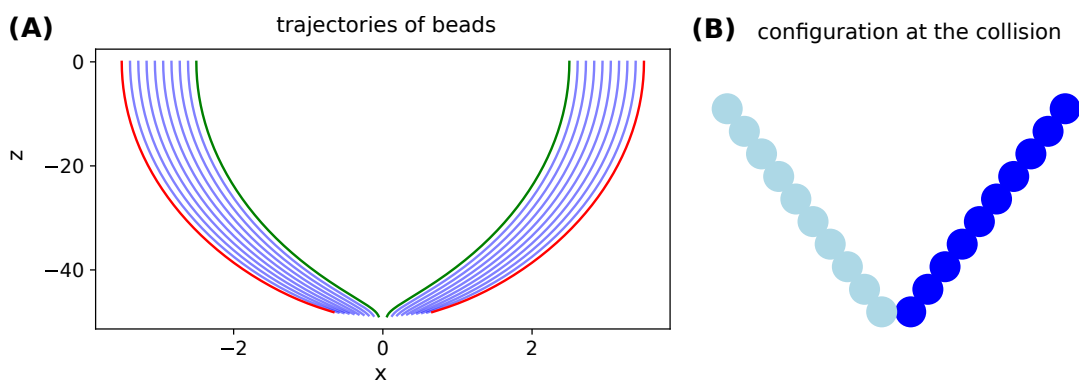


Figure 4.4: Dynamics of the rigid filaments consisting of $N = 10$ beads. (A) Trajectories of beads; (B) configuration at the collision time. Results for $x_{CM}(0) = 3$.

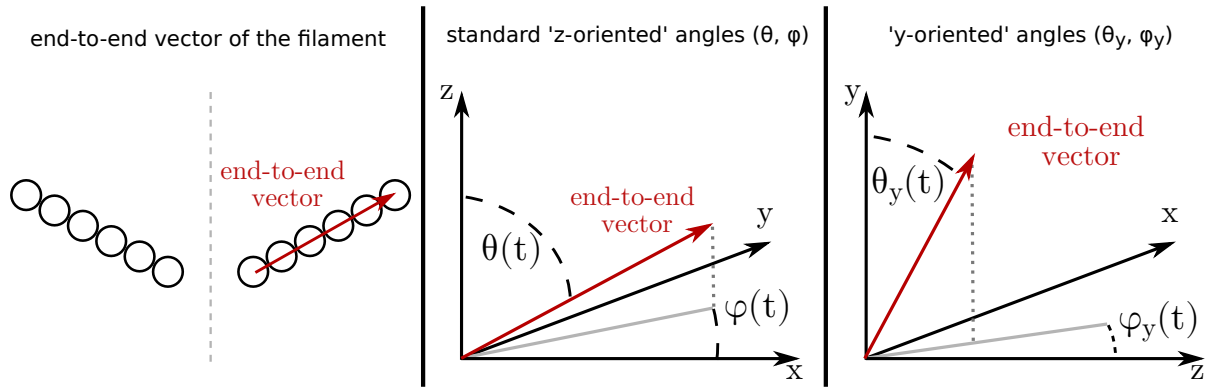


Figure 4.5: Notation used to describe orientation of the filament. End-to-end vector connects centres of the first and the last beads. The same notation will be used also for flexible filaments in chapters 6-8.

On the other hand, near-contact encounter of particles in the real world may result in amplification of existing small deviations of filaments from the vertical plane. In such case, analysis of out-of-plane particle motion is needed, what is described in the next sections for rigid particles and in chapters 7-8 for flexible filaments. Moreover, the symmetry of the system, which is implicitly assumed here, may be broken. Results for non-symmetric systems of elastic particles are presented in chapter 8. In case of rigid particles, experiments conducted by Jung et al. [23] suggest that the periodic dynamics is robust to near-contact encounters of particles.

4.2 Notation of the particles orientation in the 3D motion

For filaments in the three dimensional space it is convenient to consider their orientation described by two orientation angles. The orientation of the filament can be defined as the orientation of end-to-end vector, which connects centres of the first and the last bead. Later this description will be extend for non rigid particles.

In this dissertation orientation angles θ and φ are used, which correspond to a standard notation for spherical coordinate system (fig. 4.5). The coordinates of the orientation unit vector $\hat{\mathbf{k}} = (k_x, k_y, k_z)$ are given by:

$$k_x = \sin \theta \cos \varphi, \quad (4.1)$$

$$k_y = \sin \theta \sin \varphi, \quad (4.2)$$

$$k_z = \cos \theta. \quad (4.3)$$

Additionally a supplementary coordinate system is introduced, called here 'y-oriented'. It is given by angles θ_y and φ_y defined in an analogous way as θ and φ : θ_y is the angle between y

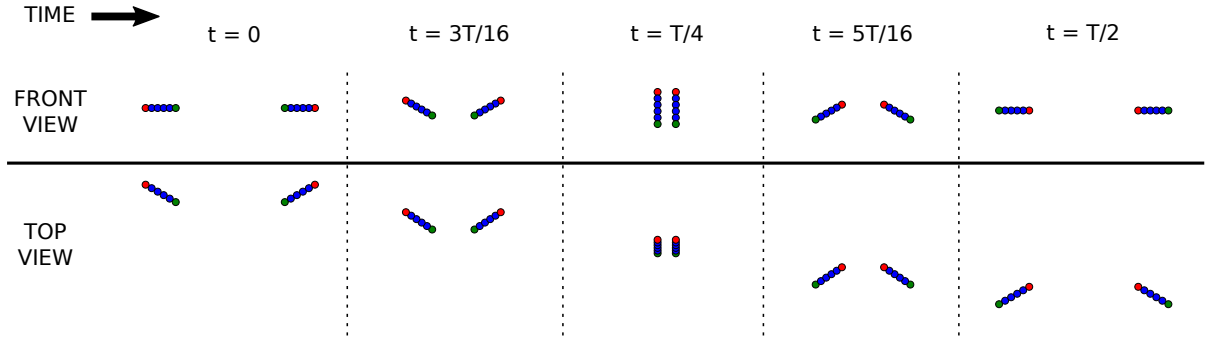


Figure 4.6: Snapshots of rigid filaments configuration at chosen moments, T denotes the period of the motion. Front and top views are presented. Results shown for $x_{CM}(0) = 2$ and $\varphi(0) = 30^\circ$. Figure reprinted from ref. [169].

axis and the orientation vector and φ_y measures the angle between projection of $\hat{\mathbf{k}}$ on the xz plane and the z axis (toward x axis), what is illustrated in figure 4.5. In (θ_y, φ_y) notation the coordinates of the orientation unit vector $\hat{\mathbf{k}} = (k_x, k_y, k_z)$ are given by:

$$k_x = \sin \theta_y \sin \varphi_y, \quad (4.4)$$

$$k_y = \cos \theta_y, \quad (4.5)$$

$$k_z = \sin \theta_y \cos \varphi_y. \quad (4.6)$$

Since the system considered here is symmetric, orientation angles θ and φ given for the ‘right particle’ (which beads have positive ‘ x ’ coordinates) define in an unambiguous way the orientation of the left particle described by angles $(\theta', \varphi') = (\theta, \pi - \varphi)$ for standard spherical coordinates and by $(\theta'_y, \varphi'_y) = (\theta_y, \pi - \varphi_y)$ for ‘ y -oriented’ coordinates.

The family of initial configurations considered for two filaments not restricted to the vertical plane consist of configurations where particles are symmetric (except for chapter 8), horizontal ($\theta(0) = \pi/2$) and in elastic equilibrium. The ‘right’ particle is rotated from the ‘ x ’ axis by an angle $\varphi(0)$ and the left by $\pi - \varphi(0)$. By convention the centre of mass of the ‘right’ particle is given by $\mathbf{r}_{CM} = (x_{CM}, 0, 0)$ and the left particle is located symmetrically at $(-x_{CM}, 0, 0)$.

4.3 Dynamics of rigid filaments out of plane

The dynamics of rigid filaments in three dimensions is similar to the one observed in the vertical plane. The particles perform periodic motions. Dynamics is illustrated by a series of snapshots in fig. 4.6 and by trajectories of beads in fig. 4.7. Similarly as for quasi two dimensional case, the particles ‘tumble’: rotate around the ‘ y ’ axis always in the inward direction. The filaments approach each other when the inner ends of particles (the ones closer to

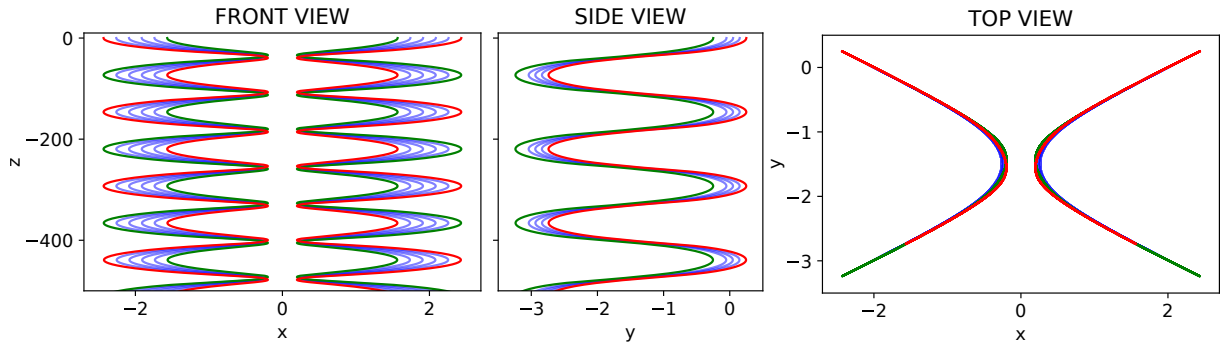


Figure 4.7: Trajectories of beads in the laboratory reference frame, shown in three different projections. Results shown for $x_{CM}(0) = 2$ and $\varphi(0) = 30^\circ$.

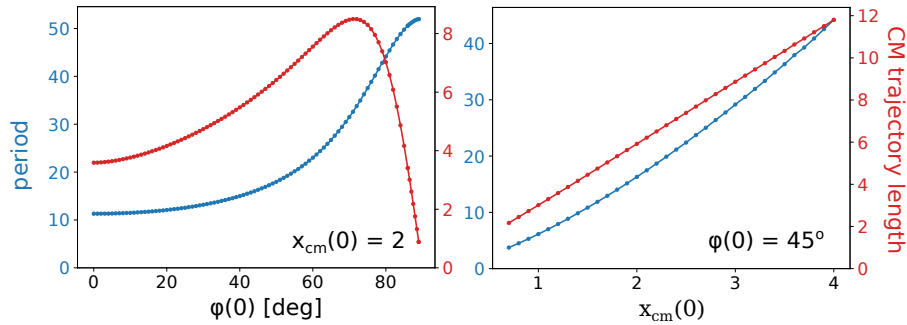


Figure 4.8: Dependence of the period and length of the trajectory in a single period on the initial configuration. Length of the trajectory is measured as the length of the path travelled by the centre of particle in the reference frame settling with the same instantaneous speed as particles. Period and trajectory length are shown as functions of (A) $\varphi(0)$ (up to 89°) for fixed $x_{CM}(0) = 2$; (B) $x_{CM}(0)$ with fixed $\varphi(0) = 45^\circ$. Figure reprinted from ref. [169].

the symmetry plane) are lower than the outer ends, and repel each other in the opposite case. In the horizontal configuration ($\theta = \pi/2$) and in the parallel, yet non-horizontal configuration ($\varphi = \pi/2$), the distance between particles is not changing. The description given in this paragraph explains the main features of the motion but is not complete, in particular the rotation of particles is not restricted to the ‘ y ’ axis, what will be elaborated later in this section.

Since the particles are not restricted to the vertical plane, they can move along the ‘ y ’ axis. The direction of motion is given by the filament orientation: the particle moves in the direction of its lower end. As a result the tumbling motion is coupled with swinging along ‘ y ’ axis, what is visible in figures 4.6 and 4.7. For the special case when the particles are initially parallel and $\varphi(0) = 90^\circ$, the tumbling does not occur (apart from settling, particles can only roll) and the distance between particles does not change during the settling.

Dependence of the period and the trajectory length in a single period on the initial configurations is presented in figure 4.8. It can be observed that for a given value of $x_{CM}(0)$ the period increases with the initial angle $\varphi(0)$. Interestingly, for $\varphi(0) \rightarrow 90^\circ$ the period converges to a finite number. Dependence of the period time on the initial distance between particles is

(A) θ and φ orientation angles during the motion **(B)** θ_y and φ_y orientation angles during the motion

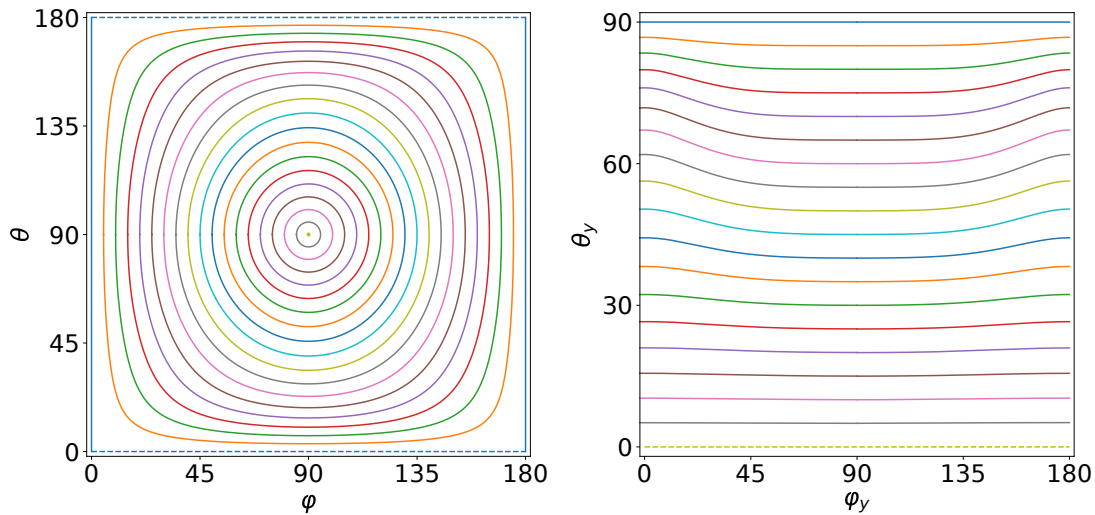


Figure 4.9: Orientation angles of the ‘right’ particle during the motion for $x_{CM}(0) = 2$ and $\varphi(0) \in \{0, 5^\circ, \dots, 90^\circ\}$. (A) Orientation shown as angles (θ, φ) . Initially $\theta(0) = 90^\circ$, $\varphi(0) \leq 90^\circ$. Angles change in the anticlockwise direction. (B) Orientation shown as angles (θ_y, φ_y) . Initially $\varphi_y(0) = 90^\circ$ and $\theta_y(0) = \varphi(0)$. Angles change from right to the left (φ_y is decreasing with time).

straightforward: the larger distance, the longer period. Length of the trajectory in one period shown in fig. 4.8 is measured for the centre of the particle in the reference frame settling with the same speed as the centre of mass of the system. In consequence, only x and y components of the centre of the particle movement are taken into account and the z coordinate is omitted – if the trajectory length is measured in the laboratory reference frame, the results are dominated by the settling distance, which mainly depends on the period duration. Considering initial configuration with the same $x_{CM}(0) = 2$, the length of the trajectory initially increases, reaches maximum (at $\varphi(0) \approx 72^\circ$ in case of $x_{CM}(0) = 2$) and subsequently decreases for even larger angle, tending to 0 for $\varphi(0) \rightarrow 90^\circ$. The relation between $x_{CM}(0)$ and the trajectory length is almost linear in the investigated range of distances, with positive slope.

For the periodic motions of rigid fibres it is particularly useful to track the dynamics in terms of orientation angles of the particles. Orientation of the particles in terms of θ and φ angles is shown in figure 4.9A for fixed $x_{CM}(0) = 2$ and different initial value of φ angle. Periodicity is clearly visible by the closed lines. The direction of the dynamics in the figure is anticlockwise: the dynamics starts at $\theta = 90^\circ$, $\varphi < 90^\circ$ and the value of θ initially decreases. The most outer trajectory shown in fig. 4.9A is the quasi 2D dynamics with $\varphi(0) = 0$, for which the φ may have values only 0 or 180° . The point in the middle of the figure represents $\varphi(0) = 90^\circ$, in which case the particles do not oscillate at all, but settle without changing the configuration.

Other interesting features of the dynamics may be observed in figure 4.9B, where θ_y and φ_y orientation angles are shown. It turns out that the value of θ_y barely changes during the motion

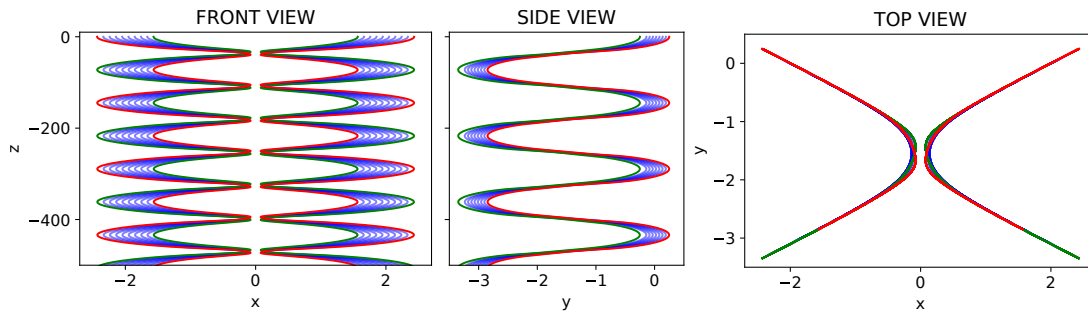


Figure 4.10: Trajectories of beads for the particles consisting of $N = 10$ beads, shown in three different projections. Results shown for $x_{CM}(0) = 2$ and $\varphi(0) = 30^\circ$.



Figure 4.11: Different types of particles used in the comparison: dumbbells ($N = 2$), trumbells ($N = 3$) and fibres consisting of $N = 6$ beads. In each case the bead radius is equal to $1/10$ of the particle length.

for all initial configurations. The changes of θ_y are the smallest for $\varphi(0)$ close to 0 and 180° , while the largest for $\varphi(0) \approx 30^\circ$. The interpretation of this result is that rotation around ‘ y ’ (which does not influence θ_y) dominates the dynamics.

In the previous section 4.1 it was shown that longer particles, with $N = 10$, located in the vertical plane collide instead of performing periodic motions. When the particles start from configuration out of the plane, fibres consisting of $N = 10$ or even larger number of beads can avoid collision and perform periodic motions, which are described above for the case $N = 6$. It is illustrated in fig. 4.10, where trajectories of beads are shown for $N = 10$, $x_{CM} = 2$ and $\varphi(0) = 30^\circ$. The reason behind possibility of periodic motions of long particles out of plane is that for $\varphi \neq 0$ the motion of particles toward each other can be much slower than for $\varphi = 0$, while the rotation around y axis is only slightly affected.

4.4 Dynamics of rigid dumbbells and trumbells

In this section the dynamics of rigid dummbells, trumbells, and filaments is investigated. As stated before, the dynamics of rigid particles with axial symmetry and fore-aft symmetry is expected to be similar for different shapes, as observed by Jung et al. [23]. Indeed, all three types of rigid particles made of beads (dumbbells, trumbells and filaments) perform periodic motions for initial configurations both in the vertical plane and out of the plane.

In order to compare the dynamics of particles consisting of different numbers of beads it is necessary to establish what bead radii should be considered. In this work the dynamics of

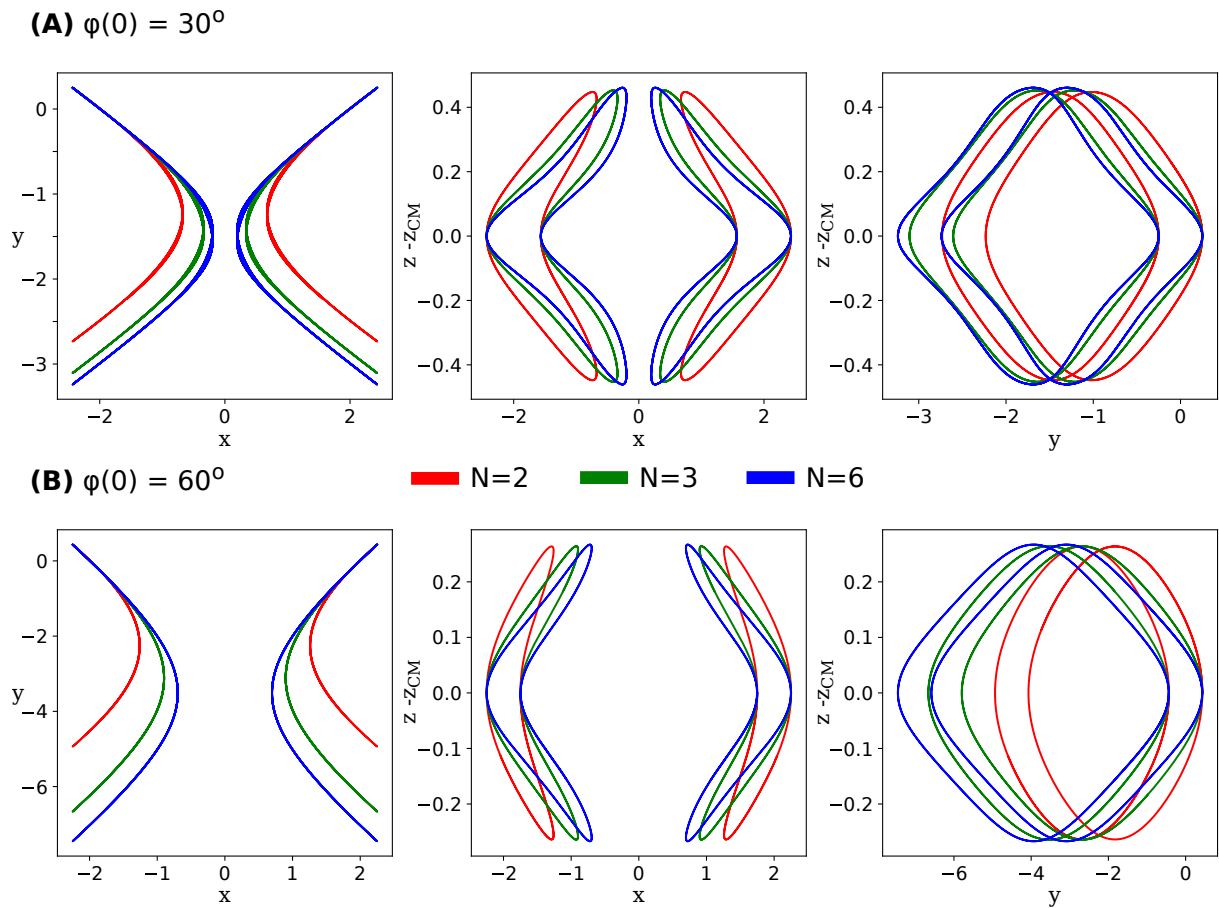


Figure 4.12: Dynamics of rigid particles consisting of 2, 3 and 6 beads, shown in terms of marginal beads trajectories in the settling reference frame. Results shown for $x_{CM}(0) = 2$ and two different initial orientation angles.

filaments consisting of $N = 6$ beads and beads radii $a = 0.1$ is compared with the dynamics of dumbbells and trumbbells with the same beads radii $a = 0.1$ (see fig. 4.11). Trajectories of marginal beads of the particles in the centre of mass reference frame are shown in figure 4.12. In all cases the particles start from the horizontal configuration and the dynamics is calculated with RPY approximation of hydrodynamic interactions.

Results show that the same pattern is observed for different initial configurations: the trajectories in both ‘ x ’ and ‘ y ’ directions are the widest for the filaments, less wide for the trumbbells and the most narrow for dumbbells. The presence of the trajectory for $N = 3$ in between results for $N = 2$ and $N = 6$ suggests a systematic dependence. Nevertheless the main conclusion from this comparison is that the dynamics is very similar for rigid particles consisting of different numbers of beads.

4.5 Periodicity of the motion

The arguments for strictly periodic motion of dumbbells in a vertical plane were described in section 3.2.1. The dynamics was proven to be periodic, given that starting from the vertical configuration the particles did not drift away, but were able to reach a horizontal configuration. Analogous reasoning can be applied to three-dimensional dynamics presented in this chapter. Since particles which are not restricted to a vertical plane cannot adopt ‘vertical’ configuration, instead a parallel configurations, in which $\varphi = \pi/2$, will be considered. Another difference with respect to the system of rigid dumbbells from section 3.2.1 is that the particles considered here initially have horizontal positions. This property ensures that the particles always reach the parallel configuration with $\varphi = \pi/2$, because the particles continuously rotate inward¹. Therefore the periodic dynamics is always observed, except for spurious collisions (which are not possible in Stokes regime) and the limiting case of initial configurations with $\varphi(0) = \pi/2$, when particles settle down without change of the configuration.

The reasoning presented in section 3.2.1 for the periodicity of two dumbbells is actually more general and can be applied also to rigid trumbbells and filaments, which are straight and lay entirely in the vertical plane (more precisely: centres of all beads lay in the vertical plane). For the particles not restricted to the vertical plane the problem is slightly more complicated. Regarding the initial, horizontal configuration, the result for sec. 3.2.1 is valid (because $M_z \mathbf{r}(0) = \mathbf{r}(0)$) and the trajectories of beads are symmetric with respect to the plane $z = z_{CM}(0)$ where $\mathbf{r}_{CM}(t) = (x_{CM}(t), y_{CM}(t), z_{CM}(t))$ is the position of the centre of the ‘right’ particle. In the three-dimensional motion, unlike for quasi-2D dynamics, such condition

¹Rotation do not vanish for any configuration of particles.

is not met for $t = T/4$ because, when particles are parallel to $x = 0$ plane, $M_z \mathbf{r}(T/4) \neq \mathbf{r}(T/4)$. However we can use the fact that $\mathbf{r}(T/4) = M_z M_y \mathbf{r}(T/4)$ and therefore $\mathbf{r}(T/4 + t) = M_z M_y \mathbf{r}(T/4 - t)$. In particular the position of particles after $t = T/2$ is a reflection of the initial configuration: therefore it is also horizontal, yet reflected with respect to $y = y_{CM}(T/4)$ plane and therefore transferred along the ‘ y ’ axis, so the centres of the particles are located at $y_{CM}(T/2) = 2y_{CM}(T/4)$ (we assume that initially $y_{CM} = 0$). Because after time $t = T/2$ the configuration of particles is symmetrical to the initial one, it can be deduced that after $t = T$ it is the same as at the beginning of the motion, with only a vertical translation due to settling.

The reasoning given in this section is a merely a sketch of the proof and the full discussion conducted by Ekiel-Jeżewska can be found in the reference [169]

5 Analysis of different forms of bending potential in bead model of elastic particles

Elastic deformations of particles include extension/compression, bending and twisting. Among them the bending is arguably the most important, due to large deformation of shape in comparison to stretching. The twist, as in vast majority of publications, in this study is omitted altogether.

In the bead model, bending stiffness is introduced by the bending potential, which usually exclusively depends on the angles between bonds, as described in sec. 2.2.2. Kratky-Porod and harmonic are the two most common forms of bending potential used in the literature. Both give the same results in the limit of vanishing bending angles, $\beta \rightarrow 0$, however so far it was not systematically studied what are the effects of the form of bending potential in the real systems of hydrodynamically interacting particles. The question is particularly relevant for trumbbells and relatively short particles, including filaments with aspect ratio around 10 studied in this dissertation.

In this chapter I investigate the differences between alternative forms of bending potential and try to indicate the preferred choice. The continuous filaments with classic model of elasticity are used as a reference for different forms of bending potential used in the bead models. As the first step, the correspondence between bead model and continuous filament needs to be established, so that bending angles in the bead model have an analogue in average curvature of the corresponding segments in continuous filament, what is done in section 5.1. In section 5.2 for each segment of the continuous filament, with known mean curvature of the segment, the lower bound for accumulated bending energy is calculated and compared to the bending energy evaluated for angles between bonds in the bead model with different forms of bending potential. Subsequently, in section 5.3 the differences between bending forces are analysed, which in general depend on triplets of consecutive angles.

The last section 5.4 of this chapter illustrates the influence of the form of bending potential on the simulated dynamics of particles. First, the existence and shape of the equilibrium configuration of a single settling trumbbell is studied for Kratky-Porod and harmonic bending models. Significant differences are found. Next, the influence of bending potential on the stationary configuration of a settling filament is investigated by a number of characteristic parameters used in the literature to describe relevant properties of filament's shape. Other

examples where bending model influences the dynamic of particles are also mentioned. The majority of results presented in this chapter was published by the author and M. Ekiel-Jezewska [159].

5.1 Correspondence between continuous and bead models

The classic theory of elasticity gives relatively simple yet powerful formulas to calculate bending energy of a continuous filament of a given shape. In order to use this theory as the reference for different forms of bending potential in bead model, first one needs to establish the correspondence between the configuration of chain of beads and the configuration of a continuous filament. The problem addressed in this section 5.1 is as follows: what can be stated about the shape of a continuous filaments knowing that it corresponds to a given configuration of a chain of beads? Although the number of possible corresponding shapes of the continuous filament remains infinite, this approach allows to determine the lower bound for its bending energy. As bead model usually intends to represent cylindrical filaments, filaments with circular cross-sections will therefore be considered.

5.1.1 Continuous filament

The shape of continuous filament with a constant, circular cross-section is described by its centreline, given by $\mathbf{r}_s^C(s)$, where parameter $s \in [0, 1]$. We denote instantaneous length of the filament as $L(t)$ and equilibrium length as L_0 . In this work we consider filaments, which are extensible and therefore the length of a given curve segment $[s_i, s_j]$ can change with time. For convenience we leave ‘ s parametrization’ as time-independent, connected with filament at rest, and alongside time-dependent ‘ l parametrization’ is introduced, $\mathbf{r}_l^C(l)$, $l \in [0, L(t)]$, which is linked to the temporary extension of the filament. As in the following text there is no risk of confusing \mathbf{r}_s^C and \mathbf{r}_l^C parametrizations, in order to avoid excessive notation the subscripts are omitted and the two functions can be distinguish by the argument: $\mathbf{r}^C(s)$ and $\mathbf{r}^C(l)$, respectively. It is worth to notice that in equilibrium $dl/ds = L_0$ everywhere along the centreline and the local strain ϵ at the centreline is given by $\epsilon = (dl/ds - L_0)/L_0$.

5.1.2 Definition of the correspondence between the bead model and the continuous model of a filament

The configuration of a continuous filament is represented by its centreline, while in bead model the configuration is given by the positions of centres of beads. In order to link continuous

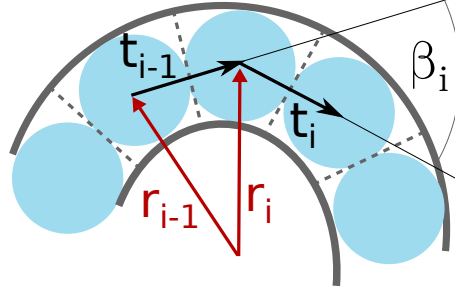


Figure 5.1: The scheme illustrates correspondence between the bead model (shown in blue) and continuous filament (solid grey lines). Dashed lines indicate division of the filament into segments, corresponding to each bead. Figure reprinted from [159].

and bead models, let us divide the continuous filament into N segments. The $(N + 1)$ borders of the segments cross centreline at points $(s_0, s_1, \dots, s_N) = (0, 1/N, \dots, 1)$ and the borders are perpendicular to the centreline. Each bead will correspond to a single segment.

Positions of beads are related with the centreline as follows. In order to link continuous and discrete models, we identify borders of segments in continuous model with a half-way positions between centres of consecutive beads. Recalling notation from chapter 2, \mathbf{r}_i denotes position of center of i -th bead and $\mathbf{t}_i = \mathbf{r}_{i+1} - \mathbf{r}_i$ denotes vector between successive beads. With this notation, we may write down the position of centreline at the border between i -th and $(i + 1)$ -th as:

$$\mathbf{r}^C(s_i) = (\mathbf{r}_i + \mathbf{r}_{i+1})/2 \quad (5.1)$$

Moreover, we assume that at the borders between segments the centreline is parallel to bonds between beads (therefore the borders themselves are perpendicular to the bonds):

$$\left. \frac{d\mathbf{r}^C}{ds} \right|_{s_i} \parallel \mathbf{t}_i \quad (5.2)$$

Correspondence between continuous and bead models is illustrated in fig. 5.1. With such model it is straightforward to assign bending angle to each segment of the continuous filament, similarly as it was done for bead model in section 2.1:

$$\beta_i = \arccos \left(\left. \frac{d\widehat{\mathbf{r}^C}(s)}{ds} \right|_{s=s_{i-1}} \cdot \left. \frac{d\widehat{\mathbf{r}^C}(s)}{ds} \right|_{s=s_i} \right) \equiv \arccos (\hat{\mathbf{t}}_{i-1} \cdot \hat{\mathbf{t}}_i), \quad (5.3)$$

where hat denotes unit vector: $\hat{\mathbf{x}} = \mathbf{x}/|\mathbf{x}|$ for any vector $\mathbf{x} \neq 0$.

Now let us draw the link between bending angle β in discrete model and curvature $\kappa(l)$ of continuous filament within the respective segment. The curvature is defined as [170] $\kappa(l) = |d^2\mathbf{r}^C(l)/dl^2|$ and for an infinitesimal segment it is related with bending angle of the curve by [171]:

$$d\beta = \kappa(l)dl, \quad (5.4)$$

where bending angle $\beta \in [0, \pi]$ of the curve segment is the angle between tangential vector at the beginning and at the end of the segment. Let us consider a curve segment $l \in [l_A, l_C]$ with a point $r^C(l_B)$, $l_A \leq l_B \leq l_C$. Denoting bending angle of a curve segment $[l_a, l_b]$ as $\beta(l_a, l_b)$ it may be noticed that $\beta(l_A, l_C) \leq \beta(l_A, l_B) + \beta(l_B, l_C)$. This result may be applied to a segment corresponding to i -th bead, $[l(s_{i-1}), l(s_i)]$, for which the bending angle of the curve $\beta(l(s_{i-1}), l(s_i))$, by eq. (5.3) is equal to β_i . Combining it with eq. (5.4) we obtain:

$$\beta_i = \beta(l(s_{i-1}), l(s_i)) \leq \int_{l(s_{i-1})}^{l(s_i)} \kappa(l) dl. \quad (5.5)$$

This formula links bending angles in bead model (β_i) with curvature of continuous filament ($\kappa(l)$). It will be used in the next paragraph to compare bending energies in continuous and discrete models. Strict equality between β_i and the integral in the relation (5.5) is obtained if the filament lays entirely in a plane and direction of bending does not change within the considered segment. Otherwise the left-hand side of the formula is strictly smaller than right-hand side.

Relation between discrete and continuous models of filament is ambiguous and many other forms of such correspondence, different than the one described in this section, may be defined. For example, one may request that the centres of beads lay on the centreline of the corresponding continuous filament, what is not provided in the approach presented here.

5.2 Comparison of energy in different bending models

In the continuous model, quadratic approximation of bending energy is usually applied [143]. Bending energy of i -th segment of elastic filament under such approximation is given by:

$$E_{b,i}^C = \frac{A}{2} \int_{l(s_{i-1})}^{l(s_i)} \kappa(l)^2 dl, \quad (5.6)$$

where A is the bending stiffness of the filament. From this equation it is clear, that in case of continuous filament bending energy of a segment depends not only on the angle between tangent vectors at the beginning and at the end of the segment, but also on the shape of the filament in between. If the bending angle of the segment is required to be β_i , bending energy is minimal if the curvature is constant and equal to $\kappa(s) = \kappa_i = \beta_i/l_i$, where l_i is the length of i -th segment:

$$E_{b,i}^C \geq \frac{Al_i \kappa_i^2}{2}. \quad (5.7)$$

In terms of bending angle we can write:

$$E_{b,i}^C \geq \frac{A\beta_i^2}{2l_i}. \quad (5.8)$$

The result shown in the inequality above suggests that in bending model the leading term of the potential should be of the order of β^2 . This indeed happens for most of bending potentials present in literature: Kratky-Porod (KP), harmonic (H) and less popular logarithmic, described in section 2.2.2. An exception to this rule is ‘cosine squared’ bending potential where energy is proportional to $(1 - \cos \beta)^2$ where the leading term in expansion around 0 is of the order of β^4 . In consequence ‘cosine squared’ bending potential does not match other potentials even in the limit $\beta \rightarrow 0$.

Most common bending potentials, Kratky-Porod U_b^{KP} and harmonic U_b^H (described also in sec. 2.2.2) are given by:

$$U_b^{KP} = \frac{A}{2l_0} \sum_{i=2}^{N-1} (\hat{\mathbf{t}}_i - \hat{\mathbf{t}}_{i-1})^2 = \frac{A}{l_0} \sum_{i=2}^{N-1} (1 - \cos \beta_i), \quad (5.9)$$

$$U_b^H = \frac{A}{2l_0} \sum_{i=2}^{N-1} \beta_i^2. \quad (5.10)$$

Comparing these formulas with eq. (5.8) we can see that harmonic bending potential is equal to the lower boundary of energy in respective segment of continuous filament, while Kratky-Porod potential systematically underestimates the energy, what becomes more pronounced for larger β . It can be noticed that equation (5.8) contains the actual length of the segment l_i , while in equations (5.9)-(5.10) equilibrium length of bonds, l_0 , is present. Although in general this fact may affect bending energies, the influence of bond lengths on bending energy is not considered in this work, because changes in bond lengths are typically very small.

The important message arising from considerations presented in this paragraph is that in the discrete model both analysed bending potentials underestimate bending energy when the curvature is not uniform. Additionally, Kratky-Porod potential underestimates this energy even for uniform curvature due to rising gap between $\beta_i^2/2$ and $1 - \cos \beta_i$ expressions for larger β_i (see fig. 5.2A,B).

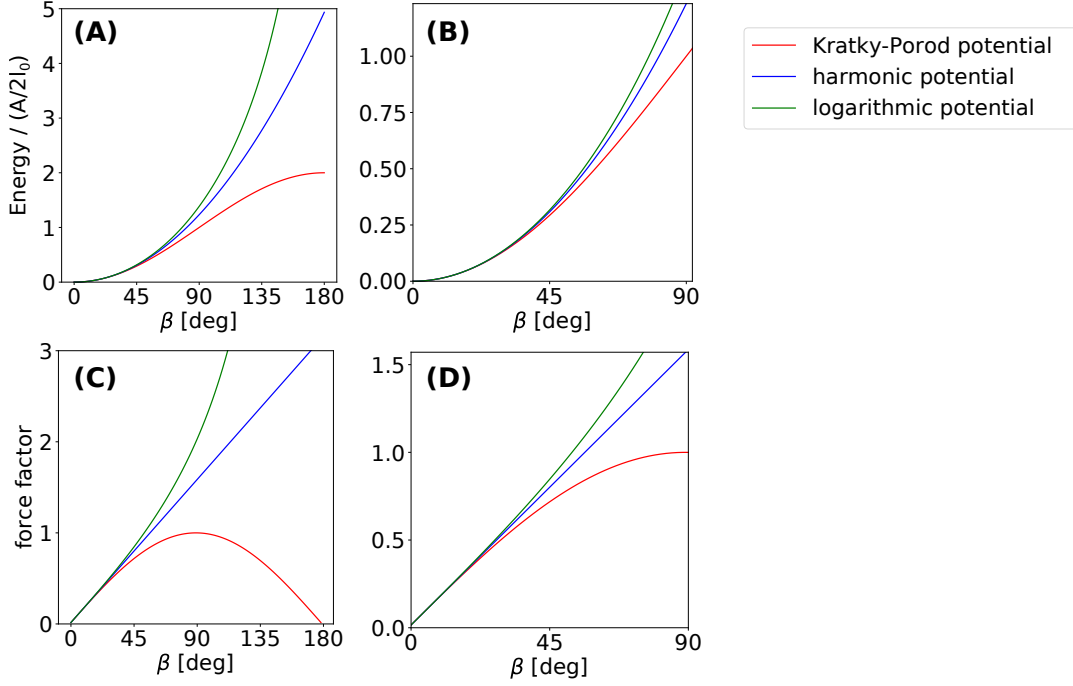


Figure 5.2: Normalized bending energy and force factor calculated for different potentials: Kratky-Porod, harmonic and logarithmic. (A) Normalized bending energy for wide range of angle β ; (B) Enlarged fragment of fig. (A) shows that the energy is similar for moderate (most common) values of bending angle; (C) Force factor for wide range of angle β ; (D) Enlarged fragment of fig. (C).

5.3 Comparison of forces in discrete models for different bending potentials

5.3.1 Bending potential derivative

In discrete bead model, the equation (2.6) for bending force acting on i -th bead can be rewritten as:

$$\mathbf{f}_i^b = \frac{\partial U^b(\mathbf{r})}{\partial \mathbf{r}_i} = \sum_{j=2}^{N-1} \frac{\partial U_b}{\partial \beta_j} \frac{\partial \beta_j}{\partial \mathbf{r}_i} = \sum_{j=\max(2,i-1)}^{\min(N-1,i+1)} \frac{\partial U_b}{\partial \beta_j} \frac{\partial \beta_j}{\partial \mathbf{r}_i} \quad (5.11)$$

where the only non-vanishing terms come from neighboring angles β_{i-1} , β_i and β_{i+1} . For different bending potentials only terms $\partial U_b / \partial \beta_j$ are altered, and therefore this term will be discussed in some details. In ref. [159] its dimensionless form, given by:

$$f(\beta_j) = \frac{l_0}{A} \frac{\partial U_b}{\partial \beta_j} \quad (5.12)$$

is called ‘force factor’, and this nomenclature is to be used also here. Force factor scales contributions to bending force originating from bending angles, but does not carry information

about direction of these contributions. Force factor has a physical interpretation for the last bead in the chain: it is proportional to the bending force multiplied by the length of bond between the last and the last but one beads. Force factors calculated for different bending potentials are as follow:

$$f_{KP}(\beta) = \sin(\beta) \quad (5.13)$$

$$f_H(\beta) = \beta \quad (5.14)$$

$$f_{Log}(\beta) = \frac{2 \sin(\beta)}{1 + \cos \beta} \quad (5.15)$$

$$f_{\cos^2}(\beta) \sim (1 - \cos \beta) \sin \beta. \quad (5.16)$$

The formulas for first three bending potentials (5.14)-(5.16) are given in equations (2.3)-(2.5), while the last form of bending potential, mentioned in the previous section and sec. 2.5, is proportional to $\sum_i (1 - \cos \beta_i)^2$. Values of force factors are plotted in fig. 5.2. From equations written above and the figure it may be observed, that in harmonic model the force factor grows linearly, while in KP model growth is slower and slower because sine function is concave in the considered range $\beta \in [0, \pi]$. Physically it means that the resistance to bending may even decrease for sufficiently large angles. Force factor for logarithmic model, which is less commonly used than the former two, was also plotted in the same figure for comparison. In logarithmic bending model forces are stronger than in harmonic one and the force factor function $f_{Log}(\beta)$ is strictly convex. For Kratky-Porod, harmonic and logarithmic potentials, in the limit $\beta \rightarrow 0$, force factors always tends to β . The last potential discussed here, $\sim (1 - \cos \beta)^2$, is an exception because its force factor tends to β^3 for vanishing β . For this reason the force factor of this potential is not shown in the fig. 5.2, due to ambiguous scaling. Force factor of $\sim (1 - \cos \beta)^2$ potential reaches maximum at 120° and subsequently decreases towards 0 at 180° . In next sections, following ref. [159], the most popular Kratky-Porod and harmonic potentials will be analysed in more details.

5.3.2 Resultant bending forces in different models

In filament, resultant bending force acting on each bead depends on three consecutive angles. For i -th bead these angles are: β_i with vertex at the centre of i -th bead, β_{i-1} and β_{i+1} . If the i -th bead is close enough to the end of the filament, not all of these angles may exist. In order to study difference in elastic forces under Kratky-Porod and harmonic bending potentials (denoted as f_i^{KP} and f_i^H respectively), the analysis of force factor is not sufficient and we need to take into account contributions from triplets of consecutive angles.

In this section 5.3.2 forces are analysed for flat configurations of beads, where centres of 5 consecutive beads (which are necessary to establish three angles) lay in a single plane. Unlike

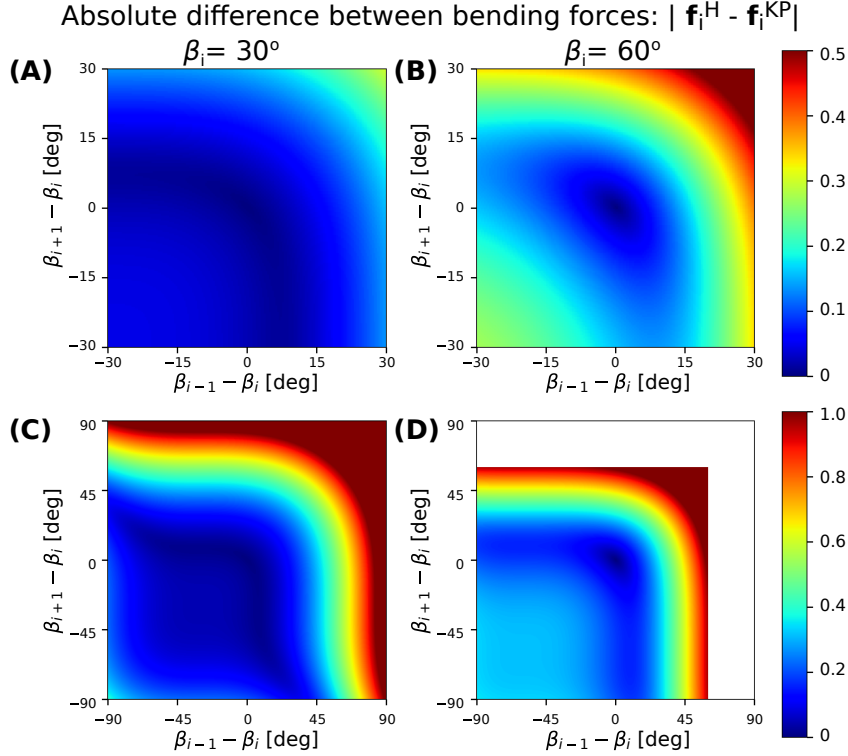


Figure 5.3: Magnitude of difference of bending force \mathbf{f}_i acting on i -th bead calculated with Kratky-Porod and harmonic potentials, normalized by A/l_0^2 . In panels (A) and (C) $\beta_i = 30^\circ$, in (B) and (D) $\beta_i = 60^\circ$. Top row (A)-(B) illustrates the range of β_{i-1}, β_{i+1} close to β_i , namely $\beta_{i-1}, \beta_{i+1} \in [\beta_i - 30^\circ, \beta_i + 30^\circ]$, while panels (C) and (D) cover wider range $\beta_{i-1}, \beta_{i+1} \in [\beta_i - 90^\circ, \beta_i + 90^\circ]$. In (D) only region of β_{i-1} and β_{i+1} smaller than 120° is shown because beads in the filament start to overlap for larger angles (for equilibrium length of bonds).

in the three dimensional space, for flat systems signed values of bending angles β_i can be used: positive values indicate the bend in the anticlockwise direction, while the negative sign the bend into clockwise direction. The allowed range of the values of a signed angle is: $\beta \in] - \pi, \pi]$ (for non-overlapping beads $\beta \in] - 2\pi/3, 2\pi/3]$). As it is useful to be able to distinct directions of bending, the signed values of angles will be used in this section.

Bending forces under distinct potentials are different both in terms of magnitude and the direction. In this section I present results for absolute difference of the forces $|\mathbf{f}_i^H - \mathbf{f}_i^{KP}|$ (fig. 5.3), relative difference $|\mathbf{f}_i^H - \mathbf{f}_i^{KP}|/|\mathbf{f}_i^H|$ (fig. 5.4) and the difference between directions of \mathbf{f}_i^{KP} and \mathbf{f}_i^H , quantified by measure of the angle between them (fig. 5.5).

The knowledge of absolute difference is important because it allows to compare uncertainty resulting from using different bending potentials with magnitude of other forces, e. g. gravitational, and gives the direct information about influence of bending potential on the velocity of beads. As the magnitude of the calculated force depends on bending stiffness A (or alternatively elasticity parameter B), in figure 5.3 it is normalized by A/l_0^2 . In order to obtain values in the normalization used elsewhere in this dissertation (force divided by G , see sec. 2.4), values from in fig. 5.3 should be multiplied by $(N - 1)^2/B$. Unsurprisingly, the

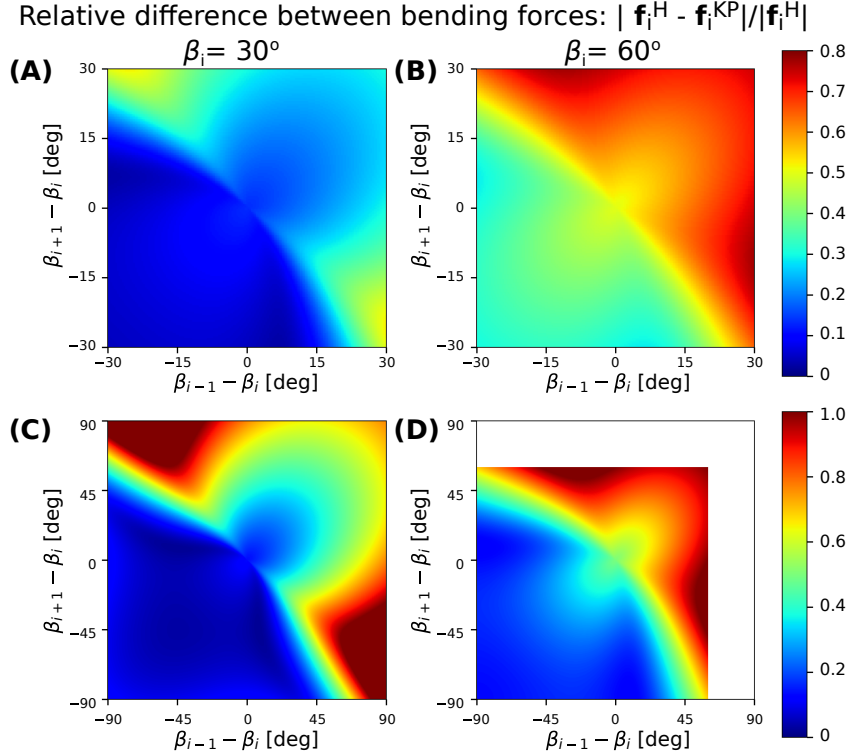


Figure 5.4: Relative difference of bending forces calculated with KP and harmonic potentials. Similarly as in fig. 5.3, left and right columns illustrate results for $\beta_i = 30^\circ$ and $\beta_i = 60^\circ$, respectively. Figures in the top row show enlarged central parts of figures in the bottom row, but with different colour scale. Figure reprinted from ref. [159].

absolute difference between forces calculated with the two bending models strongly depends on value of bending angles β_{i-1} , β_i and β_{i+1} . The largest difference is observed when the two side angles, β_{i-1} and β_{i+1} are in the upper limit of the explored range. Comparing results for $\beta_i = 30^\circ$ with those for $\beta_i = 60^\circ$ (that is 5.3A with 5.3B and 5.3C with 5.3D), a large difference in favour of larger value of β_i is visible. It should be also noted that if all three angles are equal, $\beta_{i-1} = \beta_i = \beta_{i+1}$, the absolute difference between forces \mathbf{f}_i^{KP} and \mathbf{f}_i^H is equal to 0, because in such case bending force acting on i -th bead has to vanish, what is a geometric fact valid for all forms of bending potential.

Relative error resulting from alternative forms of bending potential is shown in fig. 5.4. In some ways the relative difference between forces is more interesting than the absolute one, because it provides information about the effect of switching bending model in comparison to the actual influence of bending forces. Relative difference between forces is the smallest when both side angles β_{i-1} and β_{i+1} are smaller than central angle β_i . Larger difference is observed when the two side angles are greater than the central one, but the largest value of the difference is present when one of the side angles is smaller and the other greater than β_i . This observation holds for different values of β_i and both presented ranges of β_{i-1} and β_{i+1} . When considering influence of the value of the central angle, it can be noticed that for the case of the narrow range of β_{i-1} and β_{i+1} there is large difference between results for small central angle $\beta_i = 30^\circ$

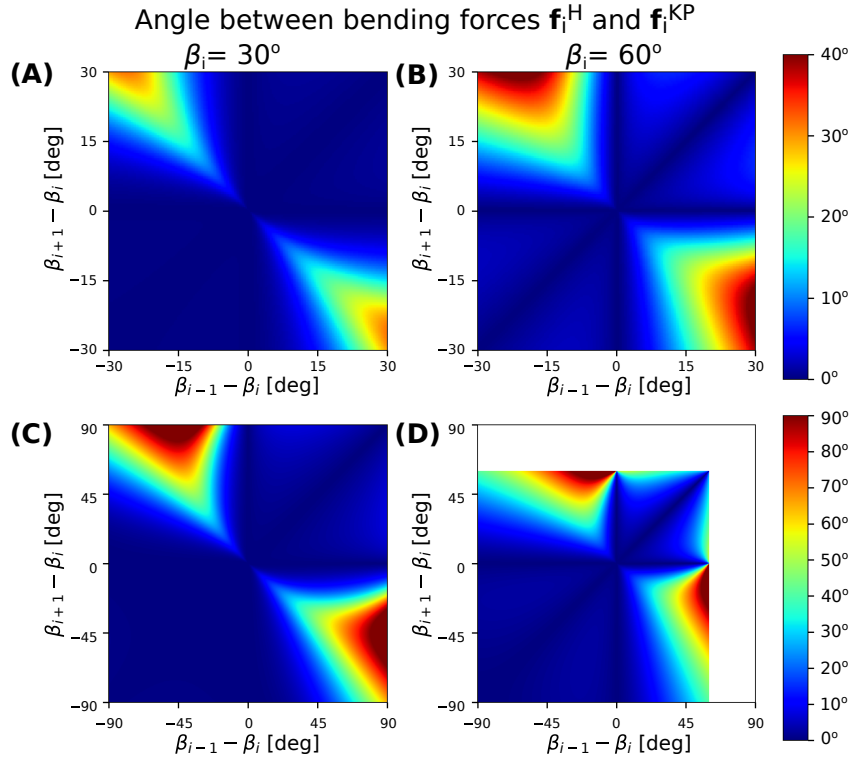


Figure 5.5: Angle between bending forces calculated with KP and harmonic potentials. Similarly as in fig. 5.3, left and right columns illustrate results for $\beta_i = 30^\circ$ and $\beta_i = 60^\circ$, respectively. Figures in the top row show enlarged central parts of figures in the bottom row, with different color scale.

and the large one $\beta_i = 60^\circ$. However, figure 5.4C shows that even for $\beta_i = 30^\circ$ the relative difference between forces can exceed 100% if the wide range of side angles is considered. Some configurations, including those with particularly large relative error, are shown in fig. 5.6. Another interesting observation is that even when the side angles are both equal to the central one, the relative difference between forces does not converge to 0, although the absolute value of bending force does.

The change of the direction of bending forces under different potentials is another feature that is worth to be analysed. Such measure is a useful supplement to absolute and relative differences of the forces. Figure 5.5 shows that direction of the bending force is almost unaffected when $\beta_{i-1} \approx \beta_{i+1}$ and can be strongly altered if $\beta_{i-1} - \beta_i$ and $\beta_{i+1} - \beta_i$ have different signs. The difference in the bending force direction between models can be as large as 30° for $\beta_i = 30^\circ$ and the narrow range of side angles, or 40° for $\beta_i = 60^\circ$ and the narrow range of side angles. For the wide range of side angles it can exceed 90° for both presented values of the central angle β_i .

The analysis provided above indicates that the error introduced by bending potential depends on the angles in a nonlinear way. It was shown that there exist some configurations where the error is large, even for not particularly unusual configurations of beads. A few examples of configurations with large difference in bending forces are presented in figure 5.6.

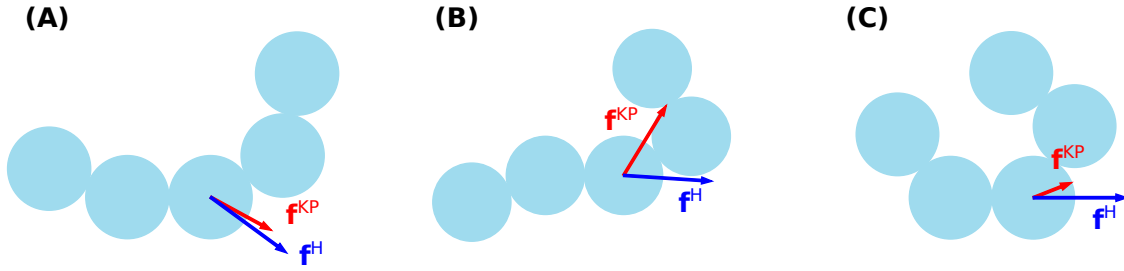


Figure 5.6: Three examples of configurations with large relative difference between forces calculated with different potentials. (A) $(\beta_{i-1}, \beta_i, \beta_{i+1}) = (20^\circ, 30^\circ, 50^\circ)$, (B) $(\beta_{i-1}, \beta_i, \beta_{i+1}) = (-20^\circ, 30^\circ, 90^\circ)$, (C) $(\beta_{i-1}, \beta_i, \beta_{i+1}) = (50^\circ, 60^\circ, 80^\circ)$

In figure 5.7 the absolute and relative differences between bending forces are summarized for wide range of angle β_i . Similarly as before in this chapter, the absolute difference is normalized by A/l_0^2 . Lines indicate maximal value of difference as a function of β_i for a given value of the threshold imposed on $|\beta_{i-1} - \beta_i| + |\beta_{i+1} - \beta_i|$. It can be noticed that the absolute value of the difference strongly depends on the chosen threshold: in other words, the absolute value of force difference remain small even for large values of bending angles, given that three consecutive angles have similar measure. In fig. 5.7A it is shown that maximal difference for $\beta_i = 120^\circ$ under 10° threshold is roughly as small as the maximal difference for 0° under 60° threshold. Figure 5.7B presents the relative difference of forces. In this case two distinct regimes may be distinguished: flat part for small value of β_i , and increasing, almost linear part for larger β_i . The length of the flat part of the plot depends on the threshold value, and is greater for larger values of the threshold. In the second phase the relative difference of the force grows with very similar rate for all threshold values. We can observe that the relative error of a few dozen percent is reached even for not very large angles, such as 30° - 60° and for small value of the threshold $|\beta_{i-1} - \beta_i| + |\beta_{i+1} - \beta_i|$ imposed on the side angles.

In conclusion, the form of bending potential may have significant effect on the resultant forces even for moderate values of angles. The differences between forces are large in terms of absolute values, relative values and the direction. As harmonic bending potential is better motivated theoretically, it should be the preferred choice.

5.4 Impact of the form of bending potential on the dynamics of elastic particles settling in a viscous fluid

In this section the dynamics of a few systems of settling elastic particles is analysed in order to reveal the influence of different forms of bending potential. These examples have been described by the author and M. Ekiel-Jezewska in ref. [159]. There exist also other systems

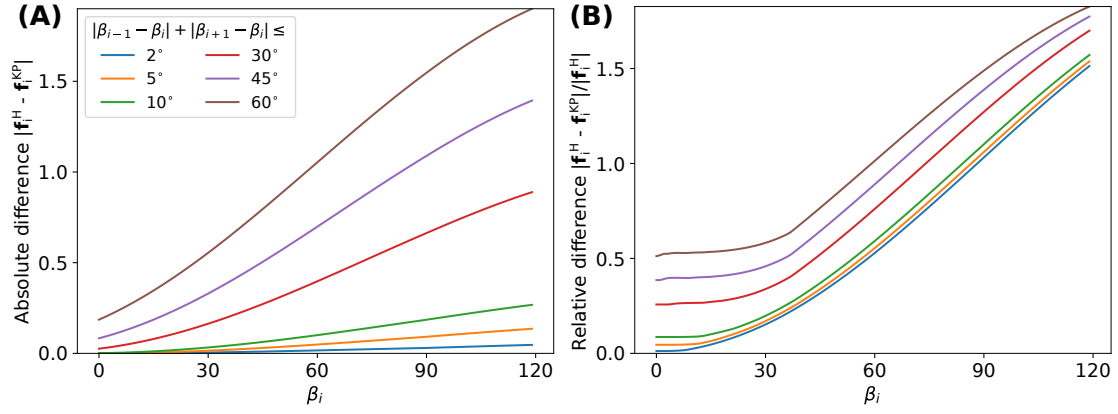


Figure 5.7: Maximal absolute (A) and relative (B) difference between models for a range of β_i . Different lines indicate different thresholds for $|\beta_{i-1} - \beta_i| + |\beta_{i+1} - \beta_i|$. Similarly as in fig. 5.3 the absolute dimensional value of force is divided here by A/l_0^2 . Panel (B) reprinted from [159].

where the form of bending potential plays a role, e.g. filament in flow, which are not shown here and can be a topic of future studies. Results presented in this section are described in terms of dimensionless variables, defined in sec. 2.4, similarly as elsewhere in this dissertation.

5.4.1 Single sedimenting trumbbell

A single sedimenting trumbbell is the simplest example studied in this chapter. Two types of trumbbells are considered: consisting of large beads, $a = a_{max} = l_0/2$, or small beads, $a = a_{max}/4 = l_0/8$. For this system, the existence and shape of the stationary configuration of the trumbbell is studied. We expect that the stable configuration of trumbbell is symmetric and restricted to the vertical plane, what reduces the number of degrees of freedom to two: bending angle β and bond length l , which is equal for the two bonds in the trumbbell (see fig. 5.8).

In order to investigate the existence of equilibrium configuration, the signs of time derivatives $d\beta/dt$ and dl/dt are evaluated in β, l phase space. Results for Kratky-Porod potential are presented in fig.5.9 for trumbbell with large beads and fig.5.10 with small ones. Results for harmonic potential are described later in the text. Different combinations of

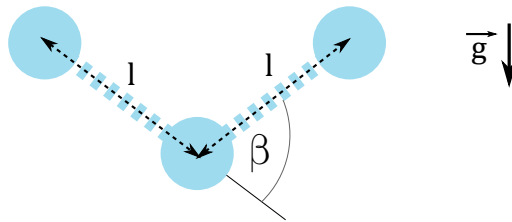


Figure 5.8: Scheme of a trumbbell in the equilibrium configuration, settling in the gravity field g . Centres of beads lay in the vertical plane. Two bonds have equal length l . β denotes the bending angle.

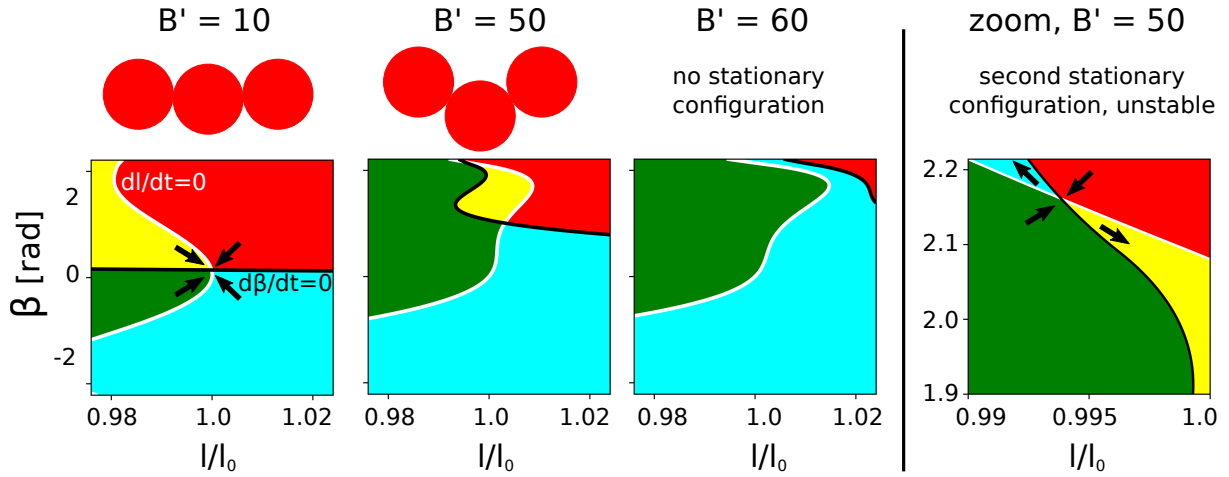


Figure 5.9: Phase space picturing signs of $d\beta/dt$ and dl/dt for KP bending potential: different colours represent different combinations of signs of derivatives, as indicated by black arrows in the first plot and explained in the main text. Above phase-space plots the equilibrium configurations of trumbell are shown, whenever exist for a given B' . In the right part of the figure the chosen region of phase-space for $B' = 50$ is enlarged in order to shown unstable stationary configuration. Figure reprinted from ref. [159].

derivatives signs are indicated in the figures with distinct colors: $(d\beta/dt < 0, dl/dt < 0)$ – red, $(d\beta/dt < 0, dl/dt > 0)$ – yellow, $(d\beta/dt > 0, dl/dt > 0)$ –green, and $(d\beta/dt > 0, dl/dt < 0)$ –blue. The line where $d\beta/dt$ changes sign is marked with black line, and the line $dl/dt = 0$ with white line. Consequently, equilibrium configurations can be found at the crossings of these lines. The full allowed range of β is shown in the figures, which is limited by the angles for which the margin beads touch each other.

Figures 5.9 and 5.10 illustrate that for trumbells with small or large beads there exists stable equilibrium configuration if particles are not too elastic. The position of this equilibrium depends on the elasticity parameter B' , defined in eq. (2.11). In particular, we can see that for both small and large beads the bending angle in equilibrium configuration is larger for more flexible particles. With Kratky-Porod model, the stationary configuration disappears for more elastic particles, without reaching maximal allowed value of β . Lack of stationary configuration is illustrated for trumbells with large beads at $B' = 60$ (fig. 5.9) and for trumbells with small beads at $B' = 75$ (fig. 5.10). Whenever stationary configuration does not exist, trumbells tend to collapse – marginal beads tend to hit each other – what can be deduced from the figures. The results for harmonic bending potentials are different, what will be discussed in later paragraphs.

Interestingly, for $B' = 50$ for trumbells with either small or large beads, a second stationary configuration is visible, which has much greater bending angle than the first one. However, these new stationary configurations are unstable, what is visible in the panels with enlarged regions of interest, shown in the right part of figures 5.9 and 5.10.

Existence of stationary configurations have been systematically investigated for different values of B' for Kratky-Porod and harmonic bending potentials. In figure 5.11 measure of

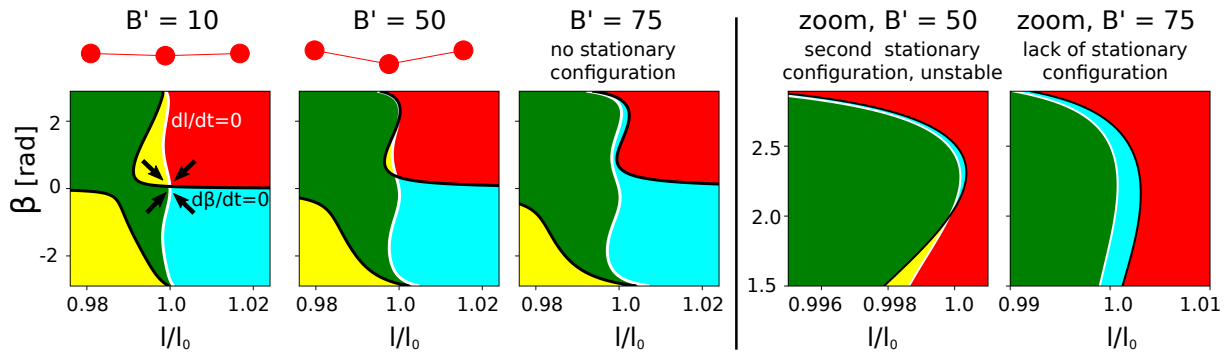


Figure 5.10: Phase space picturing signs of $d\beta/dt$ and dl/dt for a trumbbell with small beads and KP bending potential. Colour code the same as in fig. 5.9. For $B' = 10$ and $B' = 50$ stable configurations of trumbbell are drawn. In the right panel two enlarged regions are shown: first for $B' = 50$ presents unstable stationary configuration, and the second, $B' = 75$, clarifies that there is no stationary configuration even for large β . Figure reprinted from ref. [159].

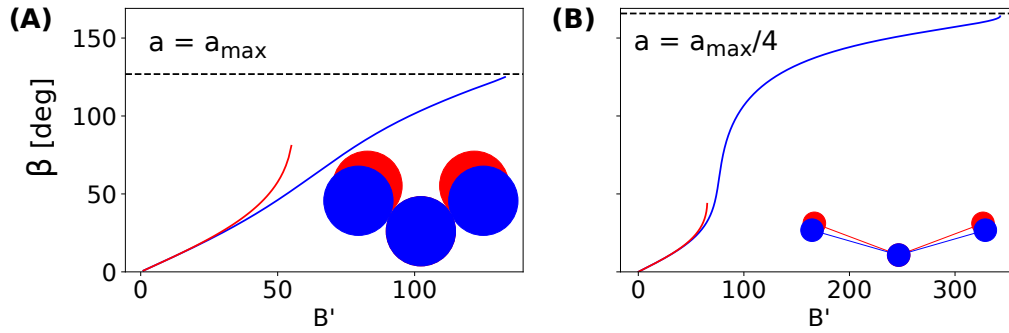


Figure 5.11: Value of the bending angle in stable configuration of trumbbell for Kratky-Porod (red) and harmonic (blue) bending potentials. Results shown for trumbbell with large (A) and small (B) beads. Stationary configurations are plotted for (A) $B' = 55$ and (B) $B' = 65$. Figure reprinted from ref. [159].

bending angle in found stationary configurations is shown. The first conclusion from the presented results is that the equilibrium configurations for trumbbells with harmonic potential can be found for much larger values of B' than with KP potential. With Kratky-Porod potential the value of bending angle at equilibrium configuration rises sharply and subsequently the stable configuration is lost for $B' < 56$ and $B' < 65.5$ in case of large and small beads, respectively. With harmonic bending potential equilibrium configuration can be found until the beads almost touch each other, what corresponds to value of β marked with dashed line in the figure. Equilibrium configurations obtained with the two bending potentials are compared in the bottom right corners of panels in fig. 5.11. Elasticity coefficient B' used in the comparison was chosen as a value close to the largest B' for which equilibrium configuration was found for both potentials. It can be observed that differences of configurations are significant, yet not striking. It is also noteworthy that in Kratky-Porod model trumbbell with small beads loses the stable configuration for very moderate bending angle β , far below value which would be intuitively guessed (at least by the author) as susceptible to subtle model differences.

In some studies, an additional very short scale repulsive potential is added to prohibit overlap of the beads [46,62], typically repulsive part of Lennard-Jones potential, which scales as $\sim r^{-12}$. In the system presented here such repulsive potential could prevent collision of beads and introduce additional stable configuration where beads are (almost) touching each other. However, such equilibrium configuration is essentially different than stationary configurations described in this section, and there is no continuity between these two kinds of stable configurations. In essence, trumbbells with short-range repulsive would still collapse at almost the same B' as shown here (due to negligible influence of introduced repulsion at long range), but the beads would stop shortly before touching each other, instead of overlap. Therefore the significant difference between dumbbells with Kratky-Porod and harmonic bending potential, described in this section, would persist.

Phase-space graphs 5.9 and 5.10 discussed in this section aim to show stability (or lack of stability) of equilibrium configuration against symmetric in-plane perturbations. Stability against random perturbations, in general non-symmetric and not restricted to the vertical plane, is analyzed in appendix B. It turns out that the stable configurations found in this section are also stable against random perturbations.

Results presented in this section indicate that the choice of bending model has a large impact on existence and location of stable equilibrium configuration for a single sedimenting trumbbell. Harmonic potential, which is in better agreement with continuous model of elastic particles than KP potential is, predicts stable stationary configurations of elastic trumbbell for broader range of B' and β .

5.4.2 Single sedimenting filament

The problem of a single sedimenting filament has been studied with bead model [6,7,10,12] as well as with slender body approximation [8,12]. It is known that for low or moderate flexibility the filament tends to a stable ‘U’-shape configuration. In this section I describe how the final shape of the filament depends on applied bending potential.

Comparison of the final configurations obtained with Kratky-Porod and harmonic bending potentials is shown in fig. 5.12A for chosen number of beads N and chosen elasticity B . It is visible, that for $N = 6$ and moderate elasticity $B = 125$, the stable shape of the filament is almost identical for the two bending potentials. For a very elastic filament $B = 300$ and $N = 6$ the difference is more significant. Values of B much greater than 300 are not shown because in Kratky-Porod model the marginal beads of filament start to overlap, what indicates that such values of parameters are beyond applicability of the model. For a filament consisting

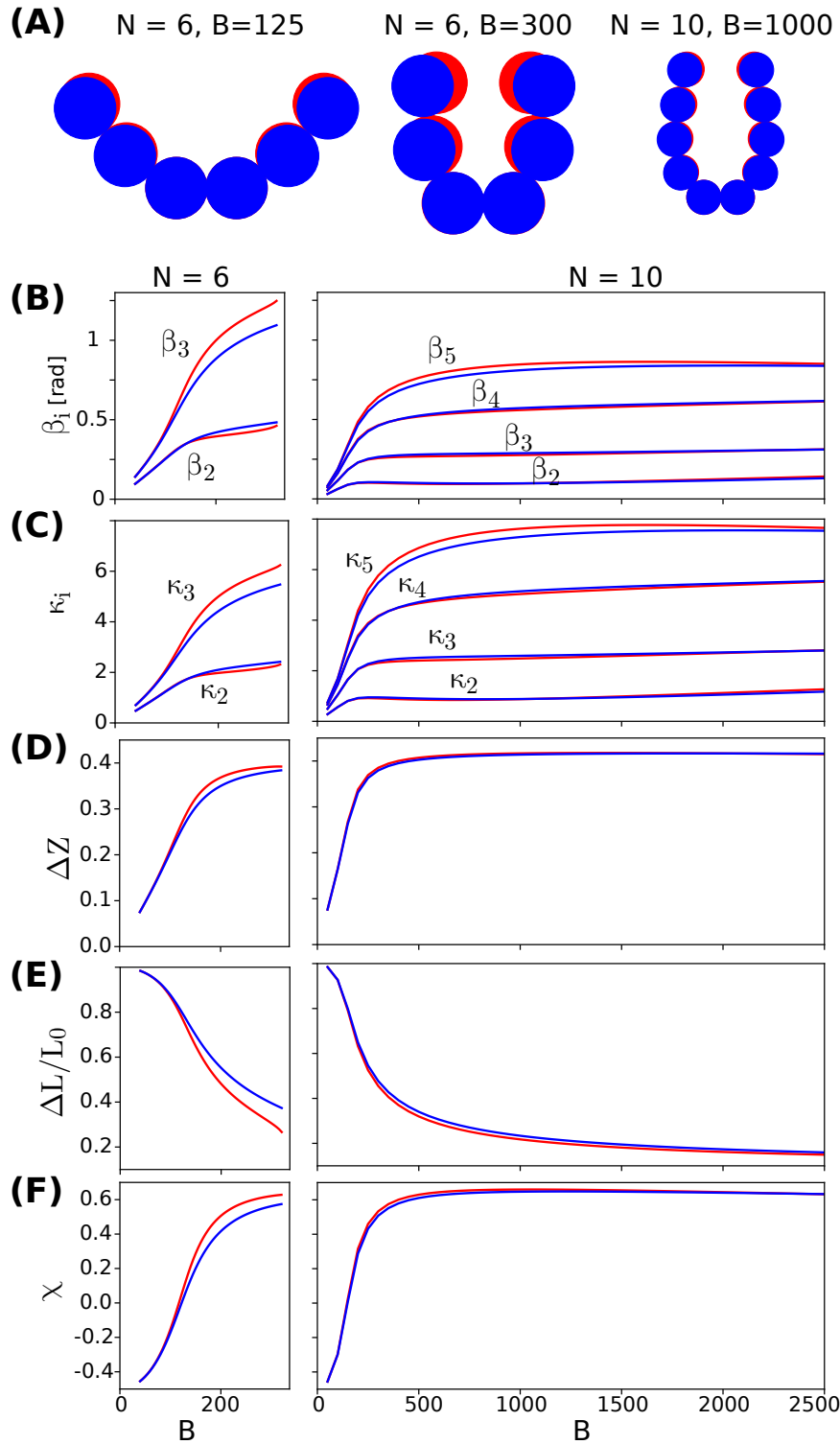


Figure 5.12: Influence of bending model on a single sedimenting filament consisting of 6 or 10 beads. Results for Kratky-Porod potential are shown in red and for harmonic potential in blue. (A) Stationary configurations shown for chosen values of N and B , (B) bending angles, (C) estimated curvatures of the segments, (D) amplitude, (E) end-to-end distance, (F) alignment parameter. Parameters shown in (B-F) are explained in the main text. Figure reprinted from [159].

of larger number of beads much greater values of B are achievable. In fig. 5.12A stationary configurations for $N = 10$ and $B = 1000$ are shown, for which it can be noticed that even for very flexible filaments the difference in the final shape for the two bending models is negligible.

In order to give more complete information about differences between stationary configurations obtained with different bending potentials a number of characteristic shape parameters was calculated, which are plotted in 5.12(B-F) against elasticity parameter B . The characteristic parameters are:

- **(B) angles β_i** – values of $(N - 2)/2$ bending angles are plotted (owing to the symmetry $\beta_i = \beta_{N+1-i}$) what allows to analyse the results in comparison with theoretical considerations on the bending angles influence, presented in sec. 5.3,
- **(C) curvature of the segment κ_i** – curvature of filament segment, estimated as $\kappa_i = \beta_i/l_0 \approx \beta_i/l_i$ which shows the difference between models in terms of parameter adequate for description of continuous filament. Similarly as for the angles, due to the symmetry of the system only $(N - 2)/2$ different curvatures κ_i are plotted,
- **(D) amplitude of fibre bend ΔZ** – the vertical distance between centres of the highest and the lowest bead. Amplitude is a measure commonly used to characterize shape of sedimenting filament [7, 8, 13],
- **(E) end-to-end distance $\Delta L/L_0$** – distance between centres of the first and last beads of filament,
- **(F) alignment parameter χ** – parameter used by Schlagberger and Netz [6], which is proportional to electric birefringence signal measured for suspension of charged filaments. The alignment parameter is given by [6] $\chi = \frac{1}{N-1} \sum_{i=1}^{N-1} \left(\frac{3}{2} (\hat{\mathbf{t}}_i \cdot \hat{\mathbf{z}})^2 - \frac{1}{2} \right)$

In agreement with predictions, differences between Kratky-Porod and harmonic potentials appear when angles are large enough. If all bending angles are smaller than 30° (0.5 radians) the curves in fig. 5.12B-F are hardly distinguishable. The values of some characteristic parameters are significantly different for short filament $N = 6$ (corresponding to small aspect ratio) with large elasticity B . The difference between models is the most pronounced in case of end-to-end distance (fig. 5.12E), alignment parameter (fig. 5.12F) and curvature/bending angles (fig. 5.12B,C). The amplitude of the filament bend remains almost unaffected (fig. 5.12D). In case of the filament with larger aspect ratio ($N = 10$) the difference between models is small for all examined values of B . This observation may be explained by values of bending angles: in fig. 5.12B,C we can see that although estimated curvatures of the filament are similar for both

analysed numbers of beads, the bending angles for $N = 10$ are significantly smaller than for shorter filament, $N = 6$.

In conclusion, for the problem of a single sedimenting filament with relatively small bending angles the form of bending potential is not relevant, unless high accuracy of the filament shape prediction is required. If bending angles become large, the differences in the filament's shape are visible.

5.4.3 Two trumbbells sedimenting in vertical plane

Unlike single trumbbell or filament, two trumbbells sedimenting in a vertical plane, in general, do not have a steady configuration toward which the dynamics converges. Therefore this problem is of a different kind than stable configuration problems described in two previous examples (sections 5.4.1 and 5.4.2).

It turns out that the form of bending potential has a huge impact on the dynamics, and Kratky-Porod can lead to spurious effects if trumbbells are too flexible – with B' of the order of 300. Both the accurate dynamics of pair of trumbbells and the spurious effects are described in sections 6.2 and 6.3 together with a short discussion.

6 Flexible particles in the vertical plane

6.1 Dynamics of filaments

The dynamics of a single filament settling under gravity in a vertical plane is relatively simple: in the range of elasticity considered in this work the particle bends to a stable ‘U’-shape configuration, which depends on the flexibility parameter B (see ref. [6–8, 10, 12] and sections 1.3.2 and 5.4.2 in this dissertation). In this chapter I will describe the system of two fibres in symmetric configurations which are restricted to the vertical plane. Such family of initial configurations has been already analysed by Llopis et al. [13] for particles consisting of 30 beads with Kratky-Porod bending potential. The chapter starts with a brief summary of their study. Later new, more general results are presented, which I obtained for shorter filaments with harmonic bending potential. The dynamics of two filaments in the vertical plane will serve also as a reference in the following chapters, describing more general case where symmetric pair of particles can perform three dimensional dynamics.

Llopis et al. [13] showed that for relatively long filaments ($N = 30$) there exist two regimes: more stiff particles approach each other and finally collide while more elastic filaments drift apart. Additionally the limit between these regimes depends on the initial distance. Results shown by the authors in their fig. 9a suggest that for B below $B \approx 150$ filaments initially attract each other even at very large distances, while for larger flexibility there exists a threshold value of distance above which filaments repel each other. Finally, for B larger than $B \approx 230$ filaments always repel each other.

The authors underline rotation of more stiff filaments and scrutinize dependence of initial angular velocity on distance between filaments (denoted as d), finding that it scales as $\sim d^{-1/2}$ at short distances and $\sim d^{-2}$ for large ones, consistently with far-field approximation. Authors speculate about tumbling motion for more rigid filaments, however for relatively long particles studied in the article, consisting of 30 beads, tumbling dynamics was not found.

6.1.1 Dynamics of short filaments

In this dissertation relatively short filaments are studied using harmonic bending potential. Similarly as in chapters 4 and 7, the particles are initially horizontal, straight and in elastic

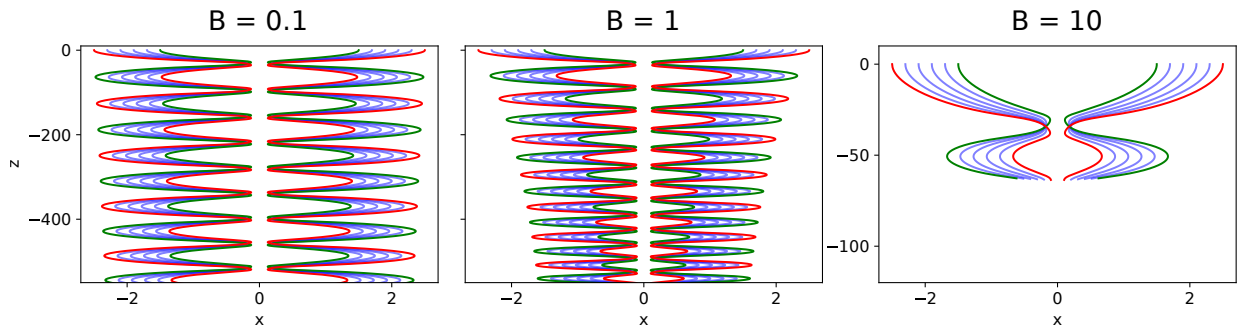


Figure 6.1: Dynamics of short ($N = 6$) and relatively stiff filaments: trajectories of all beads. For $B = 0.1$ dynamics is almost periodic, for $B = 1$ a noticeable change of trajectory shape is observed and for $B = 10$ filaments collide after one ‘tumble’. Trajectories are shown up to the collision time.

equilibrium. First, let us consider regime of weakly flexible filaments. It was already shown in chapter 4 that for stiff filaments consisting of 10 (or more) beads under Rotne-Prager approximation particles may either overlap or drift to infinity (or both), while tumbling dynamics without overlaps of beads does not exist. In agreement with the limit of stiff particles, weakly flexible filaments consisting of 10 beads approach each other and collide.

For shorter filaments $N = 6$ the tumbling dynamics is possible, as presented in fig. 6.1. For $B = 0.1$ the dynamics of filaments is almost periodic and deviation from periodicity is practically invisible. For larger $B = 1$ it can be observed that the width of trajectory decreases over time. Deviation from periodicity is greater for more flexible filaments. For $B = 10$ only a single ‘tumble’ is observed, after which particles temporarily move apart, later reach horizontal configuration, start to move back, and finally collide before the second ‘tumble’ may occur. The dynamics presented in this section, and in consequence also values of B characteristic for different types of behaviour, regard initial distance between filaments centres equal to 4 ($x_{CM}(0) = 2$). The corresponding values of B may be slightly different for other initial distances, however it was checked that for other values of $x_{CM}(0) \in [1.5, 10.0]$ the results are qualitatively the same.

For more flexible filaments the dynamics is consistent with study by Llopis et al. [13]: for smaller B filaments approach each other and collide, while for larger B filaments move away from each other. Results for $N = 6$ and $N = 10$ are shown in figures 6.2 and 6.3 respectively. If B is close to a value which separates these two types of dynamics, filaments settle almost vertically (neither attract nor repel each other), as in middle panels of figure 6.2A and 6.3A. Configuration of filaments are shown in fig. 6.2B and fig. 6.3B.

Results presented here have been obtained for initial distance between centres of particles 4 times larger than filament length. Unlike in ref. [13], the boundary between attraction and repulsion regimes was not systematically studied as a function of distance between particles.

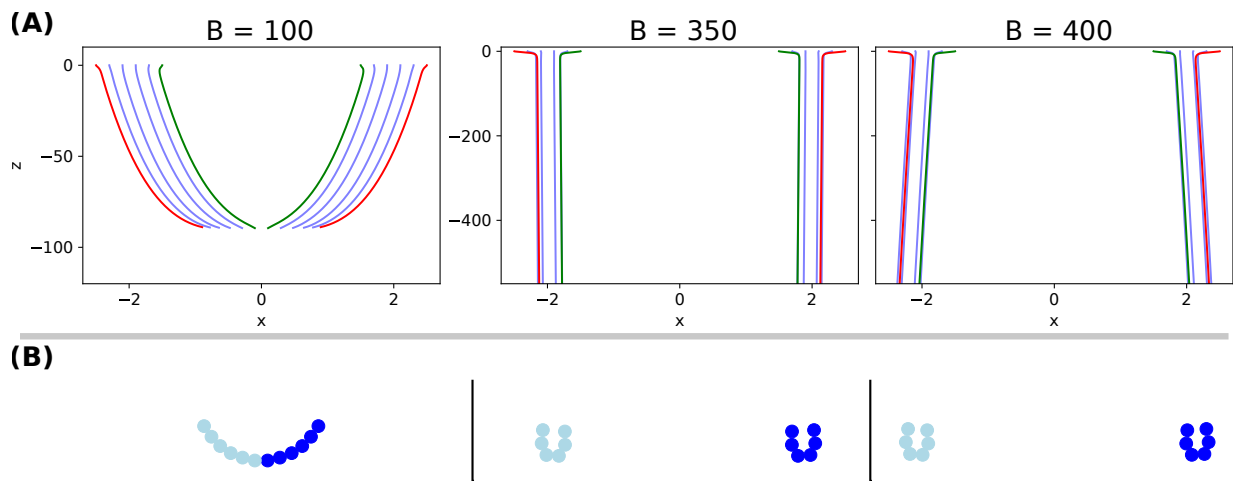


Figure 6.2: Dynamics of short ($N = 6$) and relatively flexible filaments with different values of parameter B . (A) Trajectories of beads, (B) configurations of filaments at the end of the simulation for $B = 350$ and $B = 400$ and at the collision time for $B = 100$. Less flexible filaments attract each other ($B = 100$), for $B = 350$ filaments settle almost vertically, while more elastic filaments $B = 400$ weakly repel each other.

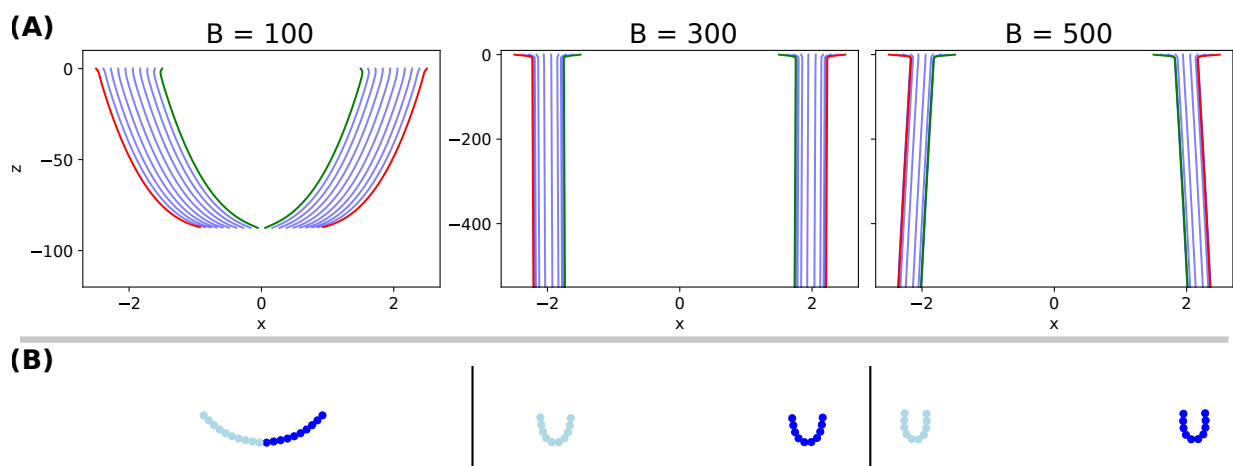


Figure 6.3: Dynamics of filaments consisting of 10 beads. (A) Trajectories of beads, (B) configurations of filaments at the end of the simulation ($B = 300$ and $B = 500$) or at the collision time for $B = 100$. Results are analogous to those for $N = 6$, shown in fig. 6.2.

6.1.2 Discussion of results

Results shown here are consistent with the known dynamics of longer filaments in plane, where attractive regime for more stiff, and repulsive regime for more flexible particles are identified. Additionally for short and relatively stiff filaments ($N = 6$) a new tumbling regime was found¹, in agreement with the limit of $B \rightarrow 0$. For longer ($N = 10$) and relatively stiff filaments, similarly as for rigid rods, particles collide. It is worth to stress again that the ‘collisions’ observed here, or in the cited articles, are only possible due to shortages of the models (lack of lubrication effects) and in principle cannot occur in the Stokes flow.

6.2 Dynamics of trumbbells

Dynamics of two elastic trumbbells in a vertical plane was studied by the author and Ekiel-Jezewska, and was described in ref. [159]. The results presented below are obtained with harmonic bending potential.

Initially, similarly as filaments, trumbbells approach each other. The motion is faster for more rigid particles and slower for more elastic, what is shown in supplementary videos of the article cited above. After the initial attraction phase the dynamics of trumbbells is different than the dynamics of filaments: if the filaments are not too flexible, periodic motions are observed. After approaching each other, the trumbbells, unlike filaments, rotate quickly enough to avoid collision and reorient themselves, so that particles move away from each other. Next, the dynamics converge to a periodic mode, illustrated in fig. 6.4. We can observe that trumbbells stay close to each other during the motion. Period of the motion shown in the fig. 6.4 is equal to $T = 8.75$ (results for $B' = 75$ and $a = a_{max}/4$). Periodic dynamics is observed for particles with different sizes of beads and different flexibility, up to a certain level of B' . The behaviour of very elastic trumbbells is described later in sec. 6.3.1.

Independently of the initial separation distance, the dynamics of trumbbells converges to a specific periodic orbit (with some time shift): period of the motion, distance between trajectories of the two particles and shape of the trajectory depend only on the trumbbell flexibility and on the beads radii. Dependence on B' and a is illustrated in figure 6.5A and B, respectively. It turns out that the shape of trajectory is only weakly sensitive to change of these parameters. In particular the distance between oscillating trumbbells is almost the same in all investigated cases. This observation leads to conclusion that elastic trumbbells within a wide range of parameters tend to approach very similar dynamics. The convergence to a single orbit form different initial separation distance is shown in fig. 6.5C.

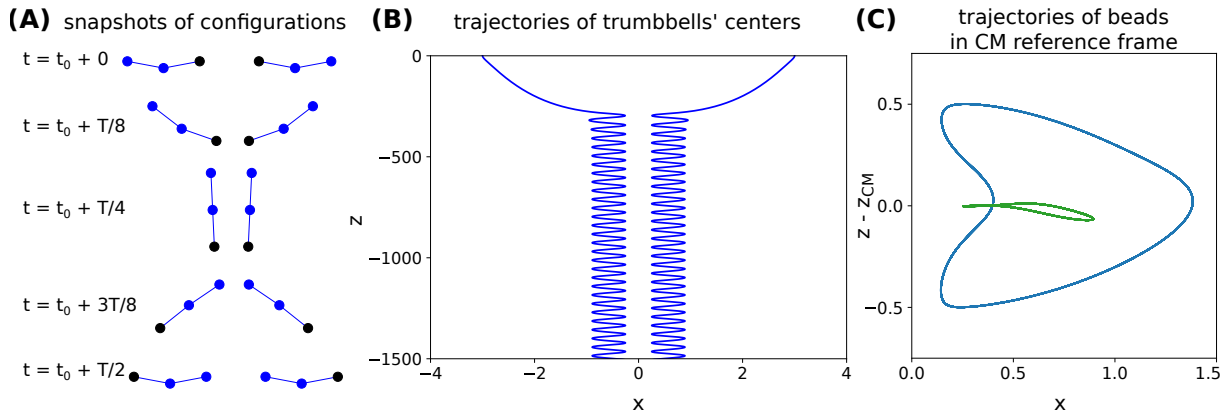


Figure 6.4: Periodic dynamics of trumbbells: (A) Snapshots of trumbbells configuration illustrate tumbling dynamics. (B) Trajectories of centres of mass of the trumbbells in the laboratory reference frame. (C) Trajectories of beads from the ‘right’ particle in the reference frame settling with the center of mass of the particles: green – central beads, blue – marginal beads. Unlike previously shown periodic trajectories, due to bending of particles there are no symmetry with respect to reflection in a horizontal plane. Graphs in panels A-C are shown for $B' = 75$ and $a = a_{max}/4$. Figure (A) reprinted from [159].

Periodicity observed in the dynamics of trumbbells is particularly interesting, because the system has three degrees of freedom. In case of dumbbells, periodic motion was found for systems with two degrees of freedom (no spring $k = 0$ or stiff joint with $k \rightarrow \infty$, sec. 3.2) and when the third degree of freedom – by the elasticity of the bond – was introduced, the dynamics became non-periodic (sec. 3.3).

¹Predicted, yet not observed by Llopis et al. [13].

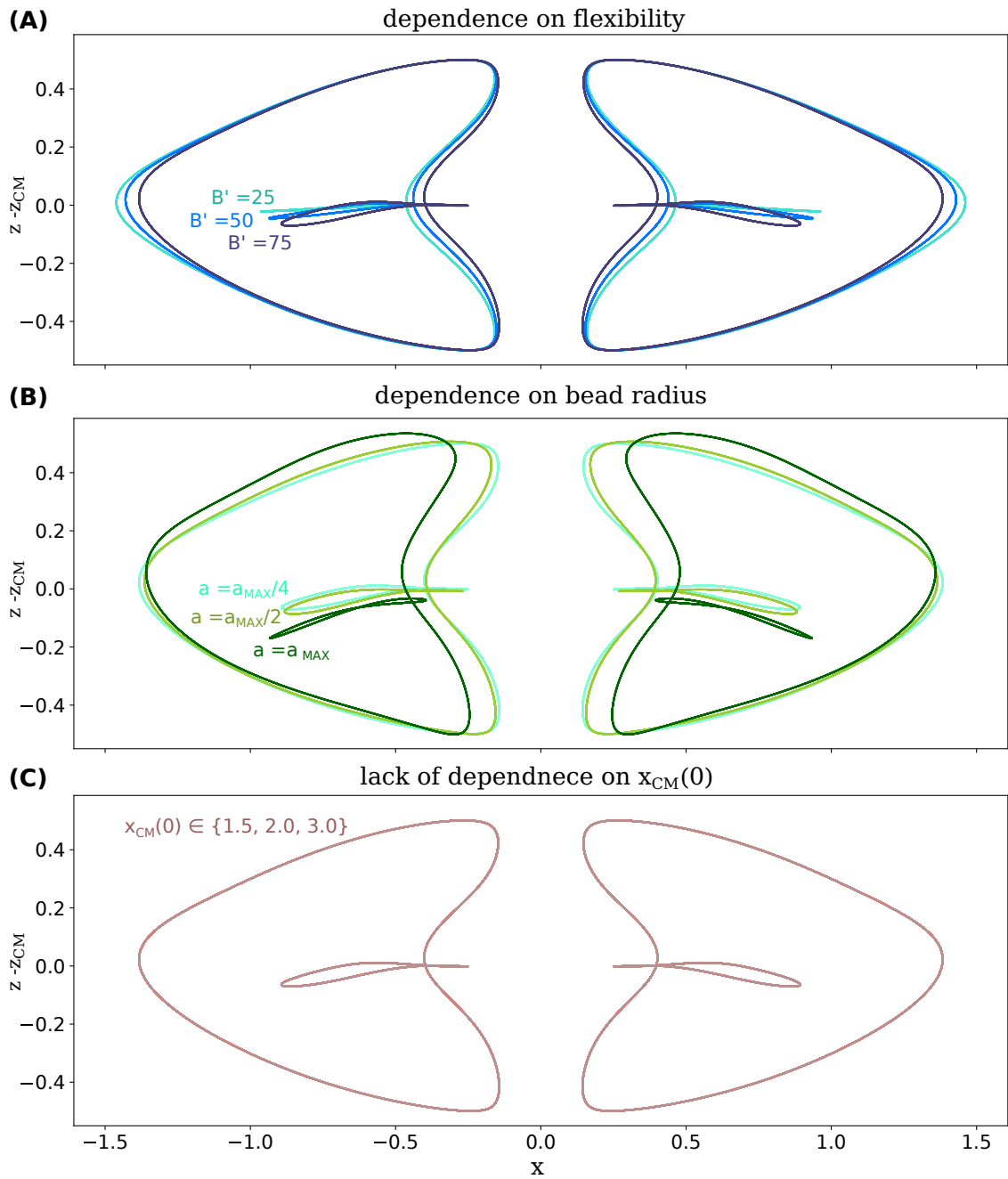


Figure 6.5: Trajectories of beads are plotted in reference frame falling with the particles. (A) Dependence on the flexibility parameter B' . (B) Dependence on the bead size. (C) Lack of dependence on the initial distance between trumbbells: trajectories calculated for different initial distances overlay. If not stated otherwise, trajectories shown for $B' = 75$ and $a = a_{max}/4$.

6.3 Example of spurious dynamics caused by inappropriate bending potential

It was previously shown in chapter 5 that different bending potentials may lead to different dynamics of particles. The question if any significant differences will occur may be difficult to be answered in advance because it depends whether the resulting differences in bending forces would amplify or attenuate in the course of the dynamics. In this section the influence of bending potential in the system of two sedimenting trumbbells is shown.

As long as the flexibility of trumbbells is not too large, results obtained with harmonic and Kratky-Porod bending potentials are very similar (fig. 6.6A): the initial attracting phase is visible, followed by the periodic oscillations. For larger B' with KP potential spurious repulsive dynamics is observed (fig. 6.6B), not present for harmonic potential neither for the same, nor for larger values of B' .

The discrepancy in the dynamics has the origin in the initial phase, when trumbbells approach each other, before oscillation phase. In this stage of dynamics the bending angle has the largest value (fig. 6.7). Indeed, it was checked by the author that if trumbbells with KP potential and $B' = 75$ start from configuration already at the periodic orbit, they do follow periodic dynamics rather than the spurious one found for horizontal initial configuration. This happens because in the periodic phase the value of bending angle is significantly smaller and therefore differences between bending models are not as large as in the relaxation phase. In the opposite situation, if we let trumbbells with harmonic potential start from a configuration taken from the repulsive phase of KP dynamics, the particles still converge to the periodic trajectory.

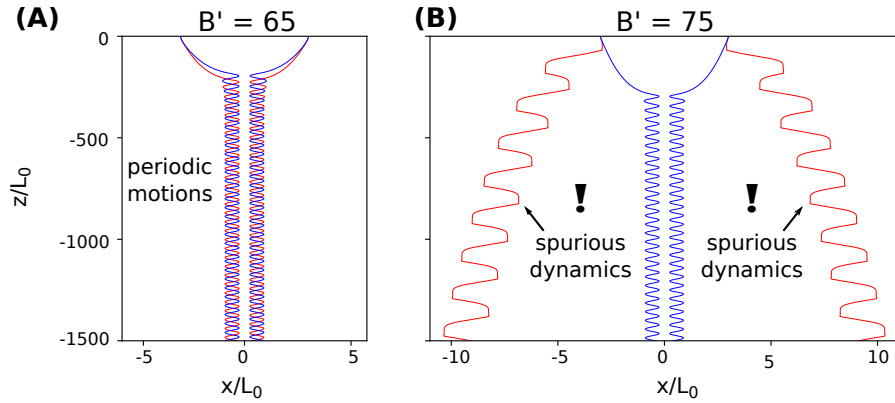


Figure 6.6: Comparison of dynamics of trumbbells calculated with Kratky-Porod (red) and harmonic (blue) bending potential: trajectories of centers of the trumbbells. (A) Periodic dynamics is obtained for both bending potentials. Trajectories are almost identical yet shifted in vertical direction. (B) Periodic dynamics is found with harmonic potential, while for Kratky-Porod potential spurious repulsive dynamics is observed. This kind of dynamics is not observed for harmonic potential even for larger B' . Results for $a = a_{max}/4$. Figure reprinted from [159].

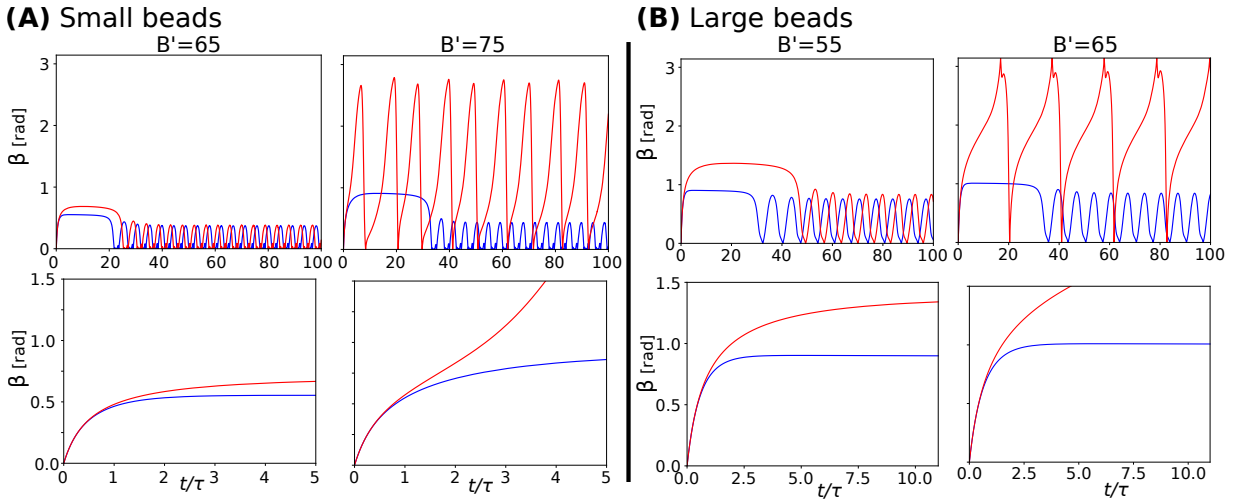


Figure 6.7: Bending angle of the trumbell in time. One can observe that value of bending angle is the largest in the initial phase of the dynamics, before trumbbells begin to oscillate. Results shown for: (A) small beads $a = a_{max}/4$, (B) large beads $a = a_{max}$. Figure reprinted from [159].

6.3.1 Very flexible trumbbells

Oscillatory, non-periodic, repulsive dynamics observed for Kratky-Porod bending potential was described as a spurious behaviour caused by the applied form of bending model. However, in order to show that the difference between different bending potentials is not only quantitative but also qualitative, it is necessary to study the dynamics of very elastic trumbbells with harmonic model. If the oscillatory repulsive dynamics in KP potential was present in harmonic model for larger B' , the conclusion would be that differences are quantitative: the form of bending potential may shift range of B' for which certain types of dynamics are observed, but do not change types of dynamics themselves, nor introduce new, spurious ones. It turns out that it is not the case and the Kratky-Porod bending potential actually introduces oscillatory, repulsive behaviour which is not observed in harmonic model even for larger flexibility. For very elastic trumbbells with harmonic bending potential different type of dynamics is obtained: particles move away from each other without oscillation. The trajectories of centres of trumbbells and their configuration are shown in figure 6.8. It is worth to notice that the same type of dynamics was observed for very elastic filaments, although it was not analysed whether the same mechanics is behind repulsion of trumbbells and filaments.

In order to further explore the influence of bending model on trumbbells dynamics, two other forms of potential were studied: logarithmic and 'improved KP', the latter introduced in ref. [159]. Logarithmic potential is even steeper than harmonic (see sec. 2.2.2) and it was used in order to study whether the dynamics observed for the harmonic model would be conserved. The 'improved KP' potential is an intermediate form of potential, between Kratky-Porod and harmonic model. It has the form:

$$\begin{aligned}
 U_{iKP}^b(\beta) &= \frac{A}{2l_0} \left[(\hat{\mathbf{t}}_2 - \hat{\mathbf{t}}_1)^2 + \frac{1}{6}(\hat{\mathbf{t}}_2 - \hat{\mathbf{t}}_1)^4 \right] \\
 &= \frac{A}{l_0} \left[(1 - \cos \beta) + \frac{1}{6}(1 - \cos \beta)^2 \right]
 \end{aligned} \tag{6.1}$$

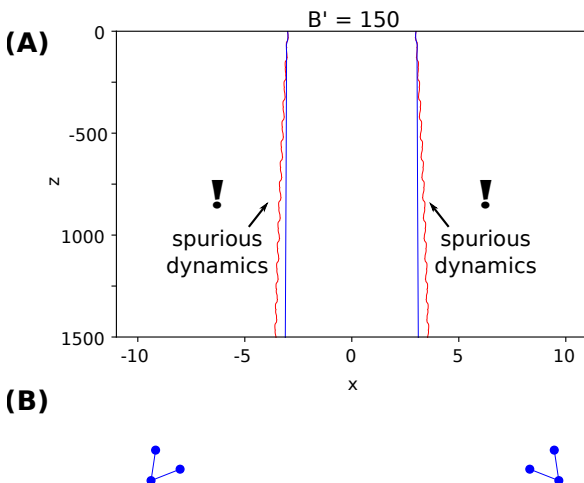


Figure 6.8: Dynamics of very elastic trumbbells. (A) Trajectories of trumbbells centers for dynamics with KP (red) and harmonic (blue) potentials. (B) Configuration of trumbbells while slowly moving apart for the harmonic potential. Figure reprinted from [159].

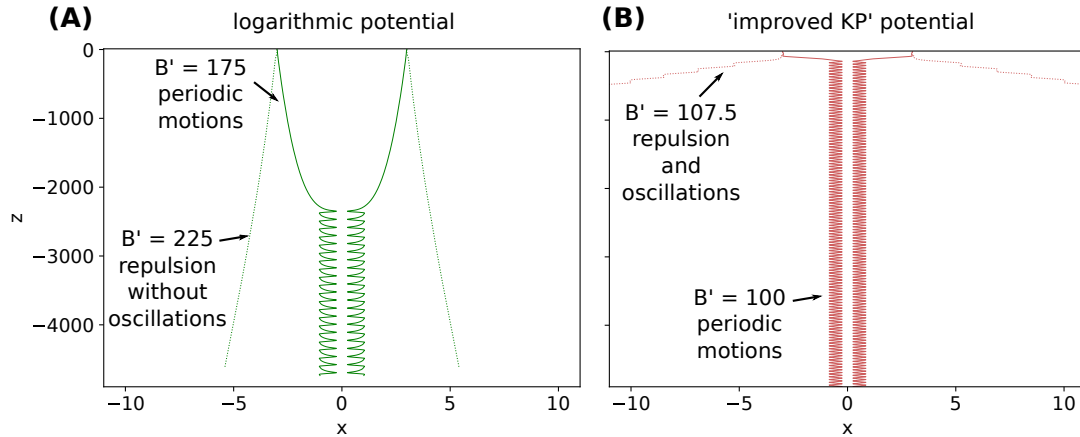


Figure 6.9: Transition from periodic to repulsive dynamics for trumbbells with alternative bending potentials: (A) logarithmic and (B) 'improved KP' (see main text for the description). Trajectories of trumbbells centres of mass are plotted for B' for which periodic motions are observed (solid lines) and larger B' for which trumbbells repel each other (dotted lines). It can be observed that repulsive dynamics is different for different forms of bending potential.

It was designed in the way that the deviation from harmonic potential is of the order of β^6 instead of β^4 as in the original KP. 'Improved KP' potential was introduced in order to study the transition between KP and harmonic models.

The results show that trumbbells with logarithmic bending potential behave in the same way as with harmonic one: for small B' periodic dynamics is observed while for larger B' particles move apart without oscillations. Differences are only quantitative: in logarithmic model transition between periodic and repulsive mode occurs for B' between 175 and 200, while for harmonic model between $B' = 135$ and $B' = 137.5$. Trumbbells with 'improved KP' bending potentials behave similarly as with KP. For B' between 105 and 107.5 (in comparison to 65 – 67.5 for 'standard' KP) transition from periodic to oscillatory repulsive dynamics is observed. Transitions between modes of dynamics described above for logarithmic and 'improved KP' bending potentials are illustrated in figure 6.9, where trajectories of trumbbells centres are plotted. The results suggest that 'improved KP' model shares the weaknesses of the KP potential, while the logarithmic model seems a reasonable alternative for the harmonic one. An additional advantage of the logarithmic bending potential is that it prevents bonds from reaching the non-physical limit of 180° , for which limit the bending energy tends to infinity.

7 Dynamics of elastic particles out of the vertical plane

In this chapter the dynamics of symmetric pair of elastic, elongated particles is analysed for initial configurations which are not restricted to the vertical plane. Both filaments and trumbbells are investigated. The behaviour of particles depends on the elasticity parameter B . The limit $B \rightarrow 0$ corresponds to the rigid particles and was described in chapter 4. In section 7.1 the general overview of the dynamics of the flexible filaments is presented for wide range of B . Subsequently in sections 7.2 and 7.3 the most important aspects of flexible filaments' behaviour are analysed. The special attention is paid to the regime of quite rigid particles, $B \leq 100$, because this range of B is the most interesting from the experimental point of view. The dynamics of trumbbells, which are the simplest models of bending particles, is described in section 7.4. Finally, in section 7.5, the main results for the symmetric pair of flexible particles are summarized.

7.1 Dynamics of filaments -general picture

The dynamics of elastic particles is very rich and depends on the flexibility parameter. Different types of the dynamics are shown in the figure 7.1. For small B the filaments initially behave similarly to the rigid particles (chap. 4): persistent oscillations are observed. However, in opposite to rigid particles case, the dynamics is not strictly periodic. Instead, the amplitude of oscillations decrease with time and finally the particles reach horizontal, aligned configuration in which they are oriented along y axis ($\theta = \pi/2$ and $\varphi \pm \pi/2$, depending whether the $\varphi(0)$ is negative or positive). This kind of the dynamics is illustrated in the figure 7.1 for $B = 10$. For more elastic particles the attenuation of oscillations is faster and for the value of B large enough the oscillations may even not be present or have negligible amplitude. In such case the particles align horizontally without significant oscillations. An example of such motion is shown in figure 7.1 for $B = 100$, where oscillations are present, yet with very small amplitude. Since the dynamics without oscillations and with oscillations of negligible amplitude (which are quickly attenuated) are from the practical point of view very similar, in this dissertation I do not focus on distinction between these two regimes.

Very elastic filaments do not align. For values of B larger than in the alignment regime the particles initially approach each other, rotate, and subsequently move apart without reaching

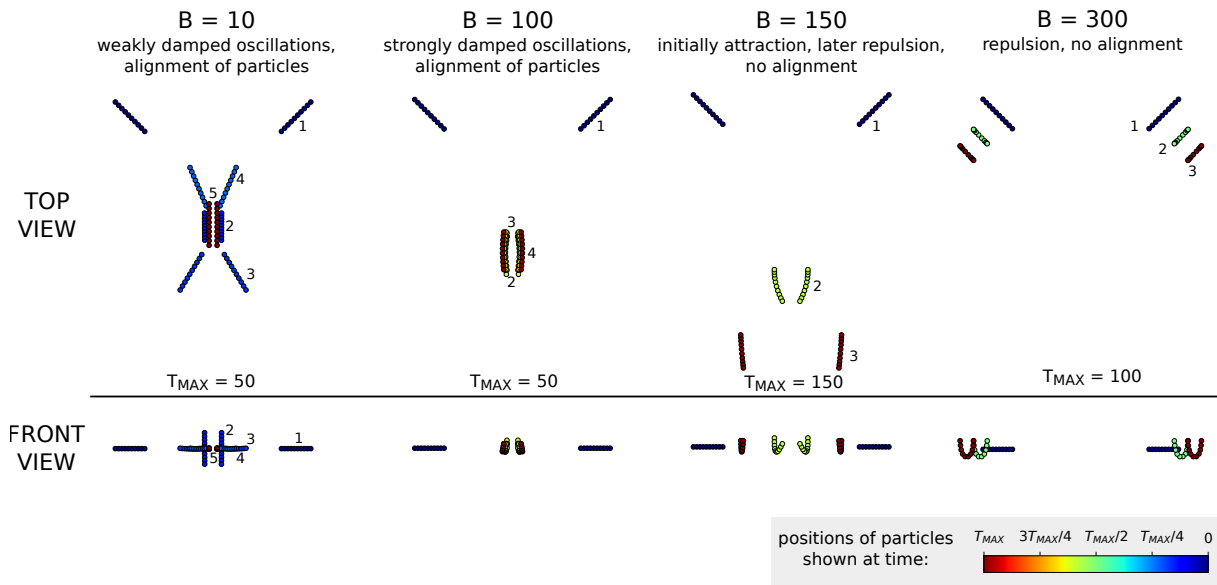


Figure 7.1: Different types of dynamics of two elastic filaments. Colour of the particles marks time when the snapshot was taken with respect to T_{MAX} , different for each B . Dynamics shown for $x_{CM}(0) = 2$ and $\varphi(0) = 45^\circ$. Figure reprinted from [169].

$\varphi = \pi/2$ (fig. 7.1 for $B = 150$), as it happens in the normal ‘tumble’ event. The drift of particles away from each other is a permanent process. It was investigated that this feature of the dynamics does not change even after 10^4 time units, in comparison to the period time $T \approx 25$ in an analogous system of rigid particles and simulation times 50 and 200 shown in the figure 7.1. Particles which are even more flexible perform yet another type of dynamics. After very short relaxation time, when the filaments form ‘U’-shape, the particles start to repel each other. Also in this case it was checked that up to the time of 10^4 time units the repulsion is still present. Apart from the three types of dynamics described above (horizontal alignment shown in fig. 7.1 for $B \in \{10, 100\}$, attraction with subsequent repulsion shown for $B = 150$ and repulsion shown for $B = 300$) there is also a fourth possibility, in which the filaments spuriously ‘collide’ when approaching each other. This behaviour is not surprising, given that this kind of behaviour was observed also in the limiting case of the dynamics restricted to the vertical plane (chap. 6).

The existence of four different modes of dynamics, described above, is illustrated in figure 7.2 for a range of B and $\varphi(0)$. It may be observed that the ‘collision’ of particles happens for small angle $\varphi(0)$ and not too large B . It is understandable, since small $\varphi(0)$ are closer to the quasi-2D limit, in which it was shown that particles consisting of $N = 10$ either collide or repel each other (chap. 6). When the angle $\varphi(0)$ is not too small and the elasticity B is not too large, the particles converge to a horizontal, aligned configuration. For the data presented in the figure 7.2 (with $x_{CM}(0) = 2$ and $\varphi(0) \leq 75^\circ$) it happens for $B < 150$ and $\varphi(0) > 30^\circ$. It should be noticed that not every aligned configuration is stationary: particles may still move, but the orientation of end-to-end vector remains unchanged, what will be described later in

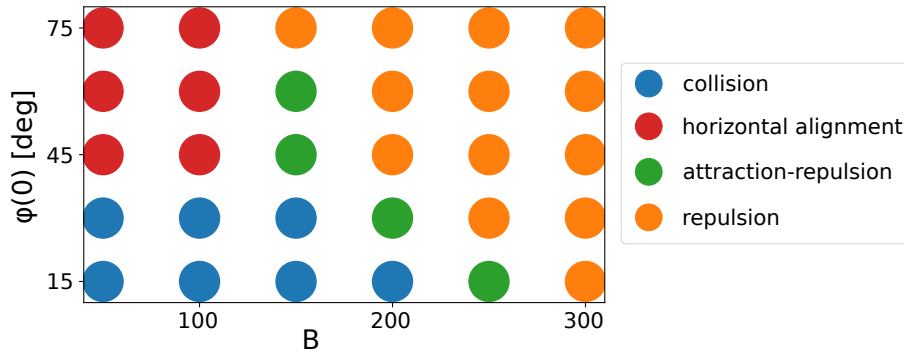


Figure 7.2: Phase diagram of different types of dynamics, described in the main text. Data for $x_{CM}(0) = 2$.

the text. The other two modes of the dynamics, shown in the phase diagram, are observed for very elastic filaments. If B is large enough, independently of the initial angle $\varphi(0)$, the particles always start to drift away immediately after relaxation. Between this repulsion mode and collisions/alignment behaviour, the last mode of the dynamics may be found, which is characterized by the initial attraction and subsequent repulsion, without reaching $\varphi = \pi/2$.

In next sections I will present the dynamics of particles which align horizontally. First, the phenomena of damped oscillations will be investigated and later the dynamics of particles after alignment.

7.2 Oscillations

7.2.1 Damping

The dynamics of weakly flexible filaments is characterized by oscillations which are effectively damped and finally the particles converge to a horizontal, aligned configuration. This behaviour is relatively easy to explain. The oscillatory dynamics has the same origin as the periodic motions observed for two rigid particles, described in chapter 4. Indeed, the shapes of weakly flexible filaments are not very different from the straight ones (see fig. 7.1 or 7.3C) and therefore hydrodynamic interactions between flexible particles are very similar to those observed for rigid ones. Oscillations of the particles are coupled with the effect of filaments flexibility, which leads to the decrease of the oscillations amplitude and finally the horizontal alignment. It is known, that a single flexible particle which bends under the external force would orient itself horizontally [6–8, 12]. In terms of notation used in this work, such an additional effect introduced by flexibility of each particle would constantly push the system toward $\theta = \pi/2$ without interfering much with the value of φ . From the phase space plots

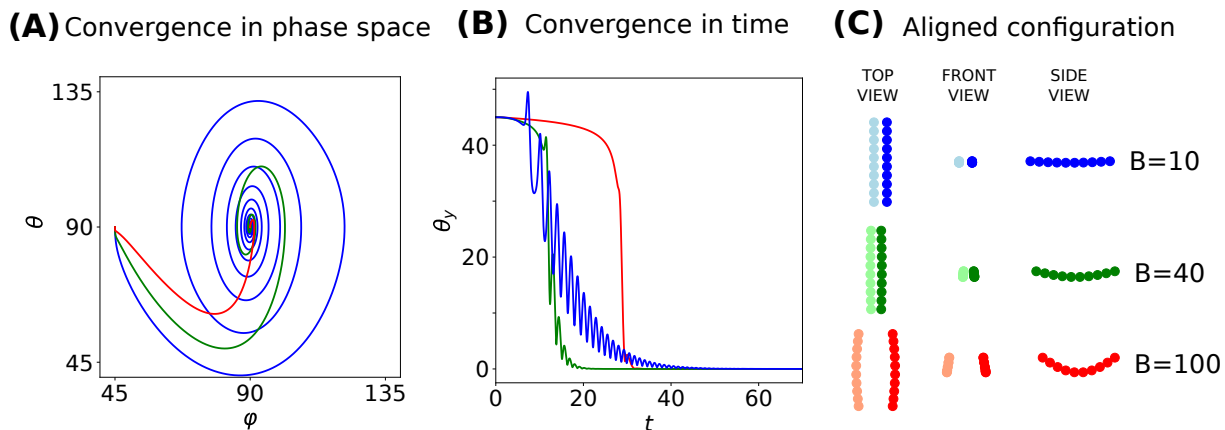


Figure 7.3: Convergence to the aligned configuration for various elasticity of the filaments, data for $x_{CM}(0) = 2$. (A) Orientation angles θ and φ : convergence to $\theta = \varphi = 90^\circ$; (B) convergence of orientation angle θ_y (defined in fig. 4.5) toward 0; (C) shapes of particles in aligned, horizontal configurations. Colours indicate value of B parameter: $B = 10$ – blue, $B = 40$ – green and $B = 100$ – red.

of the dynamics, shown in the figure 4.9A for rigid particles and fig. 7.3A for elastic ones, it may be observed that if the periodic motion of the two stiff particles (closed, circular lines) was coupled with an additional effect described above, the result would be indeed the spiral-shaped convergence toward orientation angles $\theta = \pi/2$ and $\varphi = \pi/2$, that is toward a horizontal and parallel configuration of filaments. Because in case of a single filament [6–8, 12] the particles which are more elastic in general orient themselves faster than more stiff ones (due to larger deformation), the damping effect in our two-particle system is also more intensive for larger B .

Figures 7.3A and 7.3B illustrate the convergence of filaments to an aligned configuration for $x_{CM} = 2$ and $B \in \{10, 40, 100\}$. It can be noticed that for $B = 10$ the process is long and involves a series of oscillations of a significant amplitude. For moderate value of $B = 40$ only a few oscillations are visible and their magnitudes are much smaller than for $B = 10$. Finally, for highly flexible filaments with $B = 100$ the particles converge to the aligned configuration practically without oscillations. The process of alignment in time is shown in figure 7.3B in terms of θ_y orientation angle. It may be observed that the alignment is the fastest for moderately flexible filaments with $B = 40$. Long convergence time for $B = 100$ is caused by low speed with which particles initially approach each other. Figure 7.3C illustrates aligned configurations for the chosen values of B . It shows that the filaments with $B = 10$ and $B = 40$ actually are very weakly deformed under gravity, what however turns out to be sufficient to seriously affect the dynamics. It was checked that even more stiff particles with $B = 1$ align, although the amplitude of a settling filament with such B is less than 0.0015 of the particle length. This proves that even very weak flexibility of the filaments causes two particles under gravity to orient themselves parallel to each other and perpendicular to the direction of the external force. Unless the particles are not too elastic, this effect is observed for all initial angles $\varphi(0)$ and

distances between particles (except of non physical collisions for small $\varphi(0)$).

7.2.2 Amplitude decay

There are various ways to define the amplitude of oscillations. Extrema of angles θ , φ or θ_y can be considered, as well as e.g. deviation of particle center along 'y' axis. In this work the value of angle θ was chosen, more specifically $\theta - 90^\circ$, which is the measure of the angle between orientation vector and the horizontal plane. The value of this angle in time is shown in figure 7.4A for a representative exemplary values of parameters, extrema of $\theta - 90^\circ$ are marked with dots. The decay of oscillations amplitude is exponential with respect to the number of oscillations, as shown in fig. 7.4B. In consequence the amplitude at n -th extremum, denoted as $A(n)$, can be written as:

$$A(n) = A_0 e^{-\gamma n} \quad (7.1)$$

where γ is a positive constant, or in more convenient form as:

$$A(n) = A_0 r^n \quad (7.2)$$

where

$$r = \frac{A(n)}{A(n-1)} = e^{-\gamma} \quad (7.3)$$

is the damping ratio characterizing intensity of the damping: r is equal to the ratio of a given local maximum of $|\theta - 90^\circ|$ and the preceding local maximum. Such exponential decay was not found for the time dependence, and in the figure 7.4C it may be observed that unlike in the classic problem of damped harmonic oscillator, the interval between consecutive extrema is not conserved in the studied system of two filaments.

The exponential form of amplitude decay with the oscillation count number n fits well to the the data for the amplitude in the degrees range $[0.01^\circ, 10^\circ]$ and often also well beyond (as e.g. in fig. 7.4B). However, results obtained for different initial orientation angles $\varphi(0)$ suggest that something important should be added to this description. Data for $\varphi(0) = 30^\circ$ and $\varphi(0) = 60^\circ$ are shown in figure 7.5A and B, respectively. Data points used to fit the formula are shown in green, other in orange. It is visible that although the fit is very good in the range $|\theta - 90^\circ| \in [0.01^\circ, 10^\circ]$, outside of this range the dependence of $|\theta - 90^\circ|$ on the oscillation count n is concave for $\varphi(0) < 45^\circ$ and convex for $\varphi(0) > 45^\circ$. As this observation is systematic, the mechanism behind this phenomena would be an interesting topic for the future studies.

Let us now focus again on the range $|\theta - 90^\circ| \in [0.01^\circ, 10^\circ]$, where the amplitude of oscillations decays exponentially. As stated before, the damping intensity depends on the

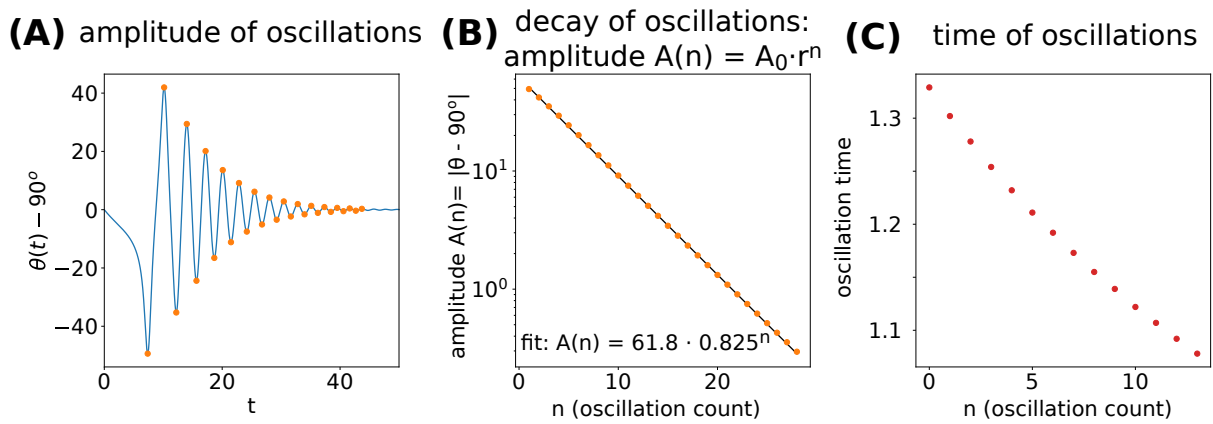


Figure 7.4: Decay of oscillations. (A) Value of $\theta - 90^\circ$ in time with extrema marked with dots. (B) Absolute values of extrema marked in panel (A) with fitted dependence on the number of oscillations. (C) Length of the intervals between consecutive extrema. All results are shown for $B = 10$, $x_{CM}(0) = 2$ and $\varphi(0) = 45^\circ$.

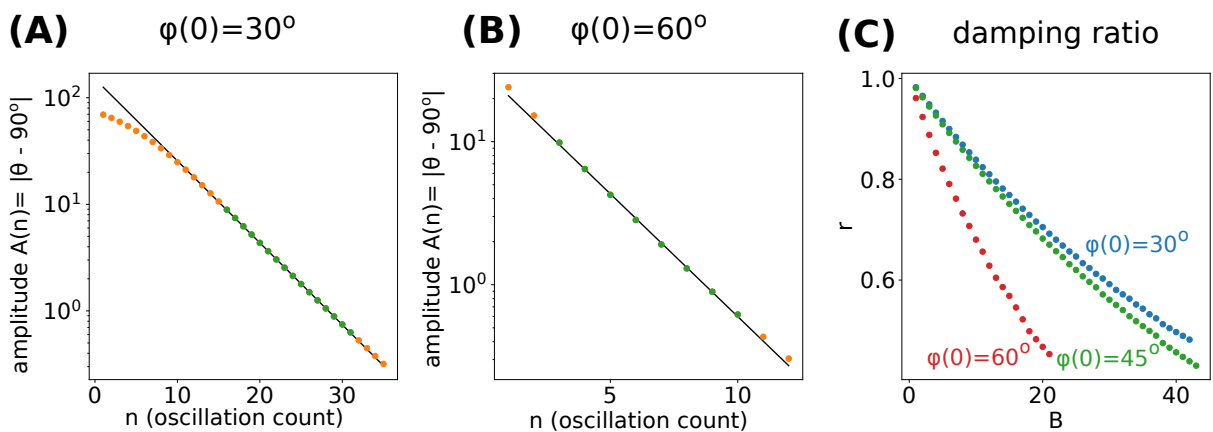


Figure 7.5: Dependence of the damping rate on $\varphi(0)$ and B . (A) Amplitude decay for $\varphi(0) = 30^\circ$ and $B = 10$. Points used to fit the line (chosen on the base of the amplitude value) are marked in green; (B) Amplitude decay for $\varphi(0) = 60^\circ$ and $B = 10$; (C) Decay rate as a function of B for different $\varphi(0)$. All results are shown for $x_{CM}(0) = 2$.

flexibility of particles and is larger for more elastic particles. Speaking in terms of elasticity parameter B and damping ratio r this statement would be expressed that the value of r decreases for larger B , what means faster decay of the oscillations. For rigid particles, $B \rightarrow 0$ the damping ratio should approach 1. The relation between B and r is illustrated in the figure 7.5C for three different initial orientation angles: $\varphi(0) \in \{30^\circ, 45^\circ, 60^\circ\}$. The results indicate that in systems which initially have larger $\varphi(0)$ the damping is significantly stronger, especially for $\varphi(0) > 45^\circ$.

7.2.3 Comparison to single filament

In previous sections of this chapter it was shown that a symmetric pair of filaments converges to an aligned, horizontal configuration. Since it is known that also an isolated, single filament orients itself horizontally, it is interesting to study whether the presence of another filament promote or hamper the filament reorientation. In other words, the question is whether two particles in a symmetric configuration converge to a horizontal configuration faster or slower than a single filament. In order to investigate this problem, the dynamics of a single filament is evaluated for the initial configuration identical to configuration of one of the pair of sedimenting filaments at chosen moments when $|\theta - 90^\circ|$ have local maxima. Representative results are presented in fig. 7.6, where values of $\theta - 90^\circ$ in the system of two particles are plotted with blue lines while the values of $\theta - 90^\circ$ for a single filament are plotted with black, dashed lines. Each dashed line corresponds to an alternative dynamics, in which the ‘left’ particle (or the right one, interchangeably) from the pair instantaneously disappears. For each simulation of the dynamics of the two particles a series of simulations of one filament was conducted, for different initial configurations. It is visible that in all cases the single filament converges toward $\theta = 90^\circ$ faster than the pair of filaments. As shown in the figure, this result holds for different values of the elasticity.

The important conclusion from this study is that the pair of filaments orient themselves horizontally slower than a single filament. This result was obtained for a strictly symmetric configurations of two filaments, however in chapter 8 it will be shown that the ‘aligning’ dynamics of filaments is robust to even large deviations from the symmetry and therefore the conclusion drawn here may be valid for wider range of the systems.

7.3 Dynamics of aligned filaments

It has been shown in previous paragraphs that for a wide range of parameters the filaments converge to a horizontal, aligned configuration. In this section the dynamics after alignment is

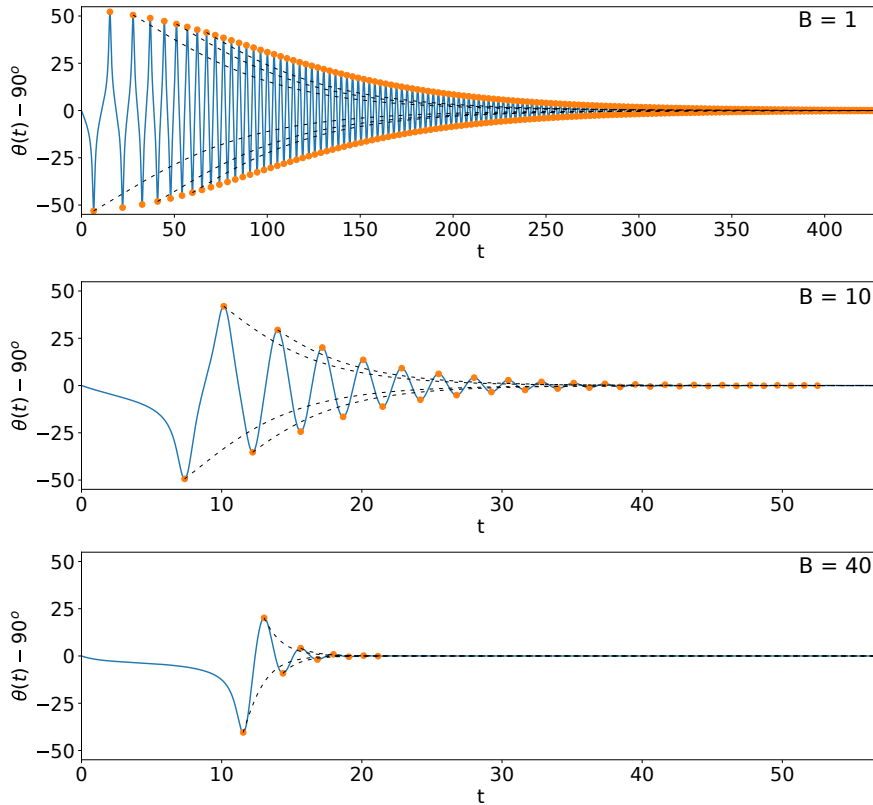


Figure 7.6: Convergence of the symmetric system of two particles toward horizontal orientation ($\theta - 90^\circ$ shown in blue), in comparison with the system of a single particle ($\theta - 90^\circ$ shown with black dashed lines). Local extrema of $\theta - 90^\circ$ are marked in orange, some of them were used to obtain initial configurations for a single filament dynamics. Note the different time scale for $B = 1$. All results shown for systems of two particles are obtained for initial configurations $x_{CM}(0) = 2$ and $\varphi(0) = 45^\circ$.

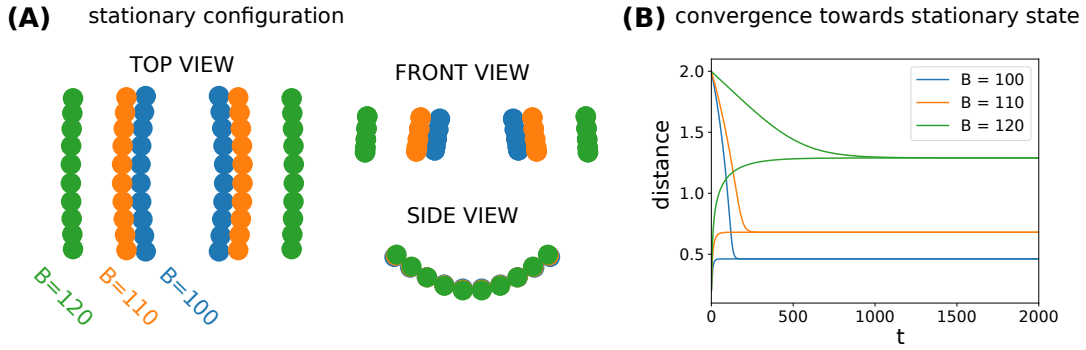


Figure 7.7: Convergence of the aligned particles to a specific distance. (A) Final configurations for $B \in \{100, 110, 120\}$. In side view the particles overlay because their shapes are almost identical. (B) Distance between centres of particles starting from $x_{CM}(0) \in \{0.1, 1\}$ for different values of B . The distance converges to a constant, flexibility-dependent value. Figure reprinted from [169].

studied, which is typically characterized by much longer time scales than the oscillation time, or even the alignment time.

In order to study the dynamics after alignment in more details, a new series of numeric simulations was carried out. This time the filaments started from the horizontal, parallel configuration: $\theta(0) = \pi/2$ and $\varphi(0) = \pi/2$. Initially the filaments were straight. The only parameter of the initial configuration was the distance between filaments, more specifically $x_{CM}(0)$. The aligned configuration of filaments, which is reached by filaments which had started from horizontal position with some $\varphi(0) \neq \pi/2$, is different from the initialization chosen here in two ways: 1) particles are bent; 2) bent particles are additionally tilted: the lowest points in the middle of the filaments become more distant from the symmetry plane than the ends of the fibres (compare fig. 7.3C, $B = 100$, front view). Considering the former issue, the bent of filaments under gravity, it is restored from the straight configuration very fast, in time of the order of $t \sim 1$, in comparison to the simulation time which is of the order of thousands time units. Therefore it is not expected to play an important role in the long-time dynamics. The characteristic time scale of the tilting of particles has not been systematically investigated yet. However, the results obtained so far indicate that the chosen family of initial configurations is able to reproduce well the dynamics of particles which have reached the aligned configuration starting from $\varphi(0) \neq \pi/2$ and therefore allows to gain the general understanding of the dynamics of particles after alignment.

Very elastic filaments ($B \geq 125$) in the parallel, horizontal configuration repel each other. This behaviour is intuitively understandable, because ‘U’-shaped filaments with a significant bending amplitude interact hydrodynamically: they tilt and drift away from each other, in a similar way as two particles in the vertical plane. The dynamics of particles with $B \leq 74$ is very different, because in this case an attraction between particles is observed what eventually leads to the collision of particles. Particles of the intermediate elasticity, $B \in [75, 124]$ drift

towards a certain stable position, which depends on their flexibility. The more flexible the filaments, the larger distance between particles in the stationary configuration. The stationary state is shown for a few chosen values of B in the figure 7.7A. The convergence toward the stationary state is illustrated in fig. 7.7B.

The dependence between filaments flexibility and the distance between particles in the stationary state is not linear. The position of particles in the stationary configuration for stiffer filaments is less sensitive to B than in case of more flexible ones, what is visible also in the fig. 7.7, where stationary configurations are more similar for values of elasticity $B = 100$ and $B = 110$ than for values $B = 110$ and $B = 120$. It was not checked yet whether for $B \geq 125$ filaments always repel each other or there exists a stationary state which is very widely separated. This question will be the subject of future studies. The results indicate that even if the stationary state exists, the equilibrium distance ‘explodes’ in the range $124 < B \leq 125$: it is smaller than 2 for $B = 124$ and larger than 100 for $B = 125$. Another important question arising from the presented result is the mechanism of attraction between more rigid filaments.

In summary, the results presented in this section show that after alignment very flexible filaments repel each other up to a very large distance (if not infinitely), particles which are rigid enough attract each other and ‘collide’, while in the intermediate range of B particles reach a stable, well separated configuration. As the collisions of particles do not happen under Stokes regime, more rigid particles are expected to attract each other to an almost touching configuration.

7.4 Trumbbells

In this section it is investigated whether the trumbbell, one of the simplest models of particle which can bend, is able to capture the main properties of the dynamics of two filaments, described above. Similarly as for the filaments, I will mostly focus on the relatively stiff particles (low $B' = B \cdot a/a_{max}$) which are the most important from the experimental point of view. Because the trumbbells in the context of this chapter intend to correspond to filaments, beads are well separated: the value of bead radius was chosen as $a = l_0/8 = a_{max}/4$.

First, let us consider different types of dynamics observed for different values of elasticity parameter B' , similarly as it was done for filaments. Trajectories of beads for representative parameters B' , $\varphi(0)$ and $x_{CM}(0)$ are shown in figure 7.8. In case of $B' = 10$ (fig. 7.8A) and $B' = 70$ (fig. 7.8B) we observe behaviours analogous to the system of two fibres: for small B' particles oscillate and converge to an aligned configuration, while for $B' = 70$ trumbbells align almost instantaneously after having approached each other. Another feature consistent

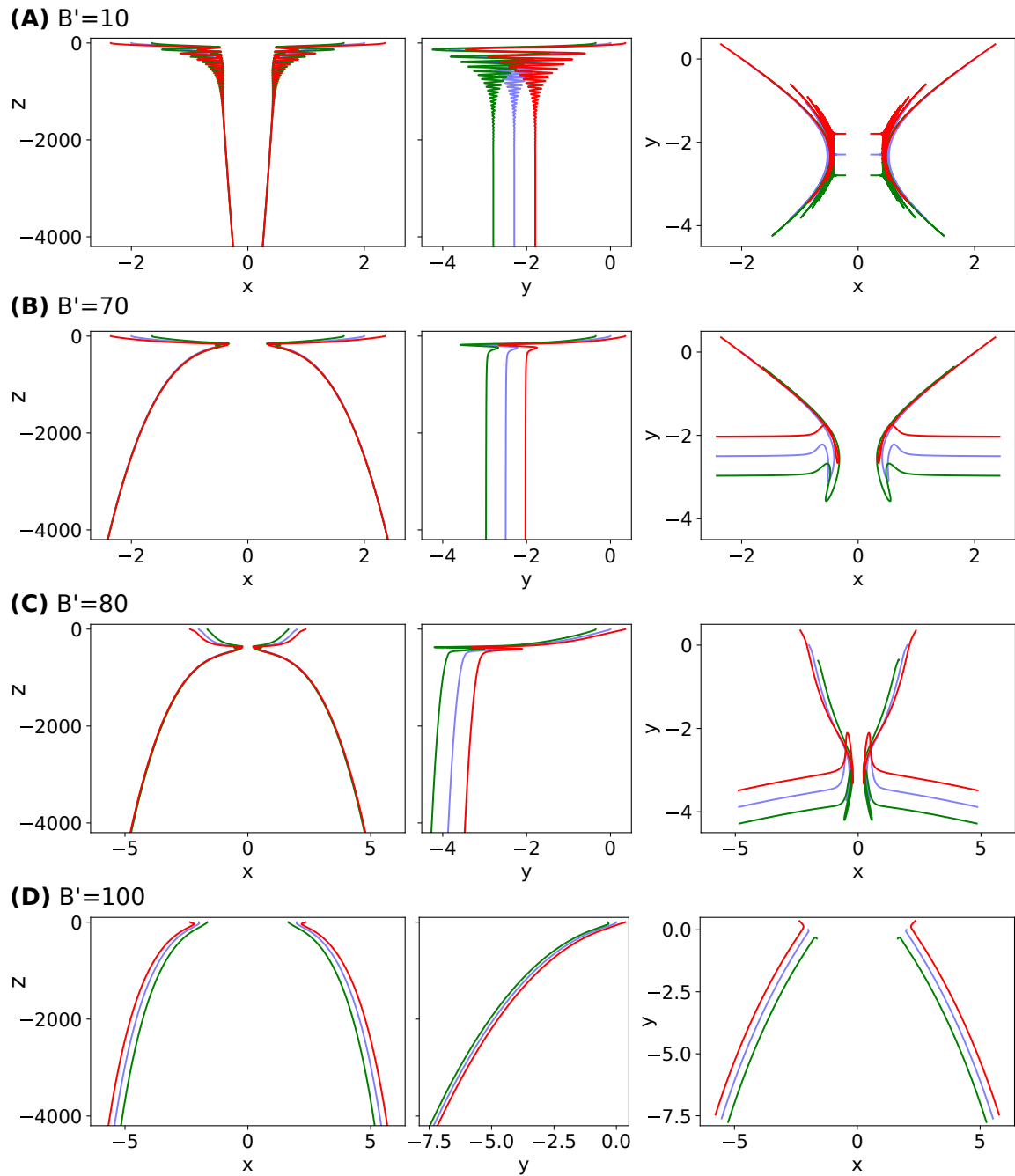


Figure 7.8: Trajectories of beads of trumbells of different elasticity B' , observed from the front (left column), side (middle column) and top (left column). Each colour corresponds to the trajectory of a different bead. Results for $a = a_{max}/4$, $x_{CM}(0) = 2$ and $\varphi(0) = 45^\circ$.

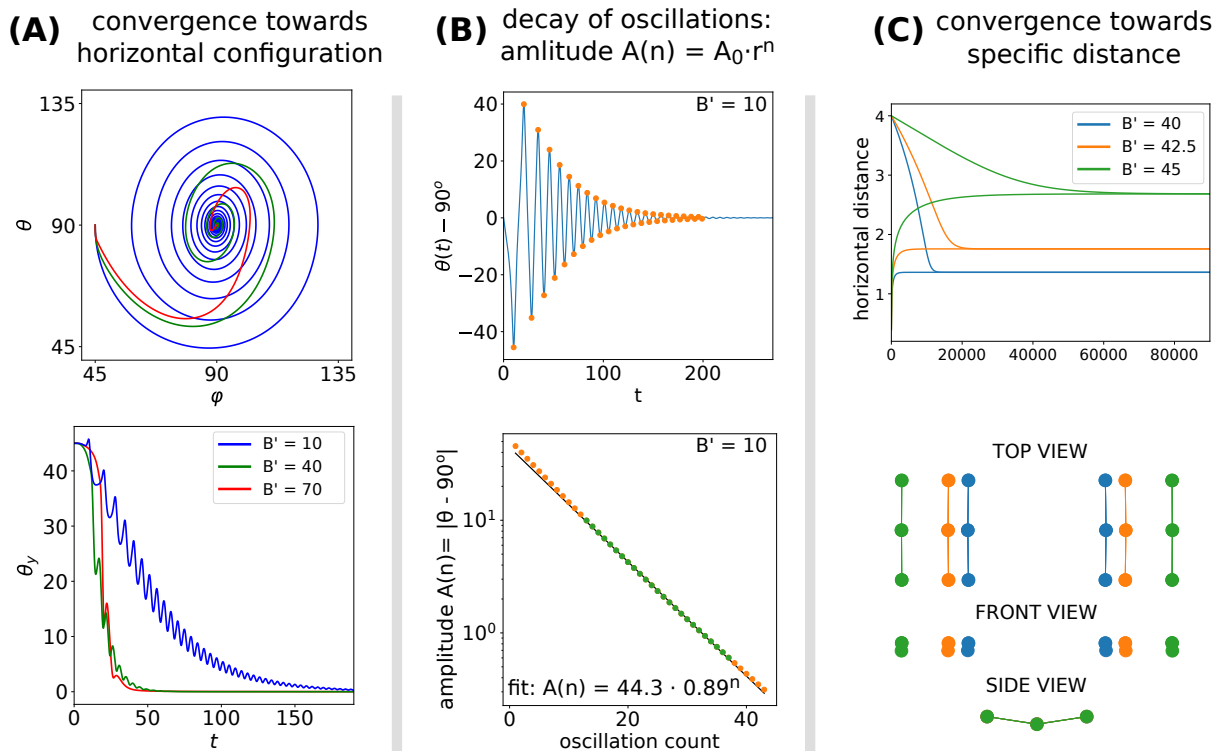


Figure 7.9: Features of the dynamics of two trumbbells. (A) Convergence to the aligned configuration shown in terms of orientation angles θ and φ (top panel) and orientation angle θ_y against time (bottom panel); (B) decay of the amplitude: $\theta - 90^\circ$ with marked extrema (top) and exponential relation between the amplitude and the oscillation count (bottom); (C) stable, horizontal and parallel configuration of trumbbells with intermediate values of B : convergence to the equilibrium distance (top) and equilibrium configurations (bottom) for the chosen values of B .

with the results for filaments is the dynamics after alignment. It is visible that more rigid trumbbells ($B' = 10$) approach each other, while more flexible ($B' = 70$) move away from each other. The analysis considering existence of stable configurations after alignment, similar to those shown for filaments in fig. 7.7, will be presented later in this section. Trajectories of beads for trumbbells with $B' = 80$ (fig. 7.8C) exhibit a new type behaviour, not observed for a pair of filaments. The trumbbells approach each other, reach parallel configuration with $\varphi = 90^\circ$ and subsequently repel each other, but not in an aligned configuration ($\varphi \neq 90^\circ$). In case of filaments the repulsion of particles with non-parallel orientation was found only in the systems where particles had not reached the parallel configuration ($\varphi \neq 90^\circ$) before. Very elastic trumbbells, with $B' \geq 100$ (fig. 7.8), similarly to very elastic filaments, drift apart just from the beginning of the simulation.

As mentioned before, the regime of small B' is particularly interesting due to its significance for experiments (see sec. 1.2). Therefore below I focus on relatively stiff trumbbells with $B' \leq 70$, what corresponds to panels (A) and (B) from figure 7.8. Convergence of trumbbells toward aligned, horizontal configuration is presented in figure 7.9A, which shows results analogous to

fig. 7.3 for elastic filaments. In terms of orientation angles θ and φ , the spiral approach toward $\theta = 90^\circ$ and $\varphi = 90^\circ$ is visible, which very well illustrates the link with periodic solutions found for rigid particles (see sec. 4.4). Similarly to filaments, the damping of the oscillations is stronger for more elastic particles.

The decay of the oscillation amplitude for trumbbells is roughly exponential (fig. 7.9B), but the deviation from the fitted exponential dependence is larger than in case of filaments. Perhaps the exponential dependence would be more suitable for another measure of amplitude than the chosen angle θ . In order to draw clear conclusions, further studies in this topic would be required. It may be noticed that the damping ratio $r = 0.89$ calculated for trumbbells with $B' = 10$ is quite similar to the value $r = 0.83$ obtained for filaments consisting of 10 beads with $B = 10$. This observation suggests that elasticity parameter B' , which takes into account radius of beads (see sec. 2.2.3), is a useful measure also in case of two trumbbells out of the vertical plane. If, instead, particles with the same parameter B (independent of a) were considered, the presented trumbbells with $B = 40$ and $r = 0.89$ would have an analogue in pair of filaments with $B = 40$ and damping ratio $r = 0.46$.

Trumbbells of a certain elasticity after the alignment converge to a stable configuration with the specific distance between particles, what is illustrated in figure 7.9C. Similarly to the filaments, more elastic particles drift apart and don't have stable configuration in the studied range of distances, which was of the order of hundreds times larger than the particle length. In the figure 7.9C the convergence toward specific position (upper panel) and the stable configurations themselves (bottom panel) are shown for a few values of B' . These results were obtained for parallel and horizontal initial positions of particles. It is noteworthy that the velocity of horizontal drift depends strongly on the distance between trumbbells and is much slower for more distant particles.

The dynamics of trumbbells described in this section is very different from the dynamics of dumbbells, presented in section 3.5.2. In general, the elastic trumbbells behave similarly to the filaments and very differently from dumbbells, which systematically repel each other and tend toward the vertical plane.

7.5 Conclusions

The dynamics of the flexible filaments is very rich with a range of different types of behaviour observed, depending on the elasticity of fibres and their initial configuration. In my opinion the most important result obtained in this chapter is the horizontal alignment of particles observed for small and moderate B , because it causes that even for a slight initial

deviation from the vertical plane xz the system converges to an aligned configuration where particles are perpendicular to this plane. Additionally, such behaviour is observed for the range of elasticity-to-gravity parameter B which is interesting from the experimental point of view. A significant effect of alignment is observed even for quite rigid particles, e.g. for mentioned before $B = 1$ which are almost straight when settling under gravity (bending amplitude is equal to 0.15% of the particle length). Very good agreement between results for filaments and trumbbells suggests that the alignment phenomena are present for different shapes of elastic particles.

The speed of convergence towards the aligned configuration was shown to depend on the elasticity of particles: more flexible filaments and trumbbells converge faster than more rigid ones. The decay of the oscillation amplitude, measured as orientation angle θ , seems to be exponential – at least in the range $\theta \leq 10^\circ$ approximately. The mechanics behind this relation has not been resolved yet.

After alignment the dynamics of particles depends on their elasticity: particles may drift apart (most flexible), converge to a stationary configuration (intermediate range) or tend to collide (most rigid). Since collisions are not possible in the Stokes regime, in the latter case the particles are expected to have a stable, almost touching stationary configuration or asymptotically converge to the contact in an infinite time.

8 Dynamics of particles in non-symmetric configurations

In previous chapters of this dissertation the dynamics of symmetric pairs of particles were described, with the symmetry embedded in the equations of motion (sec. 2.6.1). However in practice we are often interested in systems which are not exactly symmetric or we want to know how an additional perturbation would affect the motion. In particular such knowledge is relevant for the design and performance of experiments or formulation of predictions about possibility to observe the alignment phenomena in nature.

Another reason to study non-symmetric configuration is to explore the robustness of dynamics to Brownian forces or other source of noise (e.g. introduced by presence of other, more remote particles). In this context, stochastic simulations should be performed in order to adequately investigate that matter. The deterministic approach adapted in this chapter does not fully answer the noise-robustness question but at least it can exclude the possibility that the dynamics described in the previous chapters is present only in perfectly symmetric configurations.

In this chapter the dynamics of elastic particles starting from slightly non-symmetric configurations is investigated. I consider the same family of initial configurations as before, but this time with a minor non-symmetric perturbations. More details on the parameters of performed simulations are given in section 8.1. Next, in section 8.2, I describe the regime of more flexible filaments in which the perturbed pair of particles behave in the same way as a symmetric one: converges to a horizontal, parallel configuration. Subsequently in section 8.3 more complex dynamics of relatively stiff fibres is presented. Finally, drift and rotation of the whole system is analysed in section 8.4 and concluding remarks are given in sec. 8.5.

The results presented in this chapter focus on the dynamics out of the vertical plane. The reason behind that is the fact that most of random perturbation would push the system out of the vertical plane, what (as shown in the previous chapter) leads to a very different behaviour. Additionally, for particles restricted to the vertical plane, the dynamics is dominated by spurious ‘collisions’ and an adequate hydrodynamic model is required to explore this problem.

Rigid particles are not investigated here, however we study the dynamics of quite stiff particles (down to $B = 1$) and these results can be used to make some predictions regarding the limit of rigid rods, what is done in section 8.5. Dynamics of two rigid particles settling in the fluid seems to be a broad problem on its own, with some interesting properties.

8.1 Initial configurations and notation

8.1.1 Types of perturbations

Symmetric initial configurations of particles, studied in chapter 7, are described by three parameters: $\theta(0)$, $\varphi(0)$ and $x_{CM}(0)$. Filaments (or trumbbells) are straight, all bonds between beads have equilibrium length, and the centres of left and right particles are located at $(-x_{CM}(0), 0, 0)$ and $(x_{CM}(0), 0, 0)$, respectively.

In this chapter the non-symmetrical dynamics is studied for initial configuration where the position of left particle remains unchanged, while position of the right one is perturbed in one of the four different ways, as shown in figure 8.1. Each type of perturbation leaves the particle straight, but its orientation or location is changed:

- perturbed θ : orientation angle θ of the right particle is changed to $\theta(0) + \Delta\theta$,
- perturbed φ : orientation angle φ of the right particle is changed to $\varphi(0) + \Delta\varphi$,
- perturbed y_{CM} : the right particle is shifted in the horizontal y direction, so that y coordinate of its centre is moved from 0 to Δy ,
- perturbed z_{CM} : the right particle is shifted in the vertical direction, so that z coordinate of its centre is moved from 0 to Δz .

The perturbation of x coordinate of the centre of one of the particles is not considered, because it does not violate symmetry with respect to reflection in the $x = 0$ plane. Instead, perturbations in x directions correspond to symmetric configuration with different $x_{CM}(0)$, what has been studied and described in chapter 7.

8.1.2 Moving reference frame

When one of the described perturbations is introduced, the system loses chiral symmetry and may rotate. As a result, even when particles align, they end up in positions parallel to each other, but not necessary parallel to the $x = 0$ vertical plane. In order to account for the system rotation, in addition to the standard coordinates (x, y, z) , in this chapter the dynamics will be described also in (x', y', z) coordinates, which rotate together with particles. More specifically, the direction of x' axis is given by the horizontal component of the vector between centres of the 'left' (initially with negative ' x ' coordinates of all beads) and the 'right' particle. The origin of

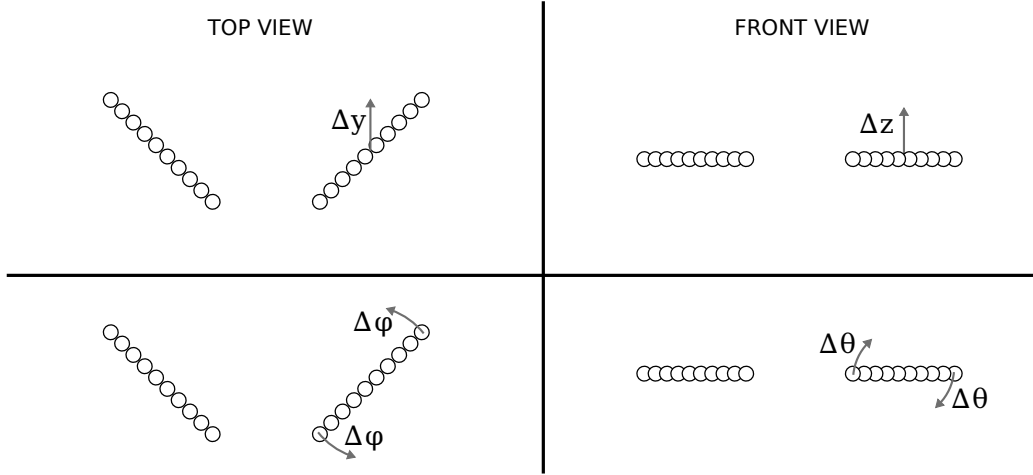


Figure 8.1: Types of perturbations of the initial configuration: Δy , Δz , $\Delta \varphi$, $\Delta \theta$. Note that for $\Delta \theta$ perturbation the rotation is around horizontal axis perpendicular to the filament.

the new coordinate system is chosen in such a way that the centres of two particles are equally distant from $x' = 0$ plane: their x' coordinates are opposite. The ' z ' axis of the (x', y', z) coordinate system is the same as in the laboratory reference, while $\hat{y}' = \hat{z} \times \hat{x}'$. Additionally we assume that y' coordinates of centres of mass of particles are always equal to 0. In the next section it will become clear that the new coordinate system, which rotates and moves together with the particles, is useful to observe alignment of particles, even if it is accompanied by a complex motion in three dimensions.

8.1.3 Parameters of performed simulations

The studied system consists of two filaments, each consisting of $N = 10$ beads. In this study the following perturbations have been investigated:

$$\Delta \theta \in \{0.1^\circ, 0.2^\circ, 0.5^\circ, 1^\circ, 2^\circ, 5^\circ, 10^\circ\}, \quad (8.1)$$

$$\Delta \varphi \in \{0.1^\circ, 0.2^\circ, 0.5^\circ, 1^\circ, 2^\circ, 5^\circ, 10^\circ\}, \quad (8.2)$$

$$\Delta y \in \{0.001, 0.002, 0.005, 0.01, 0.02, 0.05, 0.1\}, \quad (8.3)$$

$$\Delta z \in \{0.001, 0.002, 0.005, 0.01, 0.02, 0.05, 0.1\}. \quad (8.4)$$

Perturbations were introduced to the symmetric configurations described by initial parameters:

$$\theta(0) = 90^\circ \quad (8.5)$$

$$\varphi(0) \in \{45^\circ, 60^\circ\}, \quad (8.6)$$

$$x_{CM}(0) \in \{2, 3\} \quad (8.7)$$

Smaller $\varphi(0)$ have not been considered, because in these cases instead of alignment spurious collisions of filaments are observed for analysed values of the flexibility parameter (see fig. 7.2):

$$B \in \{1, 5, 10, 40, 100\}. \quad (8.8)$$

Simulations were performed for all combinations of B , $\varphi(0)$ and $x_{CM}(0)$ parameters with a single perturbation at a time. Results revealed a rich dynamics, described below.

8.2 More flexible filaments, $B \geq 10$

More flexible filaments converge to the horizontal, parallel configuration even after perturbation of the symmetric initial configuration. The results indicate that for the studied amplitudes of the perturbations, and parameters of the initial configuration $x_{CM}(0) = 2$, $\varphi(0) = 45^\circ$, the filaments with flexibility $B \in \{40, 100\}$ always align¹. For more rigid particles, with $B = 10$, the alignment is observed if non-symmetric perturbations are not too large, namely for $\Delta\theta \leq 1^\circ$, $\Delta\varphi \leq 2^\circ$, $\Delta y \leq 0.05$ and $\Delta z \leq 0.02$. If perturbations are larger, the particles ‘collide’ during the motion, indicating that further studies with more adequate hydrodynamic model are necessary in order to accurately track the dynamics. The results for different types and amplitudes of perturbations are summarized in figure 8.2. The columns correspond to perturbation types and rows to characteristic variables which describe the ‘final’ configurations of particles, taken either at the time when particles touch each other, or at the end of the simulation time, whichever happens first. Simulation time, $t = 100$, is long enough for the symmetric system to converge to the align configuration, and it was not necessary to be extended, as it will become evident later. Characteristic variables which describe the final configurations, plotted in the figure, are as follows:

- $z_R - z_L$ – difference between z coordinates of centres of right and left particles,
- $(\theta_R + \theta_L)/2$ – mean θ orientation angle of the end-to-end vectors of both particles,
- $\theta_R - \theta_L$ – difference between θ orientation angles of the end-to-end vectors of the two particles,
- ψ – angle between end-to-end vectors of the left and the right particle.

In the figure the dotted lines indicate values specific for the horizontal, aligned configuration. If (and only if) filaments have such configuration, the respective markers in all four rows are

¹other values of $x_{CM}(0)$, $\varphi(0)$ are described later

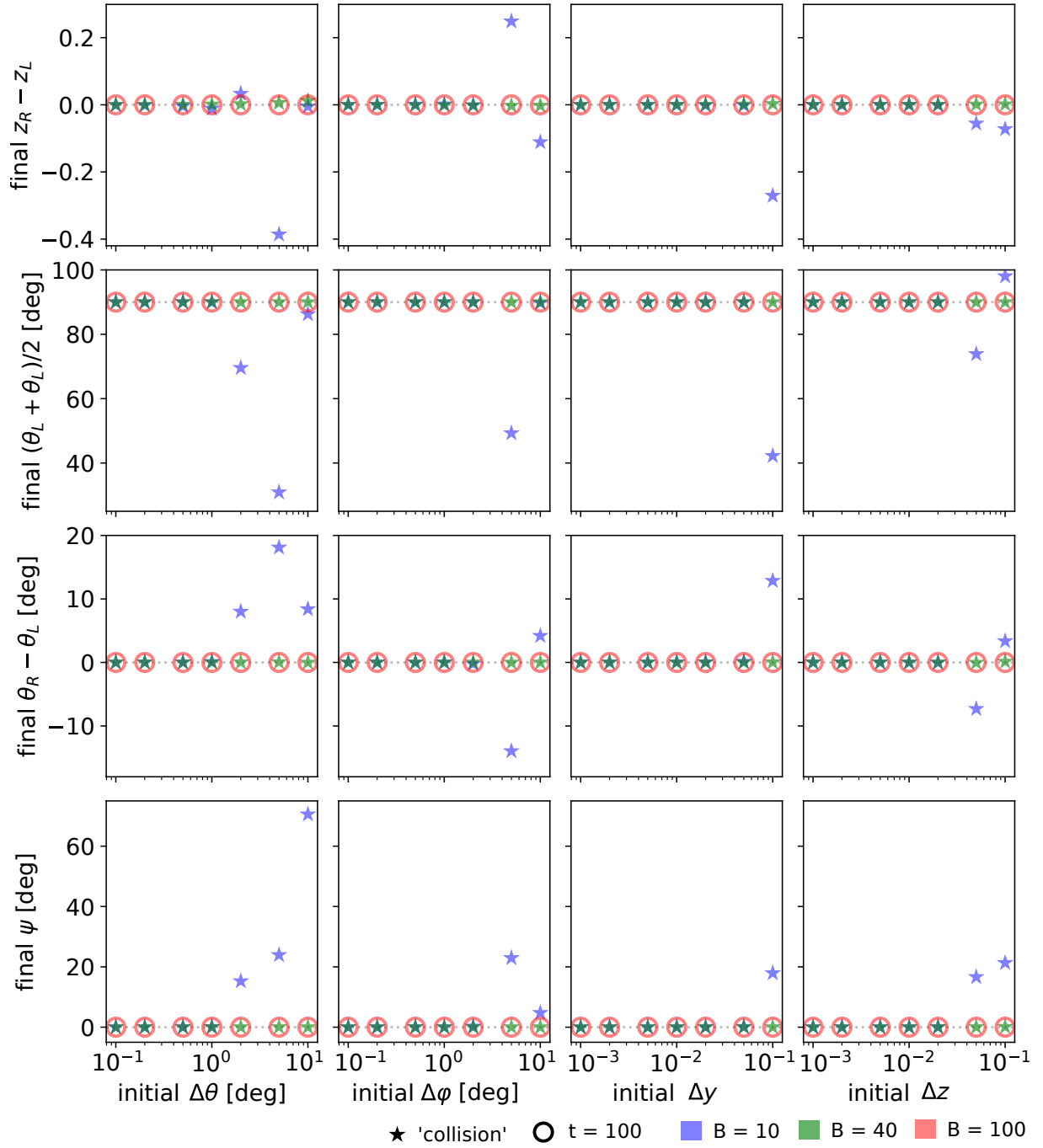


Figure 8.2: Final configurations of particles with different types and amplitudes of the non-symmetric perturbations: $\Delta\theta$, $\Delta\phi$, Δy , Δz . Stars indicate that the configuration of filament was measured at the moment of 'collision', while circles indicate that positions were taken at the end of the simulation ($t = 100$). Perturbations were introduced to initial configuration with parameters: $x_{CM}(0) = 2$ and $\varphi(0) = 45^\circ$.

located on the dotted lines. As mentioned before, up to some magnitudes of perturbations the filaments for all values of $B \in \{10, 40, 100\}$ converge to the horizontal, parallel configuration. For larger perturbations filaments with $B = 10$ ‘collide’ before the alignment. The results do not show any apparent trend in the measured characteristics of the configuration at the ‘collision’ moment. As it was described in section 7.3, after alignment the more stiff particles approach each other (e.g. for $B \in \{10, 40\}$), and the more elastic repel each other ($B \geq 125$) or converge to the specific distance (e.g. $B = 100$). This behaviour reflects in results presented in fig. 8.2: after alignment particles with $B \in \{10, 40\}$ approach and finally touch each other (what is marked with stars) and more elastic particles with $B = 100$ stay well separated until the end of simulation time (configurations marked with empty circles).

The results described above have been obtained for $x_{CM}(0) = 2$ and $\varphi(0) = 45^\circ$. In order to get the more general view, it is worth to look at different initial parameters. For larger $\varphi(0) = 60^\circ$ the convergence toward aligned configuration is stronger: parallel configuration of filaments is reached for all examined perturbations, no spurious collisions before alignment are observed. In a few cases for quite stiff filaments $B = 10$ and large perturbations of $\Delta\theta$, in the parallel configuration at the end of the simulation the particles are not at the same level. This type of long-lasting configuration is found more often for even smaller B and therefore is described in the next section 8.3. From the literature [10, 13] one may predict that although in such configuration the upper filament would finally catch up the lower one, such process is very slow, especially for more stiff filaments. The fact that the larger initial rotation angle $\varphi(0)$ enhance the alignment seems to be intuitive, since with larger initial φ the oscillation phase is shorter and the amplitude of oscillations is smaller. Smaller values of φ , such as 30° , have not been studied systematically, because in the symmetric system such initial parameter leads to ‘collision’, rather than to alignment, of particles (fig. 7.2), what was also confirmed for some perturbed initial configurations. For $\varphi(0) = 45^\circ$ but larger initial distance between particles ($x_{CM} = 3$) results are similar as for $x_{CM}(0) = 2$, described above.

Let us now discuss in details the dynamics of particles before alignment. Exemplary trajectories of beads are shown in figure 8.3A,C,E in front, side and top projections. The initial and final positions of beads are shown also in figure 8.4. It is visible, that even though in the presented simulations the alignment of particles finally occur, the trajectories of beads can be rather complex if analysed in the laboratory reference frame. Therefore in figure 8.3B,D,F the same trajectories are plotted in the reference frame that moves and rotates together with particles, which was defined in section 8.1.2. In the new reference frame it is visible that the dynamics of perturbed pair of filaments, which finally align, is actually similar to the dynamics of symmetric pair. As it will be shown in the next section, such observation is not necessarily true for more more stiff particles, for which the initial perturbation may amplify.

The initial and final configurations of particles plotted in a single graph in fig. 8.4 allow to

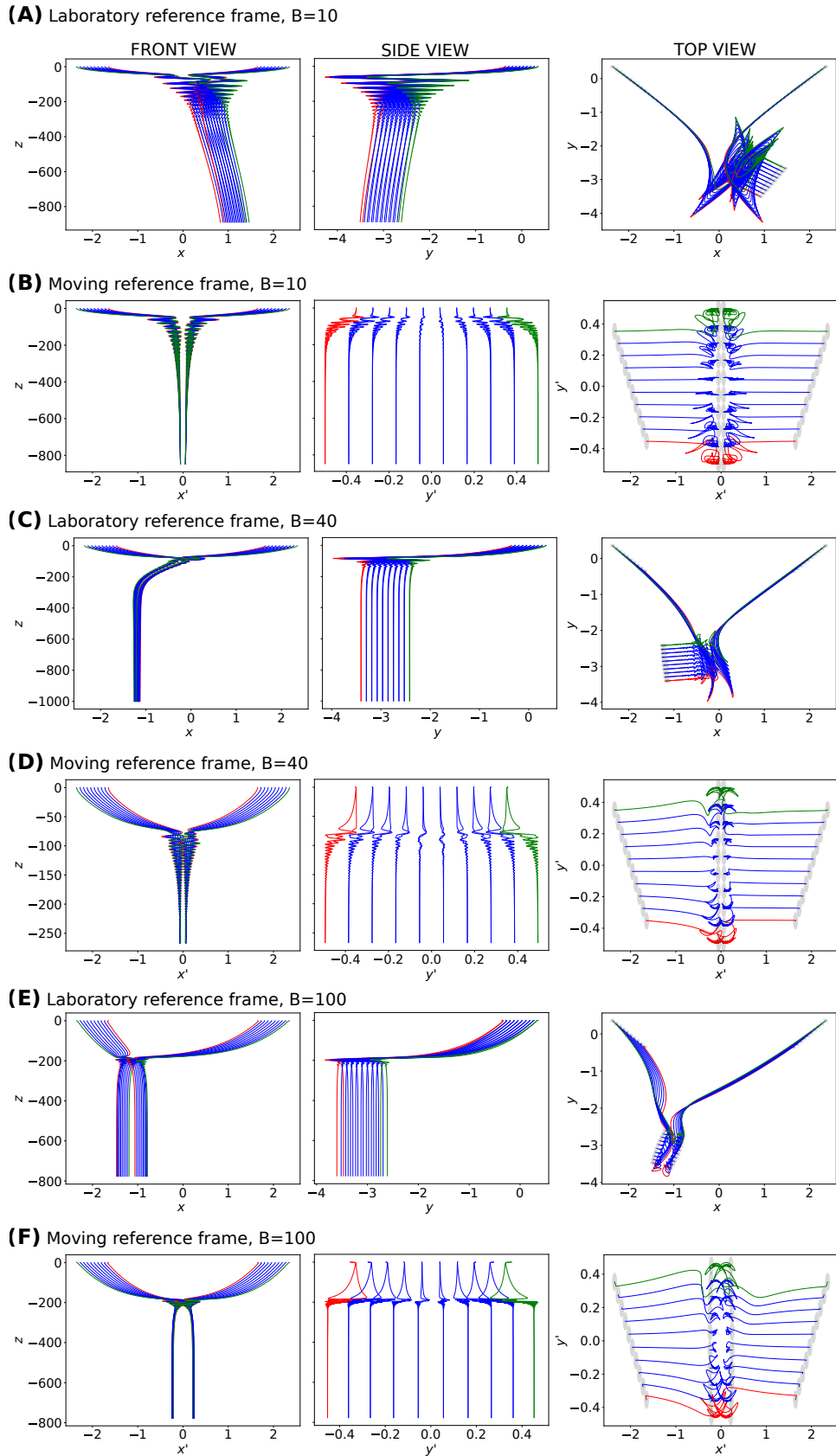


Figure 8.3: Trajectories of beads for slightly asymmetric initial configurations of the filaments. Rows A,C,E present the dynamics in the laboratory reference frame, while rows B,D,F in the moving reference frame defined in sec. 8.1.2. Gray circles indicate initial and final configurations of beads. Results shown for $x_{CM}(0) = 2$, $\varphi(0) = 45^\circ$ and perturbations $\Delta z = 0.02$ for $B = 10$ and $\Delta z = 0.1$ for $B \in \{40, 100\}$.

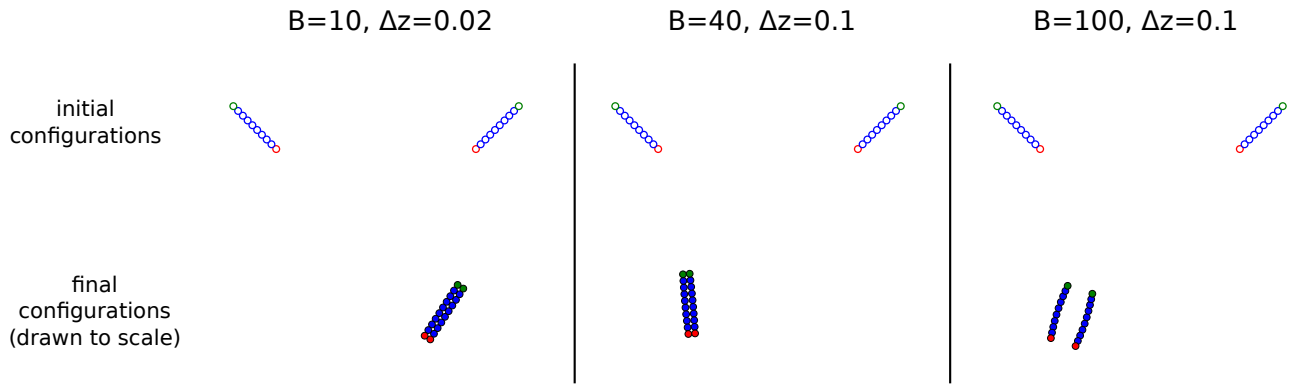


Figure 8.4: Initial and final configurations of filaments which dynamics are shown in fig. 8.3, top view. Configurations are drawn in the same reference frame and therefore drift and rotation of particles are represented accurately. Initial asymmetry is not visible, because the shift is in the vertical direction.

easily observe that, apart from relative motion and settling down, the initially perturbed particles may move together horizontally and rotate as a pair. These phenomena will be further discussed in section 8.4.

8.3 More stiff filaments, $B \leq 5$

It was already visible in the previous section that the system becomes less stable if the particles are more stiff. Let us now analyse the dynamics for filaments with small $B \in \{1, 5\}$, presented in figure 8.5 (analogous to fig. 8.2 from the previous section). If the perturbations are small, in case of $B = 5$ the results show the continuation of the trend observed for more flexible filaments: particles align horizontally at the same level. Such behaviour is present for $\Delta\theta = 0.1^\circ$, $\Delta\varphi \leq 0.2^\circ$, $\Delta y \leq 0.005$ and $\Delta z \leq 0.002$ (see fig. 8.5). An example of the aligned configuration is shown in figure 8.6A. For larger perturbations the filaments with $B = 5$ do not align (at least not at same level, as elaborated later) while for stiffer particles with $B = 1$ the alignment is not observed even for the smallest amplitudes of perturbations considered here.

During the simulations, initially the perturbations grow before the oscillations of filaments may attenuate. In this initial phase, when the asymmetry of the system vastly increases, the particle often spuriously ‘collide’ before reaching the aligned configuration. An example of the fibres configuration at the collision moment is shown in figure 8.6B. The dependence of the ‘collision’ configuration on the initial perturbation amplitude shows an interesting pattern, displayed in fig. 8.5. In some cases, for $B = 5$, it looks like linear relation in the presented semi-log scale, e.g. between the final angle between particles ψ and the logarithm of perturbation amplitudes in ranges: $\Delta\theta \in [0.2^\circ, 2^\circ]$, $\Delta\varphi \in [0.5^\circ, 5^\circ]$, $\Delta z \in [0.005, 0.05]$. It would be interesting to investigate whether such patterns occur accidentally or they reflect

deeper properties of the dynamics. In other cases configurations at the collision time seem to be quite randomly distributed, however this problem has not been studied in details.

Particles which do not ‘collide’ during the simulation time $t = 500$ in general adopt one of the following three scenarios: (1) They settle down in a horizontal and parallel (or almost parallel) configuration but not at the same level, well separated in the horizontal direction (fig. 8.6C). (2) Centres of particles are located one above the other, but their end-to-end vectors are not parallel, and the particles rotate around z axis (fig. 8.6D). (3) In all other non-colliding simulations the particles separate and, due to the large distance between them, the relative dynamics becomes very slow and does not manage to conclude in the simulation time. The three types of the dynamics given above will be further described in following paragraphs.

The extent of simulations performed so far does not allow to give a systematic view on the different types of dynamics which can occur. Because particles collide in the majority of simulations the the present ad-hoc classification of non-colliding modes is based on only a few examples² and further systematic studies on this problem are required. It is worth mentioning that simultaneously with performing one of the first two behaviours described above, sometimes the filaments perform some minor oscillations until the end of the simulation. This long persistence of oscillations follow from strong amplification of the initial perturbation. In symmetric, non-perturbed system the simulation time $t = 500$ is well sufficient to attenuate oscillations.

The first non-colliding scenario is characterized by horizontal, parallel configuration of the two particles and significant vertical distance between them. In the fig. 8.5 it is visible by the respective markers located at the dotted lines everywhere except the first row, where final vertical distance between particles is plotted.

In the second scenario the centres of the two filaments are one above the other, but the two particles are not parallel. Therefore the ψ angle between end-to-end vectors of filaments is larger than 0 (although it can be quite small) as visible in the bottom right corner of fig. 8.5 for the perturbation $\Delta z = 0.1$. The configuration of filaments which is observed under the second scenario leads to rotation of both particles around the vertical axis, as reported by Saggiorato et al. [10]. In their article, the authors discovered that after some time the upper filament would catch up the lower one and finally the particles would collide.

If the particles separate widely during the dynamics, their relative dynamics becomes very slow. In order to track their dynamics, time scales much longer than those considered here

²Parameters corresponding to different types of dynamics as follows:

- Case (1): $\Delta\varphi = 10^\circ$ with $B = 5$; $\Delta\varphi = 0.2^\circ$ or $\Delta z \in \{0.002, 0.05\}$ with $B = 1$.
- Case (2): $\Delta z = 0.1$ with $B = 5$; $\Delta z \in \{0.005, 0.1\}$ with $B = 1$.
- Case (3): $\Delta\theta = 0.5^\circ$ or $\Delta y \in \{0.005, 0.1\}$ with $B = 1$.

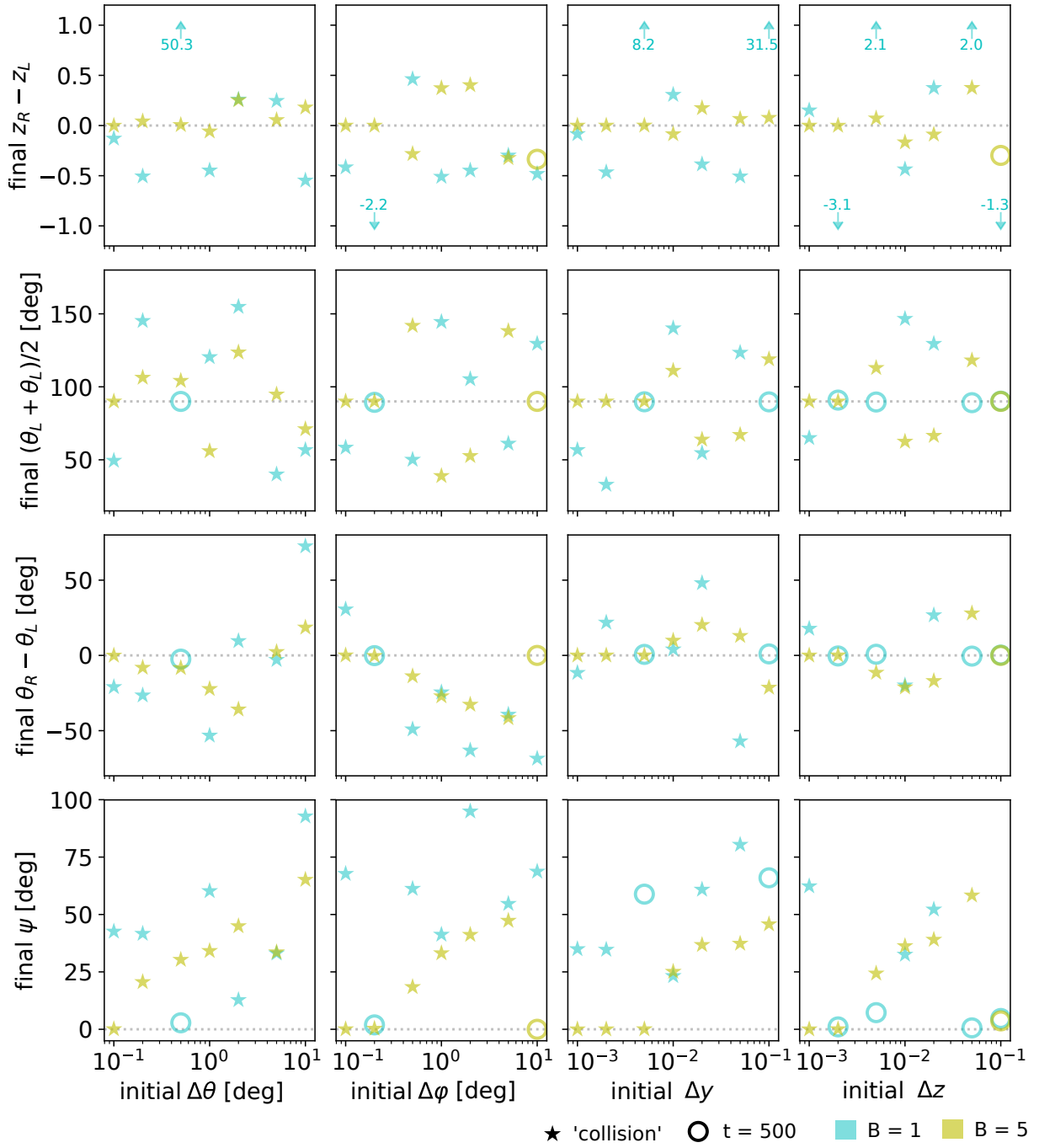


Figure 8.5: Final configurations of particles with different types and amplitudes of the non-symmetric perturbations: $\Delta\theta$, $\Delta\varphi$, Δy , Δz . Notation is the same as in fig. 8.2. In the top row, arrows represent data points outside the shown range, with the values of the final z difference indicated. Note that for all parameters measured for the final configuration, the scale is wider than in fig. 8.2. Results shown for $x_{CM}(0) = 2$ and $\varphi(0) = 45^\circ$.

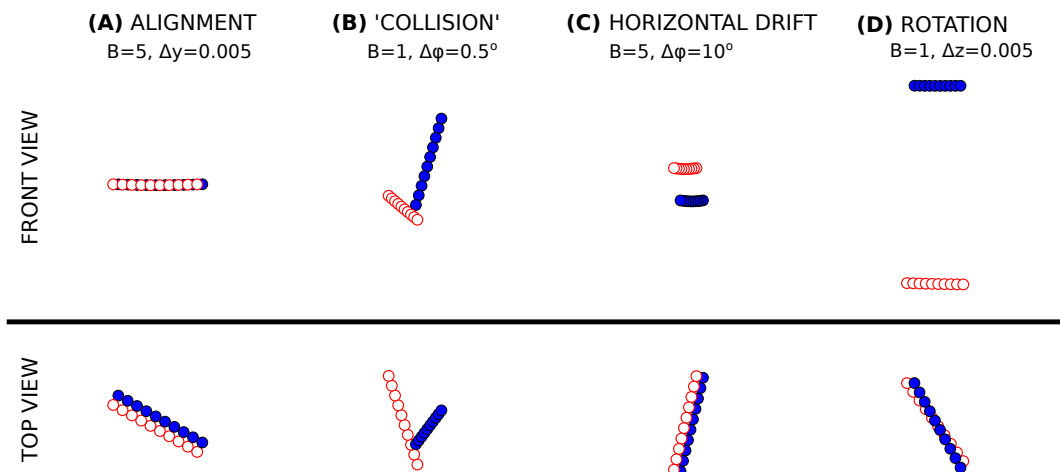


Figure 8.6: Different types of dynamics illustrated with final configurations of filaments. Snapshots taken either at the end of the simulation (A-C, $t = 500$), or at the moment when particles touch each other (B). Results for $x_{CM}(0) = 2$ and $\varphi(0) = 45^\circ$.

should be analysed. Since it is known that the upper elastic particle settles faster, it may be expected that after longer time the particles would also converge to a horizontal configuration or collide. The results presented here indicate that a systematic study of the dynamics should be based on a more accurate hydrodynamic description, eg. multipole expansion corrected for lubrication [41].

8.4 Drift and rotation of the system

The relative dynamics of two particles was the main issue of interest in the previous section, and actually throughout the whole thesis. In this chapter it is described how the pair of particles move and rotate together, after a non-symmetric perturbation of the initial configuration is introduced. For symmetric systems such problem was not considered as a separate question, because the system cannot rotate and its centre of mass can only move along y axis in a predictable manner.

In figure 8.7A the horizontal distance travelled by the centre of mass of the system is presented. The results are shown for all analysed perturbations of the initial configuration given by $x_{CM}(0) = 2$, $\varphi(0) = 45^\circ$ and for $B \in \{1, 5, 10, 40, 100\}$. Consistently, for all values of flexibility parameter B the majority of studied perturbations lead to the horizontal shift similar in magnitude to that of the unperturbed system, namely of the order of a few filament's lengths. In the figure, dots indicate final value of the shift: either at the moment when the particles touch each other or at the end of simulation. Everywhere except $B = 100$ there are some outliers which move a long horizontal distance. Such long-way travellers are most common for the

stiffest particles, $B = 1$, where in a quarter of simulations (7 out of 28) the length of horizontal drift exceeds 10. The largest drift equal to 186 was observed for $B = 5$, yet in general the distances for this value of flexibility are much shorter than for $B = 1$. For even slightly more flexible particles, $B \in \{10, 40\}$, horizontal drifts of the order of a few particle's lengths still occur in some simulations. The most flexible particles ($B = 100$) are almost insensitive to the analysed perturbations and the horizontal movement is practically the same as in symmetric system (in the figure marked with dotted line).

Apart from drifting, the system of two particles may rotate around the vertical axis as a whole. The rotation of the system is defined as the rotation of the bisector of the angle between end-to-end vectors of particles. As mentioned before, in symmetric systems the horizontal component direction of the bisector remains constant. Rotation of the system for different B and all analysed perturbations is presented in figure 8.7B. The largest rotation is observed for the most stiff filaments: in range $[-114^\circ, 75^\circ]$ for $B = 1$ (the former marked in the figure as 245°) and $[-71^\circ, 60^\circ]$ for $B = 5$ (the former marked in the figure as 289°). It was mentioned in the previous section 8.3 that in some non-colliding configurations filaments are located one above the other and the particles rotate around the vertical axis. In figure 8.7B this behaviour is particularly visible for $B = 5$ and $\Delta z = 0.1$, for which the dynamics is marked with orange, spiral line. For two other cases where analogous behaviour is observed ($B = 1$, $\Delta z \in \{0.005, 0.1\}$) the rotation of particles is much slower.

The filaments with an intermediate value of flexibility $B = 10$ also rotate, and the system can change orientation as much as $[-33^\circ, 33^\circ]$ for the analysed amplitudes of perturbations. The presented results clearly show that the type and sign of perturbation define the direction of system's rotation: positive values of Δz and $\Delta\varphi$ perturbations lead to clockwise direction, while positive values of Δy and $\Delta\theta$ to the anticlockwise.

Even more flexible filaments, with $B \in \{40, 100\}$ do not rotate significantly during the motion. What may be surprising, larger rotations of the system occur for more flexible particles with $B = 100$, which in the previous paragraph was shown to perform smaller horizontal drift than more elastic stiff with $B = 40$.

8.5 Discussion

The analysis described in this chapter has shown that the system of relatively flexible filaments ($B \geq 40$) is robust to non-symmetric perturbations. The particles converge to the aligned configuration even for deviation of the orientation angles as large as 10° and translations up to 0.1, which are the maximal analysed values.

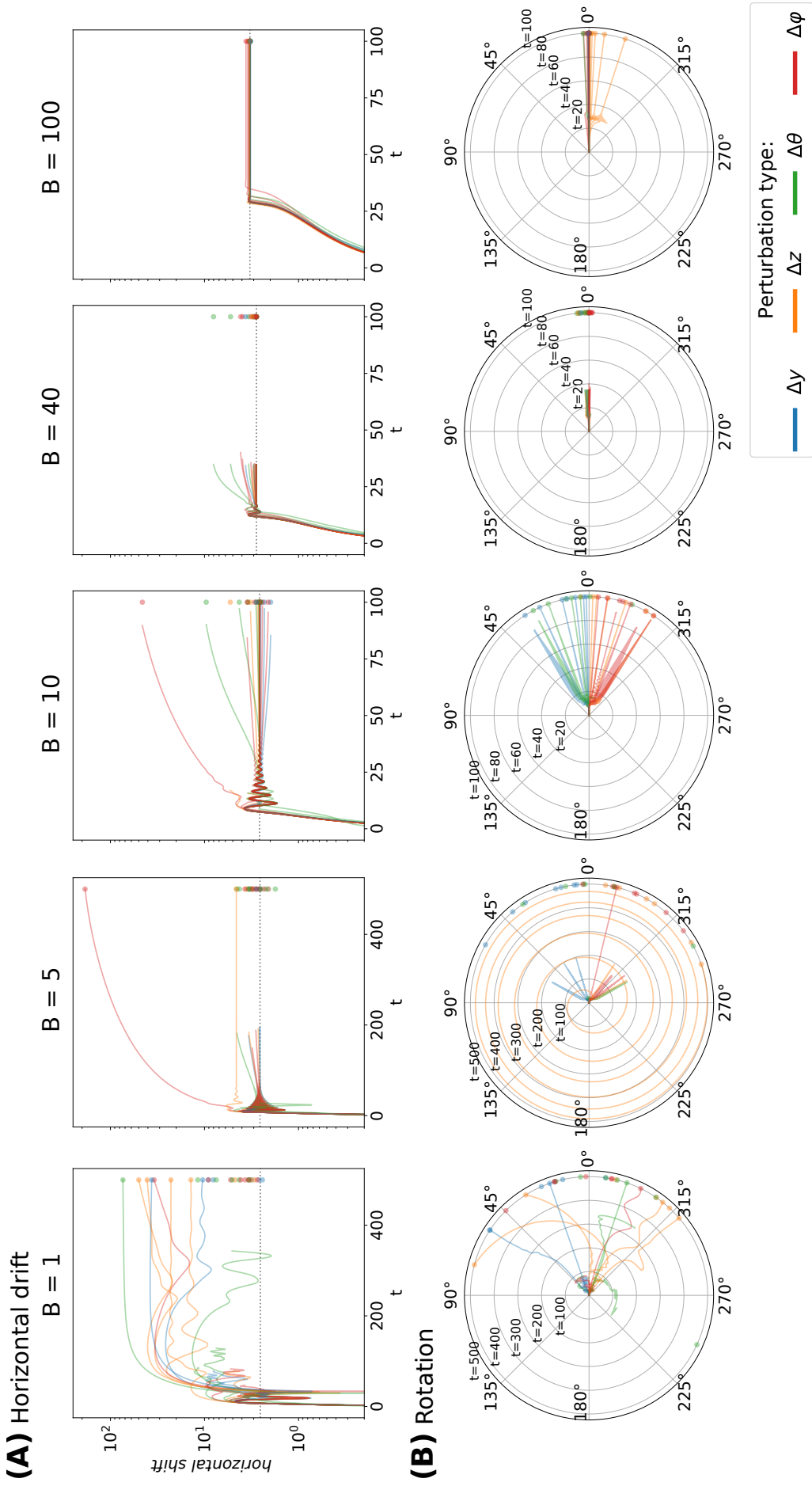


Figure 8.7: Horizontal drift (A) and rotation (B) of the system. Different colours correspond to different types of perturbations. Results are plotted until the end of simulation ($t = 500$ for $B \in \{1, 5\}$, otherwise $t = 100$) or until the particles touch each other. Additional dots at the end of time scale indicate the final values of drift and rotation for the sake of convenient comparison of results. Dotted lines in panel (A) indicate final value of horizontal drift for symmetric system with a given B . Data shown for $x_{CM}(0) = 2$ and $\varphi(0) = 45^\circ$.

Stiffer particles are more sensitive to perturbations. In my study, the dynamics for $B = 10$ was significantly more sensitive to perturbations than for $B = 40$, and dynamics for $B = 5$ more sensitive than for $B = 10$. In case of even more stiff fibres, $B = 1$, even for the smallest analysed perturbations (rotation 0.1° and translation 0.001) the dynamics was completely different than in the corresponding symmetric system. The initial perturbations initially were growing, and subsequently the particles either spuriously collided or spent long time in non-aligned configurations described in section 8.3. The main feature characteristic for non-symmetric dynamics of more flexible fibres is lost: rather stiff particles do not converge steadily toward the horizontal, parallel configuration in which the particles are at the same level. Instead, other long-lasting, ordered configurations of particles become significant for the dynamics.

In this study the analysis of the dynamics had to be terminated each time when the particles touched each other, what was allowed due to limitations of Rotne-Prager approximation. Models which include an accurate handling of near contact interactions should be used [41] in future investigations of this problem.

The fact that the dynamics of more elastic filaments is more robust to perturbations is in a good agreement with already known properties of similar systems. More flexible filaments under gravity adopt a ‘U’-shaped configuration, while more stiff remain almost straight. Fibres which are more bent quickly orient themselves horizontally (in terms of end-to-end vectors), and due to small tilt the particles have low horizontal speeds and small difference in the vertical speeds between particles. All these factors should contribute to the greater stability of the system.

One of the conclusions drawn from the obtained results is that the particles (particularly with small B) often end up in parallel or almost parallel configuration, but with a significant difference of their vertical position. In other words, the vertical deviation was usually the slowest to decay. As mentioned before, this observation is consistent with earlier articles [10, 13], which reported slow relaxation of vertical perturbations, especially for rather stiff particles. Long-lasting difference in the z coordinate of particles is the source of persistent horizontal drift or rotation in certain arrangements of particles.

An interesting problem which emerges from this study is the dynamics of rather stiff particles. The knowledge about dynamics of rigid rods in non-symmetric configuration would be very useful for deeper analysis of this problem. Unfortunately, I was not able to find any studies considering this topic. It can be easily reasoned that for some configurations rigid particles separate forever, similarly as in the symmetric system. However it is not known whether in such non-symmetric systems periodic orbits or long lasting non-periodic oscillation also exist. If the fibres are at least slightly elastic, the problem becomes even more interesting,

because flexibility, and in consequence horizontal self-orienting of the particles, excludes possibility that the particles drift apart to infinity [8]. Combining this property with the fact that two fibres which are stiff enough attract each other, at least in many arrangements which have been studied (see ref. [13] and sec. 7.3), it can be speculated that two weakly flexible filaments would interact together for a long time, possibly in a complex manner.

9 Conclusions

9.1 Summary

The task of this dissertation was to evaluate the dynamics of settling pairs of particles in symmetric configurations. One of the ideas was to carry the investigation both for rigid and elastic particles, because certain features of rigid particle dynamics can help to explain more complex dynamics of elastic particles. For the same reason simplified models of particles are considered.

The main result of this work is the discovery that elastic particles form ‘aligned’ configuration, which additionally was shown to be stable for sufficiently flexible particles. In the corresponding system of rigid rods periodic orbits have been observed and characterized. Together with results obtained for dumbbells and trumbbells, the above findings allowed to reveal the underlying mechanism of the behaviour of elastic filaments. More detailed summary of main results includes:

- Discovery and characterization of periodic dynamics of rigid particles. Reported results generalize solution obtained by Kim [100, 101] to the three-dimensional case. Chosen features of this new family of periodic motions, such as period length, have been analysed. It was also shown that during the motion particles rotate predominantly around ‘ y ’ axis.
- Different forms of bending potential have been analysed, indicating that the cosine Kratky-Porod form systematically underestimates bending energy in comparison to the continuous reference model. Harmonic and logarithmic bending potentials do not exhibit such flaw. The influence of bending potential is small in case of a single settling filament, but it becomes relevant for qualitative features of a single trumbbell dynamics, while in the system of two settling trumbbells alternative forms of bending potential can lead to completely different results.
- It was shown that pair of elastic filaments restricted to the vertical plane can tumble, as predicted in the literature [13]. During the tumbling the particles approach each other. For the bead model, the tumbling behaviour was observed only in case of very short filaments, e.g. $N = 6$. Longer particles initially attract each other and tend to collide (occurrence of collisions is an artefact of RPY approximation).

- Elastic fibres in symmetric three-dimensional configurations can exhibit a few types of behaviour, depending on their elasticity and initial configuration: (1) horizontal ‘alignment’, usually preceded by oscillations, (2) attraction and subsequent repulsion, (3) direct repulsion or (4) spurious collision (for types 2-4 particles do not reach parallel position). The alignment behaviour is the one which is further investigated in this dissertation, due to its complexity and importance for physical systems. It occurs for wide range of fibre bending stiffness, except for very flexible filaments.
- Mechanism of alignment of particles has been explained: this behaviour is caused by coupling of oscillations (two-particle effect) with a tendency of each particle to adopt horizontal position (single-particle effect). Decay of oscillations amplitude was shown to be roughly exponential.
- Dynamics of elastic particles have been analysed for horizontal, parallel positions of fibres (in terms of orientations of their end-to-end vectors). Such configuration is particularly important because it is the final stage of alignment process. It was discovered that quite stiff or moderately flexible fibres in the parallel position attract each other. More elastic ones converge toward flexibility-dependent final distance between particles, while the most flexible fibres repel each other.
- Elastic trumbbells can accurately capture the dynamics of fibres out of the vertical plane. Characteristic features are conserved: alignment of particles, exponential decay of oscillations, flexibility-dependent attraction or repulsion in the parallel configuration. If particles are restricted to the vertical plane, trumbbells, unlike the filaments, exhibit periodic motions.
- Dynamics of elastic dumbbells are different than for the trumbbells. The results show that if elastic particles under stresses are not allowed to lose their axial symmetry, they would repel each other and slowly tend *toward* vertical plane xz , unlike fibres and trumbbells which converge to the orientation *perpendicular* to this plane (in terms of end-to-end vectors of the particles).

9.2 Original elements of the thesis

Original elements of this dissertation include:

- Analysis of the bending potential: formulation of mathematically rigorous correspondence between continuous and bead models of fibres, theoretical and numerical

analysis of differences, accompanied by a few brief case studies. For the first time the influence of form of bending potential on the systems of a single settling filament, single trumbbell and two trumbbells has been investigated. Significant qualitative differences have been found.

- Dynamics of two elastic fibres were systematically analysed for a wide range of three-dimensional initial configurations. Until now, only the limiting cases of $\varphi(0) = 0$ and $\varphi(0) = \pi/2$ had been investigated [13]. Within the wide range of $\varphi(0)$ in between these limits, new types of dynamics were found, such as the alignment of filaments. Such a behaviour is important, because it transforms systems with even small deviation from the vertical plane to the final state parallel to the vertical plane, $\varphi = \pi/2$. Oscillations, with the amplitude which depends on the flexibility of fibres, were characterised. Additionally, for the initial configurations with $\varphi(0) = 0$ and short filaments, the tumbling mode has been observed for the first time. It was found that it is accompanied by attraction of fibres. For $\varphi(0) = \pi/2$ the conducted study of the long-term dynamics allowed to find an important feature of the motion: flexibility-dependent attraction or repulsion between filaments, and for some range of fibres elasticity the convergence toward a specific distance.
- An important element of this study is the investigation of different types of particles. Dynamics of rigid rods, flexible fibres, rigid or elastic dumbbells and trumbbells were determined and compared with each other. Application of many different particles in a single study allowed for more detailed analysis of the motion and better understanding of mechanisms governing the dynamics. Useful information concerning application range of simplified models has been obtained.
- The study of the symmetric systems was complemented with the investigation of the evolution of slightly non-symmetric configurations. This additional analysis has shown the robustness of the observed alignment behaviour for not too stiff filaments. It also revealed that the dynamics become much more sensitive to the perturbations for more stiff fibres. The more so, new non-symmetric and long-lasting ordered configurations of settling particles were found. Additionally, the translational and rotational motion performed by the two particles together was analysed for the first time.
- All simulations have been performed with programs written by the author in Python. The code was combined into a convenient form of a portable module. Apart from functions used to perform simulations, the module includes tools for processing of the results and visualisation.

9.3 Perspectives for future studies

During the studies conducted for this dissertation some new research questions have been formulated. Among the most important I consider the following:

- It would be worth to perform simulations of fibres and rods dynamics with an approximation of hydrodynamic interactions which is accurate even when the particles are very close to each other. This task is scheduled to be done soon, with application of advanced HYDROMULTIPOLE code with lubrication correction [41]. It was shown in this dissertation that the correct treatment of close particle surfaces is particularly relevant for symmetric systems which are restricted to the vertical plane (sec. 6.1), close to the vertical plane (small $\varphi(0)$, sec. 7.1) or for non-symmetric configurations, especially for more stiff fibres (sec. 8.3).
- Horizontal alignment of two elastic particles was shown to be the most important feature of the dynamics of two elastic particles. As the self-reorientation of a single particle is the fundamental feature behind this behaviour, other types of particles which reorient themselves under gravity should also align, and they do not need to be necessarily elastic. In particular, rigid and curved filaments seem to be good candidates because they also tend to orient themselves horizontally [97, 98]. Curved and rigid particles in bead representation can be modelled by setting very small B and modification of bending potential, so that it has the minimum for curved, rather than straight shape. E.g. if the equilibrium shape is characterized by angles $(\alpha_2, \dots, \alpha_{N-1})$, the harmonic bending potential will have the form $U_b \sim \sum_i (\beta_i - \alpha_i)^2$. Preliminary results obtained by applying this approach indeed confirm that rigid, curved particles also converge to the aligned configuration [172]. Interestingly, even the trajectories of particles and individual beads are similar to those in the system of elastic particles.
- Main results obtained in this dissertation are achievable in experiments. Robustness of the system dynamics to the non-symmetric perturbations provides a good base to hope for positive results of observations. Apart from that, as it was stated above, the alignment of particles is caused by the ability of the particle to reorient itself under gravity rather than the exact elastic properties of particles. This feature opens a possibility to observe the alignment for a wide range of different particles, including freely bending chains or rigid, curved shapes. The decay of oscillations and alignment of fibres occur after the particles have settled distance about 50 times larger than their length. In the macroscopic experiment in glycerine or the silicon oil, for the particles of the order of centimetre in length (even smaller ones can be used), the estimated height of the container is around

half of the meter, what is a reasonable size. In other configurations, where particles are closer to each other or $\varphi(0)$ is larger, the alignment may occur even faster.

- Systematic study of the two filaments behaviour for wide range of flexibility B and initial configuration would be important for better description of the system properties. Figure 7.2 presents limited, preliminary version of such analysis. The borders between different types of dynamics remain largely unknown especially for very flexible filaments $B \geq 150$ in which case the particles can attract or repel each other depending on the initial configuration. Some additional studies also for stiffer filaments would be valuable. Examination of the system for broad range of parameters could answer important questions on the fundamental properties of settling pairs of fibres: whether the particles attract or repel each other? Do they align? Do they converge to a specific, non-touching distance, as the initially parallel fibres do for $B \in [75, 124]$?
- What is the dynamics of longer particles, consisting of a larger number of beads? Preliminary results obtained for N up to 30 show that dynamics is analogous to the case of $N = 10$ described in this dissertation. Alignment is observed for $B \in \{10, 40, 100\}$. After the alignment long filaments attract or repel each other, similarly as shorter particles (sec. 7.3). The main difference with respect to the shorter fibres is larger tendency to the collision of long filaments, observed for small $\varphi(0)$, what additionally underlines the importance of applying hydrodynamic model which is adequate for near-contact interactions. In future studies filaments consisting of as much as 100 or even more beads may be considered. Having data for fibres of different lengths one may try to look for scaling laws relevant for the studied system.
- Positive experience with the system of elastic trumbbells encourages analysing even simpler models. In case of two rigid particles, Kim [100] and recently Chajwa et al. [28] showed that in some systems coupling of point approximation for hydrodynamic interactions of one particle with orientation-dependent self mobility of the other one is enough to qualitatively capture the behaviour of the system. Similar approach could be applied to the system of rigid, curved particles or even elastic ones. More general results (which do not refer to the exact shape of particle, but to its self-mobility matrix) and potentially simpler formulas, which could be tackled analytically, would be the benefit of this approach.
- The motion of two particles in non-symmetric configurations was shown in chapter 8 to be an interesting and complex issue, especially for more stiff particles. The problem of common collisions between particles could be overcome in future simulations, allowing for resolving the long-term dynamics of particles. The results obtained here for particles

which do not collide indicate that there exist several different families of long-lasting, attracting arrangements of particles. Future studies in this topic may aim to determine basins of attractions for these arrangements, characterizing chaotic properties of the system [173] and searching for other long-lasting configurations.

Some of the tasks listed above are already in progress. In particular preliminary simulations for rigid, curved particles and elastic, longer filaments have been performed and gave promising results. Experiments with macroscopic particles in glycerine and simulations with high precision HYDROMULTIPOLE code are in advanced phase of preparations.

Appendix

A Comparison of point-particle and Rotne-Prager approximations of hydrodynamic interactions in application to dumbbells' dynamics

In the main text of this dissertation point-particle approximation is used in chapter 3 which describes dynamics of elastic dumbbells and Rotne-Prager-Yamakawa approximation is applied in the rest of results (chapters 6, 7, 8) concerning dynamics of trumbbells and filaments. Here I investigate the influence of the applied hydrodynamic model on the dynamics of elastic dumbbells.

Equations (2.14) and (2.15) show that the difference between bead velocities in both models is of the order of $1/r^3$, where r is the distance between centres of beads. This means that hydrodynamic interactions between distant beads are almost insensitive to the chosen approximation, while dynamics of close beads may be more sensitive to the model.

In order to investigate the influence of chosen model of hydrodynamic interactions, here the dynamics of dumbbells is additionally calculated with Rotne-Prager approximation. Comparison of trajectories between point-particle and RPY models in the case of lack of bonds ($k = 0$) is shown in fig. 1. Unlike in the main text, vertical and horizontal axes in the figures have different scale, what visually extends the trajectory in the vertical direction. It may be observed that with both models of hydrodynamic interactions trajectories of beads are periodic and have similar shapes (see figures 1, 2). The dynamics of dumbbells was evaluated for a few values of initial length-to-distance parameter C , defined in fig. 3.1. The difference between trajectories is very small for $C = 1.65$, slightly larger for $C = 1.0$ and the largest for $C = 0.7$: note also different scale on horizontal axis in the figures). For all values of C the trajectories are wider for the point-particle model.

Similar pattern is observed for rigid dumbbells, $k = 1000$ (fig. 2). In this case for $C = 1$ and $C = 1.65$ difference between models is even smaller than for disconnected beads. Again, the alteration of trajectory is the largest for the smallest value $C = 0.7$ and the trajectory width is larger for the point-particle model than for RPY.

Figures 3 and 4 illustrate influence of hydrodynamic interaction model on dynamics of elastic dumbbells. The main effect of elasticity — hydrodynamic repulsion — is clearly observed for both models. Shapes of trajectories, shown in fig. 3, are very similar for both models. The difference between obtained trajectories is the smallest for the largest examined $k = 0.5$. We may notice that for all values of spring constant point-particle model consistently results in wider trajectories than RPY model. Figure 4 shows the horizontal distance between dumbbells

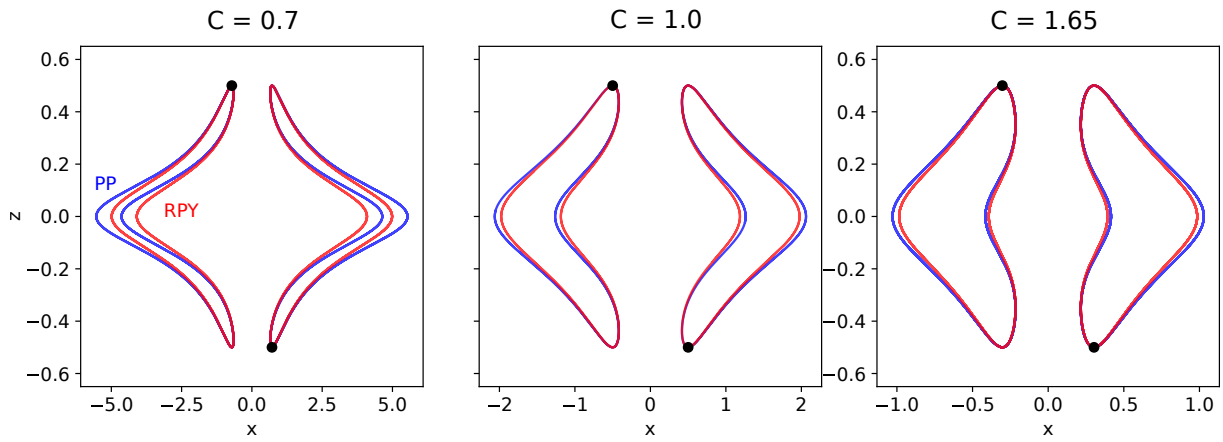


Figure 1: Comparison of beads trajectories obtained with point-particle (PP, blue) and Rotne-Prager (RPY, red) models for $k = 0$. In the left half of each plot trajectory of 1st bead is shown, in the right half - trajectory of 4th bead. Black dots indicate initial positions of beads. Note different x scale for different C .

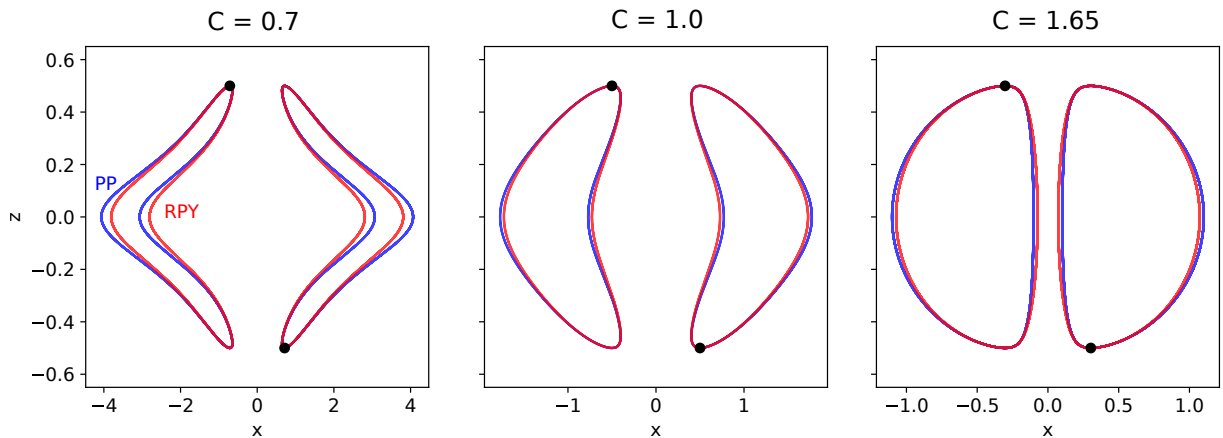


Figure 2: Comparison of beads trajectories obtained with point-particle (blue) and Rotne-Prager (red) models for practically rigid dumbbells ($k = 1000$). Note different x scale for different C .

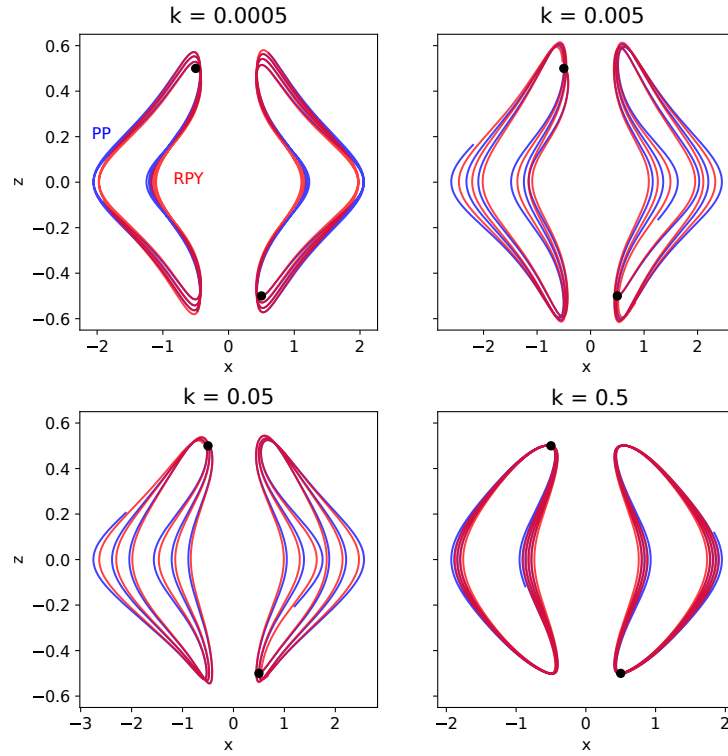


Figure 3: Comparison of beads trajectories obtained with point-particle (blue) and Rotne-Prager (red) models $C = 1$ and different elasticity values, indicated above each plot. Time of the simulations was equal to 100. Note different x scale for different k .

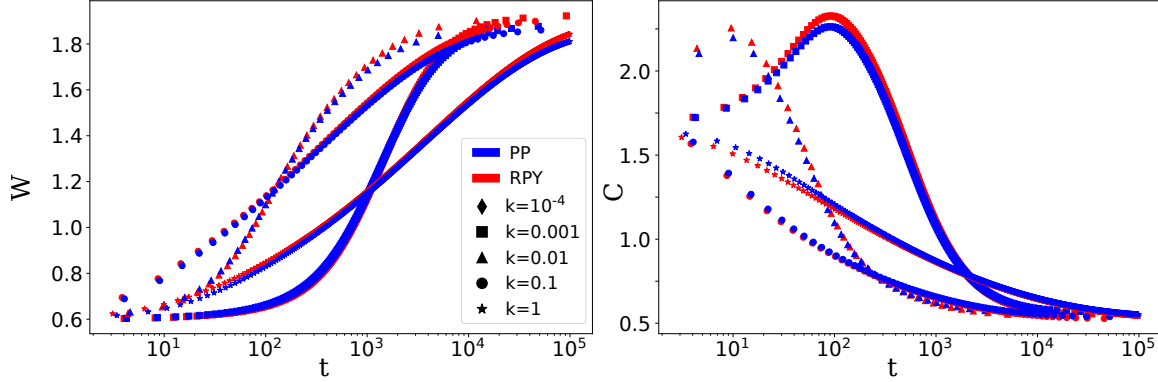


Figure 4: Values of the distance between dumbbells W and length-to-distance ratio C for dumbbells in vertical configurations. Results for point particle and Rotne-Prager-Yamakawa models of hydrodynamic interactions are shown for chosen values of the spring constant k . Note the logarithmic scale of t . Results shown for $x_{CM}(0) = 0.3$.

W and the parameter C in the vertical configuration. For all analysed spring constants k the observed values W and C are almost identical for the two hydrodynamic models.

In summary, the results described in this chapter show that the dynamics of dumbbells is qualitatively the same for point-particle and Rotne-Prager models of hydrodynamic interactions. The quantitative differences between trajectories obtained for different models are very small, yet visible. The largest differences are observed for small C (dumbbells are more separated in

the initial configuration). For all simulations in the local maxima of trajectory width (horizontal configurations) the distance between dumbbells is larger in point-particle model, but for vertical configurations (fig. 4) such systematic dependence is not present. In conclusion, the analysis conducted in this chapter suggest that the results described in chapter 3 for point-particle model remain relevant for Rotne-Prager model of hydrodynamic interactions, and that the quantitative differences introduced by switching the model are very small.

B Stability of single sedimenting trumbbell

In this appendix stability of a single sedimenting trumbbell (see sec. 5.4.1) is validated. The problem is important in context of Brownian motions: stable equilibria are likely to be robust to noise introduced by Brownian forces. For stiff trumbbells with fixed bond lengths it was shown in ref. [97] that a vertical ‘V’-shape is a stable configuration. In this appendix the model of elastic trumbbell, which is used in this dissertation, is examined.

In order to analyse stability of equilibria, the position of each bead was perturbed in a random direction. Perturbation for i -th bead has a form: $\epsilon_i = \varepsilon \hat{\epsilon}_i$, where ε is magnitude of perturbation (the same for all beads), and $\hat{\epsilon}_i$ is the direction of perturbation, which is a random unit vector, different for each bead. For each magnitude of perturbations a bunch of simulations was conducted, in order to account for the stochastic nature of results. A few values of magnitude were examined, ranging from 10^{-4} to as large as 0.1, what is equal to $1/5$ of equilibrium length of the bonds. Stability analysis described above was performed for all trumbbells analysed in sec. 5.4.1: trumbbells with large beads and $B' \in \{10, 50, 60\}$, and trumbbells with small beads and $B' \in \{10, 50, 75\}$, given that the stationary state exist for certain B and a . Both Kratky-Porod and harmonic bending potentials were examined.

Configurations of trumbbell obtained in simulations were compared with reference stationary configuration in terms of root mean square deviation (RMSD) of bead positions. Trumbbell’s configuration at each moment was first preprocessed and than root mean square deviation was calculated. RMSD between preprocessed trumbbell configuration \mathbf{r}^t and reference configuration \mathbf{r}^{ref} is given by:

$$RMSD(\mathbf{r}^t, \mathbf{r}^{ref}) = \sqrt{\sum_{i=1}^3 \left[\left(x_i^t - x_i^{ref} \right)^2 + \left(y_i^t - y_i^{ref} \right)^2 + \left(z_i^t - z_i^{ref} \right)^2 \right]}, \quad (1)$$

where x_i, y_i, z_i stand for coordinates of center of i -th bead. Preprocessing of the trumbbell configuration was done by shift in x, y, z directions and rotation around z direction, in order to minimize RMSD but without changing the shape neither tilt of the particle.

Results for all analysed parameters are consistent and clearly indicate that configurations of the trumbbell calculated in sec. 5.4.1 are stable also against random perturbations. In fig. 5 exemplary results are shown for Kratky-Porod model and $B' \in \{10, 50\}$, corresponding to results from figures 5.9 (large beads, $a = a_{max}$) and 5.10 (small beads, $a = a_{max}/4$) in the main text. Results for harmonic bending potential are very similar and therefore are not shown here. The root mean square deviation in the simulations initially decays and subsequently stays below level of 10^{-7} . It is visible that the convergence of perturbation is faster in case of more flexible filaments (as in other chapters, the time is normalized by $8\pi\eta L_0^2/G$).

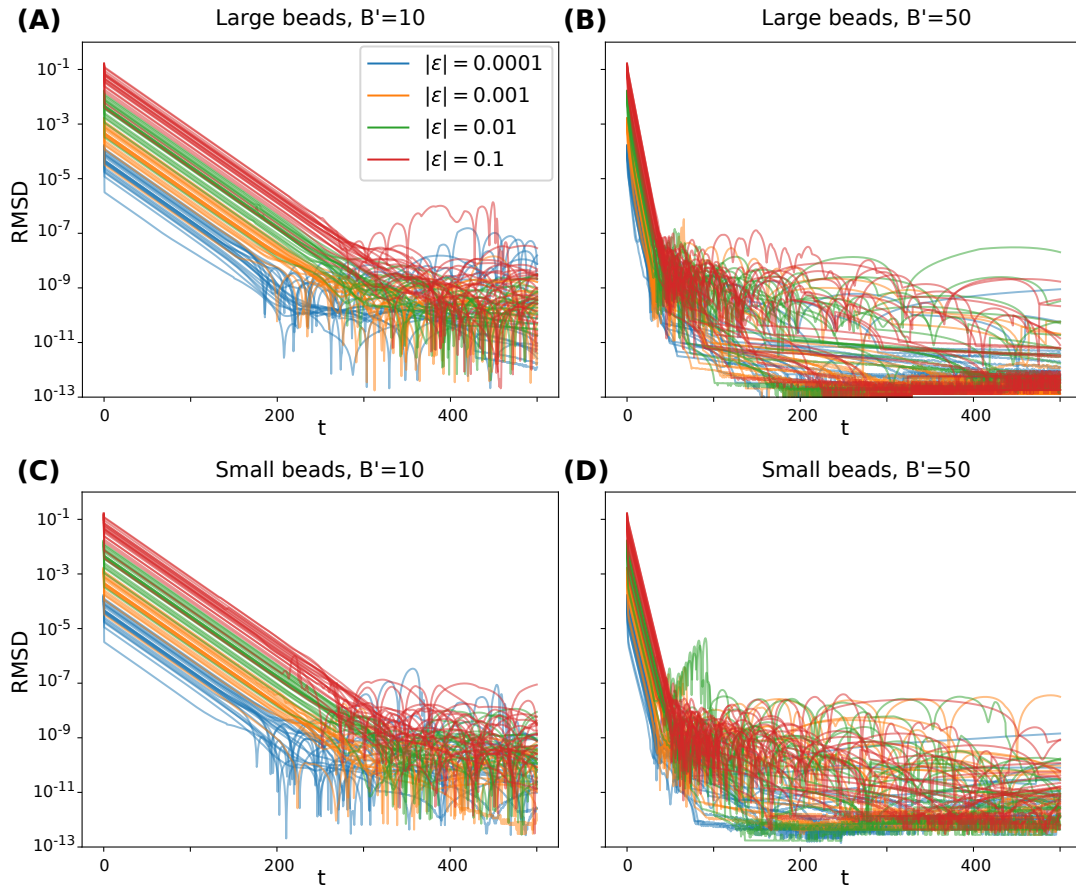


Figure 5: Convergence of trumbell configuration to a stable one from initial perturbed configuration. The magnitude of initial perturbations is labelled with color, as indicated in the (A) subplot. Results shown for Kratky-Porod bending potential with large beads $a = a_{max}$ (A,B) and small beads $a = a_{max}/4$ (C,D). The value of elasticity parameter B' is indicated over each plot.

In conclusion, in this appendix it was verified that configurations analysed in sec. 5.4.1 are stable not only against symmetric deviations of bond length and the bending angle, what was shown in the main text, but also against random perturbations even of significantly large magnitude. This conclusion holds for both Kratky-Porod and harmonic bending potentials.

Bibliography

- [1] Todd M Squires and Stephen R Quake. Microfluidics: Fluid physics at the nanoliter scale. *Reviews of modern physics*, 77(3):977, 2005.
- [2] Knut Drescher, Raymond E Goldstein, Nicolas Michel, Marco Polin, and Idan Tuval. Direct measurement of the flow field around swimming microorganisms. *Physical Review Letters*, 105(16):168101, 2010.
- [3] John M Abendroth, Oleksandr S Bushuyev, Paul S Weiss, and Christopher J Barrett. Controlling motion at the nanoscale: rise of the molecular machines. *ACS nano*, 9(8):7746–7768, 2015.
- [4] Clemens Bechinger, Roberto Di Leonardo, Hartmut Löwen, Charles Reichhardt, Giorgio Volpe, and Giovanni Volpe. Active particles in complex and crowded environments. *Reviews of Modern Physics*, 88(4):045006, 2016.
- [5] Xianghua Xu and Ali Nadim. Deformation and orientation of an elastic slender body sedimenting in a viscous liquid. *Physics of Fluids*, 6(9):2889–2893, 1994.
- [6] X Schlagberger and RR Netz. Orientation of elastic rods in homogeneous stokes flow. *Europhys. Lett.*, 70(1):129, 2005.
- [7] Marco Cosentino Lagomarsino, Ignacio Pagonabarraga, and Christopher P. Lowe. Hydrodynamic induced deformation and orientation of a microscopic elastic filament. *Phys. Rev. Lett.*, 94(14):148104, 2005.
- [8] Lei Li, Harishankar Manikantan, David Saintillan, and Saverio E Spagnolie. The sedimentation of flexible filaments. *J. Fluid Mech.*, 735:705–736, 2013.
- [9] Blaise Delmotte, Eric Climent, and Franck Plouraboué. A general formulation of bead models applied to flexible fibers and active filaments at low reynolds number. *Journal of Computational Physics*, 286:14–37, 2015.
- [10] Guglielmo Saggiorato, Jens Elgeti, Roland G Winkler, and Gerhard Gompper. Conformations, hydrodynamic interactions, and instabilities of sedimenting semiflexible filaments. *Soft Matter*, 11(37):7337–7344, 2015.

- [11] Behzad Shojaei and Hamid Dehghani. The sedimentation of slim flexible particles in stokes flow. *Indian Journal of Science and Technology*, 8(28), 2015.
- [12] Benjamin Marchetti, Veronica Raspa, Anke Lindner, Olivia du Roure, Laurence Bergougnoux, Élisabeth Guazzelli, and Camille Duprat. Deformation of a flexible fiber settling in a quiescent viscous fluid. *Physical Review Fluids*, 3(10):104102, 2018.
- [13] I. Llopis, Ignacio Pagonabarraga, Marco Cosentino Lagomarsino, and Christopher P. Lowe. Sedimentation of pairs of hydrodynamically interacting semiflexible filaments. *Phys. Rev. E*, 76(6):061901, 2007.
- [14] Donald L Koch and Eric SG Shaqfeh. The instability of a dispersion of sedimenting spheroids. *Journal of Fluid Mechanics*, 209:521–542, 1989.
- [15] Harishankar Manikantan, Lei Li, Saverio E Spagnolie, and David Saintillan. The instability of a sedimenting suspension of weakly flexible fibres. *Journal of Fluid Mechanics*, 756:935–964, 2014.
- [16] G K Batchelor. *An introduction to fluid dynamics*. Cambridge university press, 1967.
- [17] Sangtae Kim and Seppo J Karrila. *Microhydrodynamics: principles and selected applications*. Courier Corporation, 2013.
- [18] Hélène Nicolai and Elisabeth Guazzelli. Effect of the vessel size on the hydrodynamic diffusion of sedimenting spheres. *Physics of Fluids*, 7(1):3–5, 1995.
- [19] Benjamin Herzhaft, Élisabeth Guazzelli, Michael B Mackaplow, and Eric SG Shaqfeh. Experimental investigation of the sedimentation of a dilute fiber suspension. *Physical review letters*, 77(2):290, 1996.
- [20] PN Segre, Eric Herbolzheimer, and PM Chaikin. Long-range correlations in sedimentation. *Physical Review Letters*, 79(13):2574, 1997.
- [21] Bloen Metzger, Elisabeth Guazzelli, and Jason E Butler. Large-scale streamers in the sedimentation of a dilute fiber suspension. *Physical review letters*, 95(16):164506, 2005.
- [22] Gunther Machu, Walter Meile, Ludwig C Nitsche, and UWE Schaflinger. Coalescence, torus formation and breakup of sedimenting drops: experiments and computer simulations. *Journal of Fluid Mechanics*, 447:299–336, 2001.
- [23] Sunghwan Jung, SE Spagnolie, K Parikh, M Shelley, and Anna-Karin Tornberg. Periodic sedimentation in a stokesian fluid. *Phys. Rev. E*, 74(3):035302, 2006.

- [24] Bloen Metzger, Maxime Nicolas, and Élisabeth Guazzelli. Falling clouds of particles in viscous fluids. *Journal of Fluid Mechanics*, 580:283–301, 2007.
- [25] Sławomir Alabrudziński, Maria L Ekiel-Jeżewska, Daniel Chehata-Gómez, and Tomasz A Kowalewski. Particle clusters settling under gravity in a viscous fluid. *Physics of Fluids*, 21(7):073302, 2009.
- [26] Joontaek Park, Bloen Metzger, Élisabeth Guazzelli, and Jason E Butler. A cloud of rigid fibres sedimenting in a viscous fluid. *Journal of Fluid Mechanics*, 648:351–362, 2010.
- [27] Anna Myłyk, Walter Meile, Günter Brenn, and Maria L Ekiel-Jeżewska. Break-up of suspension drops settling under gravity in a viscous fluid close to a vertical wall. *Physics of fluids*, 23(6):063302, 2011.
- [28] R. Chajwa, N. Menon, and S. Ramaswamy. Kepler orbits of settling discs. pages arXiv:1803.10269 [cond-mat], 2018.
- [29] Michael Manga and HA Stone. Interactions between bubbles in magmas and lavas: effects of bubble deformation. *Journal of Volcanology and Geothermal Research*, 63(3-4):267–279, 1994.
- [30] G. I. Taylor. Low reynolds number flow. NCFM Films, 1967. <http://web.mit.edu/hml/ncfmf.html>.
- [31] Edward M Purcell. Life at low reynolds number. *American journal of physics*, 45(1):3–11, 1977.
- [32] Guy R McNamara and Gianluigi Zanetti. Use of the boltzmann equation to simulate lattice-gas automata. *Physical review letters*, 61(20):2332, 1988.
- [33] Pierre Lallemand and Li-Shi Luo. Theory of the lattice boltzmann method: Dispersion, dissipation, isotropy, galilean invariance, and stability. *Physical Review E*, 61(6):6546, 2000.
- [34] Anatoly Malevanets and Raymond Kapral. Mesoscopic model for solvent dynamics. *The Journal of chemical physics*, 110(17):8605–8613, 1999.
- [35] G Gompper, T Ihle, DM Kroll, and RG Winkler. Multi-particle collision dynamics: A particle-based mesoscale simulation approach to the hydrodynamics of complex fluids. In *Advanced computer simulation approaches for soft matter sciences III*, pages 1–87. Springer, 2009.
- [36] Jens Rotne and Stephen Prager. Variational treatment of hydrodynamic interaction in polymers. *J. Chem. Phys.*, 50(11):4831–4837, 1969.

- [37] Hiromi Yamakawa. Transport properties of polymer chains in dilute solution: hydrodynamic interaction. *J. Chem. Phys.*, 53(1):436–443, 1970.
- [38] Georges Bossis and John F Brady. Dynamic simulation of sheared suspensions. i. general method. *The Journal of chemical physics*, 80(10):5141–5154, 1984.
- [39] Louis Durlofsky, John F Brady, and Georges Bossis. Dynamic simulation of hydrodynamically interacting particles. *Journal of fluid mechanics*, 180:21–49, 1987.
- [40] Anthony JC Ladd. Hydrodynamic interactions in a suspension of spherical particles. *The Journal of chemical physics*, 88(8):5051–5063, 1988.
- [41] B Cichocki, ML Ekiel-Jezewska, and E Wajnryb. Lubrication corrections for three-particle contribution to short-time self-diffusion coefficients in colloidal dispersions. *The Journal of chemical physics*, 111(7):3265–3273, 1999.
- [42] ML Ekiel-Jezewska and E Wajnryb. Precise multipole method for calculating hydrodynamic interactions between spherical particles in the stokes flow. *Theoretical Methods for Micro Scale Viscous Flows*, pages 127–172, 2009.
- [43] Ramzi Kutteh. Methods for stokesian dynamics simulations of nonspherical particles and chains. *Physical Review E*, 69(1):011406, 2004.
- [44] Erik Gauger and Holger Stark. Numerical study of a microscopic artificial swimmer. *Phys. Rev. E*, 74(2):021907, 2006.
- [45] Agnieszka M Słowicka, Maria L Ekiel-Jezewska, Krzysztof Sadlej, and Eligiusz Wajnryb. Dynamics of fibers in a wide microchannel. *J. Chem. Phys.*, 136(4):044904, 2012.
- [46] Marco Bernabei, Petra Bacova, Angel J Moreno, Arturo Narros, and Christos N Likos. Fluids of semiflexible ring polymers: effective potentials and clustering. *Soft Matter*, 9(4):1287–1300, 2013.
- [47] Antonio F Fortes, Daniel D Joseph, and Thomas S Lundgren. Nonlinear mechanics of fluidization of beds of spherical particles. *Journal of Fluid Mechanics*, 177:467–483, 1987.
- [48] E Wacholder and NF Sather. The hydrodynamic interaction of two unequal spheres moving under gravity through quiescent viscous fluid. *J. Fluid Mech.*, 65(3):417–437, 1974.
- [49] CI Trombley and ML Ekiel-Jezewska. Stable configurations of charged sedimenting particles. *Physical Review Letters*, 121(25):254502, 2018.

- [50] Martin Golubitsky, Martin Krupa, and Chjan Lim. Time-reversibility and particle sedimentation. *SIAM Journal on Applied Mathematics*, 51(1):49–72, 1991.
- [51] LM Hocking. The behaviour of clusters of spheres falling in a viscous fluid part 2. slow motion theory. *Journal of Fluid Mechanics*, 20(1):129–139, 1964.
- [52] Russel E Caflisch, Chjan Lim, Jonathan HC Luke, and Ashok S Sangani. Periodic solutions for three sedimenting spheres. *The Physics of fluids*, 31(11):3175–3179, 1988.
- [53] Monika Bargieł, Merzik T Kamel, and Elmer M Tory. Periodic motion of four spheres in a “kite” configuration. *Powder technology*, 214(1):14–20, 2011.
- [54] Maria L Ekiel-Jezewska. Class of periodic and quasiperiodic trajectories of particles settling under gravity in a viscous fluid. *Physical Review E*, 90(4):043007, 2014.
- [55] Marta Gruca, Marek Bukowicki, and Maria L Ekiel-Jezewska. Periodic and quasiperiodic motions of many particles falling in a viscous fluid. *Physical Review E*, 92(2):023026, 2015.
- [56] Marta Gruca. *Motion of regular systems of many particles interacting hydrodynamically under gravity*. PhD thesis, IPPT PAN, 2016.
- [57] Maria Ekiel-Jezewska, Marta Gruca, and Marek Bukowicki. Particles sedimenting in a permeable medium. *Bulletin of the American Physical Society*, 2018.
- [58] ML Ekiel-Jezewska, B Metzger, and E Guazzelli. Spherical cloud of point particles falling in a viscous fluid. *Physics of Fluids*, 18(3):038104, 2006.
- [59] Gustavo Coelho Abade and Francisco Ricardo Cunha. Computer simulation of particle aggregates during sedimentation. *Computer methods in applied mechanics and engineering*, 196(45-48):4597–4612, 2007.
- [60] Imre M Jánosi, Tamás Tél, Dietrich E Wolf, and Jason AC Gallas. Chaotic particle dynamics in viscous flows: The three-particle stokeslet problem. *Phys. Rev. E*, 56(3):2858, 1997.
- [61] Piotr Szymczak, Magdalena Gruzziel-Slomka, Pawel Kondratiuk, and Maria Ekiel-Jezewska. Sedimentation of elastic loops in a viscous fluid. *Bulletin of the American Physical Society*, 2018.
- [62] Magdalena Gruzziel, Krishnan Thyagarajan, Giovanni Dietler, Andrzej Stasiak, Maria L. Ekiel-Jezewska, and Piotr Szymczak. Periodic motion of sedimenting flexible knots. *Physical Review Letters*, 121:127801, Sep 2018.

- [63] S Reddig and H Stark. Cross-streamline migration of a semiflexible polymer in a pressure driven flow. *The Journal of chemical physics*, 135(16):10B620, 2011.
- [64] Agnieszka M Słowicka, Eligiusz Wajnryb, and Maria L Ekiel-Jeżewska. Dynamics of flexible fibers in shear flow. *J. Chem. Phys.*, 143(12):124904, 2015.
- [65] Anke Lindner and Michael Shelley. Elastic fibers in flows. In *Fluid-Structure Interactions in Low-Reynolds-Number Flows*, pages 168–192. Royal Society of Chemistry, 2015.
- [66] Richard M Jendrejack, David C Schwartz, Juan J De Pablo, and Michael D Graham. Shear-induced migration in flowing polymer solutions: Simulation of long-chain dna in microchannels. *The Journal of chemical physics*, 120(5):2513–2529, 2004.
- [67] Michael D Graham. Fluid dynamics of dissolved polymer molecules in confined geometries. *Annual Review of Fluid Mechanics*, 43:273–298, 2011.
- [68] Raghunath Chelakkot, Roland G Winkler, and Gerhard Gompper. Semiflexible polymer conformation, distribution and migration in microcapillary flows. *Journal of Physics: Condensed Matter*, 23(18):184117, 2011.
- [69] O Berk Usta, Jason E Butler, and Anthony JC Ladd. Flow-induced migration of polymers in dilute solution. *Physics of fluids*, 18(3):031703, 2006.
- [70] Agnieszka M Słowicka, Eligiusz Wajnryb, and Maria L Ekiel-Jeżewska. Lateral migration of flexible fibers in poiseuille flow between two parallel planar solid walls. *The European Physical Journal E*, 36(3):31, 2013.
- [71] Steve Kuei, Agnieszka M Słowicka, Maria L Ekiel-Jeżewska, Eligiusz Wajnryb, and Howard A Stone. Dynamics and topology of a flexible chain: knots in steady shear flow. *New Journal of Physics*, 17(5):053009, 2015.
- [72] Y-N Young. Hydrodynamic interactions between two semiflexible inextensible filaments in stokes flow. *Physical Review E*, 79(4):046317, 2009.
- [73] Vasily Kantsler and Raymond E Goldstein. Fluctuations, dynamics, and the stretch-coil transition of single actin filaments in extensional flows. *Phys. Rev. Lett.*, 108(3):038103, 2012.
- [74] Ashley M Young, L Karp-Boss, PA Jumars, and EN Landis. Quantifying diatom aspirations: Mechanical properties of chain-forming species. *Limnology and Oceanography*, 57(6):1789–1801, 2012.

- [75] Markus Harasim, Bernhard Wunderlich, Orit Peleg, Martin Kröger, and Andreas R Bausch. Direct observation of the dynamics of semiflexible polymers in shear flow. *Phys. Rev. Lett.*, 110(10):108302, 2013.
- [76] Hoa Nguyen and Lisa Fauci. Hydrodynamics of diatom chains and semiflexible fibres. *Journal of The Royal Society Interface*, 11(96):20140314, 2014.
- [77] Sylwia Pawłowska, Paweł Nakielski, Filippo Pierini, Izabela K Piechocka, Krzysztof Zembrzycki, and Tomasz A Kowalewski. Lateral migration of electrospun hydrogel nanofilaments in an oscillatory flow. *PLoS One*, 12(11):e0187815, 2017.
- [78] Yanan Liu, Brato Chakrabarti, David Saintillan, Anke Lindner, and Olivia du Roure. Morphological transitions of elastic filaments in shear flow. *Proc. Natl. Acad. Sci. USA*, 115:9438, 2018.
- [79] Dietmar Lerche and Dirk Frömer. Theoretical and experimental analysis of the sedimentation kinetics of concentrated red cell suspensions in a centrifugal field: Determination of the aggregation and deformation of rbc by flux density and viscosity functions. *Biorheology*, 38(2, 3):249–262, 2001.
- [80] Peter Schuck. On the analysis of protein self-association by sedimentation velocity analytical ultracentrifugation. *Analytical biochemistry*, 320(1):104–124, 2003.
- [81] Christopher A MacRaild, Danny M Hatters, Lynne J Lawrence, and Geoffrey J Howlett. Sedimentation velocity analysis of flexible macromolecules: self-association and tangling of amyloid fibrils. *Biophysical journal*, 84(4):2562–2569, 2003.
- [82] Patrick H Brown and Peter Schuck. Macromolecular size-and-shape distributions by sedimentation velocity analytical ultracentrifugation. *Biophysical journal*, 90(12):4651–4661, 2006.
- [83] Adam Kempczyński, Maciej Bosek, and Bronisław Grzegorzewski. Fluctuations in settling velocity of red blood cell aggregates. *Optica Applicata*, 44(3), 2014.
- [84] Eric Lauga. Bacterial hydrodynamics. *Annual Review of Fluid Mechanics*, 48:105–130, 2016.
- [85] E Virginia Armbrust. The life of diatoms in the world’s oceans. *Nature*, 459(7244):185, 2009.
- [86] Knut Drescher, Kyriacos C Leptos, Idan Tuval, Takuji Ishikawa, Timothy J Pedley, and Raymond E Goldstein. Dancing volvox: hydrodynamic bound states of swimming algae. *Physical Review Letters*, 102(16):168101, 2009.

- [87] Salima Rafai, Levan Jibuti, and Philippe Peyla. Effective viscosity of microswimmer suspensions. *Phys. Rev. Lett.*, 104(9):098102, 2010.
- [88] Nathan A Baker, David Sept, Simpson Joseph, Michael J Holst, and J Andrew McCammon. Electrostatics of nanosystems: application to microtubules and the ribosome. *Proceedings of the National Academy of Sciences*, 98(18):10037–10041, 2001.
- [89] Dmitry A Fedosov, Matti Peltomäki, and Gerhard Gompper. Deformation and dynamics of red blood cells in flow through cylindrical microchannels. *Soft matter*, 10(24):4258–4267, 2014.
- [90] Fredrik Lundell, L Daniel Söderberg, and P Henrik Alfredsson. Fluid mechanics of papermaking. *Annual Review of Fluid Mechanics*, 43:195–217, 2011.
- [91] Karl MO Håkansson, Andreas B Fall, Fredrik Lundell, Shun Yu, Christina Krywka, Stephan V Roth, Gonzalo Santoro, Mathias Kvik, Lisa Prahl Wittberg, Lars Wågberg, et al. Hydrodynamic alignment and assembly of nanofibrils resulting in strong cellulose filaments. *Nature communications*, 5:4018, 2014.
- [92] Zheng-Ming Huang, Y-Z Zhang, M Kotaki, and S Ramakrishna. A review on polymer nanofibers by electrospinning and their applications in nanocomposites. *Composites science and technology*, 63(15):2223–2253, 2003.
- [93] Sylwia Pawłowska, Tomasz A Kowalewski, and Filippo Pierini. Fibrous polymer nanomaterials for biomedical applications and their transport by fluids: an overview. *Soft matter*, 14(42):8421–8444, 2018.
- [94] Manoel Manghi, Xaver Schlagberger, Yong-Woon Kim, and Roland R Netz. Hydrodynamic effects in driven soft matter. *Soft Matter*, 2(8):653–668, 2006.
- [95] Antonio Perazzo, Janine K Nunes, Stefano Guido, and Howard A Stone. Flow-induced gelation of microfiber suspensions. *PNAS*, 114(41):E8557–E8564, 2017.
- [96] S Pawłowska. Highly deformable nanofilaments in flow. In *Journal of Physics: Conference Series*, volume 760, page 012022. IOP Publishing, 2016.
- [97] Maria L. Ekiel-Jezewska and Eligiusz Wajnryb. Hydrodynamic orienting of asymmetric microobjects under gravity. *J. Phys.: Condens. Matter*, 21(20):204102, 2009.
- [98] EJ Tozzi, C Tim Scott, David Vahey, and DJ Klingenberg. Settling dynamics of asymmetric rigid fibers. *Physics of Fluids*, 23(3):033301, 2011.

- [99] Martina Palusa, Joost de Graaf, Aidan Brown, and Alexander Morozov. Sedimentation of a rigid helix in viscous media. *ArXiv e-prints*, page arXiv:1811.08491, November 2018.
- [100] Sangtae Kim. Sedimentation of two arbitrarily oriented spheroids in a viscous fluid. *Int. J. Multiphase Flow*, 11(5):699–712, 1985.
- [101] Sangtae Kim. Singularity solutions for ellipsoids in low-reynolds-number flows: with applications to the calculation of hydrodynamic interactions in suspensions of ellipsoids. *International journal of multiphase flow*, 12(3):469–491, 1986.
- [102] Tomer Goldfriend, Haim Diamant, and Thomas A Witten. Hydrodynamic interactions between two forced objects of arbitrary shape. ii. relative translation. *Physical Review E*, 93(4):042609, 2016.
- [103] Katarina Gustavsson and A-K Tornberg. Gravity induced sedimentation of slender fibers. *Physics of fluids*, 21(12):123301, 2009.
- [104] Tomer Goldfriend, Haim Diamant, and Thomas A Witten. Screening, hyperuniformity, and instability in the sedimentation of irregular objects. *Physical Review Letters*, 118(15):158005, 2017.
- [105] Maria L Ekiel-Jezewska, Tomasz Gubiec, and P Szymczak. Stokesian dynamics of close particles. *Physics of Fluids*, 20(6):063102, 2008.
- [106] David Saintillan, Eric SG Shaqfeh, and Eric Darve. The growth of concentration fluctuations in dilute dispersions of orientable and deformable particles under sedimentation. *Journal of Fluid Mechanics*, 553:347–388, 2006.
- [107] Xaver Schlagberger and Roland R Netz. Anomalous sedimentation of self-avoiding flexible polymers. *Macromolecules*, 41(5):1861–1871, 2008.
- [108] Harishankar Manikantan and David Saintillan. Effect of flexibility on the growth of concentration fluctuations in a suspension of sedimenting fibers: Particle simulations. *Physics of Fluids*, 28(1):013303, 2016.
- [109] Hongbo Ma and Michael D Graham. Theory of shear-induced migration in dilute polymer solutions near solid boundaries. *Physics of Fluids*, 17(8):083103, 2005.
- [110] Anugrah Singh. Dynamics of suspensions of spherical doublets in simple shear and pressure driven flow. *Chemical Engineering Science*, 104:17–24, 2013.
- [111] GP Alexander and JM Yeomans. Dumb-bell swimmers. *EPL (Europhysics Letters)*, 83(3):34006, 2008.

- [112] Eric Lauga and Denis Bartolo. No many-scallop theorem: Collective locomotion of reciprocal swimmers. *Physical Review E*, 78(3):030901, 2008.
- [113] Niklas Küchler, Hartmut Löwen, and Andreas M Menzel. Getting drowned in a swirl: Deformable bead-spring model microswimmers in external flow fields. *Physical Review E*, 93(2):022610, 2016.
- [114] Roland G Winkler. Dynamics of flexible active brownian dumbbells in the absence and the presence of shear flow. *Soft Matter*, 12(16):3737–3749, 2016.
- [115] Hartmut Löwen. Active colloidal molecules. *EPL (Europhysics Letters)*, 121(5):58001, 2018.
- [116] Jörn Dunkel, Victor B Putz, Irwin M Zaid, and Julia M Yeomans. Swimmer-tracer scattering at low reynolds number. *Soft Matter*, 6(17):4268–4276, 2010.
- [117] Victor B Putz, Jörn Dunkel, and Julia M Yeomans. Cuda simulations of active dumbbell suspensions. *Chemical Physics*, 375(2-3):557–567, 2010.
- [118] Antonio Suma, Giuseppe Gonnella, Gianluca Laghezza, Antonio Lamura, Alessandro Mossa, and Leticia F Cugliandolo. Dynamics of a homogeneous active dumbbell system. *Physical Review E*, 90(5):052130, 2014.
- [119] Leticia F Cugliandolo, Pasquale Digregorio, Giuseppe Gonnella, and Antonio Suma. Phase coexistence in two-dimensional passive and active dumbbell systems. *Physical Review Letters*, 119(26):268002, 2017.
- [120] Ole Hassager. Kinetic theory and rheology of bead-rod models for macromolecular solutions. i. equilibrium and steady flow properties. *The Journal of Chemical Physics*, 60(5):2111–2124, 1974.
- [121] Kyosuke Nagasaka and Hiromi Yamakawa. Dynamics of weakly bending rods: A trumbbell model. *J. Chem. Phys.*, 83(12):6480–6488, 1985.
- [122] Daniel B. Roitman. The elastic trumbbell model for dynamics of stiff chains. In *Rotational Dynamics of Small and Macromolecules*, Lecture Notes in Physics, pages 192–207. Springer, Berlin, Heidelberg, 1987.
- [123] F. G. Díaz and J. García de la Torre. Simulation of the rotational brownian dynamics of a simple, segmentally flexible model: The elastic trumbbell. *J. Chem. Phys.*, 88(12):7698–7705, 1988.

- [124] C Cruz, Francisco Chinesta, and Gilles Regnier. Review on the brownian dynamics simulation of bead-rod-spring models encountered in computational rheology. *Archives of Computational Methods in Engineering*, 19(2):227–259, 2012.
- [125] Emmanuel Lance Christopher VI Medillo Plan and Dario Vincenzi. Tumbling of a brownian particle in an extensional flow. *Proc. R. Soc. London, Ser. A*, 472(2194):20160226, 2016.
- [126] William E. Uspal and Patrick S. Doyle. Self-organizing microfluidic crystals. *Soft Matter*, 10(28):5177–5191, 2014.
- [127] Javier Atencia and David J Beebe. Controlled microfluidic interfaces. *Nature*, 437(7059):648, 2004.
- [128] Benjamin P Casavant, Erwin Berthier, Ashleigh B Theberge, Jean Berthier, Sara I Montanez-Sauri, Lauren L Bischel, Kenneth Brakke, Curtis J Hedman, Wade Bushman, Nancy P Keller, et al. Suspended microfluidics. *Proceedings of the National Academy of Sciences*, 110(25):10111–10116, 2013.
- [129] Olivier Frey, Patrick M Misun, David A Fluri, Jan G Hengstler, and Andreas Hierlemann. Reconfigurable microfluidic hanging drop network for multi-tissue interaction and analysis. *Nature Communications*, 5:4250, 2014.
- [130] Eric Lauga, Willow R DiLuzio, George M Whitesides, and Howard A Stone. Swimming in circles: motion of bacteria near solid boundaries. *Biophysical Journal*, 90(2):400–412, 2006.
- [131] Diego Lopez and Eric Lauga. Dynamics of swimming bacteria at complex interfaces. *Physics of Fluids*, 26(7):400–412, 2014.
- [132] S Ganga Prasath, Joel Marthelot, Rama Govindarajan, and Narayanan Menon. Relaxation of a highly deformed elastic filament at a fluid interface. *Physical Review Fluids*, 1(3):033903, 2016.
- [133] William H. Mitchell and Saverio E. Spagnolie. Sedimentation of spheroidal bodies near walls in viscous fluids: glancing, reversing, tumbling and sliding. *Journal of Fluid Mechanics*, 772:600–629, 2015.
- [134] F Candelier and B Mehlig. Settling of an asymmetric dumbbell in a quiescent fluid. *Journal of Fluid Mechanics*, 802:174–185, 2016.

- [135] Maria Ekiel-Jezewska, Robert Boniecki, Marek Bukowicki, and Marta Gruca. Stokes velocity generated by a point force in various geometries. *The European Physical Journal E*, 41(10):120, 2018.
- [136] Jizeng Wang and Huajian Gao. A generalized bead-rod model for brownian dynamics simulations of wormlike chains under strong confinement. *J. Chem. Phys.*, 123(8):084906, 2005.
- [137] Raghunath Chelakkot, Roland G Winkler, and Gerhard Gompper. Migration of semiflexible polymers in microcapillary flow. *Europhys. Lett.*, 91(1):14001, 2010.
- [138] R. Matthews, A. A. Louis, and J. M. Yeomans. Complex dynamics of knotted filaments in shear flow. *Europhys. Lett.*, 92(3):34003, 2010.
- [139] Ying Li and Martin Kröger. Viscoelasticity of carbon nanotube buckypaper: zipping–unzipping mechanism and entanglement effects. *Soft Matter*, 8(30):7822–7830, 2012.
- [140] Jin Suk Myung, Farzaneh Taslimi, Roland G Winkler, and Gerhard Gompper. Self-organized structures of attractive end-functionalized semiflexible polymer suspensions. *Macromolecules*, 47(12):4118–4125, 2014.
- [141] Christian O. Plaza-Rivera, Hong T. Nguyen, and Robert S. Hoy. Isostaticity and the solidification of semiflexible polymer melts. *Soft Matter*, 13(43):7948–7952, 2017.
- [142] Roger J. Lewis, Stuart A. Allison, Don Eden, and R. Pecora. Brownian dynamics simulations of a three-subunit and a ten-subunit worm-like chain: Comparison of results with trumbell theory and with experimental results from DNA. *J. Chem. Phys.*, 89(4):2490–2503, 1988.
- [143] Masao Doi and Samuel Frederick Edwards. *The theory of polymer dynamics*, volume 73. Oxford University Press, 1988.
- [144] Peter Poier, Christos N Likos, Angel J Moreno, and Ronald Blaak. An anisotropic effective model for the simulation of semiflexible ring polymers. *Macromolecules*, 48(14):4983–4997, 2015.
- [145] Otto Kratky and Günther Porod. Röntgenuntersuchung gelöster fadenmoleküle. *Rec. Trav. Chim. Pays-Bas.*, 68:1106—1123, 1949.
- [146] Joshua N. Milstein and Jens-Christian Meiners. Worm-like chain (wlc) model. In Gordon C. K. Roberts, editor, *Encyclopedia of Biophysics*, pages 2757–2760. Springer, 2013.

- [147] Stuart A Allison. Brownian dynamics simulation of wormlike chains. fluorescence depolarization and depolarized light scattering. *Macromolecules*, 19(1):118–124, 1986.
- [148] Stephen L Mayo, Barry D Olafson, and William A Goddard. Dreiding: a generic force field for molecular simulations. *J. Phys. Chem.*, 94(26):8897–8909, 1990.
- [149] Alex D MacKerell Jr, Donald Bashford, MLDR Bellott, Roland Leslie Dunbrack Jr, Jeffrey D Evanseck, et al. All-atom empirical potential for molecular modeling and dynamics studies of proteins. *J. Phys. Chem. B*, 102(18):3586–3616, 1998.
- [150] Daan Frenkel and Berend Smit. *Understanding molecular simulation: from algorithms to applications*. Elsevier, 2001.
- [151] Cornelis Storm and Philip C Nelson. Theory of high-force DNA stretching and overstretching. *Phys. Rev. E*, 67(5):051906, 2003.
- [152] Junmei Wang, Romain M Wolf, James W Caldwell, Peter A Kollman, and David A Case. Development and testing of a general amber force field. *J. Comput. Chem.*, 25(9):1157–1174, 2004.
- [153] John Kuriyan, Boyana Konforti, and David Wemmer. *The molecules of life: Physical and chemical principles*. Garland Science, 2012.
- [154] Magdalena Gruzziel, Wojciech Dzwolak, and Piotr Szymczak. Chirality inversions in self-assembly of fibrillar superstructures: a computational study. *Soft Matter*, 9(33):8005–8013, 2013.
- [155] Aamir Ali, Emmanuel Lance Christopher VI Medillo Plan, Samridhhi Sankar Ray, and Dario Vincenzi. Semiflexible particles in isotropic turbulence. *Phys. Rev. Fluids*, 1(8):082402, 2016.
- [156] RC Picu and A Sengab. Structural evolution and stability of non-crosslinked fiber networks with inter-fiber adhesion. *Soft Matter*, 14(12):2254–2266, 2018.
- [157] Andre Förtsch, Matthias Laumann, Diego Kienle, and Walter Zimmermann. Migration reversal of soft particles in vertical flows. *Europhys. Lett.*, 119(6):64003, 2017.
- [158] Lev Davidovich Landau, Evgeny Mikhailovich Lifshitz, Lev Petrovich Pitaevskii, and Arnold Markovich Kosevich. *Course of Theoretical Physics: Volume 7, Theory of Elasticity*. Butterworth-Heinemann, 1986.
- [159] Marek Bukowicki and Maria L Ekiel-Jezewska. Different bending models predict different dynamics of sedimenting elastic trumbbells. *Soft Matter*, 14:5786–5799, 2018.

- [160] BU Felderhof. Hydrodynamic interactions in suspensions with periodic boundary conditions. *Physica A: Statistical Mechanics and its Applications*, 159(1):1–18, 1989.
- [161] Anthony JC Ladd. Hydrodynamic transport coefficients of random dispersions of hard spheres. *The Journal of Chemical Physics*, 93(5):3484–3494, 1990.
- [162] Anthony JC Ladd. Dynamical simulations of sedimenting spheres. *Physics of Fluids A: Fluid Dynamics*, 5(2):299–310, 1993.
- [163] B Cichocki, BU Felderhof, K Hinsen, E Wajnryb, and J Bławdziewicz. Friction and mobility of many spheres in stokes flow. *The Journal of Chemical Physics*, 100(5):3780–3790, 1994.
- [164] Guobiao Mo and Ashok S Sangani. A method for computing Stokes flow interactions among spherical objects and its application to suspensions of drops and porous particles. *Physics of Fluids*, 6(5):1637–1652, 1994.
- [165] B Cichocki and RB Jones. Image representation of a spherical particle near a hard wall. *Physica A: Statistical Mechanics and its Applications*, 258(3-4):273–302, 1998.
- [166] Asimina Sierou and John F Brady. Accelerated stokesian dynamics simulations. *Journal of Fluid Mechanics*, 448:115–146, 2001.
- [167] S Bhattacharya, J Bławdziewicz, and E Wajnryb. Hydrodynamic interactions of spherical particles in suspensions confined between two planar walls. *Journal of Fluid Mechanics*, 541:263–292, 2005.
- [168] Marek Bukowicki, Marta Gruca, and Maria L Ekiel-Jeżewska. Dynamics of elastic dumbbells sedimenting in a viscous fluid: oscillations and hydrodynamic repulsion. *Journal of Fluid Mechanics*, 767:95–108, 2015.
- [169] Marek Bukowicki and Maria L Ekiel-Jeżewska. Sedimenting pairs of elastic filaments. *Manuscript in preparation.*, 2019.
- [170] William Prager. *Introduction to mechanics of continua*. Courier Corporation, 1961.
- [171] Oliver M O’Reilly. *Modeling Nonlinear Problems in the Mechanics of Strings and Rods*. Springer, 2017.
- [172] Marek Bukowicki and Maria Ekiel-Jeżewska. Effect of bending on sedimentation of two deformable microparticles. *Bulletin of the American Physical Society*, 2018.
- [173] Edward Ott and Tamás Tél. Chaotic scattering: An introduction. *Chaos: An Interdisciplinary Journal of Nonlinear Science*, 3(4):417–426, 1993.